# GEOCHEMISTRY OF THE EARTH'S MANTLE, NUNIVAK ISLAND, ALASKA AND OTHER AREAS: EVIDENCE FROM XENOLITH STUDIES

by

MICHAEL FRANK RODEN

A.B., Hamilton College
(1972)

M.A., University of Texas
(1977)

SUBMITTED TO THE DEPARTMENT OF EARTH AND PLANETARY SCIENCES IN PARTIAL FULFILLMENT OF THE REQUIREMENTS FOR THE DEGREE OF

DOCTOR OF PHILOSOPHY

at the

MASSACHUSETTS INSTITUTE OF TECHNOLOGY

September, 1982

Signature of Author _____
Department of Earth and Planetary Sciences
May 28, 1982

Certified by _____
Frederick A. Frey
Thesis Supervisor

Accepted by _____
Theodore R. Madden
Chairman, Departmental Committee on Graduate Students

# GEOCHEMISTRY OF THE EARTH'S MANTLE, NUNIVAK ISLAND, ALASKA AND OTHER AREAS: EVIDENCE FROM XENOLITH STUDIES

by

MICHAEL FRANK RODEN

Submitted to the Department of Earth and Planetary Sciences, M.I.T., May, 1982, in partial fulfillment of the requirements for the degree of Doctor of Philosophy

## ABSTRACT

I

The Quaternary basanites of Nunivak Island, Alaska, contain a diverse suite of ultramafic and mafic inclusions including pyroxene granulites, granuloblastic-equant (GE), coarse-equant (CE), and coarse-tabular (CT) lherzolites, and amphibole-pyroxenites. Trace element abundances and isotopic ratios were measured in representative samples of these inclusions and the associated olivine tholeiites and basanites in order to understand the petrogenesis and interrelationships of the various rock types and to document mantle heterogeneity beneath Nunivak Island

Trace element abundances in the granulites indicate that their protoliths were troctolite cumulates. Present-day $^{87}Sr/^{86}Sr$ and $^{143}Nd/^{144}Nd$ ratios of the granulites are similar to these ratios in normal mid-ocean ridge basalts (MORBs). Thus, the parental magmas of the granulite protoliths were generated relatively recently from a source similar to that presently melting to yield normal MORBs. However, trace element modelling shows that although the parental melts were K-poor, they may have had higher La/Yb and lower K/Ba ratios than normal MORBs.

The GE peridotites have La/Yb ratios less than chondrites, and clinopyroxenes from these inclusions have $^{87}Sr/^{86}Sr$ and $^{143}Nd/^{144}Nd$ ratios similar to those of normal MORBs. These clinopyroxenes have Sm-Nd model ages relative to the bulk earth of 1.6 to 1.8 x $10^9$yr. The GE peridotites appear to be petrogenetically related to normal MORBs as potential source material, however, very low K contents complicate simple models.

The CT and CE peridotites, some of which contain amphibole or glass after amphibole (ACT, ACE inclusions), all have La/Yb ratios greater than chondrites, and have high concentrations of La, K, Rb, Ba, and Sr relative to the GE inclusions. These CT, CE, ACT, and ACE inclusions are similar to metasomatized peridotites from other inclusion localities. Isotopically, these inclusions are similar to modern ocean island basalts.

Isotopic ratios of the amphibole-pyroxenites and basalts overlap those of the ACE and ACT inclusions. The amphibole-pyroxenites have metamorphic textures and are interpreted to be crystal accumulates from an alkali basalt based on their chondrite-normalized REE patterns. The basalts have high La/Yb ratios and high incompatible element abundances relative to MORBs, and thus, are similar to other alkalic basalts. The basanites have lower $^{87}Sr/^{86}Sr$ and

higher Rb/Sr ratios than the tholeiites. Other trace element ratios show systematic trends which may be the consequence of two component mixing. One endmember has high La/Yb, Rb/Sr, and low $^{87}Sr/^{86}Sr$, K/Rb, Ba/Th, Sr/Th, La/Th, and Ba/La relative to the other endmember.

We infer that the metasomatism of the ACE and ACT inclusions is the consequence of the infiltration of a H-C-O-rich fluid and/or residual silicate melt which originated in the pyroxenites. Based on consideration of isotopic data, the metasomatism occurred recently, and is petrogenetically related to the basaltic volcanism on Nunivak Island.

The mantle beneath Nunivak Island is heterogeneous in terms of isotopic and trace element ratios. Two distinct terranes are present: a terrane petrogenetically related to normal MORBs and a second terrane which is isotopically similar to oceanic island basalts. The pyroxene granulites and the GE peridotites are samples of the former terrane; this terrane may have initially obtained its geochemical characteristics approximately $1.7 \times 10^9$ yr. ago and have been melted approximately $2 \times 10^8$ yr. ago. The ACT and ACE peridotites and the amphibole-pyroxenites are samples from the second terrane which may have diapirically intruded the MORB-related terrane.

II

Ultramafic breccia diatremes in the Four Corners region of the Colorado Plateau contain peridotite and eclogite inclusions of probable upper mantle origin. Eight spinel peridotites from the Green Knobs diatreme and two eclogites from the Garnet Ridge diatreme were analyzed for the rare earth elements (REE). Lherzolites and one eclogite are relatively light REE depleted compared to chondrites while harzburgites and one eclogite have V-shaped REE patterns compared to chondrites.

All the harzburgites, one lherzolite, and one eclogite have La/Sm ratios greater than chondrites; these rocks also contain primary hydrous phases. We attribute the relative enrichment of La to mantle metasomatism by a hydrous fluid. Differences between REE patterns of the Green Knobs peridotites and metasomatized peridotites from alkali basalts may be related to fluid composition and temperature.

Because the lherzolites are relatively light REE depleted, we conclude that the mantle as represented by these peridotites has oceanic affinities. These data may indicate that mantle with oceanic affinities is widespread beneath continents. The REE data are consistent with a simple model in which the eclogites and harzburgites represent altered basaltic dikes and residues, respectively, formed by partial melting of source rocks similar to the lherzolites.

Thesis supervisor: Frederick A. Frey, Professor of Geology and Geochemistry

ACKNOWLEDGEMENTS

My supervisor, Fred Frey, first drew my attention to the Nunivak suite, and made numerous critical comments which have led to major improvements in the manuscript. Special thanks to Don Francis who provided additional Nunivak inclusions and who was always willing to share his data and petrologic expertise on the Nunivak suite. Special thanks also to Stan Hart for providing access to the mass spectrometer and clean room facilities during times of especially heavy demand on this equipment. Doug Smith generously provided the well-documented Green Knobs inclusions. R. Hickey, M. K. Roden, and S. Roy taught me the various analytical techniques used to obtain the data described herein. S. Hart, N. Shimizu, B. J. Pegram, D. Francis, and R. Coish made constructive criticisms of various portions of the manuscript prior to the defense.

Finally, thanks to my wife, Mary, for her patience, and at times lack thereof, with my somewhat erratic working habits and behavior. Without Mary's drafting, this thesis would certainly have not been finished as quickly.

TABLE OF CONTENTS

# 1. INTRODUCTION

In this study we report on the geochemistry of the upper mantle as inferred from trace element abundances and Sr and Nd isotopic compositions of ultramafic inclusions and their host alkali basalts. There are several approaches used to study mantle geochemistry. The most common method is to obtain geochemical data on basalts formed by partial melting in the mantle. However, the relationship between basalt and mantle geochemistry is not always simple because of the number of physical processes (e.g., crystal fractionation, wallrock reaction) which may affect the geochemistry of basalts during their ascent to the surface. Nevertheless, these studies have provided very important trace element and isotopic constraints on the chemistry of the mantle, especially the oceanic mantle (e.g., Gast, 1968; Hart, 1971; White and Schilling, 1978). For example, these studies show that the source for normal mid-ocean ridge basalts (MORBs; White and Schilling, 1978) has suffered a previous melting event and has La/Yb ratios less than chondrites, $^{87}Sr/^{86}Sr = 0.7023 - 0.7032$, and $^{143}Nd/^{144}Nd = 0.5130 - 0.5133$. In contrast, the source for many oceanic island basalts may have La/Yb ratios greater than chondrites, $^{87}Sr/^{86}Sr = 0.7030 - 0.7045$, and $^{143}Nd/^{144}Nd = 0.5126 - 0.5131$ (e.g., O'Nions et al., 1977; White and Schilling, 1978; Clague and Frey, 1982).

The second method involves direct analysis of mantle material in the form of tectonically emplaced peridotite massifs. An important advantage of these studies is that mantle heterogeneity can be studied in situ, limited only by the size of the massif. However, many of these

massifs have suffered a low temperature metamorphism, or have reequilibrated during transport to the surface. Thus, much of the primary phase assemblage may be replaced by secondary minerals. In order to infer the chemistry of the mantle from these studies the chemical effects of the metamorphism must be subtracted. Reconnaissance trace element and isotopic studies (Frey, 1969; Loubet et al., 1975; Menzies and Murthy, 1978; Richard and Allegre, 1980) have shown that many of these alpine bodies have La/Yb ratios less than chondrites, and clinopyroxenes from these bodies have $^{87}Sr/^{86}Sr$ and $^{143}Nd/^{144}Nd$ ratios in the range of MORBs. Thus, many of these peridotite massifs are geochemically similar to the inferred source for MORBs (e.g., White and Schilling, 1978). Detailed studies of single massifs are only beginning (e.g., Polve and Allegre, 1980; Frey and Suen, ms; Zindler and Hart, in progress); these studies are expected to provide important constraints on small scale mantle heterogeneity.

The third method used to study the geochemistry of the upper mantle is by analysis of spinel- and garnet-bearing ultramafic inclusions from kimberlites and alkali basalts. The phases in these inclusions indicate that they equilibrated in the upper mantle (e.g., Ringwood, 1975). The diverse inclusions from kimberlites include garnet peridotites, eclogites, dunites and harzburgites (Gurney and Harte, 1980). The abundance of garnet peridotite (olivine = $Fo_{88-95}$) indicates that this rock type is the predominant rock type in the upper mantle sampled by kimberlites.

Inclusions in alkali basalts are also diverse, but most polycrystalline aggregates belong to one of two groups: the group I or

Cr-diopside series and the Group II or Al-augite series (Wilshire and Shervais, 1975; Frey and Prinz, 1978). Group I inclusions are predominantly lherzolites and harzburgites containing Cr-rich diopside and spinel. Olivine compositions are typically in the range $Fo_{88-92}$. These Group I inclusions are generally thought to be accidental samples of mantle wallrock based on textural, trace element, and isotopic evidence. The relatively high abundance of the Group I inclusions indicates that spinel peridotite is the dominant rock type in the mantle sampled by alkali basalts. Group II inclusions are modally diverse but pyroxene-rich rocks with aluminous augite and olivine (Fo content less than $Fo_{85}$) are most common. Trace element studies indicate that these inclusions originated as accumulates (e.g., Frey and Prinz, 1978; Irving, 1980); isotopic studies show that some suites of Group II inclusions may be petrogenetically related to the associated volcanism (e.g., Menzies and Murthy, 1980a). However, metamorphic textures in Group II inclusions generally preclude a cognate relationship with the host basalt.

An important recent result is the recognition of metasomatized inclusions. Compositions of the constituent anhydrous silicates in these inclusions indicate that the protoliths of the metasomatized inclusions were Group I peridotites. However, relative to other Group I inclusions, metasomatized inclusions have high concentrations of K, Rb, light rare earth elements (LREE), Ti, Ba, Sr, and other incompatible elements. Metasomatized inclusions commonly contain hydrous phases, and the fluid responsible for the precipitation of these hydrous phases is believed to be the metasomatizing agent (e.g., Frey and Prinz, 1978).

There is evidence (e.g. Boettcher and O'Neill, 1980; Menzies and Murthy, 1980b) which suggests that metasomatized mantle may be the source for many alkali basalts.

Two distinct projects form the basis of this thesis. The first project (Chapters 2-3) is a detailed study of a suite of inclusions from Nunivak Island, Alaska (Figure 2-1). Nunivak is a large basaltic island located 50 km off the west coast of Alaska and approximately 600 km north of the Aleutian Islands. Basanites on the island contain a diverse suite of inclusions; we studied representative samples of pyroxene granulites, pyroxenites, and lherzolites, plus representative samples of the host basalt. Some of the lherzolites contain amphibole and phlogopite, and we inferred that these inclusions were metasomatized. We obtained trace element and isotopic data on these samples in order to understand the petrogenesis and interrelationships of various rock types. The project had four specific objectives; (1) to document the geochemical heterogeneity of the mantle sample by the Nunivak basalts, (2) to use trace element modelling in an attempt to understand the petrogenesis of various rock types, (3) to document the geochemical characteristics of metasomatism at Nunivak, and attempt to determine the source of the metasomatizing agent, and (4) use isotopic data to determine what if any interrelationships exist between the various lithologies, including the host basalts.

The second project (Chapter 4), which has not been completed, was an attempt to map the geochemistry of the mantle by analyzing inclusions from several diatremes. In particular, a transect of the mantle from the central Basin and Range to the central Colorado Plateau is being

studied by analyzing inclusions from 3 localities: Black Rock Summit, Nevada (central Basin and Range), Vulcan's Throne, Arizona (western margin of the Colorado Plateau), and Green Knobs, New Mexico (central Colorado Plateau).

The Green Knobs suite was of interest by itself because detailed petrologic studies by Smith and Levy (1976) and Smith (1979) showed that the Group I inclusions are diverse and range from anhydrous lherzolites to hydrous lherzolites and harzburgites. These Green Knobs inclusions have a unique hydrous assemblage, amphibole, chlorite, antigorite, and titanoclinohumite, relative to most other inclusion suites where only amphibole and phlogopite occur. On textural and mineralogical grounds Smith (1979) concluded that the hydrous phases formed in the mantle prior to eruption. Thus, we wished to determine whether the hydrous phases from Green Knobs are associated with the high incompatible element concentrations typical for most phlogopite- and amphibole-bearing peridotites. Unexpectedly we found that the mantle as represented by the Green Knobs inclusions has oceanic affinities. The results for the Green Knobs inclusions are described in Chapter 4.

Although samples were collected from Black Rock Summit and Vulcan's Throne, no analytical data was gathered on these samples. Thus, we do not report on either locality here.

# 2. PETROGENESIS OF PYROXENE GRANULITE XENOLITHS, NUNIVAK ISLAND, ALASKA

## I. Introduction

Sr and Nd isotopic ratios, rare earth element (REE) concentrations, and other trace element concentrations have been determined for four representative pyroxene granulite xenoliths from Nunivak Island (166°W 60°N), Alaska. Nunivak Island (Figure 2-1) is a large, 75 km diameter, basaltic island located on the Bering Sea shelf 50 km west of the Alaskan coast and 600 km north of the Aleutian Islands. The granulite xenoliths comprise approximately 9% of an inclusion population of peridotites, pyroxenites, dunites, and harzburgites (Francis, 1976a) which occurs in Quaternary basanites. The volcanism on Nunivak Island is not related to the present subduction zone under the Aleutians, but is part of a Tertiary to Recent basalt province in western Alaska and nearby islands (Figure 2-1; Hoare et al., 1968).

The samples we studied were described by Francis (1976a) and span the range of compositions exhibited by the pyroxene granulites at Nunivak. These inclusions are called pyroxene granulites after Ito and Kennedy (1970); they contain the equilibrium assemblage: clinopyroxene + orthopyroxene + spinel + plagioclase or olivine. A noteworthy petrographic feature of the granulites is the presence of coronas of clinopyroxene + orthopyroxene + spinel which record the reaction of primary olivine with primary plagioclase. These metamorphic textures preclude a cognate relationship with the host basalts and indicate that these inclusions are xenoliths. Francis (1976a) concluded

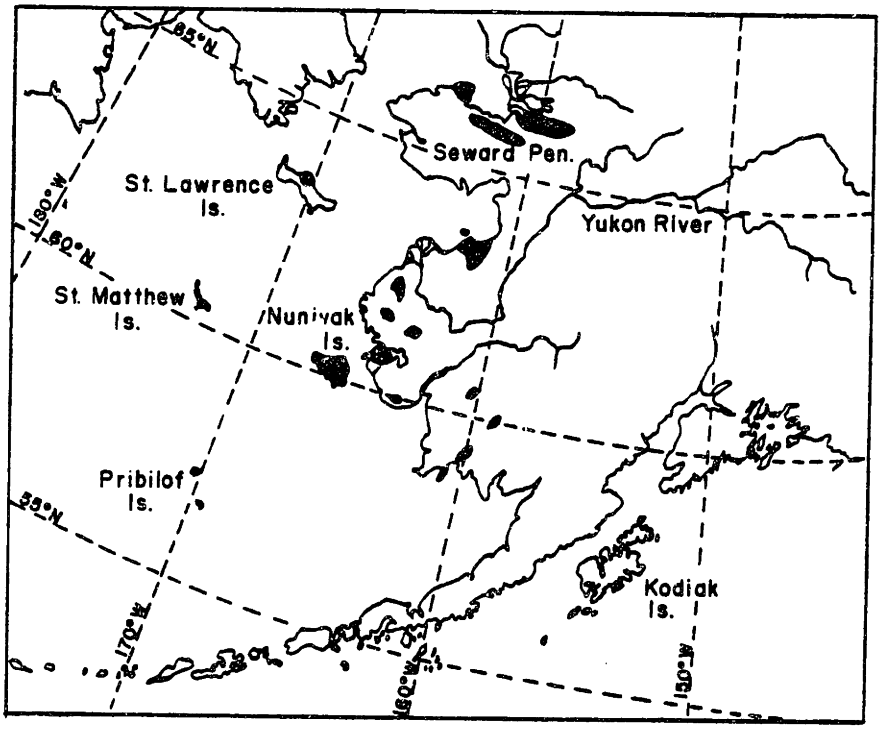
65°N
Seward Pen.
St. Lawrence
Is.
160°W
60°N
Yukon River
St. Matthew
Is.
Nunivak
Is.
Pribilof
Is.
55°N
Kodiak
Is.
170°W
160°W
150°W

Figure 2-1. Sketch map of Nunivak Island and surrounding areas. Shaded areas indicate outcrops of Late Tertiary to Recent basalts which are not associated with the Aleutian arc (after Francis, 1974).

that the granulites were originally troctolite cumulates; the original olivine and plagioclase reacted as a result of either a drop in temperature or an increase in pressure. The coronas obscure much of the igneous textures but they enable estimation of equilibration temperature, approximately 950°C, and pressure, approximately 9 kb (Francis, 1976a). These calculations indicate that the granulites are samples from near the base of the crust beneath Nunivak Island (Francis, 1976a).

Our objectives in studying these xenoliths were (1) to evaluate if the trace element abundances of the granulites are consistent with an origin as cumulates, and if so, (2) to infer the nature of the parental magma of the troctolites from the trace element and isotopic data, and (3) to provide geochemical constraints on the composition of the lithosphere beneath Nunivak Island. The composition of the lithosphere beneath Nunivak Island is of particular interest because in spite of the island's position on the Bering Sea Shelf adjacent to Alaska, both the low $^{87}Sr/^{86}Sr$ ratios, 0.7025 - 0.7033 (Mark, 1971; Menzies and Murthy, 1980a), of the basalts and the geochemistry of some of the peridotite inclusions (Roden et al., 1980) suggest that oceanic crust and mantle underlie the island.

## II. Sample Description

The following summary is taken from the detailed study of Francis (1976a). The granulites range from olivine-rich to plagioclase-rich rocks; the four samples studied here are inferred to have contained

increasing amounts of plagioclase in the sequence 12017, 12013, 12011, 12000 (Table 2-1). Many granulites possess a marked layering defined either by spinel concentrations or the oblate shape of coronas. The coronas have replaced much of the igneous mineralogy so that olivine and plagioclase are never in contact. A typical petrographic transect from olivine to plagioclase is: remnant olivine, orthopyroxene (corona), spinel-clinopyroxene symplectite (corona), remnant plagioclase. Minor amounts of primary, interstitial spinel and clinopyroxene also occur; the clinopyroxene commonly poikilitically encloses olivine or plagioclase. The present mode and the inferred primary mineralogy of the four granulites studied here are summarized in Table 2-1.

## III. Analytical Methods

The sample powders used were splits from the powders analyzed for major elements (Francis, 1976a). These powders were produced by grinding in a tungsten carbide ball mill. Sc, Cr, and Co were analyzed by instrumental neutron activation analysis (INAA) described by Frey et al. (1974; 1980). The precision of this technique can be estimated from 7 replicate analyses of mid-ocean ridge basalt standard A II 92-29-1 (Table 2-2) performed in the M.I.T. lab. Co contamination can result from the use of tungsten carbide grinding vessels (Thompson and Bankston, 1970). In the present case, Co concentration correlates with inferred, primary olivine abundance (Tables 2-1, 2-2). This correlation probably reflects the concentration of Co in olivine as the result

Table 2-1. Sample Description.[1]

| Sample | 12000 | 12011 | 12013 | 12017 |
|---|---|---|---|---|
| Present Mode: | | | | |
| Primary phases | | | | |
| olivine | 1.0 | 0.0 | 29.0 | 55.6 |
| plagioclase | 69.3 | 1.3 | 1.9 | 0.0 |
| clinopyroxene | 13.2 | 0.0 | 1.3 | 0.2 |
| spinel | 0.7 | 0.7 | 1.4 | 1.3 |
| Corona phases | 12.1 | 93.9 | 66.4 | 28.6 |
| Quench phases | 3.7 | 4.2 | 0.1 | 14.3 |
| Calculated Primary Mode[2] | | | | |
| olivine | 17.6 | 48.4 | 57.4 | 74.3 |
| plagioclase | 70.6 | 51.6 | 36.6 | 25.7 |
| clinopyroxene | 11.9 | 0.0 | 5.6 | 0.0 |
| spinel | 0.0 | 0.0 | 0.4 | 0.1 |

1. After Francis (1976a).

2. Calculated by assuming granulites are plagioclase + olivine cumulates with minor clinopyroxene + spinel.

Table 2-2. Trace element abundances (ppm).

| Sample | 12000 | 12000[1] | 12011 | 12013 | 12017 |
|---|---|---|---|---|---|
| K | 489 | | 89.7 | 111 | 60.3 |
| Sc | 20.5 | | 3.51 | 4.93 | 5.29 |
| Cr | 415 | | 1083 | 1460 | 1424 |
| Co | 29.0 | | 86.5 | 112 | 135 |
| Rb | 0.154 + 0.008[3] | | 0.097 ± 0.004[3] | | 0.050 ± 0.001[3] |
| Sr | 338 | | 170 | 136 | 57.5 |
| Cs | 0.0045 | | 0.0071 | | 0.0017 |
| Ba | 17.7 | | 6.38 | 5.10 | 5.49 |
| La | 0.91 | 0.94 | 0.22 | 0.18 | 0.10 |
| Ce | 2.6 | 2.5 | | | |
| Nd | 2.2 | | | 0.23[2] | |
| Sm | 0.66 | 0.56 | 0.059 | 0.060[2] | 0.032 |
| Eu | 0.56 | 0.54 | 0.13 | 0.10 | 0.055 |
| Tb | 0.15 | | 0.014 | 0.010 | 0.0088 |
| Yb | 0.47 | 0.41 | 0.082 | 0.060 | 0.057 |
| Lu | 0.071 | 0.065 | 0.013 | 0.012 | 0.011 |

1. INAA analysis.

2. Sm, Nd abundances measured by isotope dilution.

3. Mean of two analyses; ± indicates mean deviation from average.

Table 2-2. Continued.

| Sample | A II 92-29-1 ftnote 4 | A II 92-29-1 ftnote 5 | 10070[6] | BCR-1[7] | Ave. Num. basalt[8] |
|---|---|---|---|---|---|
| K | 1326 ±4 | | | | 12780 |
| Sc | 38.8 ±2.6 | | | | 21 |
| Cr | 246 ±20 | | | | 300 |
| Co | 58.1 ± 3.6 | | | | 52 |
| Rb | 1.20 ± 0.02 | | | | 25 |
| Sr | 131.7 ± 1.2 | | | | 698 |
| Cs | 0.028 | | | | |
| Ba | 5.20 ± 0.02 | | | | 334 |
| La | 4.00 ± 0.30 | 3.97 ± 0.34 | 0.267 ± 0.050 | 25.1 | 29 |
| Ce | 13.1 ± 0.8 | 13.7 ± 1.0 | 0.99 ± 0.18 | 54.1 | 60 |
| Nd | 12.1 ± 1.2 | 11.6 ± 0.6 | 0.99 ± 0.14 | 28.7 | 26 |
| Sm | 4.20 ± 0.24 | 4.05 ± 0.24 | 0.345 ± 0.024 | 6.63 | 5.7 |
| Eu | 1.47 ± 0.12 | 1.51 ± 0.02 | 0.146 ± 0.010 | 1.97 | 2.1 |
| Tb | 1.01 ± 0.18 | 0.99 ± 0.26 | 0.099 ± 0.012 | 1.03 | 0.86 |
| Yb | 3.95 ± 0.32 | 3.90 ± 0.32 | 0.455 ± 0.034 | 3.46 | 1.8 |
| Lu | 0.62 ± 0.04 | 0.60 ± 0.02 | 0.074 ± 0.006 | 0.54 | 0.27 |

Table 2-2. Footnotes continued.

4. Error quoted is 2 . Mean of 3 analyses (Roden) for K, Rb, Ba, Sr; mean of 7 analyses (4 by Roden, 3 by S. Roy and F. Frey) for Co, Cr, and Sc; mean of 5 RNAA analyses (Roden) for REE.

5. Error quoted is 2 . Mean of 5 INAA analyses (2 by Roden, 3 by S. Roy and F. Frey).

6. Error is 2 . Mean of 4 RNAA analyses from Chapter 3.

7. Average of isotope dilution analyses (except for Tb) from the literature (F.A. Frey, written communication, 1981). Tb value is average of INAA analyses from literature (F.A. Frey, written communication, 1981).

8. Average Nunivak basalt from Chapter 3.

of crystal-melt equilibria (e.g., Irving, 1978). Thus, we observe no anomalous behavior of Co which can be attributed to contamination from the grinding vessel. Nevertheless, we sound this cautionary note in interpreting the Co data; none of our interpretations are critically dependent on the Co data.

The rare earth elements (REE) were analyzed by radiochemical neutron activation analysis (RNAA) as described by Hickey and Frey (1982). This technique involves group separation of the REE by ion exchange following irradiation. Sc and some $Fe^{3+}$ are removed by a solvent extraction step using tri-n-butyl-phosphate. Chemical yields are estimated through the use of $^{144}Ce$ and $^{169}Yb$ tracers added during dissolution. U.S. Geological Survey standard BCR-1 was used as the primary standard, thus the REE data are reported relative to the concentrations for BCR-1 shown in Table 2-2. These values are averages of isotope dilution analyses of BCR-1 reported in the literature (F.A. Frey, written communication, 1981). The precision and accuracy of the RNAA method is comparable to that of the INAA method as indicated by a comparison of replicate analyses of A II 92-29-1 by both methods. Also, an INAA analysis of granulite 12000 is included in Table 2-2 for comparison with the RNAA analysis. The granulite analyses are less precise than the analyses of A II 92-29-1 because the granulites have lower REE concentrations than the basalt standard; the precision for the granulite analyses can be estimated from the quadruplicate analyses of Nunivak peridotite 10070 (Table 2-2).

K, Rb, Sr, Ba, and Cs were analyzed by isotope dilution according to the methods described in Hart and Brooks (1977). Based on triplicate

analyses of K, Rb, Sr, and Ba in A II 92-29-1, precision of individual analyses is less than 1% for K, Sr, and Ba, and less than 2% for Rb, all at the 95% confidence level. However, because of the low concentrations of Rb in the granulites, the precision of the granulite Rb analyses is approximately ± 5% based on duplicate analyses of Rb in 3 granulites (Table 2-2). The lower precision of these Rb analyses relative to the Rb analyses of A II 92-29-1 is probably the result of either (1) "error magnification": the increased sensitivity of the calculated concentration to the measured isotopic ratio at very low natural Rb/spike Rb ratios, or (2) variation in the blank. Five blanks measured during the course of this study show ranges of: K, 73 to 13 ngm; Rb, 0.09 to 0.02 ngm; Sr, 1.9 to 0.3 ngm; Ba, 2.9 to 2.8 ngm; and Cs, approximately 0.6 pgm. This variation is significant, although most of the high values result from a single blank that may have been catastrophically contaminated. Nominal blank corrections of -20 ngm K, -0.05 ngm Rb, -2.8 ngm Ba, -1.0 ngm Sr, and -0.6 pgm Cs have been applied to all samples where the blank contributes more than 0.5% to the measured concentration. The blank contribution to the granulite analyses does not exceed 1.3% in any case.

Isotopic ratios were measured on a nine-inch mass spectrometer at M.I.T. The methods for Sr and Nd are after Hart and Brooks (1977) and Richard et al. (1976) as described in Zindler et al. (1979). The ratios in Table 2-3 are normalized to $^{86}Sr/^{88}Sr = 0.1194$ and $^{146}Nd/^{144}Nd = 0.7219$, and are reported relative to Eimer and Amend standard $^{87}Sr/^{86}Sr = 0.70800$ and BCR-1 $^{143}Nd/^{144}Nd = 0.51264$. The quoted errors are in reference to the 95% confidence level based on within-run statistics.

Table 2-3. Isotopic ratios of Nunivak granulites.

| | $^{87}Rb/^{86}Sr$[1] | $^{147}Sm/^{144}Nd$[1] | $^{87}Sr/^{86}Sr$ | $^{143}Nd/^{144}Nd$ | |
|---|---|---|---|---|---|
| 12000 | $1.32 \times 10^{-3}$ | 0.205[2] | 0.70242<br>6 ± 5 | 0.513138<br>± 25 | |
| | | | | 0.513085<br>± 35 | 0.51311 |
| 12011 | $1.65 \times 10^{-3}$ | | 0.70248<br>± 4 | | |
| 12013 | $\leq 3.5 \times 10^{-3}$[3] | 0.156[2] | 0.70248<br>± 4 | 0.513045<br>± 38 | |
| 12017 | $2.51 \times 10^{-3}$ | | 0.70255<br>± 4 | | |

1. Atomic ratios

2. Calculated from Sm/Nd ratios measured by isotope dilution.

3. Based on nonreproducible Rb analyses.

## IV. Results

In general, the granulites have low incompatible and high compatible element contents. In the present case, by "incompatible" we refer to those elements (K, Rb, Ba, RE except Eu) which have crystal/liquid partition coefficients less than 1 (Hart and Allegre, 1980) in a silicate melt fractionating plagioclase, olivine, and minor amounts of spinel and clinopyroxene. Compatible elements (Cr, Sc, Co, Sr, Eu) are just those elements which have crystal/liquid partition coefficients greater than 1.

The incompatible and compatible elements vary in a consistent fashion relative to the calculated primary mode (Figure 2-2). For example, Sr is concentrated in the plagioclase-rich granulites while Co and Cr are concentrated in the olivine-rich granulites (Figure 2-2). Samples 12011, 12013, and 12017 have similar trace element characteristics and relative to typical basalts (compare trace element data of A II 92-29-1 and average Nunivak basalt, Table 2-2) these granulites have very low K, Rb, Sc, and REE contents, similar Ba and Sr contents (to A II 92-29-1 only), and high Cr and Co contents. Chondrite-normalized (Figure 2-3) REE curves for these granulites have large, positive Eu anomalies and are characterized by La/Sm ratios greater than chondrites. Sample 12000 differs from the other three granulites by having significantly higher incompatible element and Sc concentrations, lower Cr and Co concentrations, and a La/Sm ratio less than chondrites (Table 2-2; Figure 2-3).

The measured Sr and Nd isotopic ratios (Table 2-3) lie within the range of present day MORBs; note in particular that the $^{87}Sr/^{86}Sr$

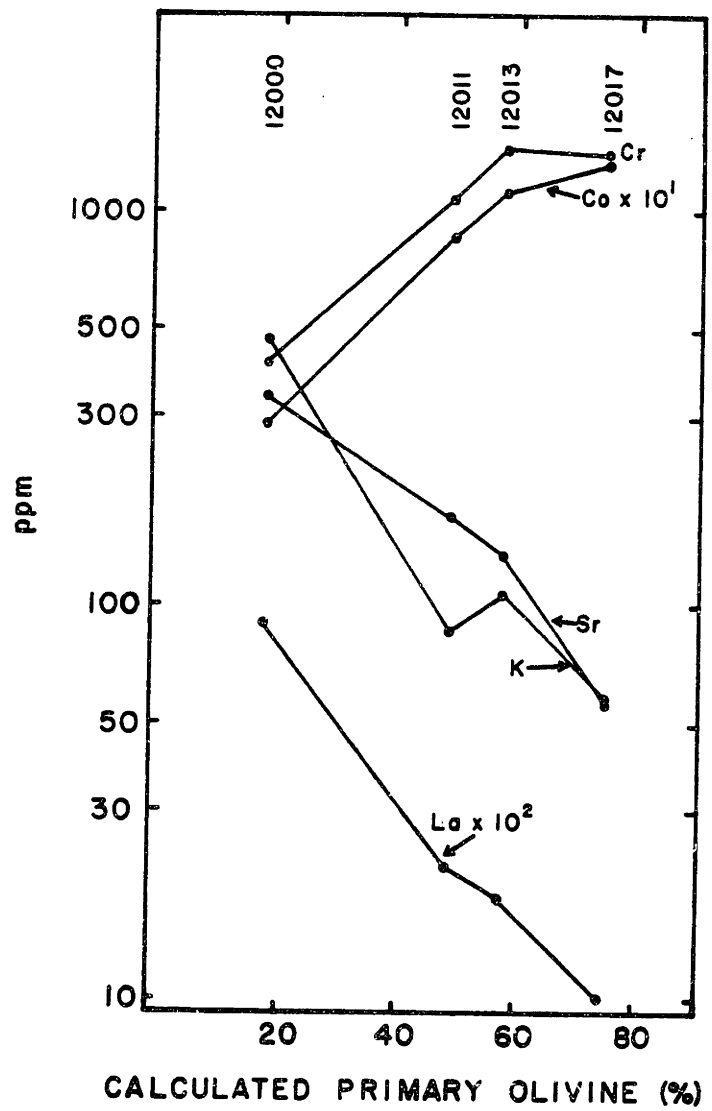
12000
12011
12013
12017
Cr
Co x 10¹
Sr
K
La x 10²
1000
500
300
100
50
30
10
ppm
20
40
60
80
CALCULATED PRIMARY OLIVINE (%)

Figure 2-2. Plot of trace element concentrations versus calculated primary olivine (Table 2-1) for the Nunivak granulites.

ratios of the granulites are lower than those of modern basalts from oceanic islands (Figure 2-4). The range of the $^{87}Sr/^{86}Sr$ ratios for the granulites is only slightly larger than analytical error.

## V. Discussion

### (A) Confirmation of the cumulate hypothesis

We interpret the systematic variation of trace element concentrations with calculated primary mineralogy to confirm the hypothesis of Francis (1976a) that the granulites formed from cumulate protoliths. The trace element characteristics of a cumulate are defined by at least 3 parameters: crystal/liquid partition coefficients, composition of the liquid, and the amount of trapped melt. In cumulates with very small amounts of trapped melt, trace element concentrations will be controlled by the first two parameters mentioned above. As a result, in such cumulates trace element concentrations are positively correlated with the modal proportion of their principle host phase. Thus, plagioclase-rich cumulates will have La/Sm ratios greater than chondrites, a large positive Eu anomaly (assuming $f_{O_2} \sim$ QFM), and high Sr concentrations (see for example Table 2-4, or Arth, 1976). Olivine-rich cumulates will be characterized by low REE concentrations although a positive Eu anomaly will occur if any plagioclase is present, high Co contents, and high Cr contents if as is common, chromite precipitation accompanied olivine precipitation (see for example Table 2-4 or Arth, 1976).

The Nunivak granulites are characterized by low incompatible

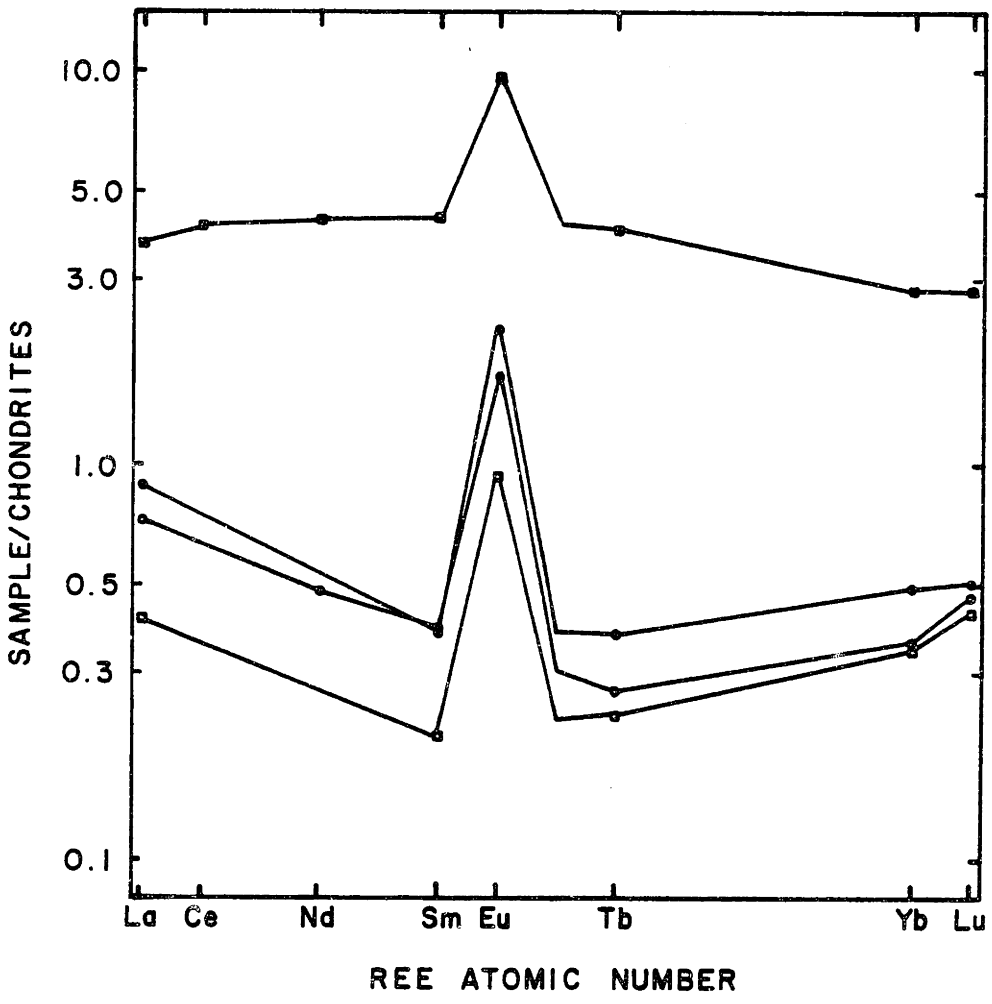
10.0
5.0
3.0
1.0
0.5
0.3
0.1
SAMPLE/CHONDRITES
La
Ce
Nd
Sm
Eu
Tb
Yb
Lu
REE ATOMIC NUMBER

Figure 2-3. Chondrite-normalized REE patterns of Nunivak granulites 12000 (■), 12011 (●), 12013 (○) and 12017 (□). Chondrite values from Evensen et al. (Table 3, "CI Average", 1978).

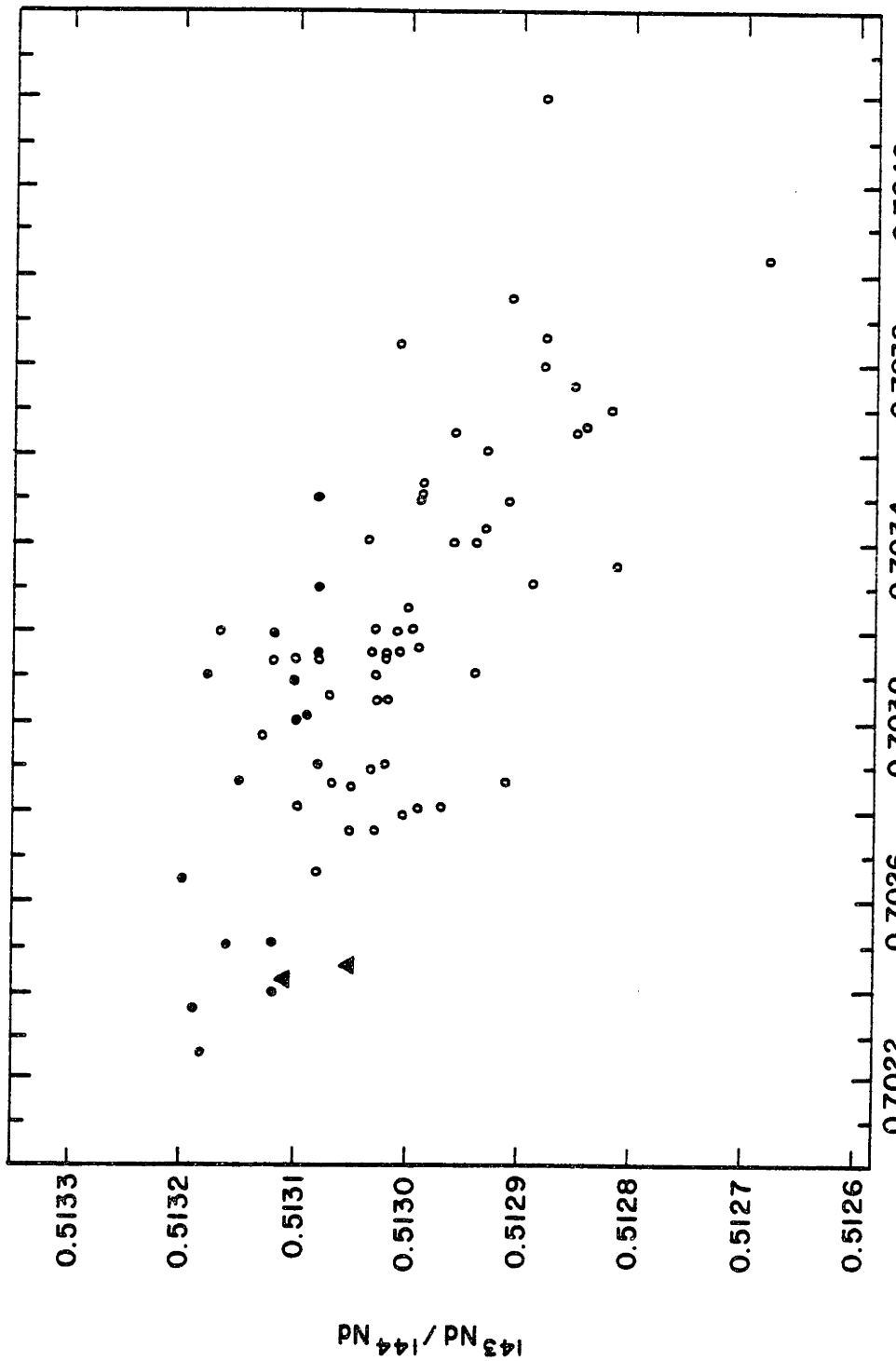
0.5133
0.5132
0.5131
0.5130
0.5129
0.5128
0.5127
0.5126
$^{143}Nd/^{144}Nd$
0.7022
0.7026
0.7030
0.7034
0.7038
0.7042
$^{87}Sr/^{86}Sr$

Figure 2-4. $^{87}Sr/^{86}Sr$ and $^{143}Nd/^{144}Nd$ ratios of Nunivak granulites (▲) 12000 and 12013 compared to these ratios in MORBs (●) and basalts from oceanic islands (○). Data from DePaolo and Wasserburg (1976a, 1976b); O'Nions et al. (1977); Richard et al. (1976); Carlson et al. (1978); Zindler et al. (1978); White and Hofmann (197 ).

element abundances, and large positive Eu anomalies (Figure 2-3). Sr correlates with the amount of calculated primary plagioclase (Figure 2-2) and Co and Cr correlate with the amount of calculated primary olivine (Figure 2-2). These observations are consistent with the hypothesis of Francis (1976a) that the protoliths of the granulites were troctolite cumulates. No other simple model for the origin of the granulites can explain the low incompatible element abundances, the bulk compositions, textures consistent with a cumulate origin, the correlation of trace element abundances with modes, and the large positive Eu anomalies.

Granulite 12000 has significantly higher REE, K, Sr, Sc, and Ba concentrations than the other granulites (Table 2-2); this sample also contains poikilitic clinopyroxene enclosing subhedral plagioclase, and the composition of the calculated primary olivine is significantly more Fe-rich, $Fo_{72}$, than that, $Fo_{78-82}$, of the calculated primary olivine of the other three granulites (Francis, 1976a). Either the presence of trapped melt as suggested by the poikilitic clinopyroxene or crystallization from a more differentiated liquid than the other granulites probably accounts for the geochemistry of 12000. The similarity between the composition of the calculated primary olivine, $Fo_{72.4}$, and the composition of relic olivine, $Fo_{71.7}$, in 12000 indicates that if trapped melt is present, it did not significantly alter the bulk rock $Fe^{2+}/Mg$ ratio.

Our reasons for the use of "cumulate" must be clarified in view of the controversy concerning the use of this term with respect to inclusions in basalts (e.g., Wilshire et al., 1980). "Cumulate" implies

separation of crystals from liquid under the influence of gravity in a floored magma chamber. Many Group II inclusions are geochemically indistinguishable from cumulate rocks (e.g., Frey and Prinz, 1978), although these inclusions are believed to be derived from dike-like bodies in the upper mantle (Wilshire et al., 1980). This habit precludes an origin by gravitational separation, and Frey (1980) uses "accumulate" to avoid the connotation of gravity settling with regard to pyroxenites from Hawaii. We retain "cumulate" in the case of the Nunivak granulites primarily because these inclusions are layered in hand specimen (Francis, 1976a). We also note that the granulites are geochemically distinct from typical Group II pyroxenites (e.g., Frey and Prinz, 1978) which have higher REE concentrations and lack positive Eu anomalies. There is no evidence to the authors' knowledge to indicate that the granulites form dikes in the upper mantle or lower crust.

(B) Isotopic constraints on the parental magma

The isotopic ratios (Table 2-3) of the granulites provide important constraints on the nature of the parental magma both in terms of the isotopic characteristics of the magma, and on the age of crystallization. In order to infer the isotopic characteristics of the parental magma, we assume that the granulites have behaved isochemically since crystallization. This assumption is consistent with the static, fluid-absent metamorphism caused by isobaric cooling and/or crustal thickening envisioned by Francis (1976a), and with the trace element data which require an origin as plagioclase- and olivine-rich cumulates.

On a plot of $^{143}Nd/^{144}Nd$ ratio versus $^{147}Sm/^{144}Nd$ ratio (Figure 2-5) the data points for 12000 and 12013 define a line whose slope specifies an age of $2.1 \times 10^8$ yr. ($\lambda = 6.54 \times 10^{-12} yr^{-1}$). We note that this age is poorly constrained because there are only two data points; for example, the data are marginally consistent with a horizontal line (t = 0) or with a line whose slope specifies an age of $3.7 \times 10^8$ yr. (Figure 2-5). Because we assume closed system evolution as indicated above, we interpret this age, approximately $2 \times 10^8$ yr., to be the age of crystallization from the parent magma.

The evolution of $^{143}Nd/^{144}Nd$ ratios in the granulites relative to the bulk earth and "most depleted MORB source" is consistent with the age derived from the isochron. The growth curve for 12013 which has the smallest average slope on a neodymium evolution diagram (Figure 2-6) intersects the growth curve for the most depleted MORB source at approximately $5 \pm 0.6 \times 10^8$ yr. ago. This age is an upper limit to the age of crystallization because at greater ages the growth curve for 12013 lies in a field where no known terrestial samples occur. We note further that because cumulates must be in isotopic equilibrium with their parental magma, the observation that the growth curves for both 12000 and 12013 have $^{143}Nd/^{144}Nd$ ratios greater than the bulk earth growth curve for the last $5 \times 10^8$ yr., indicates that the source for the parental magma must have had a history of relative LREE depletion relative to the bulk earth.

The $^{87}Sr/^{86}Sr$ ratios of 12000 and 12013 projected back through time are analytically indistinguishable over the past $10^9$ yr. (Figure 2-7) and thus are consistent with the inferred age relationship

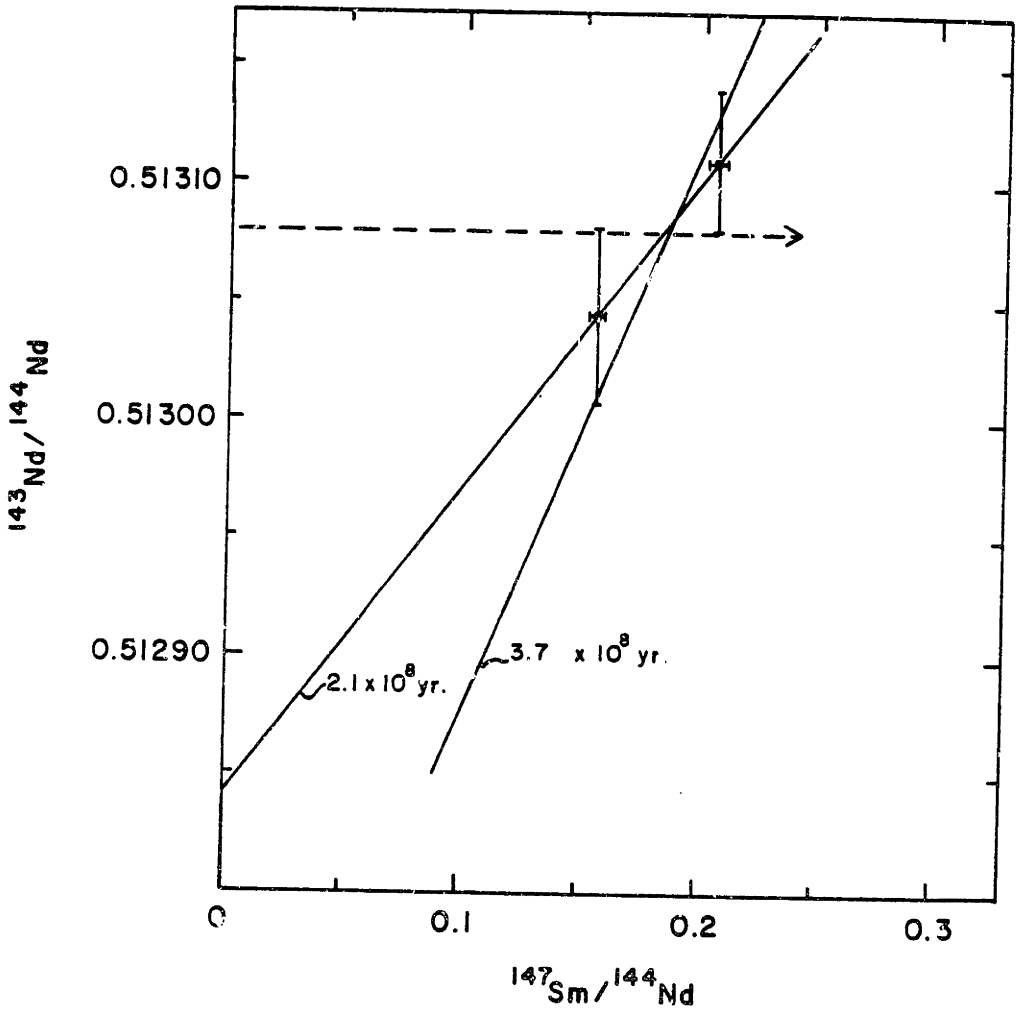
0.51310
0.51300
0.51290
$^{143}Nd/^{144}Nd$
2.1 x 10^8 yr.
3.7 x 10^8 yr.
0
0.1
0.2
0.3
$^{147}Sm/^{144}Nd$

Figure 2-5. $^{143}Nd/^{144}Nd$ versus $^{147}Sm/^{144}Nd$ (Table 2-3) for granulites 12000 and 12013. The line defined by the two points corresponds to an age of $2.1 \times 10^8$ yr. Note that the data are marginally consistent with the other two lines in the figure which specify ages of 0 (dashed line) and $3.7 \times 10^8$ yr.

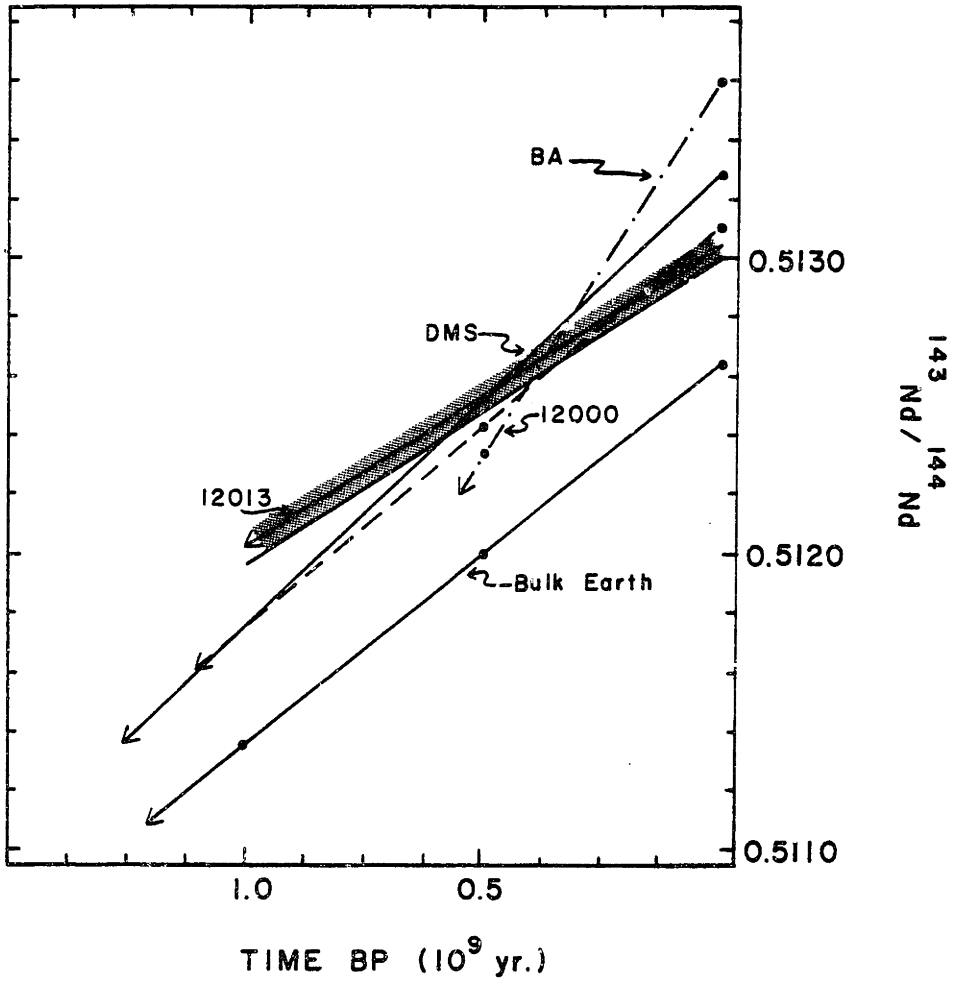
BA
DMS
12000
12013
Bulk Earth
0.5130
0.5120
0.5110
1.0
0.5
TIME BP (10⁹ yr.)
143Nd/144Nd

Figure 2-6. $^{143}Nd/^{144}Nd$ evolution diagram. Curves labelled 12000 and 12013 are for Nunivak granulites. Curve labelled "BA" is for a sample from the Baldissero orogenic lherzolite (Richard and Allegre, 1980); this sample is the most radiogenic modern basalt or peridotite measured to date. Bulk earth curve was calculated by assuming that bulk earth $^{143}Nd/^{144}Nd = 0.51264$ and $^{147}Sm/^{144}Nd = 0.1967$ (Jacobsen and Wasserburg 1980; Wasserburg et al., 1981). The curve labelled "DMS" is an estimate of the evolution of the most radiogenic MORB source based on a first order transport model after Zindler et al. (1981) in which $^{143}Nd/^{144}Nd)_o = 0.5133$, $^{143}Nd/^{144}Nd)_{4.6} = 0.50663$, $K = -4.5 \times 10^{-11} yr^{-1}$, and the age of the earth is assumed to be $4.6 \times 10^9$ yr. The shaded region indicates the uncertainty in the growth curve of 12013 as calculated from the uncertainty in the $^{143}Nd/^{144}Nd$ ratio of 12013 (Table 2-3) and assuming 1% uncertainties in the abundances of Sm and Nd.

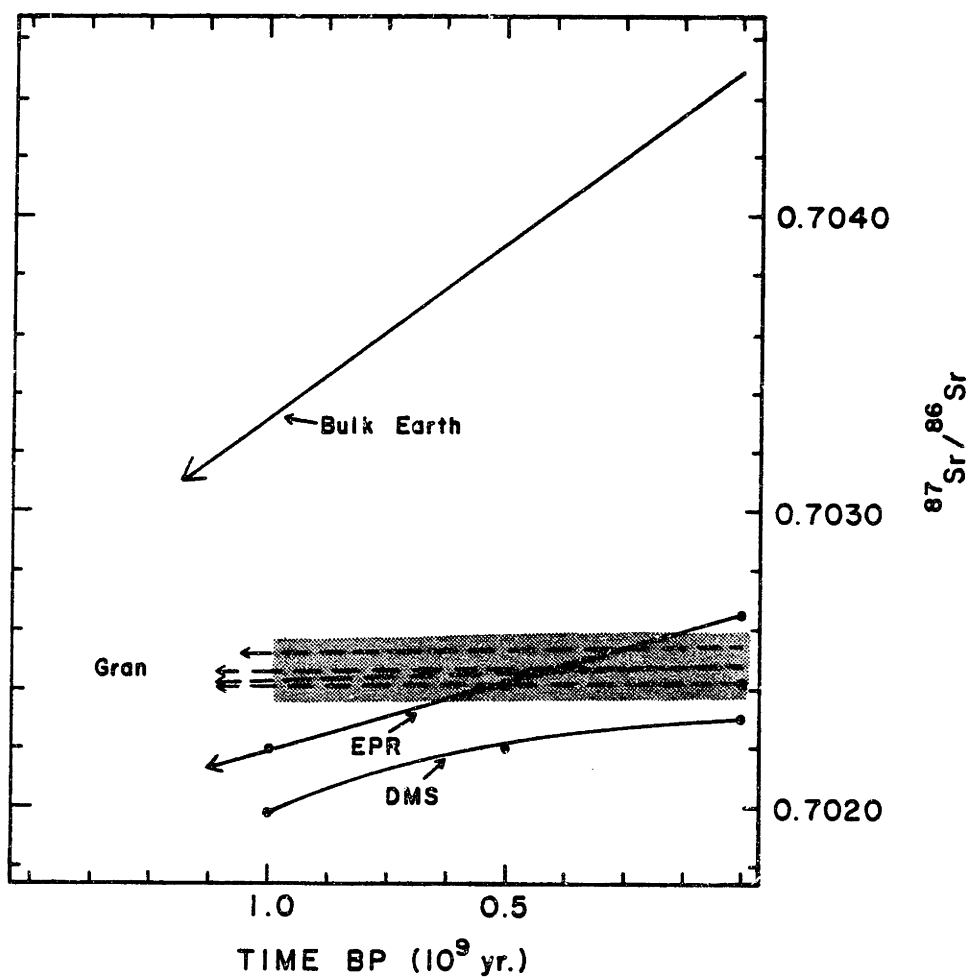
0.7040
0.7030
0.7020
$^{87}Sr/^{86}Sr$
Bulk Earth
Gran
EPR
DMS
1.0
0.5
TIME BP ($10^9$ yr.)

Figure 2-7. $^{87}Sr/^{86}Sr$ evolution diagram for Nunivak granulites ("Gran"). Bulk earth line is constrained by $^{87}Sr/^{86}Sr = 0.7045$ (DePaolo and Wasserburg, 1976b) and $^{87}Sr/^{86}Sr)_{4.6} = 0.699$. Curve labelled "EPR" is based on average values for $^{87}Sr/^{86}Sr$ and Rb/Sr ratios for East Pacific Rise basalts (Brooks et al., 1976). The curve labelled "DMS" is an estimate of the evolution of the least radiogenic MORB source based on a first order rate equation after Zindler et al. (1981) where $^{87}Sr/^{86}Sr)_o = 0.7023$, $^{87}Sr/^{86}Sr)_{4.6} = 0.699$ $K = 2.5 \times 10^{-10} yr.^{-1}$, and the age of the earth is assumed to be $4.6 \times 10^9 yr$. The shaded region reflects the uncertainties in the present-day $^{87}Sr/^{86}Sr$ ratios of the granulites (Table 2-3).

between these two samples. Because of the very low $^{87}Rb/^{86}Sr$ ratios (Table 2-3) of the granulites, the $^{87}Sr/^{86}Sr$ ratios are presently increasing at a rate of less than 6 parts in 70,000 per $10^9$ yr. (Figure 2-7). Hence, the measured $^{87}Sr/^{86}Sr$ ratios provide an accurate estimate of the initial $^{87}Sr/^{86}Sr$ ratios of the parental magma or magmas. This narrow range, 0.70236-0.70259 (Figure 2-7), lies within the range of present day MORBs. For the last $10^9$ years the growth curves for the granulites lie within the region occupied by sources depleted in $^{87}Sr$ relative to the bulk earth (Figure 2-7); this observation is consistent with the inference from the neodymium isotopic data that the cumulate protolith for the granulites crystallized from a magma derived by partial melting of a source which had a long history of depletion in incompatible elements.

When projected back through time, the strontium and neodymium isotopic data indicate that the protolith for the granulites crystallized from a magma derived from a source similar to the source of young MORBs (Figure 2-8). Based on a first order transport model (Zindler et al., 1981) which assumes continuous differentiation of mantle reservoirs since the accretion of the earth, over the past $6 \times 10^8$ yr. the most depleted oceanic island source lies at lower $^{143}Nd/^{144}Nd$ and higher $^{87}Sr/^{86}Sr$ ratios than the growth curves for the Nunivak granulites (Figure 2-8). Thus, assuming that the protoliths for the granulites precipitated in equilibrium from a melt within the last $6 \times 10^8$ yrs as suggested above, it is unlikely that the parent magma was a typical oceanic island basalt, or for that matter a continental basalt (e.g., Carlson et al., 1981). Possible parent magmas with appropriate

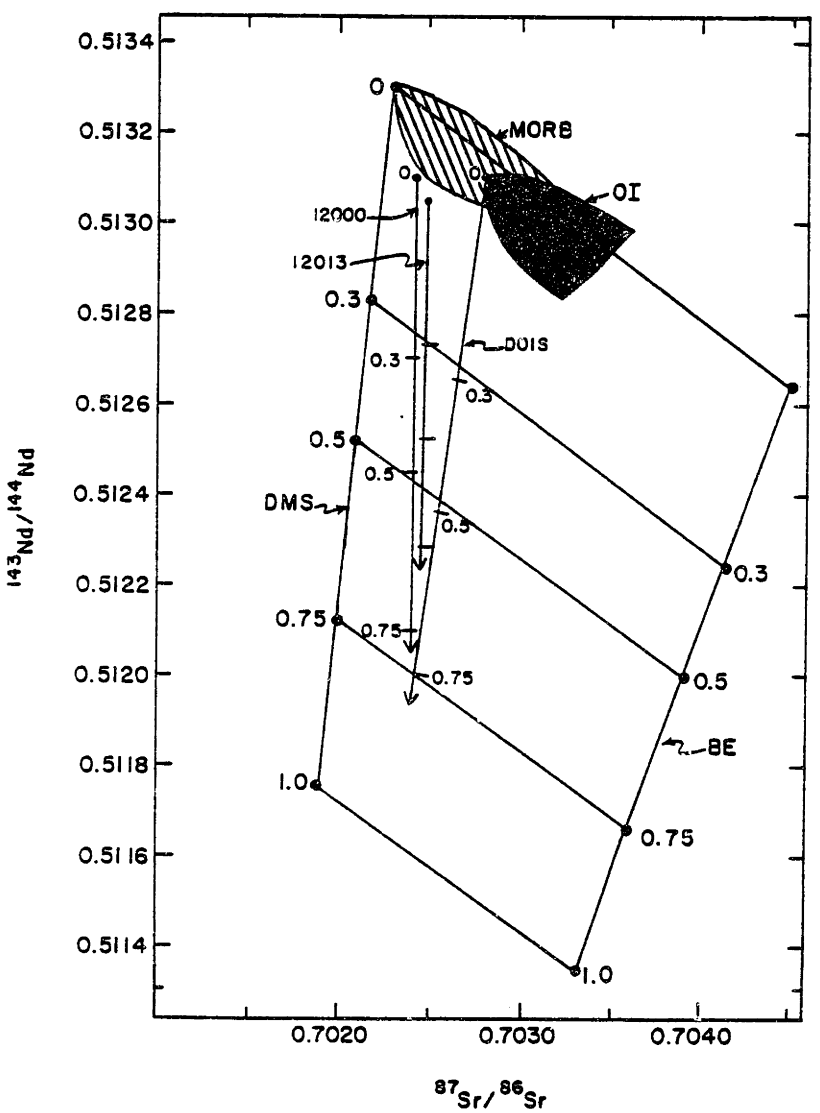
0.5134
0.5132
0.5130
0.5128
0.5126
0.5124
0.5122
0.5120
0.5118
0.5116
0.5114
$^{143}Nd/^{144}Nd$
0.7020
0.7030
0.7040
$^{87}Sr/^{86}Sr$
MORB
OI
DUPAL
BE
DMS
12000
12013
0
0.3
0.5
0.75
1.0

Figure 2-8. The mantle array compared to the growth curve of granulites 12000 and 12013 in time-$^{143}Nd/^{144}Nd$-$^{87}Sr/^{86}Sr$ space projected onto the $^{143}Nd/^{144}Nd$-$^{87}Sr/^{86}Sr$ plane. For simplicity, only the bulk earth (BE), most depleted MORB source (DMS), and most depleted oceanic island source (DOIS) were projected back in time. The MORB and oceanic island (OI) fields are from Figure 2-4. The values for the DMS and BE curves are from Figures 2-6 and 2-7; the DOIS curve was calculated using present day $^{87}Sr/^{87}Sr$ and $^{143}Nd/^{144}Nd$ ratios estimated from Figure 2-4 and a first order transport model (Zindler et al., 1981). The "mantle array plane" is contoured in time, $10^9$yr.; tic marks and numbers along the growth curves of 12000, 12013, and DOIS, also denote time in $10^9$yr. The limits of the plane as depicted are defined by t = 0, t = 1 x $10^9$yr. B.P., and by the bulk earth and DMS values from Figures 2-6 and 2-7.

isotopic characteristics besides MORBs include some back-arc basin basalts (e.g., Hawkesworth et al., 1977) and some island arc tholeiites (e.g. DePaolo and Johnson, 1979). In evolutionary models for the earth which are based on more recent and more rapid differentiation of mantle reservoirs than the continuous differentiation model, the difference in average slopes of the granulite growth curves and the growth curve for the most depleted ocean island source will be increased. Thus, the above conclusions will be strengthened.

(C) Trace element constraints on the parental magma

Based on the isotopic data of the granulites and assuming closed system evolution since the crystallization of their cumulate protoliths, we infer that the parental magma for these cumulates was similar to present-day MORBs. This inference can be tested for consistency with the trace element data by: (1) comparing the trace element abundances in the granulites to plagioclase-olivine cumulates from ophiolites and the ocean floor, and (2) inferring the trace element abundances in the parental magmas from trace element modelling.

(1) Comparisons with cumulates from ophiolites

Although cumulate gabbroic rocks are common in many ophiolites, clinopyroxene commonly appears as a cumulate phase before plagioclase (e.g., Cameron et al., 1980) and most cumulate gabbros from ophiolites analyzed for the REE have convex upward chondrite-normalized REE patterns with La/Yb ratios less than chondrites (Figure 2-9). This relative LREE depletion of the gabbros reflects the important role of

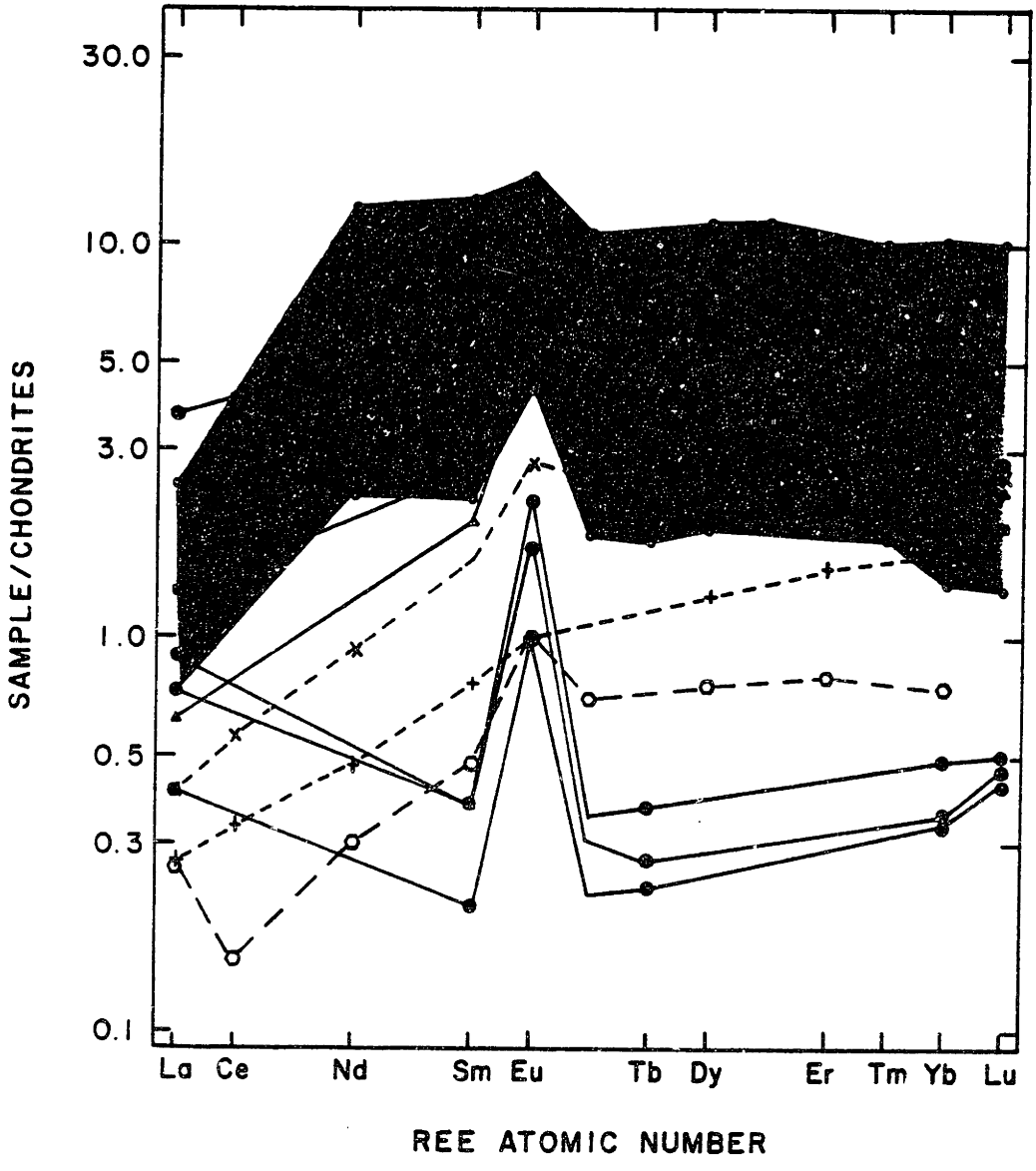
30.0
10.0
5.0
3.0
1.0
0.5
0.3
0.1
SAMPLE/CHONDRITES
La
Ce
Nd
Sm
Eu
Tb
Dy
Er
Tm
Yb
Lu
REE ATOMIC NUMBER

Figure 2-9. Chondrite-normalized REE patterns of Nunivak granulites (●) compared to individual ophiolite gabbros from the Troodos (dashed lines; Kay and Senechal, 1976) and the Bay of Islands (E,L; Suen et al., 1979) complexes. Also shown as the shaded region is the range for gabbros from the Samail ophiolite (Pallister and Knight, 1981).

clinopyroxene as a cumulate phase (e.g., Suen et al., 1979) and probably, crystallization from a parental magma with a La/Yb ratio less than chondrites. These clinopyroxene-rich ophiolitic gabbros contrast strongly with the Nunivak granulites both with respect to La/Sm ratios (Figure 2-9) and with respect to the inferred clinopyroxene-poor cumulate mineralogy of the Nunivak granulites. However, some ophiolites contain troctolite cumulates. These ophiolites are the Type D ophiolites of Church and Riccio (1977) such as the Pindos and parts of the Bay of Islands complexes. Serri (1980) also described "Mg-gabbros" from northern Appennine ophiolites which are dominantly olivine-plagioclase cumulates with poikilitic clinopyroxene, and Jacques and Chappell (1980) described a troctolite from the Papuan Ultramafic belt. To the writers' knowledge REE data do not exist for these occurrences, but the Papuan troctolite has Cr, Sr, K, and Sc contents similar to those of the Nunivak granulites. We conclude that, although troctolites are uncommon in many ophiolites, rocks analogous to the inferred protoliths of the granulites occur in some ophiolites. Unfortunately, in the absence of trace element data for these ophiolite occurrences, no direct comparison to the Nunivak xenoliths can be made.

(2) Comparison with cumulates from the ocean floor

In that the inferred crystallization sequence for ocean-floor basalts is olivine (± spinel), olivine (± spinel) + plagioclase, olivine (± spinel) + plagioclase + clinopyroxene (Basaltic Volcanism Study Project, 1981), troctolite cumulates should be fairly common on the ocean floor. Surprisingly, most cumulate gabbros described from the

ocean floor are clinopyroxene-bearing and have convex-upward chondrite-normalized REE patterns with La/Yb ratios less than chondrites (Figure 2-10). Tiezzi and Scott (1980), however, described cumulate gabbros which in spite of containing significant amounts of clinopyroxene have flat REE patterns and positive Eu anomalies relative to chondrites, i.e., similar to the REE patterns of 12011, 12013, and 12017 but offset to higher REE concentrations. Shih (1972) described what is perhaps the best analogue for the Nunivak rocks: a troctolite dredged from 24°N near the Mid-Atlantic Ridge. This troctolite is similar in major element composition, REE abundances (Figure 2-10), Sr, and Ba concentrations to samples 12011, 12013, and 12017. Clinopyroxene-bearing gabbros with La/Yb ratios less than chondrites (Figure 2-10) were associated with this troctolite (Shih, 1972). To summarize, rocks similar in composition and mineralogy to the Nunivak granulites occur in ophiolites and in present-day ocean crust, but they appear to be subordinate to clinopyroxene-bearing gabbros with La/Yb ratios less than chondrites.

(3) Inferred trace element abundances in parental magmas

The second method by which to test the proposed origin of the granulites for consistency with the trace element data is to infer the parental magma composition from the trace element abundances in the granulites. We base our model on the assumption of equilibrium between melt and cumulate according to $D^i = C_s^i/C_l^i$ where $C_s^i$ is the concentration of element i in the solid, $C_l^i$ is the concentration of element i in the liquid and $D^i = D^{i'}(1-\alpha) + \alpha$ where $\alpha$ is the weight fraction of trapped

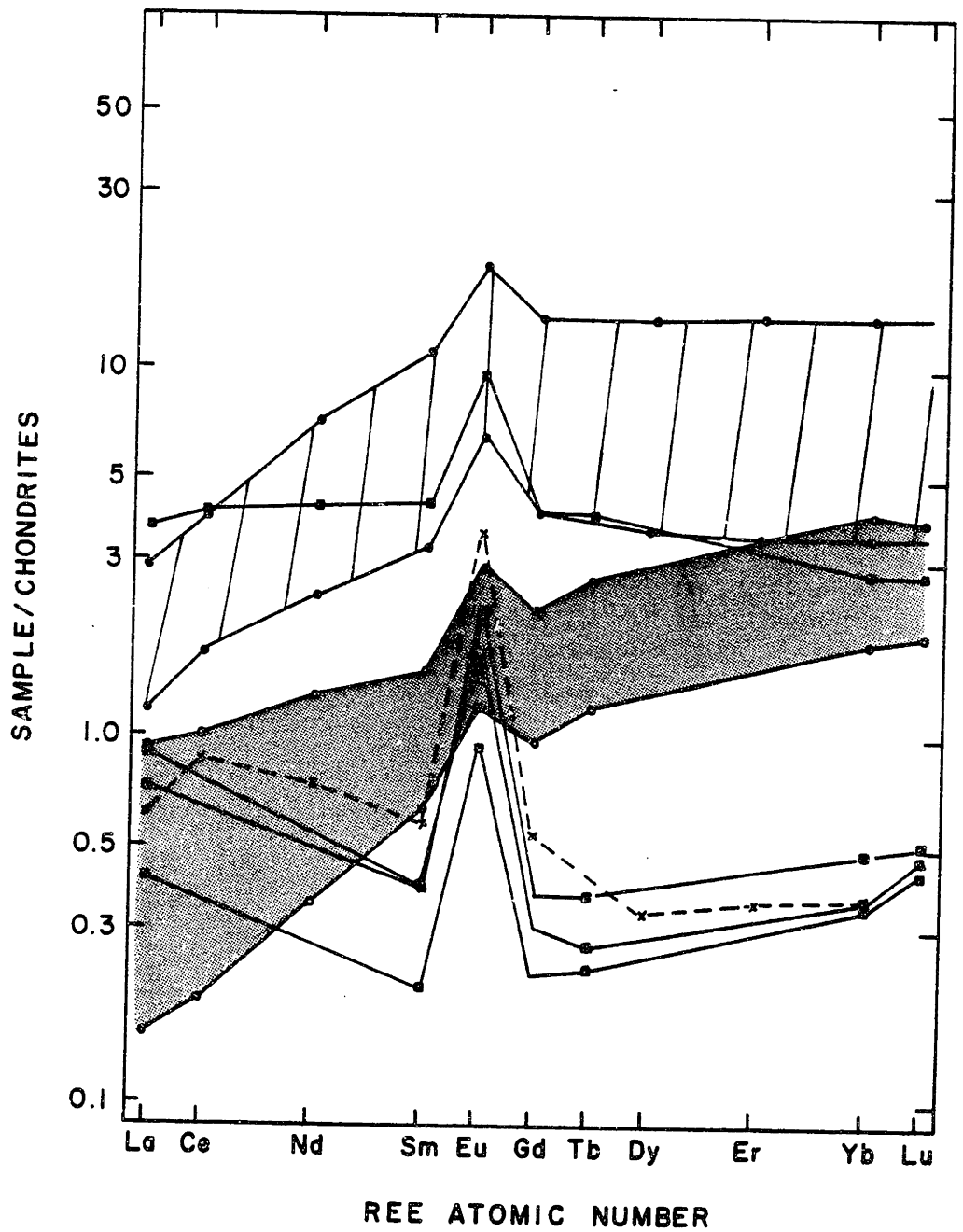
50
30
10
5
3
1.0
0.5
0.3
0.1
SAMPLE/CHONDRITES
La
Ce
Nd
Sm
Eu
Gd
Tb
Dy
Er
Yb
Lu
REE ATOMIC NUMBER

Figure 2-10. Chondrite-normalized REE patterns of Nunivak granulites (■) compared to the range of REE patterns for ocean gabbros (lined region), a troctolite (dashed line) from the Mid-Atlantic Ridge near 24°N (Shih, 1972), and gabbros (shaded region) from site 334 of leg 37 of the DSDP (Dostal and Muecke, 1978).

liquid and $D^{i}$, is the bulk distribution coefficient determined from the cumulate mineral partition coefficients (Table 2-4) and their respective weight fractions in the cumulate (after Albarede, 1976).

There are a number of problems inherent in the procedure of inferring the concentrations of trace elements in a parental liquid from the concentrations in a cumulate rock. Firstly, if the calculations are to yield an accurate estimate of the parental magma, then the cumulate crystals must be homogeneous and have equilibrated with the parental magma (e.g., Haskin and Korotev, 1977). If the crystals are zoned then calculation of a parental magma composition is difficult. However, in the slow cooling which presumably accompanies the formation of layered cumulates one would expect conditions to be favorable for the formation of homogeneous crystals, and indeed, many cumulates contain unzoned cumulus phases (Cox et al., 1979). The layered aspect of the granulites indicates that these xenoliths may be fragments of a layered complex, and that the cumulate minerals may be unzoned. Relict olivine grains are unzoned (Francis, 1976a) and thus are consistent with the assumption of homogeneous crystals. However, much of the original igneous mineralogy is replaced by corona minerals, thus, we cannot be certain that the original cumulus grains were homogeneous.

A serious problem may lie in the assumption that the cumulus minerals equilibrated with the parental liquid. If any orthocumulus growth occurred in the presence of differentiated interstitial melt, then the calculated incompatible element abundances of the parental melt will be too high, and the calculated compatible element abundances of the parental melt will be too low (Haskin and Korotev,

Table 2-4. Mineral partition coefficients.

| | plagioclase | olivine | clinopyroxene |
|---|---|---|---|
| K | 0.18[1] | 0.00021[1] | 0.0123[1] |
| Sc | 0.02[2] | 0.15[3] | 2.7[4] |
| Co | 0.05[5] | 3.3[6] | 0.9[7] |
| Sr | 2.0[1] | 0.000067[1] | 0.092[1] |
| Ba | 0.33[1] | 0.00045[1] | 0.014[1] |
| Ce | 0.047[8] | 0.000032[9] | 0.04[10] |
| Nd | 0.038[8] | 0.000063[9] | 0.09[10] |
| Sm | 0.031[8] | 0.000084[9] | 0.14[10] |
| Tb | 0.027[8] | 0.00038[9] | 0.19[10] |
| Er | 0.023[8] | (0.0016)[9] | (0.20)[10] |
| Yb | 0.022[8] | 0.0038[9] | 0.20[10] |

---

Values in parentheses are interpolated

Data sources:

1. Averaged partition coefficient from Hart and Brooks (1974) and Zindler (1980).
2. 1135°C, Lindstrom (1976).
3. Average from Dale and Henderson (1972).
4. 1250°C, Drake and Weill (1975).
5. 1170°C, Lindstrom (1976).
6. 1250°C, summary in Irving (1978).
7. Lindstrom and Weill (1978).
8. Shih (1972).
9. Stosch (1982).
10. Frey et al. (1978).

1977). The petrologic data are insufficient to evaluate the seriousness of this problem because of the coronas, however, the results of the trace element model (described below) appear to indicate that some orthocumulus growth occurred.

Secondly, it is difficult to accurately estimate the amount of trapped melt present. Two samples, 12000 and 12013, may contain trapped melt: 12000 has poikilitic clinopyroxene enclosing cumulate plagioclase, has a relatively high K content (Table 2-2), and contains clinopyroxene in the recalculated mode (Table 2-1). Although 12013 does not contain poikilitic clinopyroxene, it has more K than 12011 in spite of containing less of the major cumulate host, plagioclase, for K than 12011; also 12013 contains clinopyroxene in the recalculated mode. In order to allow for the presence of trapped melt in these two samples we calculated two model liquids for these two samples. In the first case, we assumed that there was no trapped melt, that is, the clinopyroxene equilibrated with the parent melt just as the cumulus phases did. In the second case, we arbitrarily set $\alpha$ equal to the percent clinopyroxene in the recalculated mode.

Thirdly, the granulites may have been contaminated by the host basanites. The incompatible elements which are in low abundance in the granulites are particularly sensitive to contamination by host alkali basalt. However, this problem does not appear serious for the Nunivak granulites. Five Nunivak basanites (Table 3-14) contain 27-56 ppm La. The very low La concentration, 0.1 ppm (Table 2-2), in 12017 limits the maximum amount of contamination by these basalts to 0.4%. But even this much contamination is unlikely because the systematic

behavior of K, and La relative to the inferred variation of cumulate minerals (Figure 2-2) suggest that these elements are contained in cumulate plagioclase.

Finally, the absolute value of the mineral partition coefficients vary as functions of temperature, pressure, and composition of the equilibrating phases. Thus, mineral/melt partition coefficients for a given element may have changed during the formation of a cumulate; this variation can result in an inaccurate estimate of the concentration of a given element in the parental liquid.

We used partition coefficients (Table 2-4) which are appropriate for MORBs because of our conclusion based on the isotopic data that the parental magma was isotopically similar to MORBs. The particular partition coefficients used are in general near the low end of the range of published partition coefficients, and where possible are derived from careful mineral separate-matrix studies. We chose to use these values where possible because recent detailed studies (e.g., Hart and Brooks, 1974) have shown that many of the relatively high partition coefficients for incompatible elements may be due to impure mineral separates. Furthermore, it is a general observation that the partition coefficients for many trace elements are lower in Mg-rich basalts than in more silica-rich magmas (e.g., Arth, 1976; Watson, 1977; Hart and Davis, 1978).

Most of the elements modelled are to some degree compatible in olivine or plagioclase. In view of the uncertainty concerning the choice of an appropriate partition coefficient, caution should be exercised in evaluating the absolute concentrations of the model liquids (Table 2-5) because calculated compatible element concentrations are very sensitive

Table 2-5. Model parental melts (ppm).

| | 12000 $\alpha = 0$ | 12000 $\alpha = 0.12$ | 12011 | 12013 $\alpha = 0$ | 12013 $\alpha = 0.056$ |
|---|---|---|---|---|---|
| K | 3761 | 1956 | 965 | 1657 | 925 |
| Sc | 57 | 128 | 42 | 21 | 33 |
| Co | 40 | 39 | 54 | 56 | 56 |
| Sr | 241 | 225 | 170 | 184 | 172 |
| Ba | 77 | 51 | 38 | 43 | 28 |
| Ce | 68 | 17 | (20) | (22) | (5.6) |
| Nd | 57 | 15 | (13) | (12) | (3.3) |
| Sm | 17 | 4.7 | 3.7 | 3.2 | 1.0 |
| Tb | 3.6 | 1.1 | 1.0 | 0.48 | 0.15 |
| Er | (13) | (3.8) | (5.6) | (2.5) | (0.82) |
| Yb | 12 | 3.4 | 6.3 | 2.9 | 0.91 |

Values in parentheses are interpolated

Table 2-5. Continued

| | 12017 | KD 11[1] | Typical MORB Range |
|---|---|---|---|
| K | 1311 | 1400 | 430-2154[3] |
| Sc | 44 | | 30-52[2] |
| Co | 54 | | 36-60[2] |
| Sr | 113 | 135 | 95-166[3] |
| Ba | 65 | 46 | 2.7-39[3] |
| Ce | (19) | 12 | |
| Nd | (13) | 9.5 | |
| Sm | 4.0 | 3.1 | |
| Tb | 1.2 | | |
| Er | (6.9) | 3.0 | |
| Yb | 6.7 | 2.9 | |

1. Sample KD from Kay et al. (1970).

2. Range of normal MORBs (Frey et al., 1974; Sun et al., 1979).

3. Range of MORBs not including 3 samples from 46°N (Hart, 1976).

to the values of partition coefficients. Calculate elemental ratios are more reliable, especially ratios of elements which have similar partition coefficients, and which are concentrated in only one phase such as olivine or plagioclase. Elemental ratios are less sensitive to the choice of partition coefficients because ratios of partition coefficients are much less sensitive to variations in pressure, temperature, and composition than single partition coefficients. For example, while Arth's (1976) basaltic melt/plagioclase partition coefficients for Ce and Sm are greater by a factor of two than Shih's (1972) values, $D^{Ce}/D^{Sm}$ for Arth's set is 1.79 while the same ratio for Shih's set is 1.52. Hence, elemental ratios such as K/Ba, La/Sm, and La/Yb of the model parental melts are probably more accurate estimates of the chemistry of the melt than absolute concentrations.

In spite of the above problems, we infer from the trace element modelling that: (1) it is unlikely that the protoliths for the granulites were related to the Nunivak volcanism, (2) there is little or no trapped melt present in 12000 and probably 12013, and (3) the parental melts for 12011, 12013, and 12017 were similar to normal MORBs in having low K abundances but the parental melts may have had higher Ba abundances and higher La/Yb ratios than normal MORBs.

The trace element modelling provides further evidence that the granulite inclusions are not petrogenetically related to the host basalts. As noted previously, only two basanites have $^{87}Sr/^{86}Sr$ ratios within analytical error of the granulites (Mark, 1971; Menzies and Murthy, 1980a). The Nunivak basanites have significantly higher incompatible element abundances, K = 11403-20988 ppm, Sr = 639-1046

ppm, Ba = 310-541 ppm; La = 27-56 ppm (Table 3-14), and significantly higher chondrite-normalized Ce/Yb ratios, 32-44, than the incompatible element abundances (Table 2-5) and chondrite-normalized Ce/Yb ratios, 2.9 to 7.5, of the calculated parental melts. Thus, it is unlikely that there is any relation between the cumulate protoliths of the granulites and the basaltic volcanism on Nunivak Island.

The Sc content of the parental magma inferred from granulite 12000 (Table 2-5) appears to be unreasonably high unless a significant amount of the poikilitic clinopyroxene, a major host for Sc, is heterad in origin. For example, if the clinopyroxene represents trapped melt then the Sc content of the parental liquid is inferred to be 128 ppm. Most basalts have less than 60 ppm Sc (e.g., Norman and Haskin, 1968). In contrast, if the clinopyroxene is the result of heterad crystallization, i.e., clinopyroxene which equilibrated with parental melt, then the model parent has 55 ppm Sc which is within the range of Sc concentrations of oceanic basalts (Norman and Haskin, 1968; Frey et al., 1980). A larger olivine partition coefficient for Sc such as 0.27 (Frey et al., 1978) will lower the Sc abundance in the calculated model melt. However, the effect is not significant: the calculated Sc concentration of the liquid in the trapped melt model using 0.27 for the olivine partition coefficient is still unrealistically high at 113 ppm. Also, the calculated primary olivine composition, $Fo_{72}$, is analytically indistinguishable from relict olivine composition, $Fo_{71.7}$ (Francis, 1976a). Thus, there can be little or no Fe-rich interstitial melt present in this sample. We conclude that most of the clinopyroxene in 12000 must be heterad in origin and that there is little trapped

melt present.

The case of 12013 which also contains clinopyroxene in the recalculated mode (Table 2-1) is more equivocal than that of 12000. The no-trapped-melt model is more likely because the REE content of the parent liquid is similar to that of the model parental melts for 12011 and 12017 (Table 2-5). The REE model is then consistent with the indistinguishable $^{87}Sr/^{86}Sr$ ratios of these granulites and the inferred narrow range in the compositions of primary olivine ($Fo_{78-82}$) and plagioclase ($An_{66-73}$ ; Francis, 1976a).

The calculated concentrations of K, Sc, Co, and Sr in the model liquids inferred from 12011, 12013, and 12017 (Table 2-5) are within the range of normal MORBs ("normal MORBs of Sun et al., 1979; Group I MORBs of Bryan et al., 1976). However, these parental melts have higher La/Yb ratios (Figure 2-11), higher REE concentrations (Figure 2-11), and higher Ba abundances (thus lower K/Ba ratios, Table 2-5) than LIL-element depleted MORBs. We presently cannot resolve the problem as to whether this inference is valid or whether it is a consequence of invalid assumptions in the model. For example, the high total REE abundances, relative to normal MORBs (Figure 2-11) and mafic basalts from back-arc basins (e.g. Hawkesworth et al., 1977) or island arcs (e.g., DePaolo and Johnson, 1979) may be the result of equilibration of cumulate, adcumulate, and heteradcumulate phases with interstitial melt.

Granulite 12000 appears to have equilibrated with a highly differentiated melt because its inferred parental melt (no-trapped-melt model) has high incompatible element concentrations and because the

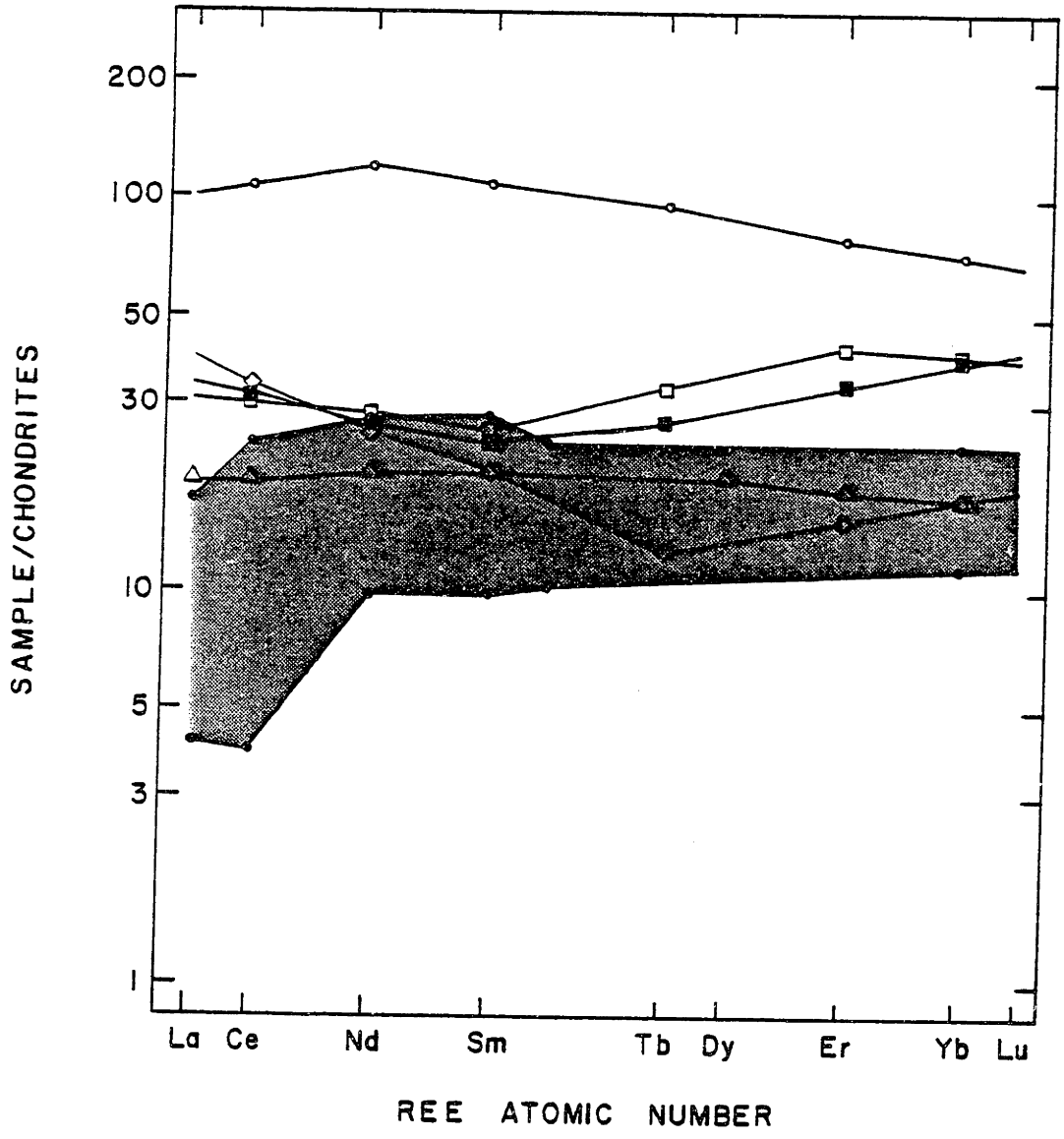
200
100
50
30
10
5
3
1
SAMPLE/CHONDRITES
La
Ce
Nd
Sm
Tb
Dy
Er
Yb
Lu
REE ATOMIC NUMBER

Figure 2-11. Chondrite-normalized REE patterns of model liquids (Table 2-5) in equilibrium with 12000 (o), 12011 (■), 12013 (◇), and 12017 (□). Also shown is sample KD 11 (△) from Kay et al. (1970) and the range (shaded region) for normal MORBs from Frey et al. (1974) and Sun et al. (1979).

calculated primary olivine in 12000 is more Fe-rich, Fo72, than that, $Fo_{78-82}$, of the other granulites.

There are at least some basalts erupted from oceanic ridges which are similar to the calculated parental melts for 12011, 12013, and 12017. For example, sample KD 11 (Table 2-5) from the Gorda Ridge shares with the model parental melts similar K abundances and has high Ba abundances and La/Yb ratios relative to normal MORBs (Table 2-5; Figure 2-11). To our knowledge this sample has not been analyzed for isotopic composition, but samples from the Juan de Fuca Ridge and the Gorda Ridge have $^{87}Sr/^{86}Sr$ ratios, 0.7023-0.7027 (Sun et al., 1979), similar to the ratios of the granulites. Some basalts from back-arc basins and island arcs also have La/Yb ratios similar to the calculated parental melts (Hawkesworth et al., 1977; DePaolo and Johnson, 1979) but the former basalts typically have higher K abundances (Hart et al., 1972; Jacobsen and Wasserburg, 1979) while the latter commonly have higher $^{87}Sr/^{86}Sr$ ratios then the inferred parental basalts (e.g., DePaolo and Johnson, 1979). In summary, although we believe that the most likely parental magma was geochemically similar to oceanic-ridge basalts we cannot eliminate the possibility that the parental magma was a back-arc basin basalt with lower than average K abundances or a low-K island arc tholeiite that did not have the relatively high $^{87}Sr/^{86}Sr$ signature that many island arc basalts have (DePaolo and Johnson, 1979). We emphasize that the similar REE abundance in a troctolite from near the Mid-Atlantic Ridge (Figure 2-10) and granulites 12011, 12013, and 12017 may indicate that our inference that the La/Yb ratio of the parental melts was significantly higher than

normal MORBs is an artifact of the trace element model.

## VI. Summary: Implications for the Composition of the Lithosphere

Several lines of geochemical evidence indicate that some inclusions at Nunivak Island are samples of oceanic lithosphere which underlies Nunivak Island at least in part:

(1) The isotopic and trace element geochemistry of the granulites require an oceanic basalt as a parental melt. This basalt was most likely an oceanic ridge basalt, but possible parental melts also include back-arc basin basalts and island arc tholeiites. Consideration of the Sm-Nd data for the granulites indicates that the cumulate protoliths for the granulites crystallized less than $5 \times 10^8$ yr. ago, most likely at approximately $2 \times 10^8$ yr. ago.

(2) Granuloblastic-equant lherzolite inclusions (Chapter 3) which are associated with the granulite inclusions at Nunivak Island are probably samples of the same oceanic terrane as the granulites. The low La/Yb ratios relative to chondrites, and the similar $^{87}Sr/^{86}Sr$ and $^{143}Nd/^{144}Nd$ ratios to present-day MORBs of these inclusions indicate that the granuloblastic-equant lherzolites are petrogenetically related to MORBs. We propose (Chapter 3) that these inclusions represent potential source rocks for MORBs. Relative to the bulk earth, the granuloblastic equant lherzolites have Sm-Nd model ages of approximately 1.6 to $1.8 \times 10^9$ yr.

One possible explanation for the oceanic affinities of the granulites and the granuloblastic-equant peridotites is that they are samples of oceanic lithosphere which underlies Nunivak Island. Indeed, the basalts on Nunivak have $^{87}Sr/^{86}Sr$, 0.70251-0.70330 and $^{143}Nd/^{144}Nd$, 0.51281-0.51315, ratios (see Chapter 3) which reflect no interaction with continental crust. We speculate that the Sm-Nd model ages of the granuloblastic-equant lherzolites represent the time at which this oceanic terrane became a geochemical entity. A portion of this terrane similar in geochemistry to the granuloblastic-equant lherzolites was melted at approximately $2 \times 10^8$ yr. ago at a ridge crest. The cumulate protoliths of the granulites formed in magma chambers near the base of the crust at this time. The reaction of olivine and plagioclase recorded in the corona textures of the granulites was probably a consequence of the cooling of oceanic lithosphere as it moved away from the ridge crest, but it may also reflect gradual thickening of the crust (Francis, 1976a). We suggest that this oceanic terrane is part of the Yukon-Koyukuk terrane, an oceanic terrane accreted to western Alaska during the Cretaceous period (Churkin et al., 1980).

Thus, we suggest that laterally accreted oceanic lithosphere is the source terrane of the Nunivak granulites and granuloblastic equant lherzolites. This lithosphere may be gradually converted to continental crust by crustal thickening as suggested by Francis (1976a). Indeed, we support the suggestion of Polve and Allegre (1980) that lateral accretion of oceanic lithosphere is the explanation of the recently

recognized occurrence of peridotite nodules with oceanic affinities in continental alkali basalts (Jagoutz et al., 1980; Stosch et al., 1980; Chapters 3 and 4, this study).

# 3. GEOCHEMISTRY OF PERIDOTITE AND PYROXENITE INCLUSIONS, NUNIVAK ISLAND, ALASKA, AND THEIR RELATIONSHIP TO ASSOCIATED VOLCANISM

## I. Introduction

Compositional and isotopic heterogeneity in the earth's upper mantle has been inferred from many studies of basalts (e.g., White and Schilling, 1978; Hofmann and Hart, 1978), however, mantle heterogeneity can be most directly studied by analyzing samples of the upper mantle such as alpine peridotites and peridotite inclusions in alkali basalts and kimberlites. Because of their large size (commonly more than 10 $km^2$), alpine peridotites provide structural information on the size and interrelationships of various lithologies. However, these bodies are frequently metamorphosed and/or partially serpentinized, and thus, their geochemistry may not be simply related to mantle processes. On the other hand, ultramafic inclusions are usually fresh and their geochemistry can be directly related to mantle processes. Inclusions are generally less than a meter in diameter and hence, inclusion studies provide little information on structural relationships besides the pressure estimates derived from phase equilibrium. Companion geochemical studies of inclusion-bearing basalts are especially important because the basalt-xenolith association represents an instantaneous sampling of the upper mantle involving wallrock (inclusions) and partial melts (basalts). Combined studies of basalts and upper mantle xenoliths maximizes the amount of information obtained

from any one locality.

We studied the Nunivak Island, Alaska (Figure 2-1), inclusion suite because previous studies of the petrography and mineral chemistry of the inclusions (Francis, 1976b, 1976c, 1978) provide a framework for geochemical studies. In particular, Francis (1978) showed that the lherzolite inclusions are texturally and mineralogically diverse, thus, we expected to observe trace element abundance and possibly isotopic heterogeneity. In this paper we report Sr and Nd isotopic ratios and trace element concentrations in lherzolite and pyroxenite inclusions and associated basalts from Nunivak Island. This study had several major objectives: (1) to document mantle heterogeneity beneath Nunivak Island in terms of trace element and isotopic geochemistry, (2) to evaluate and understand the role of mantle metasomatism in this region, (3) to use isotopic data to ascertain if any of the rock types were genetically related, and (4) to develop a geochemical model for the upper mantle beneath Nunivak Island.

In the past decade mantle metasomatism has frequently been invoked to explain the geochemistry of the source rocks for alkali basalts (e.g., Boettcher and O'Neill, 1980). Based on trace element modelling these source rocks appear to be highly enriched in incompatible trace elements, e.g., K, Rb, Ba, La, P, etc., relative to alpine peridotite or pyrolite (e.g., Clague and Frey, 1982), yet the Sr and Nd isotopic ratios of many alkali basalts indicate that their source rocks have had a time-integrated history of depletion in incompatible elements relative to the bulk earth (e.g., Roden et al., 1981). The Nunivak Island inclusion

suite is especially suitable for determining the nature of mantle metasomatism because many of the peridotite inclusions contain the hydrous minerals such as amphibole and mica typically associated with mantle metasomatism (e.g., Lloyd and Bailey, 1975).

## II. Background

### (A) General background

Nunivak Island (166°W, 60°N) is a large, 75 km in diameter, basaltic island located on the Bering Sea shelf 50 km west of the Alaskan coast and 600 km north of the Aleutian Islands (Figure 2-1). The island consists predominantly of thin olivine tholeiite flows capped by less voluminous alkali basalt flows and associated cinder cones and maars. The volcanism on Nunivak is all younger than 6.1 million years and was episodic in nature with the center of volcanism moving to the east with time (Hoare, 1968). This volcanism is part of a late Tertiary to Recent province of dominantly tholeiitic activity which includes volcanic centers on the Pribilof Islands, St. Matthews Island, St. Lawrence Island, and Seward Peninsula (Figure 2-1). In addition to Nunivak Island, ultramafic inclusions occur in alkali basalts of the Seward Peninsula and the Pribilof Islands.

On Nunivak Island, ultramafic inclusions and megacrysts of anorthoclase, clinopyroxene, and kaersutite are common at most of the alkalic centers. The inclusions studied here were associated with the last episode of basaltic volcanism ranging in age from 1 million years to perhaps only a few thousand years (Francis, 1974). Lherzolites (84.4%) are the most abundant inclusion followed in abundance by

dunites and harzburgites (6.5%), pyroxene granulites (8.5%), and amphibole-bearing pyroxenites (0.3%, Francis, 1978). This chapter concerns the lherzolites, pyroxenites, and host basalts; the petrogenesis of the pyroxene granulites was discussed in Chapter 2.

Several important constraints on the geochemistry of the upper mantle beneath Nunivak Island have been established by isotopic studies on the host basalts and associated xenoliths. Mark (1971) first reported the relatively low $^{87}Sr/^{86}Sr$ ratios, 0.7025 to 0.7033, of the Nunivak basalts. These ratios are within the range of modern mid-ocean ridge basalts (MORBS, Hofmann and Hart, 1978). Mark (1971) further noted a correlation between basalt chemistry and $^{87}Sr/^{86}Sr$ ratio with the most alkalic basalts having the least radiogenic Sr. The Pb isotopic ratios of a basalt and a lherzolite are also similar to modern abyssal tholeiites (Zartman and Tera, 1973). Most recently, Menzies and Murthy (1980a) found that the Sr and Nd isotopic ratios of basalts and amphibole-bearing peridotites were indistinguishable and that these peridotites had Sm/Nd ratios less than chondrites. The present-day $^{143}Nd/^{144}Nd$ ratios of these amphibole-bearing peridotites require a long term depletion in the light rare earth elements (LREE) relative to the bulk earth. Menzies and Murthy (1980a) postulated a recent metasomatic event to explain this anomaly. Overall, the isotopic data indicate that the basalts have not been contaminated by continental crust and that the source for the Nunivak basalts is isotopically similar to the source of many oceanic basalts.

(B) Textures and mineralogy of the peridotite and pyroxenite inclusions.

The peridotite inclusions are spinel peridotites, and consist of, in order of decreasing abundance: olivine, orthopyroxene, clinopyroxene, and spinel. Francis (1978) divided the peridotites into three textural groups: coarse-equant, coarse-tabular, and granuloblastic equant (nomenclature of Harte, 1977). The coarse-equant and coarse-tabular inclusions were further subdivided on the basis of whether or not they contained amphibole or glass after amphibole; the granuloblastic-equant inclusions never contain amphibole. In the coarse-equant and coarse-tabular inclusions the amphibole or glass typically occurs as rims around amoeboid spinel (Figure 3-1). Francis (1976b) postulated that the amphibole formed by the reaction of anhydrous phases with a water-rich fluid.

Magnesium content, $Fo_{88-91}$, of olivine shows no correlation with texture, however, $TiO_2$ and $Al_2O_3$ in clinopyroxene increase and molar Cr/Cr + Al in spinel decreases in the sequence coarse-equant, coarse-tabular, granuloblastic-equant (Figure 3-2). Both clinopyroxene and spinel are more abundant in the granuloblastic-equant (herein abbreviated GE) inclusions than the other two groups of peridotites. The GE inclusions are the most fertile with respect to basaltic components and are texturally and chemically distinct from the coarse-equant (herein abbreviated CE, or ACE if they contain amphibole or glass after amphibole) and coarse-tabular (herein abbreviated CT, or ACT if they contain amphibole or glass after amphibole) groups

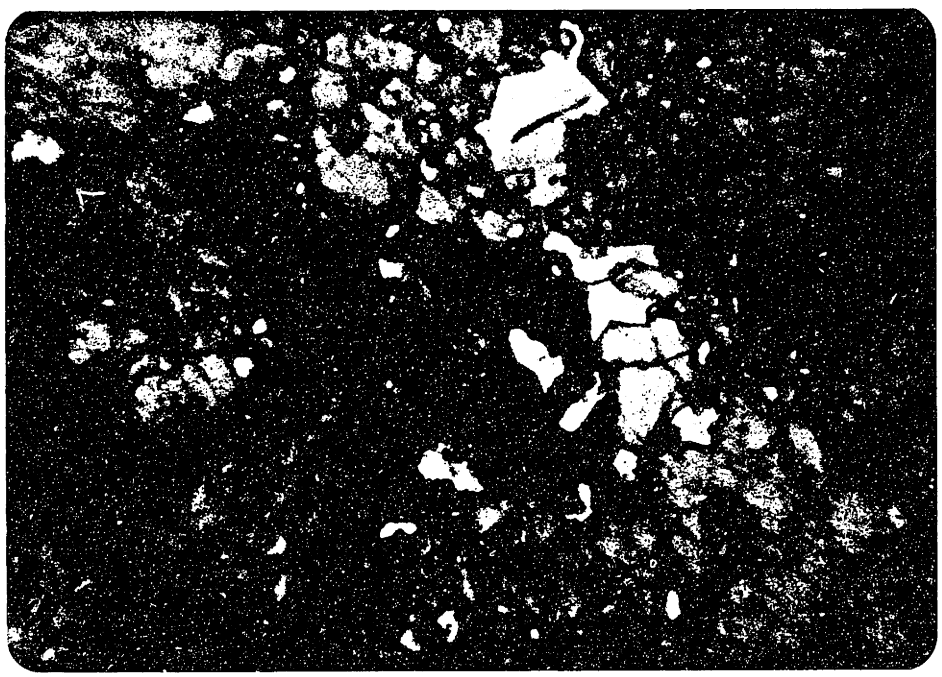

Figure 3-1. Photomicrograph of brown amphibole rimming black spinel in ACT inclusion 10067 (long dimension is 2.5 mm).

(Figure 3-2). In contrast, there appears to be a gradational textural transition from the CE to the CT inclusions. Associated with the presence of amphibole in the ACE and ACT groups is a greater amount of jadeite component in the clinopyroxene, and a lower molar $Mg/(Mg + Fe^{2+})$ ratio in clinopyroxene and olivine than in the CE and CT groups (Francis, 1978).

The amphibole pyroxenites (Francis, 1976c) consist predominantly of amphibole oikocrysts and anhedral black augite with lesser amounts of virtually Cr-free spinel, orthopyroxene, and pyropic garnet. Textures in these pyroxenites, including composite augite grains with an inner zone rich in orthopyroxene lamellae and an outer zone free from lamellae, jackets of garnet around spinel, and corroded and embayed augite in contact with amphibole, indicate a complex history for these xenoliths. Francis (1976b) suggested that the amphibole formed in a manner analogous to the amphibole in the peridotites following a period of cooling and recrystallization in the upper mantle.

## III. Sample Description

Eighteen peridotite and pyroxenite xenoliths, which are described below, were chosen to provide a sampling of the various textural groups defined by Francis (1978; 1976b). Modes are shown in Figure 3-3. The peridotites are predominantly lherzolites, although some harzburgites are present. Basalt samples, which are also described below, were selected from a suite collected by Francis in order to cover as completely as possible the range of basalt compositions present on

## TEXTURAL CLASSIFICATION OF NUNIVAK SPINEL LHERZOLITES

| Gradational → | | Granuloblastic-Equant (GE) |
|---|---|---|
| Coarse Equant | Coarse Tabular | |
| Amphibole-Free (CE) | Amphibole-Free (CT) | No Amphibole<br>Green Spinel<br>Jadeitic Clinopyroxene |
| ← Interstitial Brown Spinel → | | |
| 10007 | 10004, 10008 | |
| Amphibole or Glass-Bearing (ACE) | Amphibole or Glass-Bearing (ACT) | |
| Spinel as Vermicular Grains in Glass, Amphibole, Phlogopite, or Clinopyroxene | | |
| Clinopyroxene Relatively Jadeite Rich | | |
| 10002, 10006, 10055 | 10051, 10067, 10075 | 10070, 10068, 10026, 10211 |

CHEMICAL GRADIENTS {
- Increasing $TiO_2$ in Clinopyroxene →
- Increasing $Al_2O_3$ in Clinopyroxene →
- Decreasing Cr/Cr+Al in Spinel →

Figure 3-2. Schematic illustration of compositional and textural variations in peridotite inclusions from Nunivak Island (after Francis, 1978). Samples used for the present study are shown in their appropriate textural group.

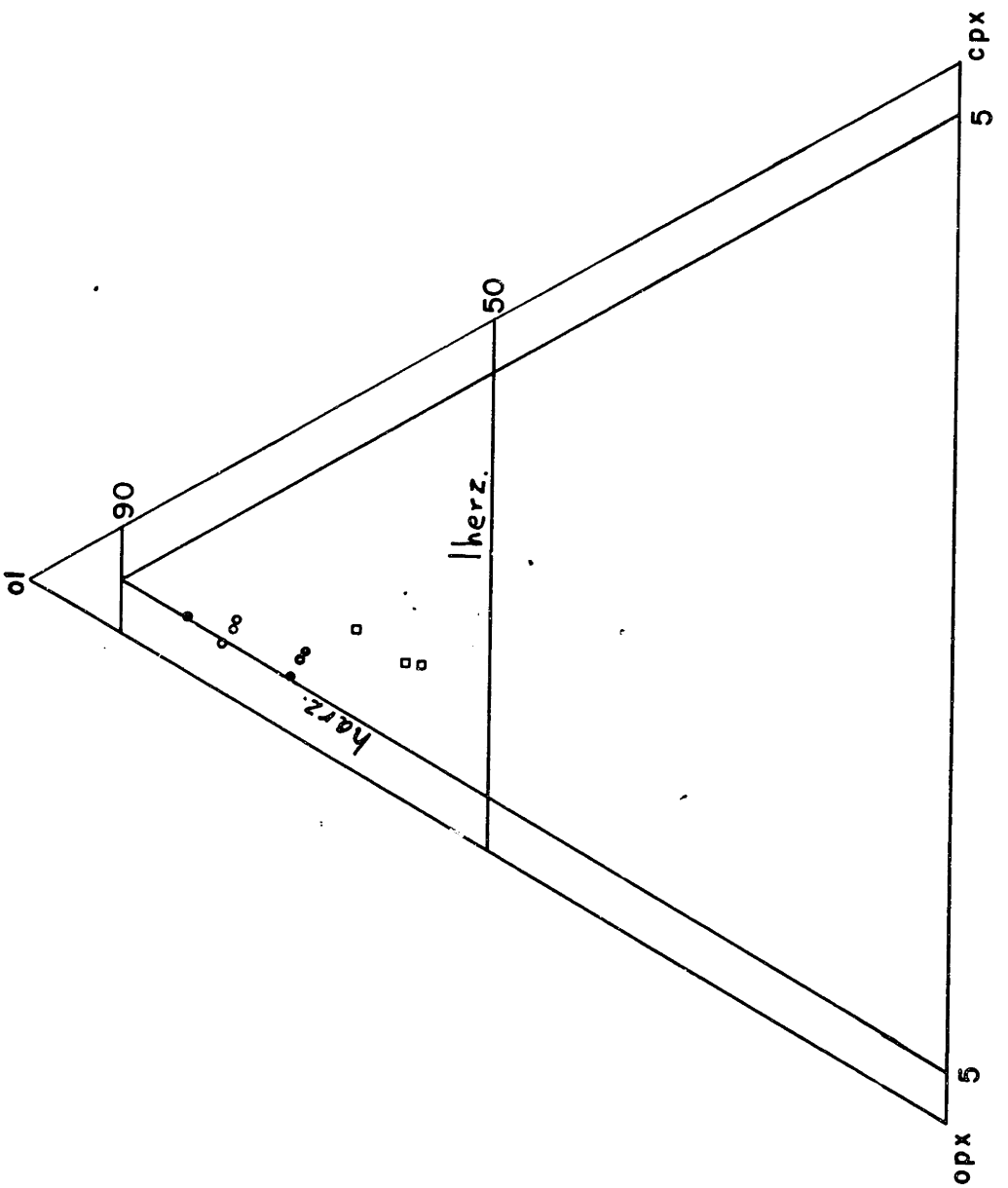
ol
90
50
cpx
5
5
opx
lherz.
harz.

Figure 3-3. Modes of GE (□), CE and CT (●), and ACE and ACT (○) inclusions projected onto the olivine (ol)-orthopyroxene (opx)-clinopyroxene (cpx) triangle from spinel + amphibole/glass.

Nunivak. More general descriptions of lithologies can be found in papers by Francis (1976b,c, 1978), Mark (1971), and Hoare et al. (1968).

(A) Peridotites

Coarse-equant, no amphibole or glass (CE)

10007: coarse-grained, 4 phase lherzolite dominated by large (to 7 mm maximum dimension) somewhat tabular, kinked olivine which contains uncommon elliptical inclusions of spinel and pyroxene. Interstitial to the olivine are regions of finer-grained (less than 3 mm) olivine, pyroxene, and brown spinel.

Coarse-equant, containing amphibole or glass (ACE)

10002: coarse-grained lherzolite with elliptical pods (to several mm in diameter) of glass enclosing amoeboid, brown spinel. Large (to 4 mm), kinked, somewhat tabular olivine grains surrounded by regions consisting of smaller olivine neoblasts, orthopyroxene, and clinopyroxene. Clinopyroxene contains rare subhedral apatite inclusions (less than 100 μ long) and large (to 50 μ diameter) spherical fluid inclusions which are now empty.

10006: Glass and amphibole-bearing harzburgite. Rock dominated by somewhat tabular, kinked olivine to 5 x 3 mm with less abundant orthopyroxene (less than 2 mm). Clinopyroxene is typically developed along olivine and orthopyroxene grain boundaries embaying or replacing these silicates. Interiors of the clinopyroxenes are crowded with several morphologic types of fluid inclusions including large vacuoles as in

10002. Apatite inclusions in clinopyroxene are also present. Spinel occurs as amoeboid grains surrounded by glass as in 10002; remnant amphibole and phlogopite grains are present within the glass.

10055: An unusual lherzolite in which clinopyroxene and its breakdown products rim amoeboid spinel. This inclusion lacks amphibole but is included with ACE inclusions on the basis of textural similarities. Much of the clinopyroxene has been replaced by very fine grained intergrowths of euhedral spinel (less than 3 μ diameter) + a silicate (less than 0.05 mm). The remaining clinopyroxene contains common fluid inclusions, and possibly some apatite. Another unusual feature of this xenolith is that the orthopyroxene contains abundant, fine lamellae of clinopyroxene. The olivine is similar in habit to that in 10002.

Coarse-tabular, no amphibole or glass (CT)

10004: A four phase lherzolite with a foliation defined by tabular grains of olivine 1 to 3 mm in size. Interstitial to these larger olivines and some large orthopyroxenes are small, 1 mm or less neoblasts of olivine, orthopyroxene, and clinopyroxene. Spinel is brown and blocky. Clinopyroxene contains uncommon, large (to 100 μ diameter) spherical fluid inclusions, now empty.

10008: A four phase lherzolite, very similar to 10004 except that clinopyroxene is free of large, i.e. greater than 25 μ diameter, fluid inclusions.

Coarse-tabular, containing amphibole or glass (ACT)

10051: An amphibole (4.3%)-bearing lherzolite notable for the

presence of thin (less than 5 mm) veinlets of phlogopite, and for complex textures involving amphibole, phlogopite, and clinopyroxene. Olivine forms large (to 6 x 4 mm), tabular, kinked grains with numerous subgrain boundaries. Small (less than 0.2 mm), unstrained olivine neoblasts are common along grain boundaries and as stringers within olivine porphyroclasts. Phlogopite inclusions are common within olivine and clinopyroxene grains. In olivine, these inclusions are often surrounded by radial expansion cracks. Phlogopite also occurs as interstitial aggregates and as small inclusions in amphibole. Clinopyroxene occurs as pale green, small (less than 0.5 mm) grains, commonly molded to or embaying olivine and especially orthopyroxene. In some places clinopyroxene forms a concentric ring between amphibole enclosing spinel and the other silicates, whereas elsewhere the clinopyroxene contains wisps of amphibole or occurs as small round inclusions in amphibole. The amphibole occurs as grain aggregates enclosing spinel, sometimes rimmed by clinopyroxene. Elsewhere, the amphibole occurs as interstitial grains often with round inclusions of phlogopite, clinopyroxene, and olivine.

10067: An amphibole-rich (amphibole + glass = 14.7%) lherzolite with extremely complex textures. This lherzolite contains two texturally distinct regions: a relatively coarse-grained region consisting of kinked olivine (3 x 1 mm) with serrated grain boundaries and pyroxenes crowded with a variety of fluid inclusions. A second region consists of finer-grained (less than 0.5 mm), relatively unstrained neoblasts with straight grain boundaries and rare orthopyroxene

porphyroclasts. With the exception of neoblasts, both pyroxenes are cloudy due to abundant fluid inclusions. The fluid inclusions are abundant and variable in morphology ranging from curving, planar arrays of tubular to spherical inclusions generally less than 1μ in diameter to larger, isolated spherical cavities to 50μ in diameter. Apatite, as subhedral prisms to 100μ long and containing minute red-brown inclusions, occurs as inclusions in clinopyroxene. The amphibole occurs in aggregates of grains (0.5 mm in diameter) preferentially nucleated around amoeboid spinel, but also as isolated single grains or groups of grains. Although both fluid and mineral inclusions occur in the amphibole, they are noticeably less common than in the pyroxenes.

10075: lherzolite containing small amounts of amphibole (0.3%) and phlogopite (0.5%). This sample is most notable for a concentric zoning of the hydrous minerals around amoeboid spinel: a ring of phlogopite separates amphibole from spinel.

Granuloblastic-equant (GE)

10070: A fine-grained (0.5 - 1 mm. average grain size), clinopyroxene-and green spinel-rich lherzolite. Both clinopyroxene and spinel are significantly more abundant than in the CE, CT, ACE, and ACT groups. Rare 2+ mm orthopyroxene porphyroclasts occur in a granuloblastic matrix of olivine, orthopyroxene, clinopyroxene, and spinel.

10068: similar in all essential features to 10070.

10026: similar to 10070 except iddingsitized. Red-brown iddingsite occurs on grain surfaces and along fracture surfaces within olivine grains.

10211: similar in all essential features to 10026.

Composite xenolith

10056: A layered, composite xenolith consisting of peridotite and two types of pyroxenite. Measured normal to the plane of the layers, the rock consists of a 1 cm thick band of orthopyroxenite between a 3.5 cm band of peridotite and a 1 cm band of spinel clinopyroxenite. The peridotite is coarse-equant in texture and contains pods of glass enclosing red-brown, amoeboid spinel. The orthopyroxenite consists of equant, kinked grains of orthopyroxene, 4 to 5 mm in diameter. Extensive subsolidus exsolution of clinopyroxene is indicated by concentrations of small clinopyroxene grains (less than 0.2 mm) along boundaries and in linear zones within orthopyroxene crystals. Reddish-green spinel is anhedral and interstitial. Spinel clinopyroxenite consists of large, to 5 mm diameter, clinopyroxene grains with wormy exsolution lamellae of spinel and smaller (to 2 mm diameter) anhedral grains of orthopyroxene.

(B) Pyroxenites

13004, 13007: garnet-bearing amphibole pyroxenites, subhedral to euhedral black spinel (13%) (less than 0.3 mm) enclosed in clinopyroxene (48%; 0.2 to 1 mm) and oikocrysts of amphibole (36%; to 3 mm) with minor orthopyroxene (1.2%) and garnet (1.5%). Modes refer to 13004. In places the clinopyroxene is embayed adjacent to amphibole and contains wisps of amphibole. Exsolution lamellae of orthopyroxene

in clinopyroxene and rare spinel (?) in amphibole occur. Garnet is distributed heterogeneously and is absent from amphibole-rich regions.

13002, 13005: Coarse grained pyroxenites composed predominantly of clinopyroxene (62%, 1-2 mm) and amphibole (38%, more than 1 cm diameter) with minor spinel (0.5%), phlogopite (tr) and orthopyroxene (1.3%). Mode refers to 13002. Lamellae of orthopyroxene and spinel are common in clinopyroxene and amphibole respectively. Clinopyroxenes are occasionally complexly zoned with a core rich in exsolution lamellae, and a rim free of such lamellae.

(C) Basalts

The basalts on Nunivak range in composition from olivine tholeiites with normative hypersthene to basanites with more than 5% normative nepheline (nomenclature of Green and Ringwood, 1967). They contain up to 10% olivine phenocrysts commonly with chromite inclusions, ± augite phenocrysts, and rarely plagioclase phenocrysts. The groundmass is subophitic to intersertal and dikytaxitic and consists of plagioclase, olivine, clinopyroxene, oxides, and glass (Hoare et al., 1968). Analcime and nepheline have been identified in the groundmass of some basanites (Mark, 1971). Xenolithic debris is also common in some basanites. The specific characteristics of the basalts studied here are shown in Table 3-1; the reader is referred to Hoare et al. (1968) for further descriptions of the basalts.

Table 3-1. Basalt petrography.

| Sample | Rock type | Phenocrysts (maximum dimension in mm) | | | | |
|---|---|---|---|---|---|---|
| | | olivine | chromite | clinopyroxene | plagiocluse | Xenolithic debris |
| B-1 | olivine tholeiite | 1.5 | abundant | np | np | np |
| B-12 | olivine tholeiite | 2 | abundant | np | np | np |
| B-5 | olivine tholeiite | 1 | np(?) | 1[g] | np | metamorphic wehrlites and clinopyroxenites |
| B-6 | basanite | 1 | abundant | 1 | np | np |
| B-7 | basanite | 1 | np(?) | 1[g] | np | abundant peridotites |
| B-9 | basanite | 1 | rare | 0.5 | np | abundant peridotites |
| B-10 | basanite | 2 | present | np | np | rare |
| B-13 | basanite | 1.5 | present | 0.5[g] | np | rare (?) |

---

np stands for "not present"

g indicates that glomerocrysts are common

Table 3-1. Basalt petrography, continued.

| Sample | Groundmass | Comments |
|---|---|---|
| B-1 | intersertal: plagioclase + clinopyroxene + magnetite + ilmenite + mesostasis | |
| B-12 | intergranular: plagioclase + clinopyroxene + magnetite + ilmenite | |
| B-5 | intersertal: plagioclase + clinopyroxene + magnetite + ilmenite + mesostasis | glomerocrysts of clinopyroxene are very common |
| B-6 | intersertal: plagioclase + clinopyroxene + magnetite + ilmenite + mesostasis | broken hopper crystals of olivine are common |
| B-7 | intersertal: plagioclase + clinopyroxene + magnetite + mesostasis | "green-cored" and spongy clinopyroxenes are common |
| B-9 | intersertal: plagioclase + clinopyroxene + magnetite + mesostasis | skeletal olivine phenocrysts |
| B-10 | intersertal: plagioclase + clinopyroxene + magnetite + mesostasis | |
| B-13 | intersertal: plagioclase + clinopyroxene + magnetite + mesostasis | flow aligned olivine + plagioclase; vesicles lined with analcime (?) |

## IV. Analytical Methods

Rocks were slabbed and then sanded with silicon carbidesand paper. Slabs were crushed in a steel jaw crusher and then ground to finer than 100 mesh in an agate grinder. Some samples (10002, 10004, 10006, 10008) were powdered in a tungsten carbide ball mill during the course of previous studies. Co contents in these samples may be elevated due to contamination from the grinding vessel.

Mineral separates were obtained by handpicking a coarse 16-40 mesh size. This rough separate was then crushed in a steel percussion mortar and a final separate obtained by handpicking the 40-60 mesh size. Final separates were essentially 100% pure with the following qualifications: (1) some of the clinopyroxene separates (10002, 10004, 10067) contain fluid and/or mineral inclusions (see following section "Results" and Francis 1976b), (2) the 10067 amphibole separate contains spinel inclusions (see Francis 1976b), (3) the 10002 glass separate contains spinel and quench silicate grains (see Francis 1976b). Clinopyroxene separates were leached for 10 minutes in 2.5 N HCl at 50°C and 20 minutes in 5% HF at 50°C (see Shimizu, 1974). The amphibole and glass separates were leached only in 2.5 N HCl. All the reagents used during the leaching were doubly distilled.

Most of the analyses were performed using standard analytical techniques described previously. The basalts were analyzed for major elements by X-ray fluorescence (X-ray Assay Labs, Francis, 1976a). The whole rock analyses are normalized to 100% water-free, and the $Fe^{2+}/Fe^{3+}$ (atomic) ratio has been set at 3:1. This ratio is

reasonable in view of the $Fe^{2+}/Fe^{3+}$ ratios of analyzed fresh basalts (e.g., Carmichael et al., 1974), and has been used in previous studies of alkali basalts (Sun and Hanson, 1975; Kesson, 1973). The electron microprobe analyses were performed either using the MIT MAC probe or a JEOL probe at Cornell Univ. using Bence-Albee reduction schemes. Ion probe analyses were obtained on the MIT-Harvard-Brown Cameca IMS-3F under the supervision of N. Shimizu and using the energy filtering technique described in Shimizu et al. (1978).

K, Rb, Sr, Ba, and Cs were analyzed by isotope dilution according to the methods described in Hart and Brooks (1977). Based on triplicate analyses of K, Rb, Sr, and Ba in MORB basalt standard A II 92-29-1, precision of individual analyses is less than 1% for K, Sr, and Ba, and less than 2% for Rb at the 95% confidence level (Table 3-2). Precision of K, Rb, and Ba analyses for samples with very low concentrations of these elements (20 ppm or less K, 0.5 ppm or less Rb, 2.5 ppm or less Ba for a nominal 50 mg sample) is higher (approximately ± 5% based on duplicate measurements of Rb concentrations in Nunivak granulites, Table 2-2) due to variation in the blank (see below) and the problem of "error magnification": the increased sensitivity of the calculated concentration to the measured isotopic ratio at very low natural K, Rb, or Ba to spike K, Rb, or Ba ratios. The Rb and Sr concentrations of U.S. Geological Survey standard dunite DTS-1 reported here (Table 3-2) are within 10% of the "preferred" values, 0.053 ppm Rb and 0.35 ppm Sr, of Flanagan (1976).

Because of the low concentrations measured in some samples, the blank contribution to the observed concentration can be significant.

Table 3-2. Standard analyses (ppm).

| | A II 92-29-1[1] | A II 92-29-1[2] | DTS-1 | PCC-1[3] | BCR-1[4] |
|---|---|---|---|---|---|
| K | 1326 ± 4 | | 9.49 | | |
| Sc | 38.8 ± 2.6 | | 3.56 | | |
| Cr | 246 ±20 | | 4350 | | |
| Co | 58.1 ± 3.6 | | 144 | | |
| Rb | 1.20 ± 0.02 | | 0.058 | | |
| Sr | 131.7 ± 1.2 | | 0.320 | | |
| Cs | 0.028 | | 0.0068 | | |
| Ba | 5.20 ± 0.04 | | 0.323* | | |
| La | 4.00 ± 0.30 | 3.97 ± 0.34 | 0.024 | 0.034 ± 0.004 | 25.1 |
| Ce | 13.1 ± 0.8 | 13.7 ± 1.0 | | | 54.1 |
| Nd | 12.1 ± 1.2 | 11.6 ± 0.6 | | | 28.7 |
| Sm | 4.20 ± 0.24 | 4.05 ± 0.24 | 0.004 | 0.007 ± 0.002 | 6.63 |
| Eu | 1.47 ± 0.12 | 1.51 ± 0.06 | 0.002 | 0.003 ± 0.001 | 1.97 |
| Tb | 1.01 ± 0.18 | 0.99 ± 0.26 | | | 1.03 |
| Yb | 3.95 ± 0.32 | 3.90 ± 0.32 | 0.011 | 0.025 ± 0.003 | 3.46 |
| Lu | 0.62 ± 0.04 | 0.60 ± 0.04 | 0.003 | 0.006 ± 0.001 | 0.54 |

Table 3-2. Footnotes.

All errors are at the 95% confidence level except for PCC-1 for which the errors represent the average deviation from the mean for 2 analyses.

*indicates that the blank correction amounted to more than 10%.

1. MORB standard (Staudigel, 1980). Mean of 3 analyses (Roden) for K, Rb, Ba, Sr; mean of 7 analyses (4 by Roden, 3 by S. Roy and F. Frey) for Co, Cr, and Sc; mean of 5 RNAA analyses (Roden) for REE.

2. Mean of 5 INAA analyses (2 by Roden, 3 by S. Roy and F. Frey).

3. Mean of two RNAA analyses.

4. Average of isotope dilution analyses (except for Tb) from the literature (F.A. Frey, written communication, 1981). Tb value is average of INAA analyses from the literature (F.A. Frey, written communication, 1981).

Five blanks measured during the course of this study show ranges of: K, 73 to 13 ngm; Rb, 0.09 to 0.02 ngm; Sr, 1.9 to 0.3 ngm; Ba, 2.9 to 2.8 ngm; and Cs, approximately 0.6 pgm. This variation is significant, although most of the high values result from a single blank that may have been catastrophically contaminated. Nominal blank corrections of -20 ngm K, -0.05 ngm Rb, -2.8 ngm Ba, -0.5 ngm Sr, and -0.6 pgm Cs have been applied to all samples where the blank contributes more than 0.5% to the measured concentration. Because of the variation in the measured blank, this blank correction can introduce a significant error where the blank correction is large. All concentrations where the blank correction is greater than 10% are indicated by an asterisk (*); these values should be interpreted with caution.

Sc, Cr, Co, REE, Hf, Ta, and Th were analyzed by neutron activation techniques, either instrumentally (INAA) or radiochemically (RNAA). The INAA technique was described in detail by Frey et al. (1974; 1980). The precision of this technique can be estimated from 5 replicate analyses for the REE and 7 replicate analyses for Sc, Co, and Cr on mid-ocean ridge basalt standard A II 92-29-1 (Table 3-2). The precision is better than 10% at the 95% confidence level for all elements except Tb. The absolute values compare well with the values reported in Staudigel (1980). REE concentrations in the peridotites and pyroxenites were measured by a RNAA technique described in Hickey and Frey (1981). U.S. Geological Survey standard BCR-1 was used as the primary standard; thus the REE data for the peridotites and pyroxenites

are reported relative to the values for BCR-1 in Table 3-2. These BCR-1 values are averages of isotope dilution analyses of BCR-1 from the literature (F.A. Frey, written communication, 1981). There are no significant differences between the average of 5 INAA analyses of A II 92-29-1 and 5 RNAA analyses of the same standard performed during the course of this study (Table 3-2), although the INAA analyses are reported relative to a synthetic standard. Based on the replicate analyses by RNAA of A II 92-29-1, the precision for the two methods is approximately the same (Table 3-2) in spite of an additional yield correction being applied to the RNAA data. Better counting statistics for the RNAA technique apparently counterbalances any error introduced due to uncertainty in the yield of the radiochemical procedure. Precisions for the peridotites can be estimated from four replicate analyses of peridotite 10070 (Table 5) which indicate precisions ($2\sigma$) of 10 to 20% for La, Ce, Nd, and Tb and less than 10% for Sm, Eu, Yb, and Lu. For rocks with very low REE concentrations such as U.S. Geological Survey standards PCC-1 and DTS-1, precision is considerably worse, and on the order of 50% for La, Sm, and Eu, and 20% for Yb and Lu based on duplicate analyses of PCC-1 (Table 3-2).

Isotopic ratios were measured on a nine-inch mass spectrometer at MIT. The methods for Sr and Nd are described in Hart and Brooks (1977) and Zindler et al. (1979) respectively. The Nd technique follows that of Richard et al. (1976). The isotopic ratios are normalized to $^{86}Sr/^{88}Sr = 0.1194$ and $^{146}Nd/^{144}Nd = 0.7219$, and are reported relative to Eimer and Amend standard $^{87}Sr/^{86}Sr = 0.70800$ and

BCR-1 $^{143}Nd/^{144}Nd = 0.51264$. The errors are quoted at the 95% confidence level based on within-run statistics.

## V. Results

### (A) Summary

Our results are given in the following three sections but we summarize our most important observations in this paragraph. Firstly, the GE inclusions have convex-upward chondrite-normalized REE patterns with La/Yb ratios less than chondrites (Figure 3-4). These inclusions have $^{87}Sr/^{86}Sr$ and $^{143}Nd/^{144}Nd$ ratios within the range of normal MORBs (Figure 3-11). Secondly, the CE, CT, ACE, and ACT inclusions have La/Yb ratios greater than chondrites (Figures 3-5, 3-6) and have $^{87}Sr/^{86}Sr$ and $^{143}Nd/^{144}Nd$ ratios in the range of oceanic island basalts and some MORBs (Figure 3-11). Thirdly, the $^{87}Sr/^{86}Sr$ and $^{143}Nd/^{144}Nd$ ratios of the amphibole-pyroxenites and the ACE and ACT peridotites lie within the field defined by the Nunivak basalts $^{143}Nd/^{144}Nd$ versus $^{87}Sr/^{86}Sr$ diagram (Figure 3-11). Fourthly, subhedral apatite inclusions and several types of fluid inclusions in clinopyroxene correlate with high incompatible element concentrations in the ACE and ACT inclusions. These apatites have high concentrations of the LREE and Sr relative to the host clinopyroxene.

### (B) Peridotites

#### (1) Trace element abundances

REE element abundances in the Nunivak peridotites correlate with

the textural groups of Francis (1978). The GE inclusions have La/Yb ratios less than chondrites with Yb = 2 to 3 x chondrites and La = 0.8 to 1.1 x chondrites (Table 3-3, Figure 3-4). Leached clinopyroxenes separated from these inclusions have chondrite-normalized REE patterns similar to the whole rock patterns but displaced to higher concentrations with Yb = 12 to 15 x chondrites and La = 3.8 to 5.6 x chondrites (Figure 3-4). Similar relatively LREE depleted inclusions occur at other continental inclusion localities such as Kilbourne Hole (Jagoutz et al., 1979), Dreiser Weiher (Stosch and Seck, 1980), and Green Knobs (Chapter 4).

In contrast to the GE inclusions, the CE, CT, ACE, and ACT inclusions are heterogeneous in terms of both their absolute and relative REE abundances although all have La/Yb ratios greater than chondrites (Table 3-5, Figures 3-5, 3-6). There is no obvious correlation between textural group and REE pattern relative to chondrites. However, the ACE and ACT inclusions have higher concentrations of the LREE than the CE or CT inclusions. The CE, CT, and many of the ACE and ACT inclusions have REE patterns with La/Ce ratios greater than chondrites, a steep, negative slope from La to Tb, and an essentially flat pattern from Tb to Lu on chondrite-normalized REE plots (Figures 3-5, 3-6). Note that sample 10075 is an exception to the above generalization in that it has an essentially constant, negative slope from La to Lu. Some ACE and ACT inclusions, e.g., 10051 (Figure 3-6) have La/Ce ratios less than chondrites and have chondrite-normalized REE patterns with a maximum in the vicinity of

Table 3-3. Trace element abundances (ppm) of the GE inclusions.

| | 10068 cpx | 10068 wr | 10070 cpx | 10070[1] wr |
|---|---|---|---|---|
| K | 22.0 | 16.5 | 28.8 | 9.01 |
| Sc | | 16.0 | | 15.9 |
| Cr | | 2799 | | 2370 |
| Co | | 110 | | 112 |
| Rb | 0.0603 | 0.107 | 0.021* | 0.011* |
| Sr | 72.2 | 12.9 | 93.2 | 15.8 |
| Cs | 0.0081 | 0.013 | 0.0045 | 0.00058 |
| Ba | 0.37* | 0.559 | | 0.834 |
| La | 0.92 | 0.26 | 1.37 | 0.267 ± 0.050 |
| Ce | 3.8 | 1.1 | 5.5 | 0.99 ± 0.18 |
| Nd | 4.0 | 0.76 | 6.1 | 0.99 ± 0.14 |
| Sm | 2.05 | 0.29 | 2.07 | 0.345 ± 0.024 |
| Eu | 0.823 | 0.121 | 0.859 | 0.146 ± 0.010 |
| Tb | 0.54 | 0.080 | 0.56 | 0.099 ± 0.012 |
| Yb | 2.46 | 0.39 | 2.26 | 0.455 ± 0.034 |
| Lu | 0.36 | 0.061 | 0.35 | 0.074 ± 0.006 |

cpx = clinopyroxene and wr = whole rock

*indicates that the blank correction amount to more than 10%

1. REE abundances are average of four analyses. Errors are quoted at the 95% confidence level.

Table 3-3. Continued.

| | 10026 cpx | 10026 wr | 10211 cpx |
|---|---|---|---|
| K | 5.0* | 102 | |
| Sc | | 15.9 | |
| Cr | | 2891 | |
| Co | | 112 | |
| Rb | 0.0087* | 0.090 | |
| Sr | 64.0 | 12.0 | |
| Cs | 0.00042 | | |
| Ba | 0.59* | 1.74 | |
| La | | 0.20 | 0.97 |
| Ce | | 0.83 | 4.4 |
| Nd | | 0.84 | 4.3 |
| Sm | | 0.28 | 1.75 |
| Eu | | 0.116 | 0.752 |
| Tb | | 0.078 | 0.46 |
| Yb | | 0.38 | 2.04 |
| Lu | | 0.060 | 0.31 |

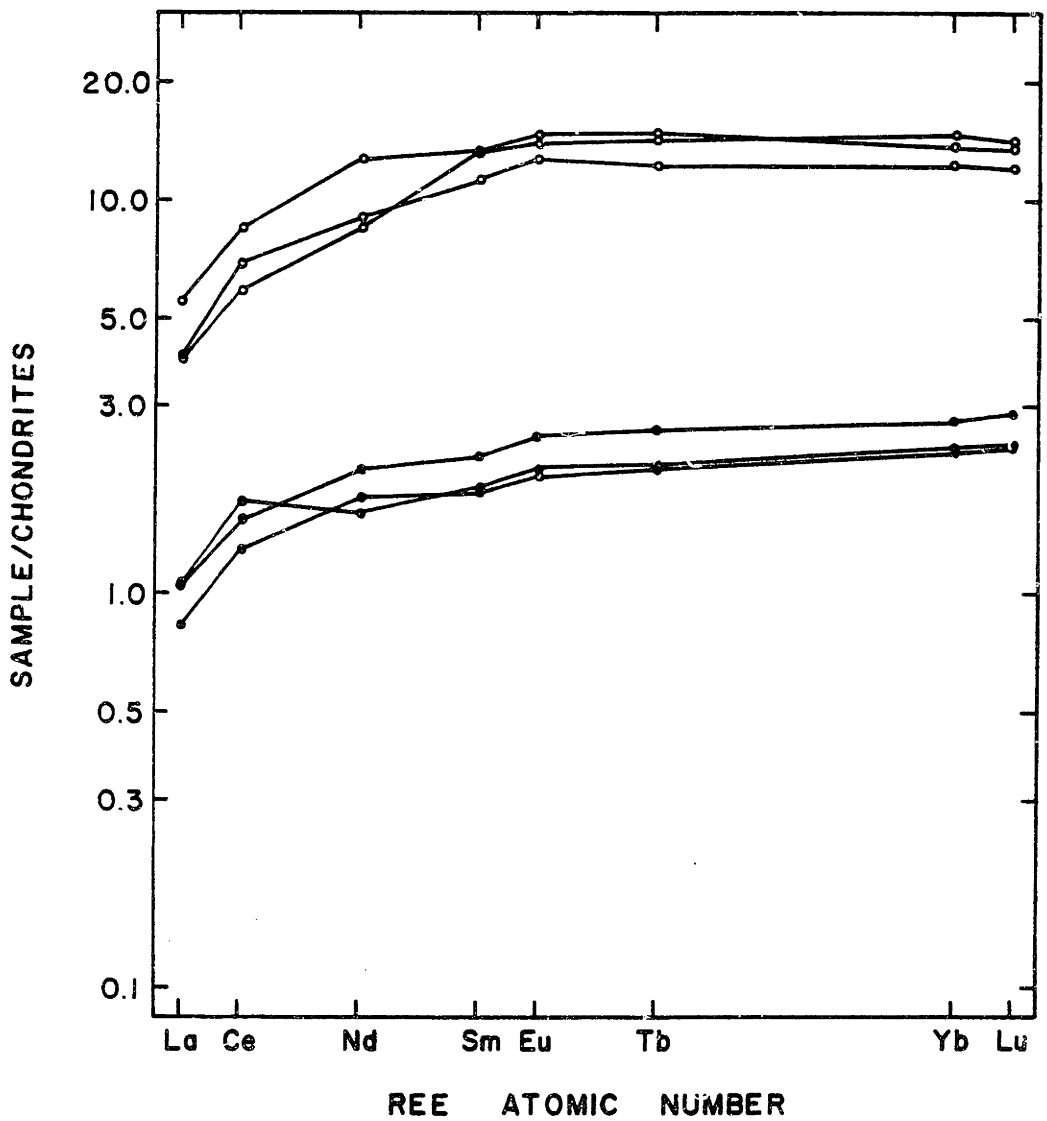
20.0
10.0
5.0
3.0
1.0
0.5
0.3
0.1
SAMPLE/CHONDRITES
La
Ce
Nd
Sm
Eu
Tb
Yb
Lu
REE ATOMIC NUMBER

Figure 3-4. REE abundances of GE inclusions (●) and clinopyroxenes (o) normalized to chondrites. Chondrite values from Evensen et al. (Table 3, "CI Average", 1978).

Table 3-4. Mass balance calculations.

Percentage of bulk rock elemental abundance contained in clinopyroxene (cpx) and glass (gl)

| textural group | 10070 cpx GE | 10068 cpx GE | 10004 cpx CT | 10002 cpx ACE | 10002 gl ACT |
|---|---|---|---|---|---|
| K | 40 | 19 | 1.4 | 0.4 | |
| Rb | 25 | 8 | 1.3 | 0.3 | |
| Sr | 74 | 79 | 78 | 56 | |
| Ba | | 9.3 | 4.3 | 1.0 | |
| La | 65 | 49 | 86 | 35 | 58 |
| Ce | 70 | 49 | 85 | 44 | 60 |
| Nd | 78 | 75 | 96 | 49 | 60 |
| Sm | 76 | 101 | 111 | 50 | 66 |
| Eu | 74 | 97 | 115 | 51 | 69 |
| Tb | 71 | 97 | 85 | 43 | 61 |
| Yb | 63 | 89 | 61 | 52 | 47 |
| Lu | 60 | 84 | 57 | 53 | 47 |

Table 3-5. Trace element abundances (ppm) of CE, CT, ACE, and ACT inclusions.

| | 10007 wr | 10004[1] wr | 10004 cpx | 10008 wr | 10006[1] wr |
|---|---|---|---|---|---|
| textural group | CE | CT | CT | CT | ACE |
| K | 118 | 172 | 28.6 | 80.4 | 195 |
| Sc | 7.53 | 12.4 | | 10.7 | 11.0 |
| Cr | 2535 | 3059 | | 2877 | 2591 |
| Co | 127 | 114 | | 118 | 113 |
| Rb | 0.0577 | 0.0419 | 0.0639 | 0.187 | 0.215 |
| Sr | 12.2 | 31.1 | 285 | 11.0 | 53.5 |
| Cs | 0.00081 | | 0.0094 | 0.0034 | 0.0021 |
| Ba | 7.88 | 8.05 | 4.08 | 3.79 | 6.93 |
| La | 0.29 | 0.91 ±0.04 | 9.26 | 0.88 | 8.3 ±0.7 |
| Ce | 0.70 | 2.5 ±0.1 | 25.0 | 1.6 | 14.0 ±0.9 |
| Nd | | 1.1 ±0.05 | 12.6 | 0.68 | 4.6 ±0.6 |
| Sm | 0.061 | 0.180 ±0.001 | 2.36 | 0.099 | 0.54 ±0.04 |
| Eu | 0.020 | 0.060 ±0.000 | 0.815 | 0.033 | 0.156 ±0.007 |
| Tb | 0.008 | 0.036 ±0.002 | 0.362 | 0.019 | 0.052 ±0.002 |
| Yb | 0.037 | 0.188 ±0.002 | 1.34 | 0.097 | 0.190 ±0.002 |
| Lu | 0.0075 | 0.032 ±0.002 | 0.21 | 0.017 | 0.033 ±0.001 |

cpx = clinopyroxene and wr = whole rock

1. Errors indicate deviation from the mean of two analyses.

Table 3-5. Continued.

| | 10002 wr | 10002 cpx | 10002 gl | 10055[1] wr |
|---|---|---|---|---|
| textural group | ACE | ACE | ACE | ACE |
| K | 206 | 11.3 | | 682 |
| Sc | 13.1 | | | 7.78 |
| Cr | 3174 | | | 2666 |
| Co | 115 | | | 124 |
| Rb | 0.226 | 0.0098 | | 0.323 ±0.001 |
| Sr | 82.2 | 676 | | 50.0 |
| Cs | 0.0027 | 0.0018 | | 0.0032 |
| Ba | 7.03 | 1.04 | | 3.68 |
| La | 3.65 | 18.8 | 23.9 | 1.68 |
| Ce | 6.5 | 42.1 | 44.2 | 4.9 |
| Nd | 2.1 | 15.0 | 13.9 | 3.3 |
| Sm | 0.25 | 1.80 | 1.83 | 0.77 |
| Eu | 0.084 | 0.628 | 0.648 | 0.258 |
| Tb | 0.030 | 0.19 | 0.20 | 0.11 |
| Yb | 0.145 | 1.11 | 0.76 | 0.320 |
| Lu | 0.24 | 0.19 | 0.13 | 0.52 |

---

cpx = clinopyroxene, gl = glass, wr = whole rock

error for 10055 indicates deviation from the mean for duplicate analyses.

Table 3-5. Continued

| | 10051[1] wr | 10051 cpx | 10075 wr | 10067 amp | 10067 cpx |
|---|---|---|---|---|---|
| textural group | ACT | ACT | ACT | ACT | ACT |
| K | 1065 | | 968 | | |
| Sc | 7.75 | | 11.7 | | |
| Cr | 2817 | | 2967 | | |
| Co | 121 | | 115 | | |
| Rb | 2.83 | | 1.9 | | |
| Sr | 42.4 | | 67.1 | | |
| Cs | 0.023 | | 0.019 | | |
| Ba | 27.1 | | 42.3 | | |
| La | 1.48 ±0.11 | 13.5 | 3.59 | 16.1 | 12.1 |
| Ce | 4.6 ±0.3 | 47.2 | 8.5 | 41.9 | 34.9 |
| Nd | 3.3 ±0.2 | 40.7 | 5.3 | 23.1 | 23.0 |
| Sm | 0.82 ±0.08 | 10.3 | 1.22 | 5.06 | 5.22 |
| Eu | 0.262 ±0.013 | 3.44 | 0.390 | 1.72 | 1.77 |
| Tb | 0.12 ±0.01 | 1.42 | 0.16 | 0.685 | 0.730 |
| Yb | 0.284 ±0.003 | 3.15 | 0.396 | 1.74 | 2.16 |
| Lu | 0.045 ±0.001 | 0.48 | 0.060 | 0.27 | 0.33 |

cpx = clinopyroxene, wr = whole rock, amp = amphibole

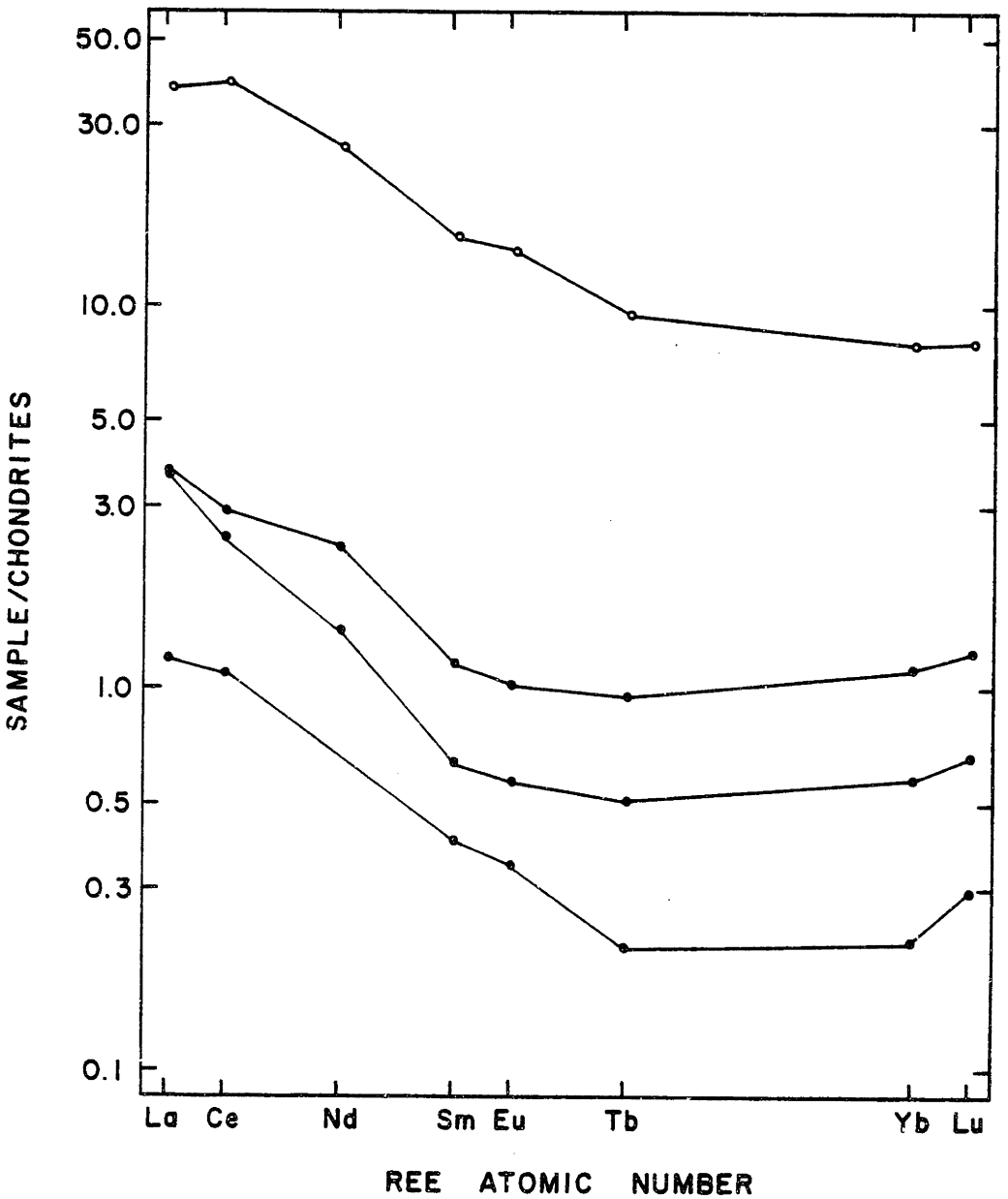
50.0
30.0
10.0
5.0
3.0
1.0
0.5
0.3
0.1
SAMPLE/CHONDRITES
La
Ce
Nd
Sm
Eu
Tb
Yb
Lu
REE ATOMIC NUMBER

Figure 3-5. Chondrite-normalized REE abundances of CT and CE inclusions (●) and 10004 clinopyroxene (o).

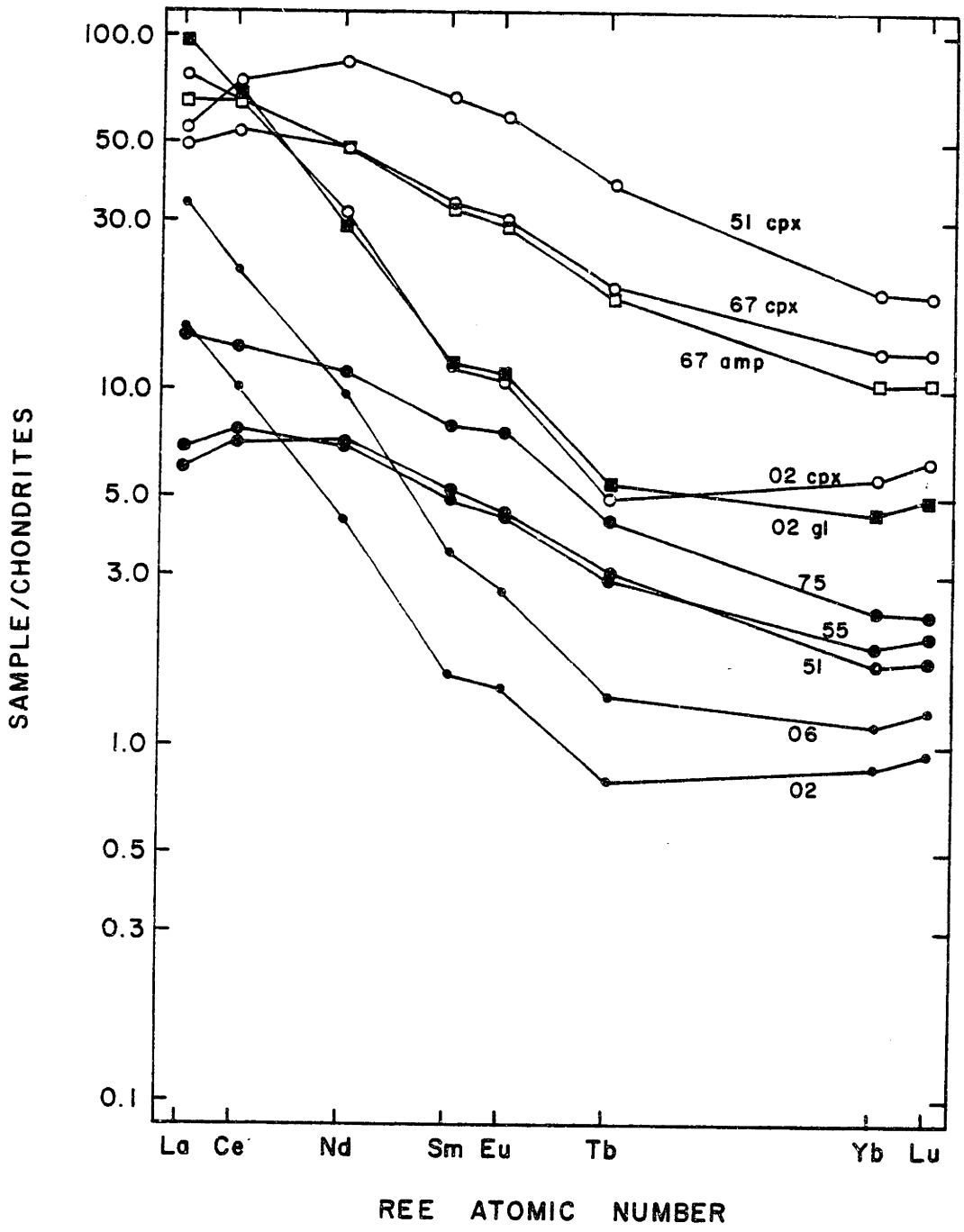
100.0
50.0
30.0
10.0
5.0
3.0
1.0
0.5
0.3
0.1
SAMPLE/CHONDRITES
51 cpx
67 cpx
67 amp
02 cpx
02 gl
75
55
51
06
02
La
Ce
Nd
Sm
Eu
Tb
Yb
Lu
REE ATOMIC NUMBER

Figure 3-6. Chondrite-normalized abundances of ACT and ACE inclusions and their constituent minerals. First three digits are left off sample numbers. "Cpx" indicates clinopyroxene, "gl" indicates glass, and "amp" indicates amphibole.

Figure 3-6. Chondrite-normalized abundances of ACT and ACE inclusions and their constituent minerals. First three digits are left off sample numbers. "Cpx" indicates clinopyroxene, "gl" indicates glass, and "amp" indicates amphibole.

Ce or Nd, and a negative, near constant slope from Nd to Lu (Figure 3-6).

Acid-leached minerals have chondrite-normalized REE patterns which mimic the bulk rock patterns (Figures 3-5, 3-6), and thus, indicate that the distinction drawn above on the basis of La/Ce ratios is an inherent feature of individual inclusions and not related to basalt-inclusion interaction (e.g., compare 10051 clinopyroxene to 10051 whole rock, Figure 3-6).

The relative REE abundances in an amphibole-clinopyroxene pair is similar to the relative REE abundances in a glass-clinopyroxene pair (Figure 3-7), thus confirming the conclusion of Francis (1976b) that the glass formed by melting of interstitial amphibole during transport to the surface. The nearly constant ratio of REE abundances between clinopyroxene and amphibole is consistent with the relative partitioning of the REE in these minerals (e.g., see summary in Frey and Prinz, 1978). However, the abundance of the REE in clinopyroxene relative to amphibole is higher then would be predicted from mineral/melt partition coefficients; this result is probably the consequence of the presence of apatite inclusions in 10002 and 10067 clinpyroxene.

A final point to note with regard to the REE is the complexity of the REE patterns exhibited by the clinopyroxenes separated from composite inclusion 10056 (Table 3-6; Figure 3-8). The peridotite clinopyroxene has a high La/Yb ratio relative to chondrites, and a REE pattern similar to 10002 clinopyroxene (Figure 3-6); these

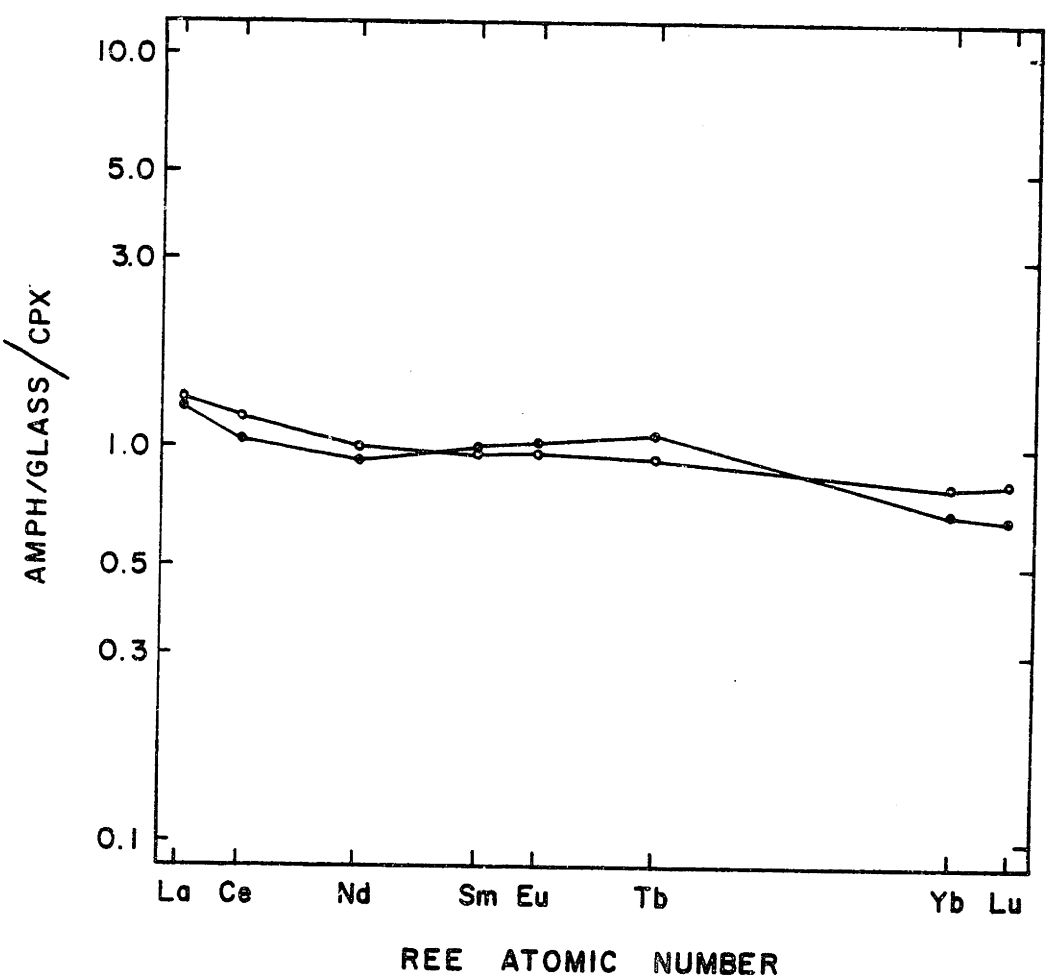
10.0
5.0
3.0
1.0
0.5
0.3
0.1
AMPH/GLASS / CPX
La
Ce
Nd
Sm
Eu
Tb
Yb
Lu
REE ATOMIC NUMBER

Figure 3-7. REE abundances of 10002 glass (●) and 10067 amphibole (⊙) normalized to the REE abundances of their respective coexisting clinopyroxenes.

Table 3-6. REE abundances (ppm) in composite inclusion 10056.

| | peridotite clinopyroxene | clinopyroxenite clinopyroxene |
|---|---|---|
| La | 25.1 | 2.99 |
| Ce | 48.3 | 3.7 |
| Nd | 17.0 | 0.99 |
| Sm | 3.15 | 0.264 |
| Eu | 1.01 | 0.171 |
| Tb | 0.364 | 0.13 |
| Yb | 1.51 | 0.735 |
| Lu | 0.22 | 0.12 |

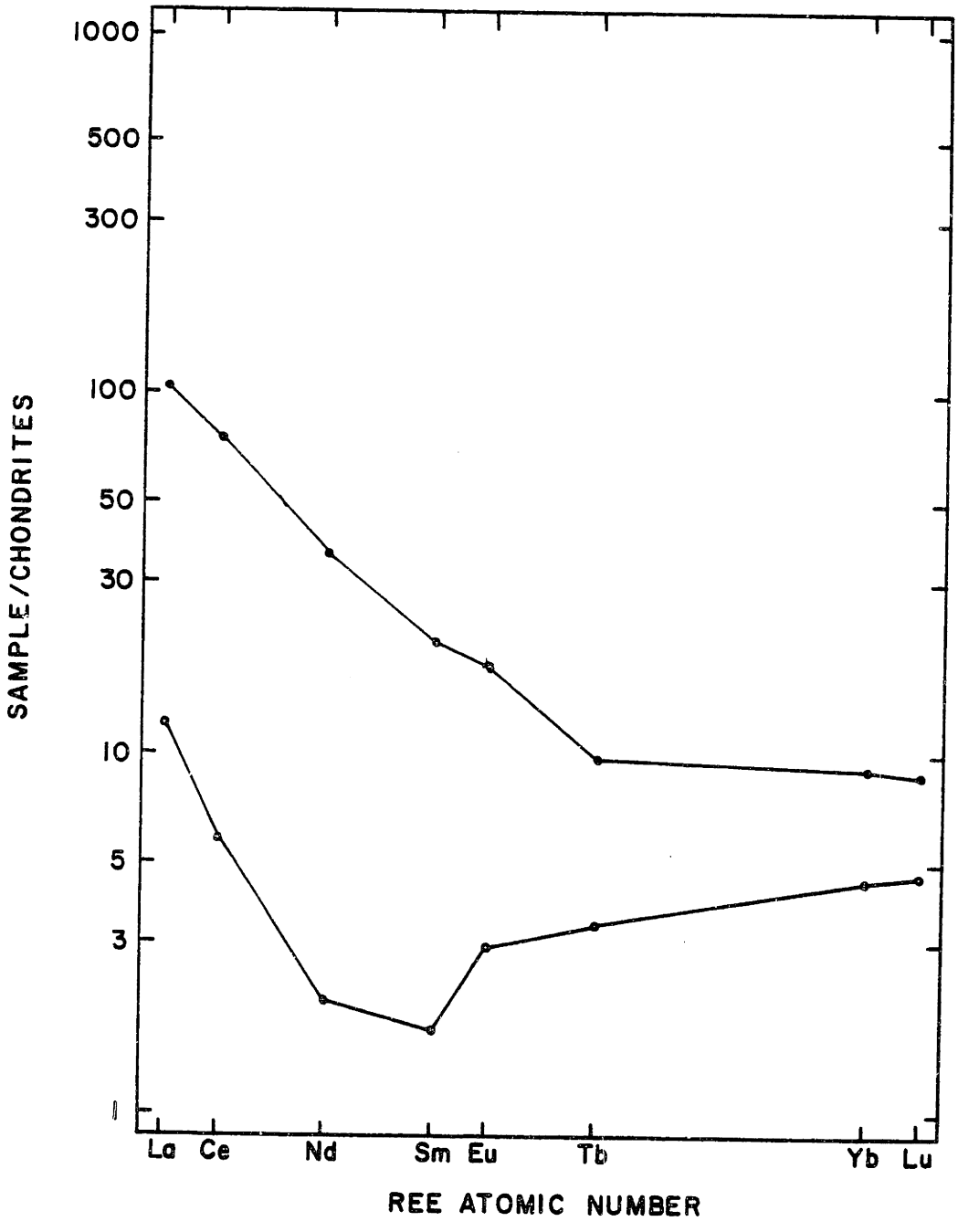
1000
500
300
100
50
30
10
5
3
1
SAMPLE/CHONDRITES
La
Ce
Nd
Sm
Eu
Tb
Yb
Lu
REE ATOMIC NUMBER

Figure 3-8. Chondrite-normalized REE abundances of peridotite clinopyroxene (•) and clinopyroxenite clinopyroxene (o) from composite inclusion 10056.

observations are consistent with both the coarse-equant texture of the peridotite and the major element composition (Table 3-7) of the clinopyroxene (see Figure 4 of Francis, 1978). In contrast, the clinopyroxene separated from the clinopyroxenite of 10056 has a complex chondrite-normalized REE pattern (Figure 3-7) with a minimum at Nd and a La/Yb ratio greater than chondrites. The latter clinopyroxene is more calcic and aluminous but less sodic than the peridotite clinopyroxene (Table 3-7).

Concentrations of the other incompatible elements (K, Rb, Ba, Sr) correlate positively with La concentration in the CE, CT, ACE, and ACT inclusions. For example, relative to an average of the GE inclusions (Table 3-8, Figure 3-9), the CE, CT, ACE, and ACT inclusions are enriched in Rb, Ba, Sr, and K in a manner broadly consistent with relative incompatibilities (Wood, 1979) although Rb and Ba abundances are lower relative to K then would be predicted from relative incompatibilities. The ACE and ACE inclusions are more highly enriched in incompatible elements than the CE and CT inclusions (Figure 3-9). In the case of the compatible elements Sc, Cr, and Co, Sc has lower and Cr and Co have slightly higher concentrations in the CE, CT, ACE, and ACT groups relative to the GE inclusions (Figure 3-9).

Overall, the GE inclusions bear a remarkable similarity to the "primitive", relatively LREE depleted inclusions described by Jagoutz et al. (1979), while the CE, CT, ACT, and ACE groups are similar to metasomatized inclusions from Dreiser Weiher (Stosch and Seck, 1980), San Carlos (Frey and Prinz, 1978), and Victoria (Frey and Green, 1974).

Table 3-7. Average clinopyroxene analyses (wt. %) from composite inclusion 10056.

| | peridotite | clinopyroxenite |
|---|---|---|
| $SiO_2$ | 54.8 | 52.9 |
| $TiO_2$ | 0.10 | 0.12 |
| $Al_2O_3$ | 3.79 | 4.56 |
| $Cr_2O_3$ | 0.50 | 0.16 |
| FeO | 2.50 | 2.78 |
| MnO | 0.11 | 0.11 |
| MgO | 16.0 | 16.8 |
| CaO | 20.6 | 23.6 |
| $Na_2O$ | 1.90 | 0.30 |
| $K_2O$ | 0.02 | 0.02 |
| Total | 100.3 | 101.4 |
| Atomic proportions[1] | | |
| Si | 1.964 | 1.892 |
| Ti | 0.003 | 0.003 |
| Al | 0.160 | 0.192 |
| Cr | 0.014 | 0.005 |
| Fe | 0.075 | 0.083 |
| Mn | 0.003 | 0.003 |
| Mg | 0.857 | 0.896 |
| Ca | 0.791 | 0.903 |
| Na | 0.132 | 0.021 |
| K | 0.001 | 0.001 |
| Total | 3.997 | 3.999 |

Analyst: D.M. Francis

1. Normalized to 6 oxygens

Table 3-8. Average trace element abundances (ppm) for various Nunivak rock types.

| | GE[1] | CT, CE | ACT, ACE | basalts average | basalts range |
|---|---|---|---|---|---|
| K | 12.8 | 123 | 489 | 12780 | 6988-20988 |
| SC | 15.9 | 10.2 | 10.3 | 21 | 15.6-25.4 |
| Cr | 2670 | 2824 | 2843 | 300 | 203-348 |
| Co | 111 | 120 | 118 | 52 | 41.1-58.2 |
| Rb | 0.059 | 0.22 | 1.06 | 25 | 10.9-45.7 |
| Sr | 13.6 | 18.1 | 51.4 | 698 | 469-1046 |
| Ba | 0.70 | 6.6 | 13.7 | 334 | 187-541 |
| La | 0.24 | 0.70 | 3.73 | 29 | 13-56 |
| Ce | 0.97 | 1.6 | 7.7 | 60 | 30-101 |
| Nd | 0.86 | 0.70 | 3.7 | 26 | 17-39 |
| Sm | 0.30 | 0.11 | 0.72 | 5.7 | 4.2-7.4 |
| Eu | 0.13 | 0.038 | 0.23 | 2.1 | 1.6-2.6 |
| Tb | 0.085 | 0.021 | 0.094 | 0.86 | 0.73-1.0 |
| Yb | 0.41 | 0.11 | 0.27 | 1.8 | 1.6-2.3 |
| Lu | 0.065 | 0.019 | 0.043 | 0.27 | 0.23-0.34 |

1. K, Rb, and Ba abundances of 10026 are not included in the average because this sample is iddingsitized.

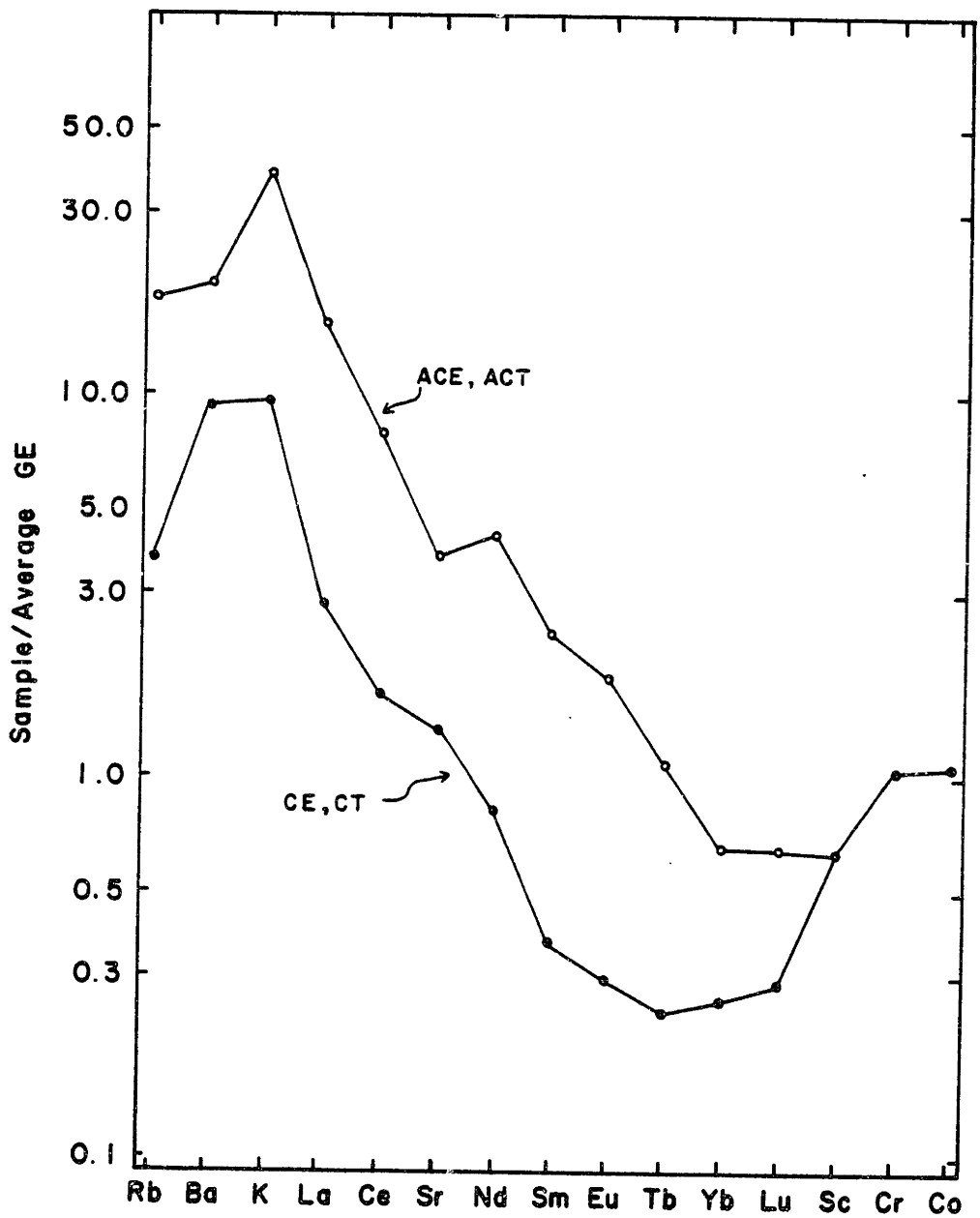
50.0
30.0
10.0
5.0
3.0
1.0
0.5
0.3
0.1
Sample/Average GE
ACE, ACT
CE, CT
Rb Ba K La Ce Sr Nd Sm Eu Tb Yb Lu Sc Cr Co

Figure 3-9. Average trace element abundances (Table 3-8) of ACE and ACT (ⓞ), and CT and CE (●) inclusions normalized to the average for the GE inclusions.

(2) Isotopic ratios

The isotopic data (Table 3-9) for the peridotites also show systematic trends with respect to trace element abundances (Figure 3-10). The GE inclusions which are relatively depleted in incompatible elements, e.g., La/Yb ratios are less than chondrites, have lower $^{87}Sr/^{86}Sr$ ratios than the other peridotite inclusions. Acid-leached clinopyroxenes separated from the GE inclusions have $^{87}Sr/^{86}Sr$ and $^{143}Nd/^{144}Nd$ ratios within the range of modern MORBs (Figure 3-11). These clinopyroxenes have Sr isotopic ratios which are analytically indistinguishable from the bulk rock ratios (Table 3-9). We obtained no bulk rock $^{143}Nd/^{144}Nd$ ratios for the GE inclusions but note that in a geochemically similar inclusion from Kilbourne Hole, bulk rock and clinopyroxene $^{143}Nd/^{144}Nd$ ratios were analytically indistinguishable (Jagoutz et al., 1980). The measured isotopic ratios for the GE bulk rocks and clinopyroxenes are similar to isotopic ratios for other lherzolite inclusions with La/Yb ratios less than chondrites from Kilbourne Hole (Jagoutz et al., 1980) and Dreiser Weiher (Stosch et al., 1980), and to some clinopyroxenes from orogenic lherzolites (Menzies and Murthy, 1978; Richard and Allegre, 1980; Polve and Allegre, 1980).

The CE, CT, ACE, and ACT inclusions have higher $^{87}Sr/^{86}Sr$ and lower $^{143}Nd/^{144}Nd$ ratios than the GE inclusions (Table 3-9); the ACE and ACT inclusions have a more restricted range of $^{87}Sr/^{86}Sr$ ratios, 0.70289-0.70313 compared to 0.70293-0.70375, than the CE and CT inclusions. Of the two separated clinopyroxenes, 10002 clinopyroxene

Table 3-9. Isotopic ratios.

| | $^{87}Rb/^{86}Sr$ | $^{147}Sm/^{144}Nd$ | $^{87}Sr/^{86}Sr$ | $^{143}Nd/^{144}Nd$ |
|---|---|---|---|---|
| GE peridotites | | | | |
| 10070 wr | 0.0020 | | 0.70262 ± 4 | |
| cpx | 0.00066 | 0.245[1] | 0.70264 ± 2 | 0.51321[2] ± 5 |
| 10026 wr | 0.0216 | | 0.70216 ± 9 | |
| cpx | 0.00039 | 0.255[1] | 0.70203 ± 3 | 0.513277 ± 20 |
| 10068 cpx | 0.00242 | 0.257[1] | 0.70232 ± 5 | 0.513295 ± 17 |
| CE and CT peridotites | | | | |
| 10007 wr | 0.0137 | | 0.7033 ± 2 | |
| 10004 wr | 0.0390 | | 0.70375 ± 9 | |
| cpx | 0.00065 | 0.113 | 0.70344 ± 5 | 0.513136 ± 18 |
| | | | 0.70341 ± 3 | |
| 10008 wr | 0.0492 | | 0.70293 ± 4 | |
| ACE and ACT peridotites | | | | |
| 10002 wr | 0.00795 | | 0.70297 ± 6 | |
| | | | 0.70305 ±10 | |
| cpx | 0.000042 | 0.0722 | 0.70298 ± 3 | 0.513093 ± 35 |
| 10006 wr | 0.0116 | | 0.70303 ± 8 | |
| 10055 | 0.0186 | | 0.70289 ± 4 | |
| 10051 | 0.193 | | 0.70303 ± 7 | |
| 10075 | 0.0746 | | 0.70313 ± 4 | |

Table 3-9. Continued

| | $^{87}Rb/^{86}Sr$ | $^{147}Sm/^{144}Nd$ | $^{87}Sr/^{86}Sr$ | $^{143}Nd/^{144}Nd$ |
|---|---|---|---|---|
| Pyroxenites | | | | |
| 13002 | 0.120 | 0.185 | 0.70288 ± 6 | 0.513095 ± 32 |
| 13004 | 0.0184 | 0.253 | 0.70288 ± 6 | 0.513103 ± 22 |
| 13005 | 0.0535 | | 0.70297 ± 7 | |
| 13007 | 0.0153 | | 0.70297 ± 10 | |
| Basalts | | | | |
| B-1 | 0.0672 | 0.154 | 0.70306 ± 4 | 0.513018 ± 21 |
| B-5 | 0.0783 | 0.150 | 0.70298 ± 4 | 0.513149 ± 19 |
| | | | | 0.513148 ± 24 |
| B-6 | 0.103 | 0.139 | 0.70294 ± 3 | 0.513105 ± 19 |
| B-9 | | 0.115 | | 0.513097 ± 20 |
| B-10 | 0.121 | 0.128 | 0.70279 ± 4 | 0.513071 ± 30 |
| | | | 0.70285 ± 4 | |
| B-12 | 0.0676 | 0.154 | 0.70327 ± 3 | 0.513084 ± 19 |
| | | | | 0.513083 ± 18 |
| B-13 | 0.0955 | 0.135 | 0.70288 ± 5 | 0.513122 ± 24 |

1. Analyzed by isotope dilution.

2. Corrected for $^{144}Sm$ interference.

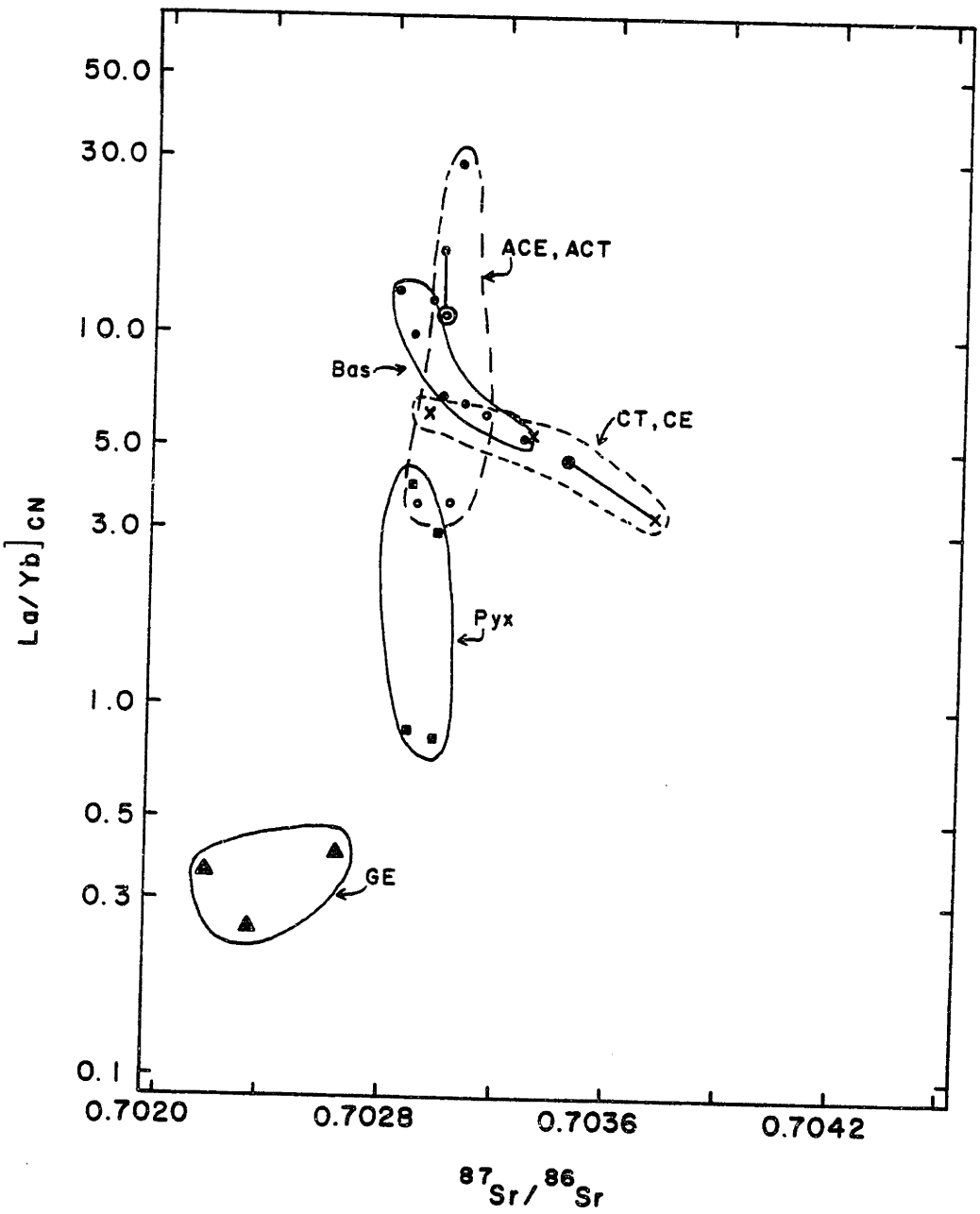
50.0
30.0
10.0
5.0
3.0
1.0
0.5
0.3
0.1
La/Yb]CN
0.7020
0.7028
0.7036
0.7042
87Sr/86Sr
ACE, ACT
Bas
CT, CE
Pyx
GE

Figure 3-10. Chondrite-normalized La/Yb ratios plotted versus $^{87}Sr/^{86}Sr$ for Nunivak basalts (●), GE clinopyroxenes (▲), CE, CT whole rocks (✗), CT clinopyroxene (●), ACE, ACT whole rocks (o), ACE clinopyroxene (◎), and pyroxenites (■). Tie lines connect clinopyroxenes to their respective whole rocks.

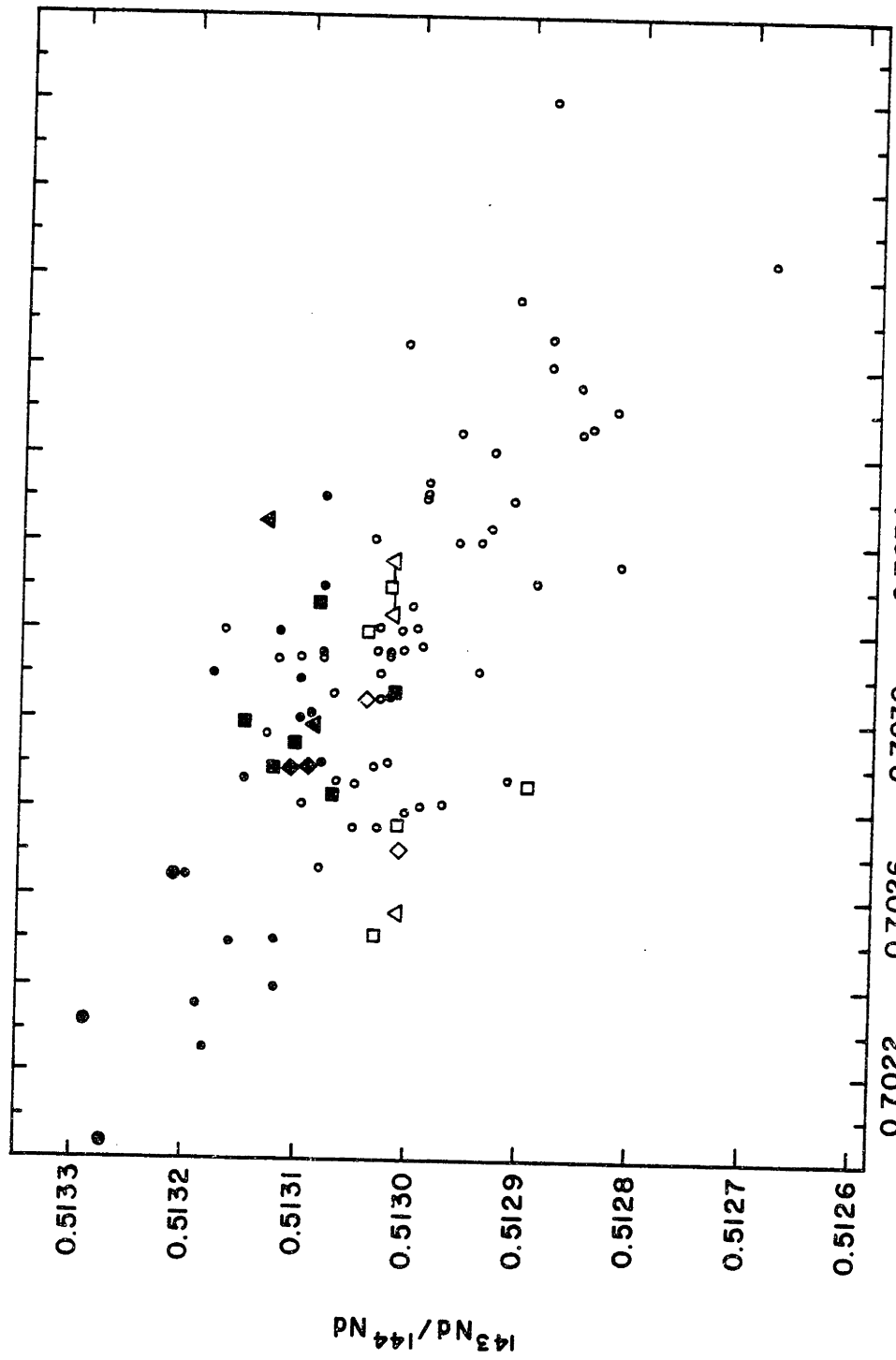
0.5133
0.5132
0.5131
0.5130
0.5129
0.5128
0.5127
0.5126
$^{143}Nd/^{144}Nd$
0.7022
0.7026
0.7030
0.7034
0.7038
0.7042
$^{87}Sr/^{86}Sr$

Figure 3-11. $^{143}Nd/^{144}Nd$ and $^{87}Sr/^{86}Sr$ for Nunivak samples compared to MORBs (●) and oceanic island basalts (○). Symbols used: (◉) clinopyroxenes from GE inclusions, (△, ▲) clinopyroxenes from CE, CT, ACT, ACE inclusions, (◇, ◆) pyroxenites and minerals from pyroxenites, (□, ■) basalts. Open symbols from Menzies and Murthy (1980a), filled symbols from the present study. Oceanic basalt data from DePaolo and Wasserburg (1976a, 1976b), O'Nions et al. (1977), Richard et al. (1976), Carlson et al. (1978), Zindler et al. (1979), and White and Hofmann (1978).

lies within error of the bulk rock ratio while 10004 clinopyroxene has a significantly lower $^{87}Sr/^{86}Sr$ ratio than the bulk rock (Table 3-9). Both the bulk rock and clinopyroxene from 10004 have higher $^{87}Sr/^{86}Sr$ ratios than any of the other peridotites. 10004 clinopyroxene lies slightly to the high $^{87}Sr/^{86}Sr$ side of the mantle array (Figure 3-11). In contrast, 10002 clinopyroxene lies within the region defined by oceanic island basalts (Figure 3-11).

The correlation between several important trace element ratios and isotopic ratios are illustrated in Figures 3-10, 3-12, and 3-13. In these figures the GE inclusions occupy fields distinct from the other peridotite inclusions because of their relatively low Rb/Sr, La/Yb, and $^{87}Sr/^{86}Sr$ ratios and their relatively high Sm/Nd and $^{143}Nd/^{144}Nd$ ratios. These general features are closely paralleled by the suite of inclusions from Dreiser Weiher studied by Stosch and Seck (1980) and Stosch et al. (1980).

Of particular note in the Nunivak suite is the relatively small range in $^{87}Sr/^{86}Sr$ and the relatively large range in $^{87}Rb/^{86}Sr$ displayed by the ACE and ACT inclusions (Figure 3-12).

The line defined by the $^{87}Sr/^{86}Sr$ and $^{87}Rb/^{86}Sr$ ratios of 10004 bulk rock and 10004 clinopyroxene specifies an age of $5.8 \times 10^8$ yr. assuming closed system evolution. Besides this relationship, there appears to be no systematic relation between $^{87}Rb/^{86}Sr$ and $^{87}Sr/^{86}Sr$ or $^{147}Sm/^{144}Nd$ and $^{143}Nd/^{144}Nd$ ratios in the peridotites (Figures 3-12, 3-13).

Menzies and Murthy (1980a) previously reported Sr and Nd isotopic

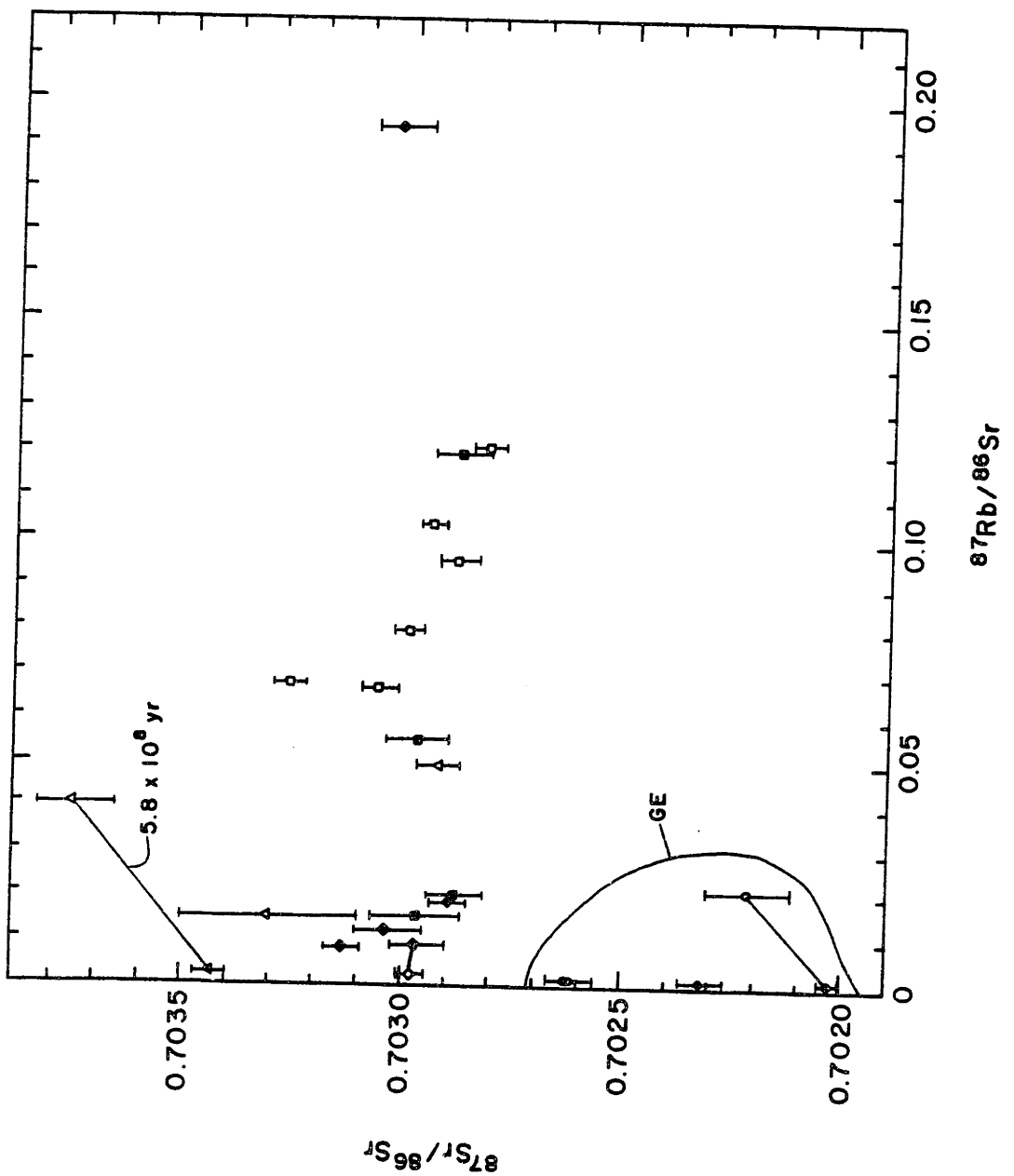
0.7035
0.7030
0.7025
0.7020
$^{87}Sr/^{86}Sr$
0
0.05
0.10
0.15
0.20
$^{87}Rb/^{86}Sr$
5.8 x 10$^{9}$ yr
GE

Figure 3-12. $^{87}Sr/^{86}Sr$ versus $^{87}Rb/^{86}Sr$ for GE clinopyroxenes (●), GE whole rocks (○), CT, CE whole rocks (△), CT clinopyroxene (▲), ACE, ACT whole rocks (◆), ACE clinopyroxene (◇), pyroxenites (■) and basalts (□). Tie lines connect coexisting clinopyroxene and bulk rock. All data from Table 3-9.

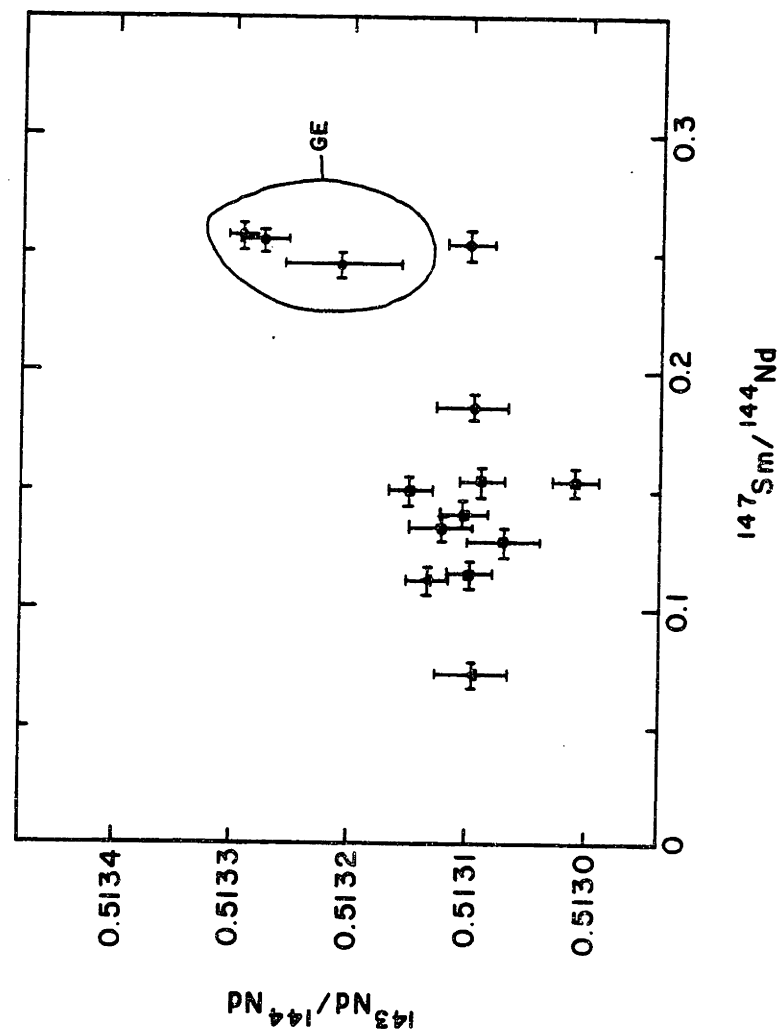
GE
0.5134
0.5133
0.5132
0.5131
0.5130
0
0.1
0.2
0.3
$^{143}Nd/^{144}Nd$
$^{147}Sm/^{144}Nd$

Figure 3-13. $^{143}Nd/^{144}Nd$ plotted versus $^{147}Sm/^{144}Nd$ for GE clinopyroxenes (●), ACE and CT clinopyroxenes (▲), pyroxenites (◆) and basalts (■). All data from Table 3-9.

ratios for several basalts, pyroxenites, megacrysts, and two amphibole or phlogopite-bearing peridotite inclusions from Nunivak Island. Their data is plotted in Figure 3-11 for comparison to our data. We note that there appears to be a systematic difference in the measured $^{143}Nd/^{144}Nd$ ratios with our values being substantially higher, although the ranges reported overlap. We do not understand the reason for this discrepancy but note that within each data set the relationship of basalt to pyroxenite to amphibole-bearing peridotite is the same, thus each set is internally consistent. For the purposes of the discussion to follow, our data will be used primarily in order to avoid complications due to interlaboratory bias.

(3) Textures and mineral chemistry

Because a major aim of this study is to provide constraints on the nature of the metasomatic process in the upper mantle, the textural relations and mineral chemistry of fluid and mineral inclusions, and phases associated with amphibole were investigated. In particular, a correlation between the presence of mineral and fluid inclusions of various types and high bulk rock La/Yb ratios were observed and are described below. Also, zoning at grain boundaries in ampibole-bearing xenoliths was studied with the use of the electron microprobe, primarily to determine whether the amphibole was in equilibrium with the anhydrous phases. Francis (1976b) earlier showed that significant zoning occurred at amphibole and spinel grain boundaries.

An important observation is the variation of phase proportions in amphibole- or glass-spinel clusters in the ACE and ACT inclusions. In

a typical cluster amphibole or glass rims amoeboid spinel (Figure 3-1). In some of these inclusions clinopyroxene also rims orthopyroxene (Figure 3-14A) and contains small inclusions of olivine and orthopyroxene, and in one case, an earlier generation of clinopyroxene (Figure 3-14B). The texture indicates a replacement origin for the clinopyroxene as well as the amphibole. In other inclusions, clinopyroxene instead of amphibole rims amoeboid spinel (Figure 3-15A) or concentric rings of amphibole and phlogopite rim spinel (Figure 3-15B). The most complex relationships are found in sample 10051 in which textures indicate the existence of two generations of hydrous and associated minerals. The first generation consists of phlogopite and possibly clinopyroxene. The phlogopite occurs in veinlets, interstitial grains, and anhedral inclusions in anhydrous silicates. Some of these inclusions have radially dispersed expansion cracks surrounding them (Figure 3-16). These cracks may have resulted from decompression during the transport of the xenolith to the surface as a consquence of the different compressibilities of phlogopite and olivine (Birch 1966). This feature further indicates a high pressure origin for the hydrous phases. The second generation of hydrous minerals in 10051 consists of amphibole and associated clinopyroxene (Figure 3-18). The amphibole contains small inclusions of phlogopite (Figure 3-17) and in places, clinopyroxene. This amphibole appears to have replaced both minerals. Within the same thin section however, amphibole elsewhere appears to be in textural equilibrium with clinopyroxene (Figure 3-18) but not with phlogopite. The above observations indicate

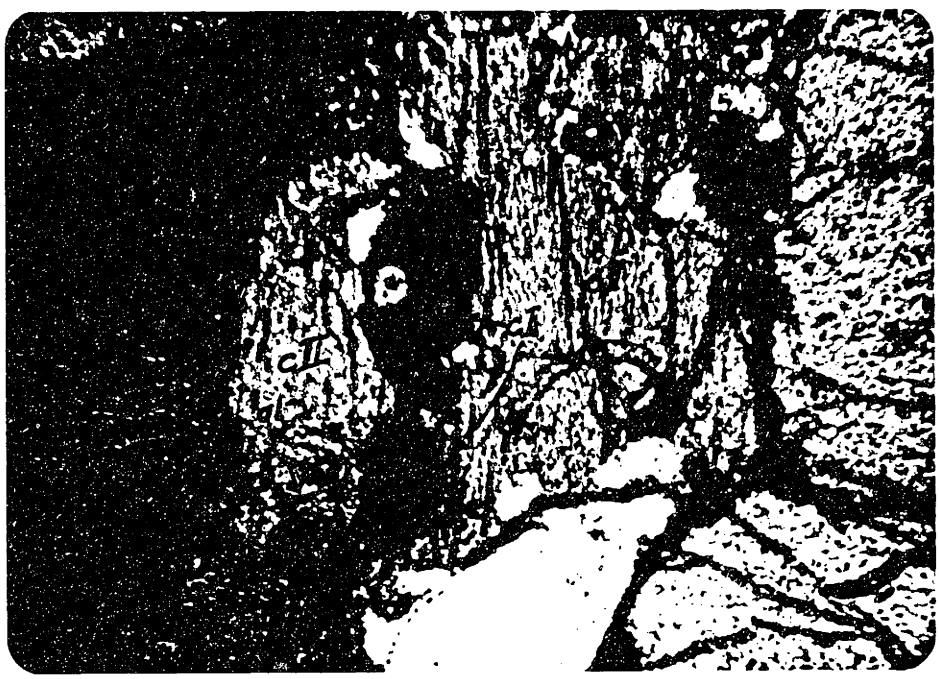

B

A

Figure 3-14. A. Photomicrograph of clinopyroxene (c) rimming orthopyroxene ( ) in ACE inclusion 10006 (crossed nicols; long dimension is 2 mm).

B. Two generations of clinopyroxene in ACE inclusions 10006. Large clinopyroxene (cII) encloses remnant clinopyroxene (cI) and small olivine grains (ol); a remnant grain boundary (lined in) between olivine and clinopyroxene cI is also preserved (crossed nicols; long dimension is 2 mm).

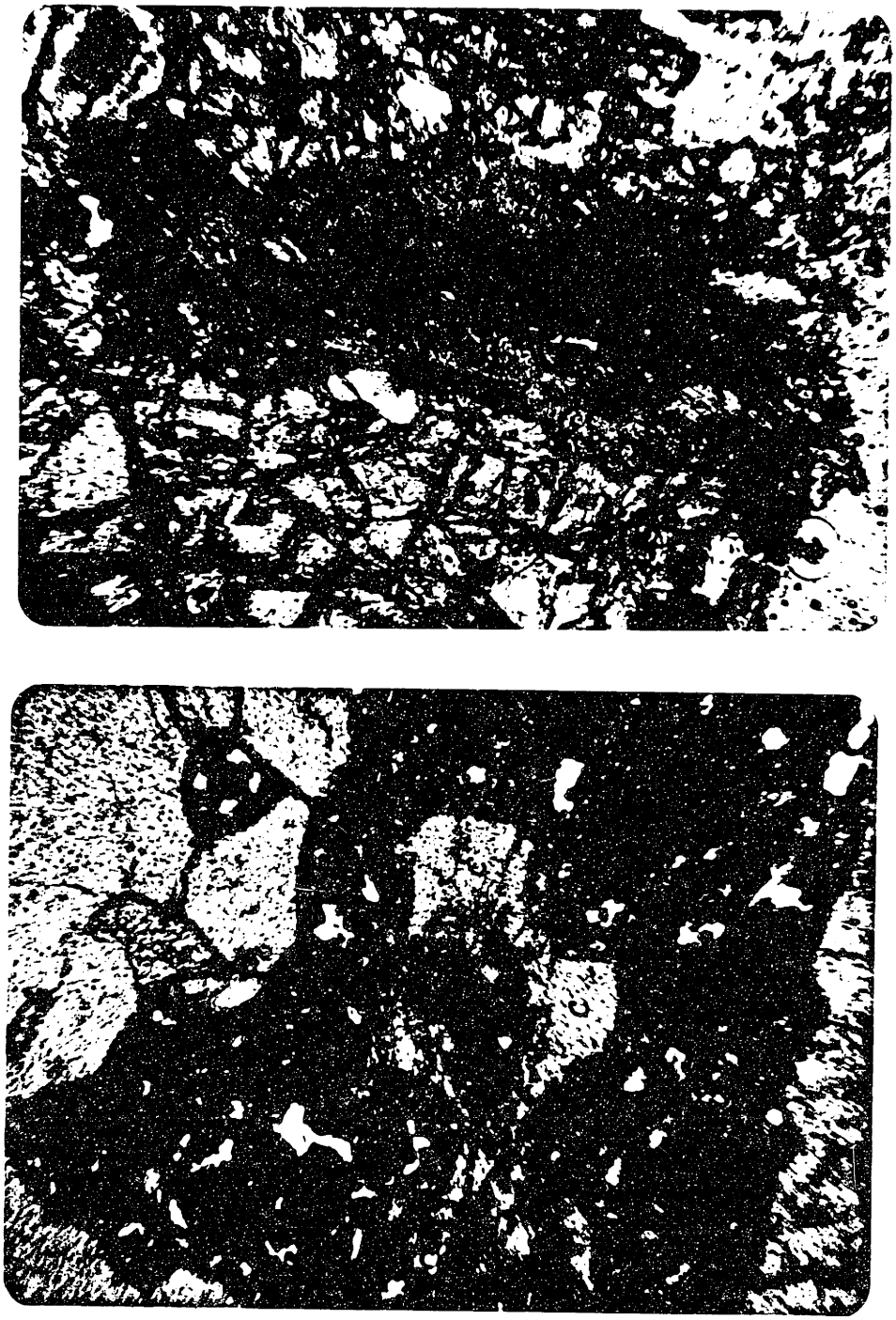

B

A

Figure 3-15. A. Clinopyroxene (c) and its breakdown products rimming black, amoeboid spinel in ACE inclusion 10055 (long dimension is 2 mm).

B. Concentric rims of amphibole (A) and phlogopite (P) around black, amoeboid spinel in ACT inclusion 10075 (long dimension is 2 mm).

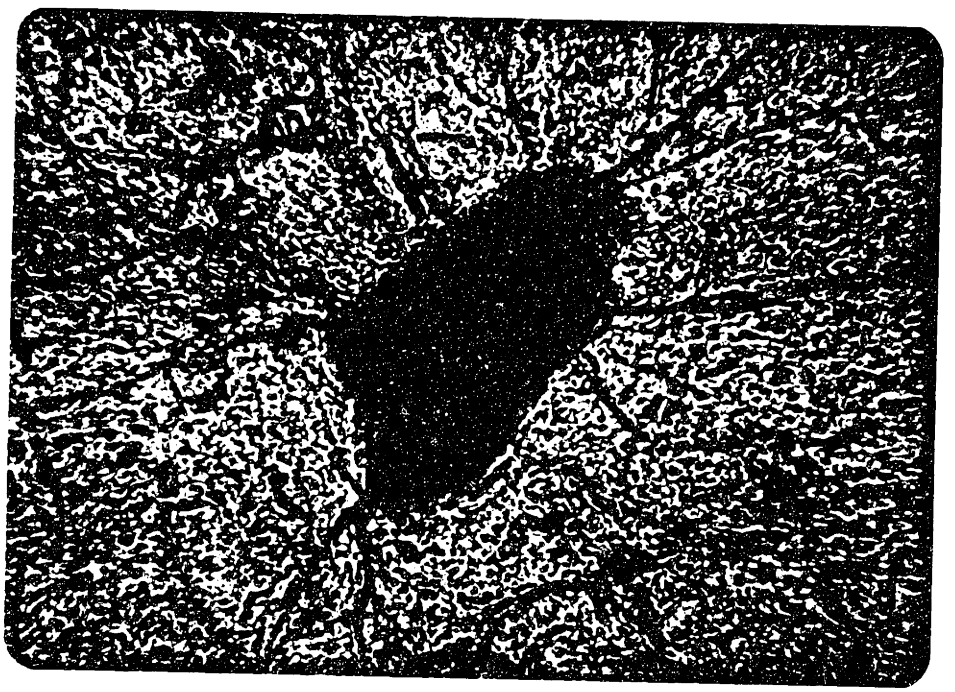

Figure 3-16. Phlogopite (P) inclusions in olivine (ol) of ACT inclusion 10051. Note radially disposed expansion cracks (EC) surrounding inclusions (long dimension is 0.6 mm).

Figure 3-17. Amphibole (A) with phlogopite inclusion (P) in ACT inclusion 10051 (long dimension is 0.6 mm).


A
B
C

Figure 3-18. Amphibole (A) and clinopyroxene (c) rimming black spinel in ACT inclusion 10051 (long dimension is 2 mm).

that phases associated with amphibole are variable and furthermore, textural relations between these phases are variable. We define an "amphibole-associated" assemblage as follows: amphibole + clinopyroxene ± phlogopite.

A second important petrographic feature is that the number and morphology of fluid inclusions correlates with textural group. Firstly, the volume (as estimated visually) occupied by fluid inclusions increases in the sequence GE, CE and CT, ACE and ACT. Secondly, the morphology of fluid inclusions varies from textural group to textural group. One type of fluid inclusion, herein denoted as "Type III" is common to all the textural groups. Type III fluid inclusions are tubular to spherical, generally less than 1μ in diameter and occur in planar, curving arrays (Figure 3-19). Some arrays can be traced into fractures or grain boundaries; other arrays are radially disposed around mineral inclusions or larger Type II inclusions (described below). Type III inclusions are present in all silicates, but are most common in clinopyroxene. The presence of Type III inclusions is <u>not</u> correlated with high incompatible element concentrations. Similar fluid inclusions in ultramafic and mafic xenoliths have been described by Roedder (1965) and Selverstone (Type III, secondary, ms); these are generally $CO_2$-filled and may in part be related to the exsolution of a vapor phase from the host basalt at relatively shallow depths. A second type of fluid inclusion, herein termed Type II (Figure 3-20) are large, to 50μ diameter, isolated spheres which are now empty and which may have a very thin black layer

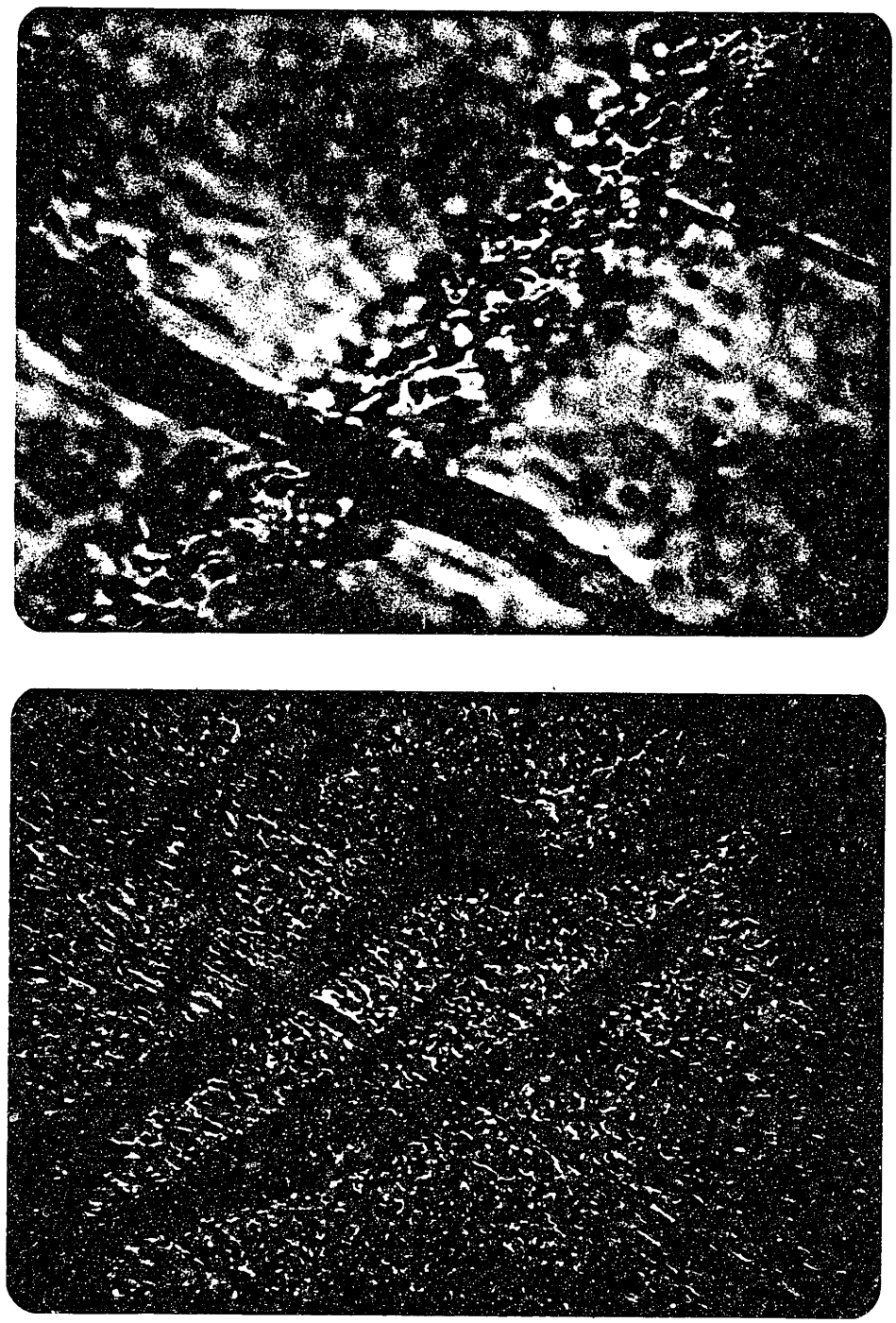

B

A

Figure 3-19. A. Type III fluid inclusion array in clinopyroxene of GE inclusion 10211 (long dimension is 0.6 mm).

B. Enlarged view of fluid inclusion train of Figure 3-19A (long dimension is 0.15 mm).


II
c

Figure 3-20. Type II fluid inclusion (II) in clinopyroxene (c) of ACT inclusion 10067. Also note Type III inclusions (III). Long dimension is 0.6 mm.

plated on the inside walls. Many of these Type II inclusions have an array of radially disposed cracks surrounding them. Type II fluid inclusions are found only in clinopyroxene and amphibole, are absent from the GE xenoliths, and are much more common in the ACE or ACT xenoliths than in the CE or CT nodules. A third type of fluid inclusion, Type I is oval to lenticular to faceted to irregular shaped and less than 20μ in diameter. These inclusions are concentrated in clinopyroxenes of the ACE and ACT inclusions. Type I inclusions form planar arrays, some of which cross grain boundaries; but these inclusions also occur as isolated bodies. Many of the Type I inclusions are characterized by high internal reflection; similar inclusions were shown by Roedder (1965) to be filled with $CO_2$.

The Type I and III inclusions are similar to the secondary fluid inclusions in gabbroic xenoliths described by Selverstone (ms). She argued that these inclusions resulted from the penetration along fractures of a vapor phase related to the host basalt. The larger Type II inclusions may predate the incorporation of the xenoliths into the basalt because they are spatially associated with amphibole. The presence of Type II and Type I inclusions correlate with high bulk rock incompatible element concentrations.

Mineral inclusions are also found in some amphibole- or glass-bearing coarse-equant and coarse-tabular xenoliths. Apatite sporadically occurs as subhedral prisms (Figure 3-21) with rounded terminations to 150μ long in clinopyroxene. These apatites are crowded with micron-sized inclusions, and some have complex structures with a clear, sharply defined euhedral core (Figure 3-21B). Similar occurrences of

B

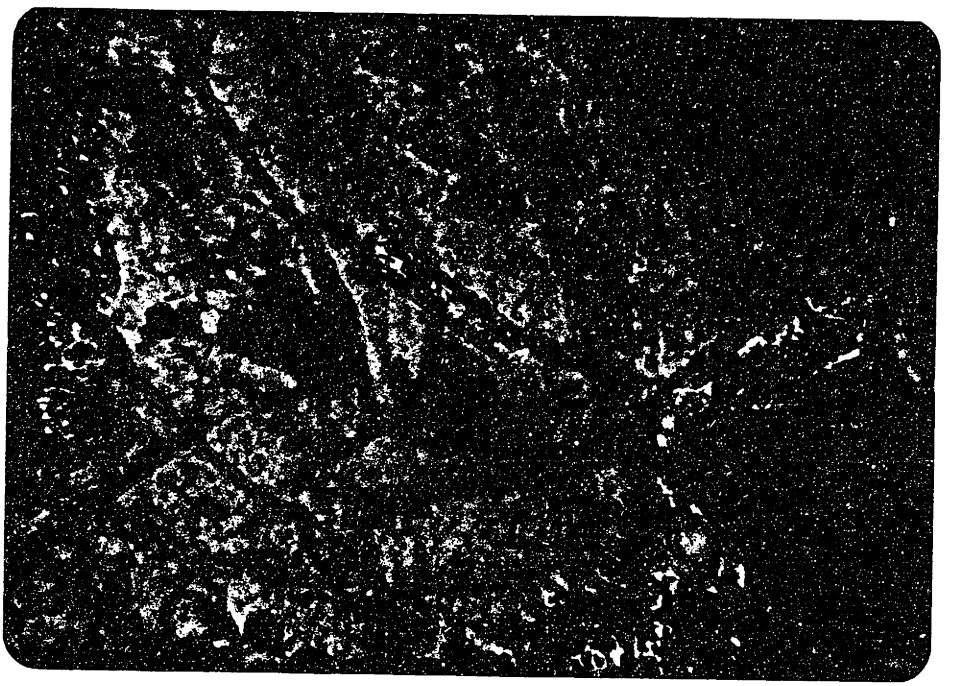

A

Figure 3-21. A. 100 micron-long apatite (Ap) inclusion in clinopyroxene of ACT inclusion 10067; note associated Type II fluid inclusions (II; crossed nicols; long dimension is 0.6 mm).

B. Composite apatite inclusion with euhedral core in clinopyroxene (c) of ACT inclusion 10067 (long dimension is 0.15 mm).

apatite inclusions in mantle-derived clinopyroxene have been noted by Hervig and Smith (1981) and Wass (1979). A second type of mineral inclusion is a rare, unidentified, acicular phase with high relief and birefringence observed in one amphibole grain. By analogy with other amphibole or phlogopite-bearing suites, this phase is probably rutile or zircon (e.g. Dawson and Smith, 1977). Amphibole and phlogopite also occur as inclusions in some anhydrous silicates. All these mineral inclusions occur in peridotites with relatively high bulk rock incompatible element concentrations.

The mineral chemistry studies of Francis (1976b, 1978) have been augmented through the use of the electron and ion probe on samples 10067 and 10006 primarily to determine the compositions of the apatite inclusions, the relationship of apatite inclusions to host clinopyroxene, and to study zoning at grain boundaries. Typical compositions of minerals associated with amphibole are shown in Table 3-10. The amphibole ranges from pargasite or pargasitic hornblends in the lherzolites to ferroan pargasite or kaersutite in the amphibole-pyroxenites (nomenclature of Leake, 1978). Mica associated with amphibole is characterized by low $TiO_2$, and high $Cr_2O_3$, $Al_2O_3$, and $Na_2O$ relative to micas from kimberlites and their xenoliths (e.g. Boettcher and O'Neill, 1980). The apatite contains measurable $SiO_2$, FeO, MgO, and $Na_2O$. Although edge effects could account for some of these oxides, 3 of 4 analyses of 4 different apatite grains show narrow ranges of these oxides: $SiO_2$, 0.33 to 0.34%; FeO, 0.44 to 0.46%; MgO, 1.42 to 1.50%; and $Na_2O$, 1.66 to 1.94% (uncorrected for

Table 3-10. Representative mineral analyses.

| | 10067 amp | 10067 cpx | 10006[1] amp | 10006 cpx | 10006[2] ap |
|---|---|---|---|---|---|
| Rock type | ACT | ACT | ACE | ACE | ACE |
| $SiO_2$ | 43.8 | 53.5 | 46.0 | 55.3 | 0.45 |
| $TiO_2$ | 0.36 | 0.01 | 0.08 | 0.00 | 0.00 |
| $Al_2O_3$ | 14.5 | 5.56 | 12.9 | 3.83 | 0.09 |
| $Cr_2O_3$ | 2.04 | 0.83 | 3.14 | 0.58 | 0.05 |
| FeO | 3.80 | 3.17 | 3.42 | 2.90 | 0.67 |
| MnO | 0.09 | 0.17 | 0.07 | 0.16 | 0.11 |
| MgO | 18.5 | 16.7 | 18.5 | 16.2 | 1.26 |
| CaO | 9.70 | 18.3 | 9.07 | 18.3 | 41.1 |
| $Na_2O$ | 3.33 | 2.24 | 4.67 | 2.48 | 1.67 |
| $K_2O$ | 1.26 | 0.03 | 0.92 | 0.05 | 0.04 |
| Total | 97.4 | 100.5 | 98.8 | 99.8 | 45.4 |
| | | | Atomic proportions[3] | | |
| Si | 6.248 | 1.918 | 6.449 | 1.977 | |
| Ti | 0.048 | 0.000 | 0.008 | 0.000 | |
| Al | 2.455 | 0.235 | 2.134 | 0.189 | |
| Cr | 0.224 | 0.023 | 0.348 | 0.018 | |
| Fe | 0.466 | 0.095 | 0.401 | 0.087 | |
| Mn | 0.018 | 0.005 | 0.008 | 0.005 | |
| Mg | 3.840 | 0.894 | 3.856 | 0.868 | |
| Ca | 1.504 | 0.703 | 1.363 | 0.705 | |
| Na | 0.918 | 0.156 | 1.302 | 0.173 | |
| K | 0.253 | 0.000 | 0.165 | 0.002 | |
| Total | 15.974 | 4.031 | 16.035 | 4.009 | |

cpx = clinopyroxene, amp = amphibole, ap = apatite

1. Analysis from Francis (1976a).
2. Average of four point analyses.
3. Normalized to 23 oxygens for amphibole, 6 oxygens for clinopyroxene, and 22 oxygens for mica.

Table 3-10. Representative mineral analyses, continued.

| | 10016[1] mica | 13004[4] amp | 13004[4] cpx |
|---|---|---|---|
| rock type | ACE | AP[4] | AP[4] |
| $SiO_2$ | 39.9 | 39.6 | 48.7 |
| $TiO_2$ | 0.20 | 4.57 | 1.23 |
| $Al_2O_3$ | 17.8 | 15.3 | 8.84 |
| $Cr_2O_3$ | 2.17 | 0.05 | 0.00 |
| FeO | 3.43 | 10.7 | 7.91 |
| MnO | 0.05 | 0.11 | 0.20 |
| MgO | 23.8 | 13.7 | 13.4 |
| CaO | 0.00 | 10.2 | 18.5 |
| $Na_2O$ | 1.47 | 3.17 | 1.93 |
| $K_2O$ | 7.30 | 1.33 | 0.02 |
| Total | 96.1 | 97.5 | 100.7 |
| | Atomic proportions[3] | | |
| Si | 5.540 | 5.781 | 1.788 |
| Ti | 0.021 | 0.501 | 0.381 |
| Al | 2.904 | 2.625 | 0.033 |
| Cr | 0.238 | 0.004 | 0.000 |
| Fe | 0.398 | 1.304 | 0.242 |
| Mn | 0.006 | 0.013 | 0.005 |
| Mg | 4.916 | 2.985 | 0.734 |
| Ca | 0.000 | 1.595 | 0.727 |
| Na | 0.396 | 0.896 | 0.137 |
| K | 1.293 | 0.244 | 0.000 |
| Total | 15.712 | 15.947 | 4.047 |

4. Amphibole pyroxenite; analyses from Francis (1976c).

$P_2O_5$ content). It is unlikely that the limited concentration ranges observed are the result of random penetration of grain boundaries by the electron beam; more likely these oxides are related to the abundant inclusions within the apatite grains. Hervig and Smith (1981) found measurable $SiO_2$ and Frey and Green (1974) found measurable $SiO_2$, FeO, MgO, and $Na_2O$ in apatite from megacryst and xenolith occurrences respectively.

Ion microprobe analyses of apatite inclusions (Table 3-11) in a clinopyroxene from sample 10006 confirmed the optical and electron probe identification of apatite. These apatite inclusions also contain significant amounts of the LREE as represented by $^{139}La$ and Sr as represented by $^{88}Sr$ relative to host clinopyroxene (Table 3-11). The host clinopyroxene contains 390 ppm Sr based on calibration curves derived from natural diopsides in the MIT lab (N. Shimizu, personal communication). The high Sr and La concentrations in apatite relative to the host clinopyroxene are consistent with published partition coefficients for these elements in clinopyroxene and apatite (Irving, 1978; Watson and Green, 1982).

Further observations on the relationship between apatite and host clinopyroxene were made by the use of the University of Paris ion microprobe (D.M. Francis, unpublished data). Specifically, clinopyroxenes from the GE xenoliths have lower La/Y ratios than clinopyroxenes from the other peridotite nodules which is consistent with bulk rock and clinopyroxene RNAA analyses (Figures 3-4, 3-5, 3-6) because Y is geochemically similar to the heavy REE. Relative to the

Table 3-11. Ion probe analyses of minerals from peridotite 10006 (counts)

| | apatite inclusion | host clinopyroxene |
|---|---|---|
| $^{31}P/^{28}Si$ | 38.6 | 0.0004 |
| $^{40}Ca/^{28}Si$ | 2010 | 1.05 |
| $^{88}Sr/^{28}Si$ | 33.5 | 0.0012 |
| $^{139}La/^{28}Si$ | 3.65 | 0.00004 |

host clinopyroxene, the apatite inclusions in samples 10006 and 10067 have higher La/Y ratios, 4.6 to 5.8 versus 0.40 to 0.68. Thus, the $(La/Y)_{apatite}/(La/Y)_{clinopyroxene}$ ratio is approximately 10; this ratio is similar to an equilibrium value of $(La/Lu)_{apatite}/(La/Lu)_{clinopyroxene}$ ratio based on partition coefficients for the REE in apatite and clinopyroxene (Frey et al., 1978; Watson and Green, 1982).

There appears to be no zoning at apatite-clinopyroxene grain boundaries, nor does there appear to be any systematic distribution of apatite relative to zoning of the host clinopyroxene. Figure 3-22 is a major element map of a host clinopyroxene with 3 apatite inclusions. The host clinopyroxene has a small sharply defined region depleted in $Al_2O_3$, $Na_2O$ and enriched in CaO, MgO, and $Cr_2O_3$; this region was probably near a grain boundary (see Francis 1976b). A diffuse, linear region relatively enriched in jadeite traverses the center of the crystal. This type of zoning may be related to the clear-cloudy distinction of Francis (1976b). The distribution of the three apatite inclusions show no relation to the zoning of the host diopside (Figure 3-22). Ion and electron probe traverses between two apatite grains (Figure 3-22) show no zoning at diopside-apatite grain boundaries (Figures 3-23, 3-24). The compositional gradients observed within 5 to 10μ of the grain boundary are attributed to edge effects because of sympathetic variation of several elements including P (Figures 3-23, 3-24).

Zoning was also studied at grain boundaries between amphibole and

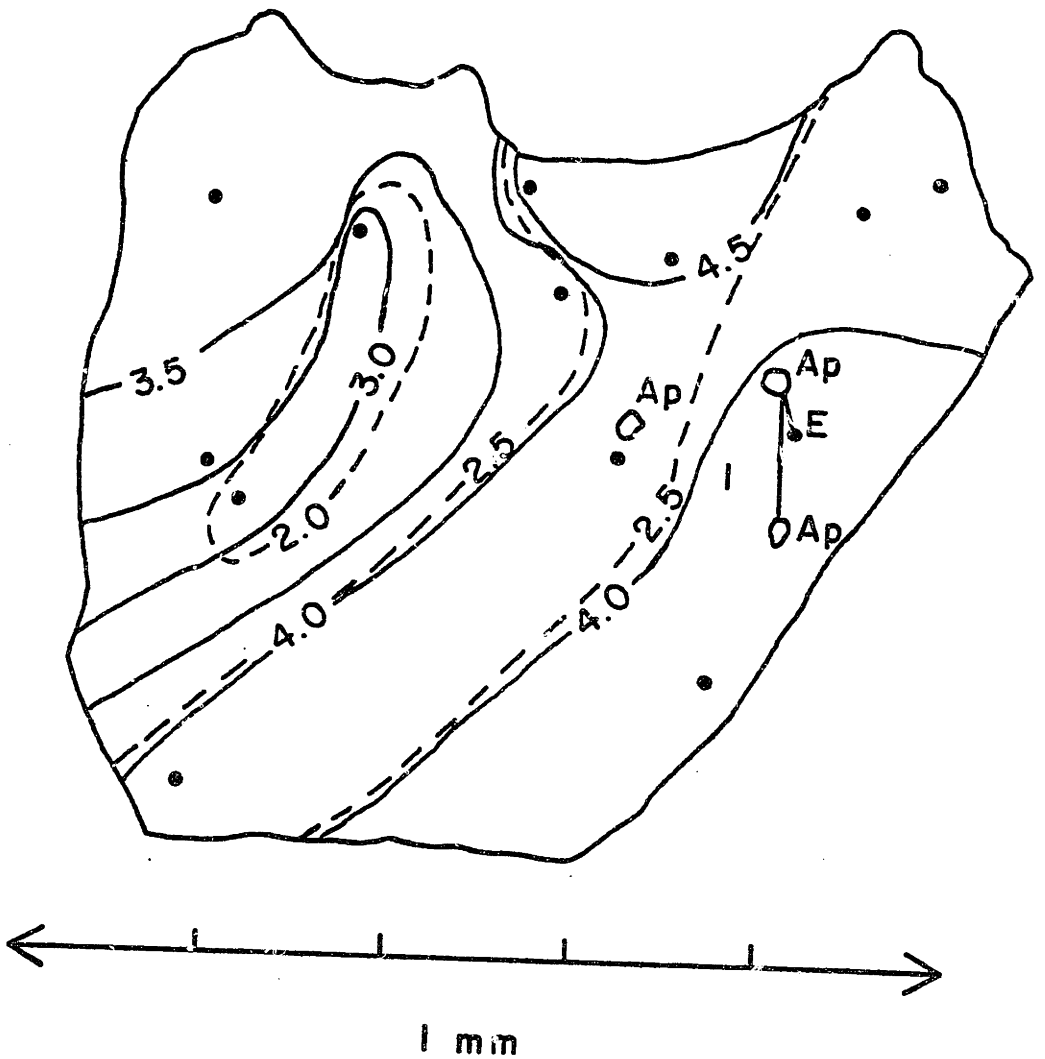
3.5
3.0
2.0
2.5
4.0
4.5
Ap
Ap
E
Ap
1 mm

Figure 3-22. Compositional map of 10006 clinopyroxene grain with apatite inclusions (Ap). Grain is contoured in terms of $Al_2O_3$ concentrations (solid lines) and $Na_2O$ concentration (dashed lines). Filled circles indicate locations of point analyses. Location of ion probe (I; Figure 3-23) and electron probe (E; Figure 3-24) traverses across apatite-clinopyroxene grain boundaries are also shown.

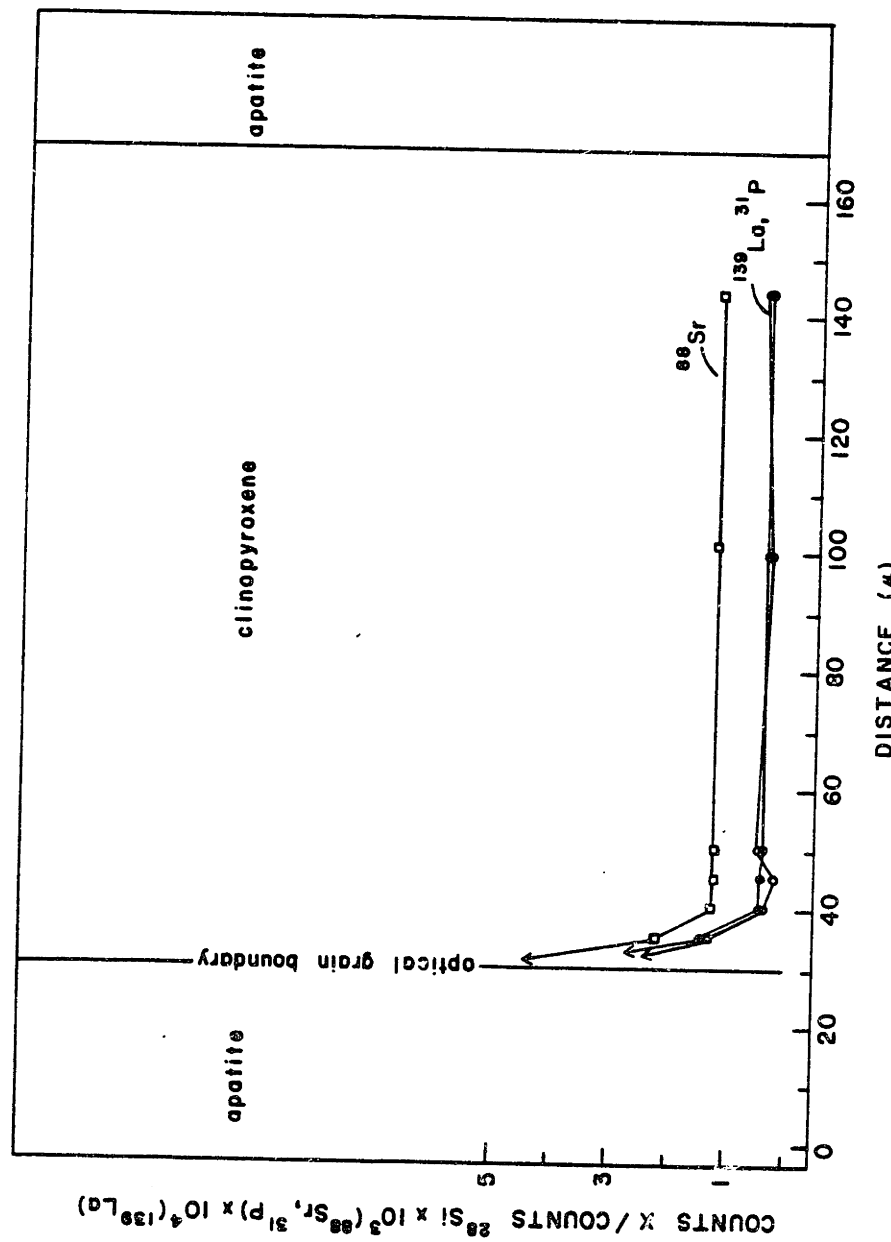
apatite
clinopyroxene
apatite
optical grain boundary
$^{88}Sr$
$^{139}La, ^{31}P$
0
20
40
60
80
100
120
140
160
DISTANCE (μ)
1
3
5
COUNTS χ / COUNTS $^{28}Si \times 10^3 (^{88}Sr, ^{31}P) \times 10^4 (^{139}La)$

Figure 3-23. Ion probe traverse into clinopyroxene from apatite, ACE inclusion 10006. Plotted in terms of $^{28}Si$ normalized counts x $10^3$ for $^{88}Sr$ (□) and $^{31}P$ (●), and $^{28}Si$ normalized counts x $10^4$ for $^{139}La$ (○).

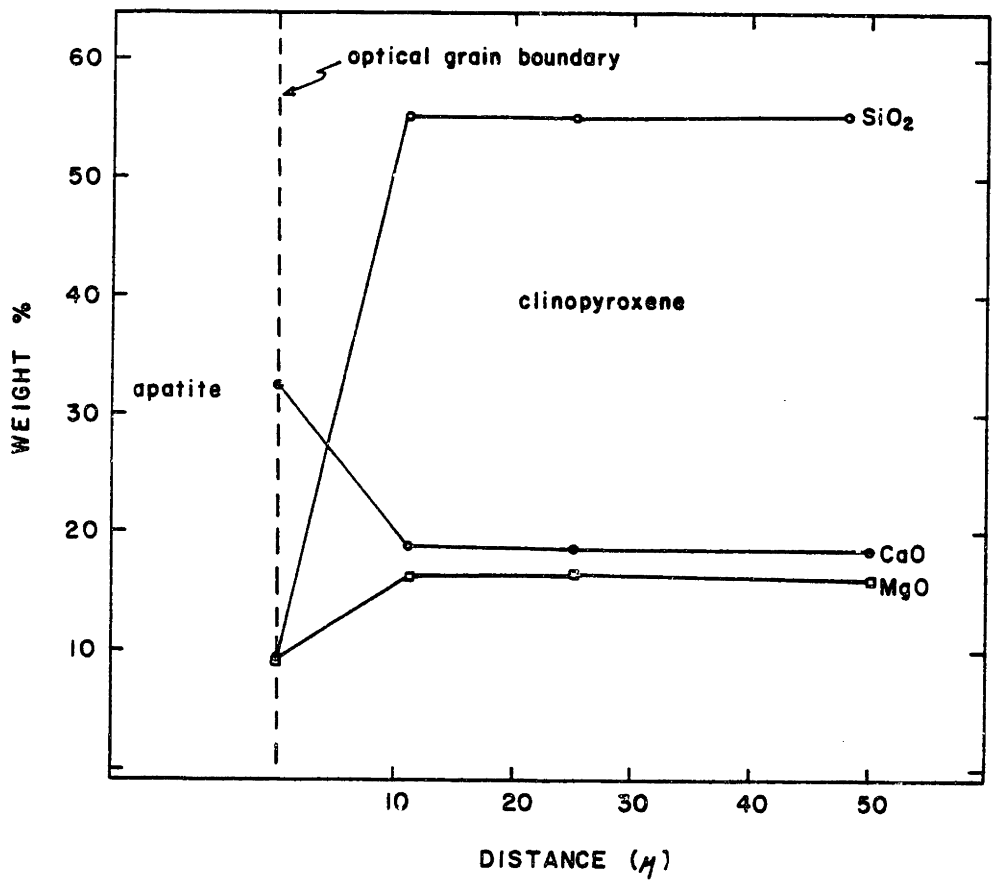
optical grain boundary
SiO2
clinopyroxene
apatite
CaO
MgO
WEIGHT %
60
50
40
30
20
10
10
20
30
40
50
DISTANCE (μ)

Figure 3-24. Electron microprobe traverse from clinopyroxene into apatite, see Figure 3-22 for location.

other minerals in sample 10067 which has the greatest amount of fresh amphibole of any of the samples studied. In contrast to the results of Francis (1976b) for other Nunivak samples, no strong zoning was found at any grain boundaries. Zoning that was observed is near the resolution limits of the microprobe but was encountered in several traverses and appears to be real. For example, in three amphibole-spinel traverses (Figure 3-25) CaO was detectable to depths of approximately 50μ from the grain boundary in spinel, and within 50μ of the grain boundary, $Cr_2O_3$ increased from 2.0 to 2.2 or 2.5% in amphibole towards the grain boundary (Figure 3-25). FeO in spinel and olivine and $Cr_2O_3$ and $TiO_2$ in clinopyroxene showed similar gradients in single traverses.

(C) Pyroxenites

The pyroxenites are texturally bimodal with samples 13002 and 13005 being coarse-grained, spinel-poor amphibole-pyroxenites, and 13004 and 13007 being fine-grained, spinel-rich amphibole pyroxenites. The trace element data (Table 3-12) correlate with rock textures. The fine-grained pyroxenites with abundant spinel have convex-upward REE patterns relative to chondrites with La/Yb ratios approximately equal to chondrites (Figure 3-26). Relative to the coarse-grained pyroxenites, the fine-grained pyroxenites have low Cr, Rb, Sr, and higher Co (Table 3-21). The Cr results are particularly surprising in view of the abundant spinel in the fine-grained pyroxenites. However, Francis (1976c) noted that this spinel was virtually Cr-free. The

Table 3-12. Pyroxenite trace element abundances (ppm).

| | 13004 | 13007 | 13002 | 13005 |
|---|---|---|---|---|
| Sc | 33.6 | 35.3 | 40.3 | 34.4 |
| Cr | 137 | 107 | 1021 | 1370 |
| Co | 84.3 | 79.4 | 52.7 | 60.9 |
| Rb | 0.348 | 0.265 | 8.58 | 2.38 |
| Sr | 54.8 | 50.1 | 207 | 129 |
| La | 1.83 | 1.76 | 6.89 | 4.33 |
| Ce | 6.1 | 6.4 | 16.9 | 11.1 |
| Nd | 7.1 | 7.1 | 11.1 | 7.9 |
| Sm | 2.98 | 3.05 | 3.40 | 2.55 |
| Eu | 1.11 | 1.16 | 1.19 | 0.90 |
| Tb | 0.63 | 0.65 | 0.58 | 0.46 |
| Yb | 1.41 | 1.44 | 1.15 | 0.98 |
| Lu | 0.19 | 0.20 | 0.16 | 0.14 |

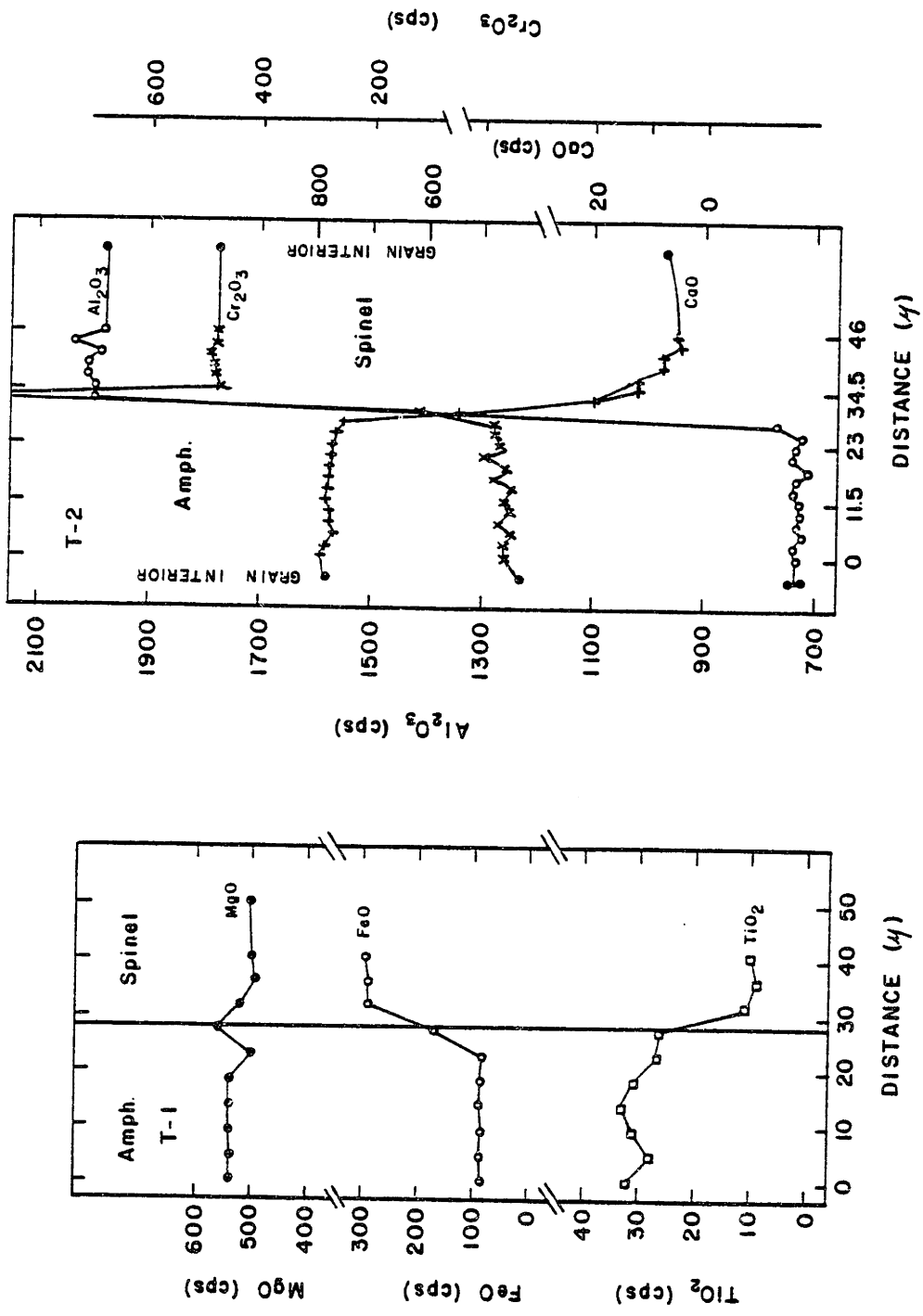
Cr2O3 (cps)
600
400
200
CaO (cps)
800
600
20
0
GRAIN INTERIOR
Al2O3
Cr2O3
Spinel
CaO
T-2
Amph.
GRAIN INTERIOR
2100
1900
1700
1500
1300
1100
900
700
Al2O3 (cps)
0 11.5 23 34.5 46
DISTANCE (μ)
MgO (cps)
FeO (cps)
TiO2 (cps)
600 500 400 300 200 100 0
40 30 20 10 0
Spinel
MgO
FeO
TiO2
Amph.
T-1
0 10 20 30 40 50
DISTANCE (μ)

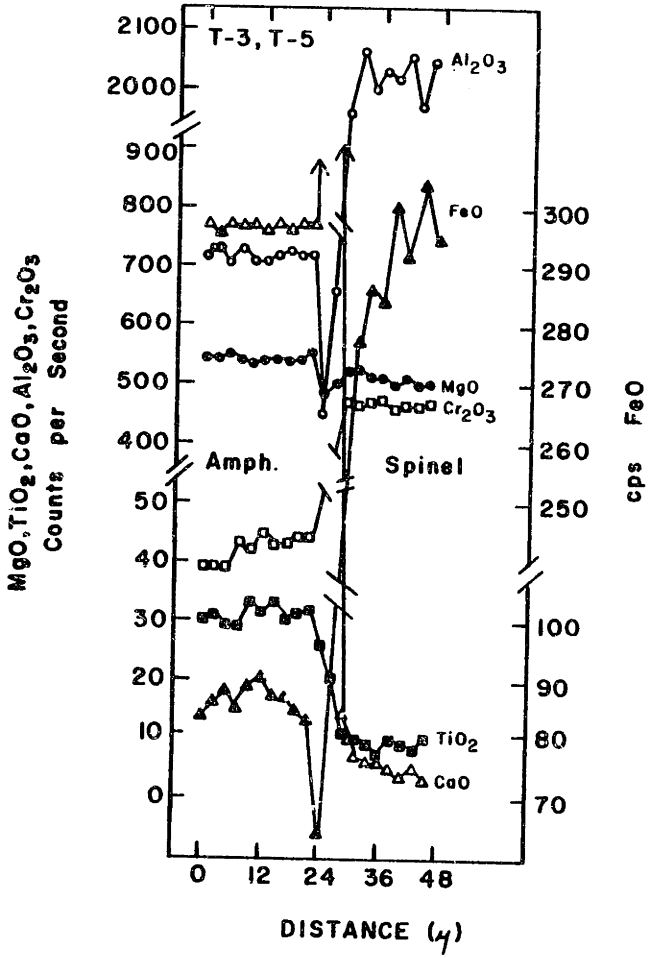
T-3, T-5
$Al_2O_3$
FeO
MgO
$Cr_2O_3$
$TiO_2$
CaO
Amph.
Spinel
MgO, $TiO_2$, CaO, $Al_2O_3$, $Cr_2O_3$
Counts per Second
cps FeO
DISTANCE (μ)

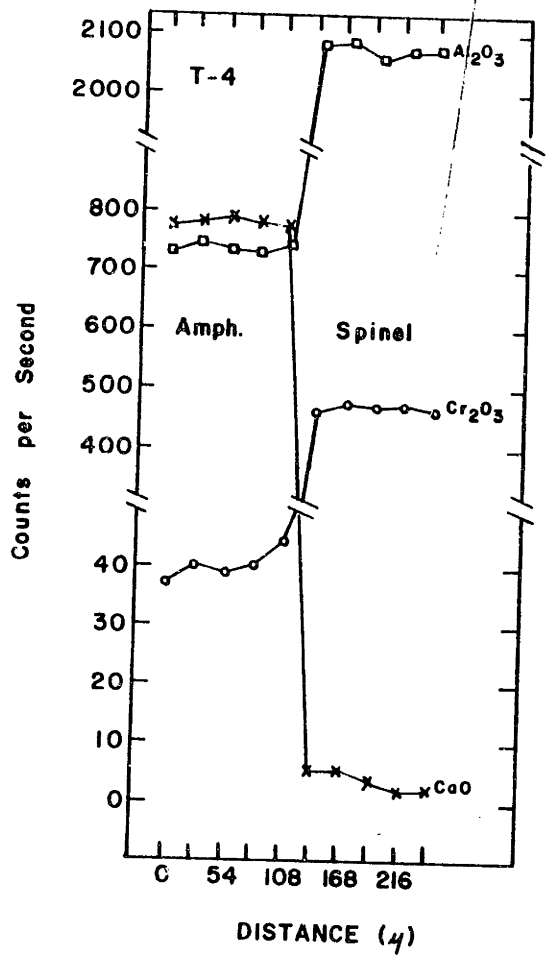
T-4
$Al_2O_3$
$Cr_2O_3$
CaO
Amph.
Spinel
Counts per Second
DISTANCE (μ)

Figure 3-25. Electron microprobe traverses across four spinel-amphibole grain boundaries in inclusion 10067.

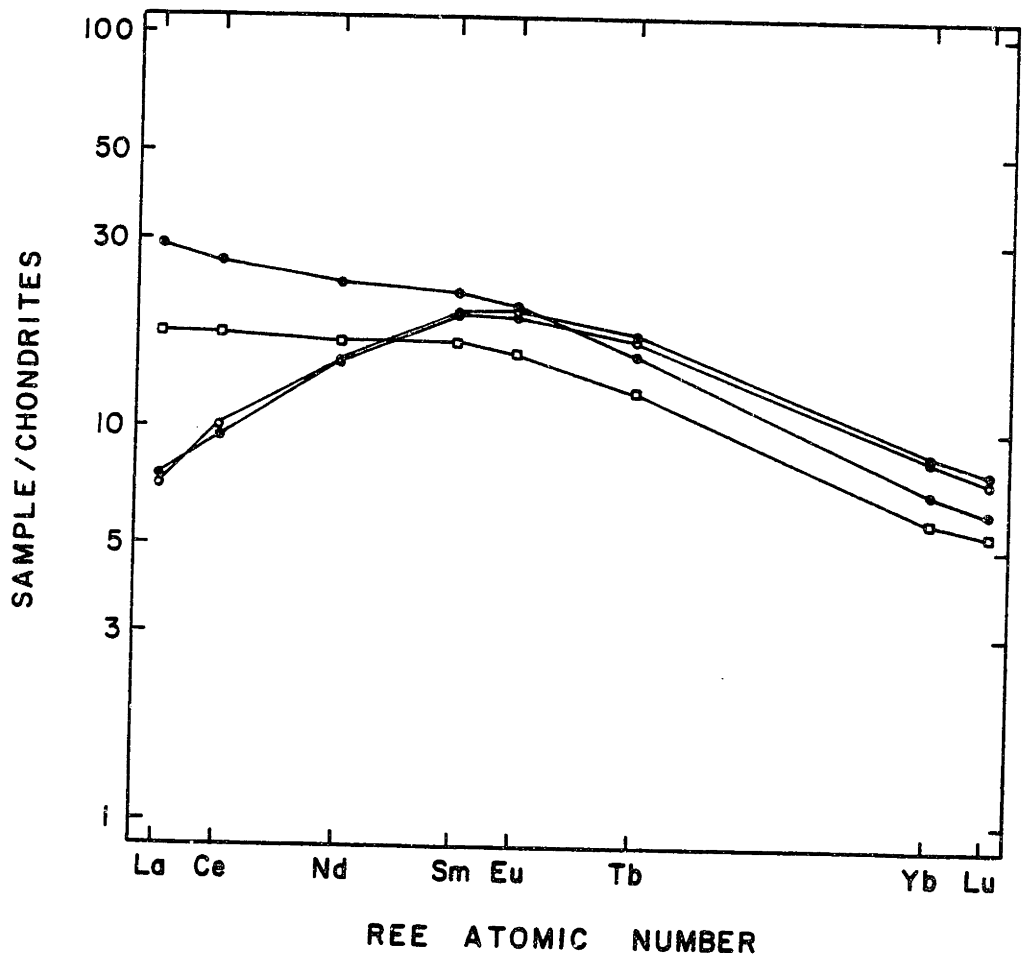
100
50
30
10
5
3
1
SAMPLE / CHONDRITES
La
Ce
Nd
Sm
Eu
Tb
Yb
Lu
REE ATOMIC NUMBER

Figure 3-26. Chondrite-normalized REE patterns for the Nunivak amphibole-pyroxenites.

coarse grained pyroxenites have heavy REE abundances similar to the fine-grained pyroxenites, but have La/Sm ratios greater than chondrites (Figure 3-26). The trace element data for both textural types of pyroxenites are similar to data for other Al-augite or Group II pyroxenites from San Carlos (Frey and Prinz, 1978).

The $^{87}Sr/^{86}Sr$ ratios of the pyroxenites all lie within error and lie within the range defined by the measured $^{87}Sr/^{86}Sr$ ratios of the ACE and ACT inclusions (Figure 3-12). The $^{143}Nd/^{144}Nd$ ratios of the pyroxenites (Table 3-9) lie within error of this ratio for 10002 clinopyroxene. On the plot of $(La/Yb)_{cn}$ (where "cn" indicates the chondrite-normalized ratio) versus $^{87}Sr/^{86}Sr$ (Figure 3-10) the pyroxenites form a linear extension of the trend formed by the ACE and ACT inclusions. This trend is characterized by essentially constant $^{87}Sr/^{86}Sr$ but variable $(La/Yb)_{cn}$.

(D) Basalts

The basalts studied range from basanites with more than 5% normative nepheline (nomenclature of Green and Ringwood, 1967) to hypersthene-normative olivine tholeiites (Table 3-13). The range of normative nepheline and hypersthene is similar to that reported for the larger sample suite studied by Mark (1971). Our suite does not as completely cover the spectrum of normative compositions as Mark's, and in particular we lack basalts with less than 8% nepheline or 7% hypersthene. In contrast to the range of normative compositions, the basalts in Table 3-13 have a narrow range in molar $Mg/(Mg + Fe^{2+})$,

Table 3-13. Nunivak basalt major element abundances (wt.%),

| | B-1 | B-5 | B-12 | B-6 | B-7 |
|---|---|---|---|---|---|
| rock type | ol. thol. | ol. thol. | ol. thol. | bas. | bas. |
| $SiO_2$ | 48.78 | 48.88 | 48.65 | 46.70 | 44.60 |
| $TiO_2$ | 1.86 | 2.19 | 2.03 | 2.50 | 2.47 |
| $Al_2O_3$ | 14.29 | 14.24 | 14.09 | 14.54 | 13.20 |
| $Fe_2O_3$ | 3.24 | 3.04 | 3.15 | 3.22 | 3.32 |
| FeO | 8.76 | 8.25 | 8.49 | 8.68 | 8.97 |
| MnO | 0.18 | 0.18 | 0.19 | 0.19 | 0.19 |
| MgO | 9.80 | 9.60 | 9.81 | 8.77 | 12.17 |
| CaO | 8.89 | 9.48 | 9.47 | 9.05 | 9.71 |
| $Na_2O$ | 3.01 | 2.64 | 2.82 | 3.96 | 3.40 |
| $K_2O$ | 0.87 | 1.07 | 0.97 | 1.75 | 1.37 |
| $P_2O_5$ | 0.34 | 0.41 | 0.34 | 0.62 | 0.59 |
| Total | 100.02 | 99.98 | 100.01 | 99.98 | 99.99 |
| $MG/(Mg+Fe^{2+})$ | 66.6 | 67.4 | 67.3 | 64.3 | 70.8 |
| equilibrium olivine | $Fo_{87}$ | $Fo_{87}$ | $Fo_{87}$ | $Fo_{86}$ | $Fo_{89}$ |
| | CIPW norms | | | | |
| or | 5.14 | 6.32 | 5.73 | 10.34 | 8.10 |
| ab | 25.47 | 22.34 | 23.86 | 18.75 | 11.48 |
| an | 22.91 | 23.84 | 22.92 | 16.73 | 16.71 |
| ne | - | - | - | 8.00 | 9.37 |
| di | 11.08 | 12.30 | 12.96 | 14.10 | 17.18 |
| he | 4.22 | 4.20 | 4.62 | 5.35 | 4.94 |
| en | 5.45 | 8.26 | 5.04 | - | - |
| fs | 2.38 | 3.23 | 2.06 | - | - |
| fo | 9.69 | 6.98 | 9.38 | 10.73 | 15.66 |
| fa | 4.67 | 3.01 | 4.22 | 5.14 | 5.70 |
| mt | 4.70 | 4.41 | 4.57 | 4.67 | 4.81 |
| il | 3.53 | 4.16 | 3.86 | 4.75 | 4.69 |
| ap | 0.79 | 0.95 | 0.79 | 1.44 | 1.37 |

Table 3-13. Nunivak basalt major element abundances (wt.%), Continued.

| | B-9 | B-10 | B-13 |
|---|---|---|---|
| rock type | bas. | bas. | bas. |
| $SiO_2$ | 47.27 | 46.04 | 45.01 |
| $TiO_2$ | 1.92 | 2.34 | 2.21 |
| $Al_2O_3$ | 14.88 | 14.80 | 14.04 |
| $Fe_2O_3$ | 3.03 | 3.27 | 3.25 |
| FeO | 8.18 | 8.82 | 8.77 |
| MnO | 0.22 | 0.19 | 0.21 |
| MgO | 8.37 | 9.13 | 11.36 |
| CaO | 7.81 | 8.04 | 9.93 |
| $Na_2O$ | 5.06 | 4.54 | 3.39 |
| $K_2O$ | 2.47 | 2.08 | 1.34 |
| $P_2O_5$ | 0.78 | 0.76 | 0.50 |
| Total | 99.99 | 100.01 | 100.01 |
| $Mg/(Mg+Fe^{2+})$ | 64.6 | 64.9 | 69.8 |
| equilibrium olivine | $Fo_{86}$ | $Fo_{86}$ | $Fo_{89}$ |
| CIPW norms | | | |
| or | 14.60 | 12.29 | 7.92 |
| ab | 16.38 | 16.14 | 12.15 |
| an | 10.59 | 13.86 | 19.14 |
| ne | 14.32 | 12.07 | 8.96 |
| di | 13.23 | 12.29 | 16.42 |
| he | 5.40 | 4.70 | 5.14 |
| en | - | - | - |
| fs | - | - | - |
| fo | 10.31 | 11.95 | 14.49 |
| fa | 5.32 | 5.78 | 5.74 |
| mt | 4.39 | 4.74 | 4.71 |
| il | 3.65 | 4.44 | 4.20 |
| ap | 1.81 | 1.77 | 1.16 |

0.64 to 0.71. $K_2O$, $Na_2O$, and $P_2O_5$ increase as the basalts become more $SiO_2$-undersaturated (Table 3-13). All the basalts have the high La/Yb ratios relative to chondrites (Table 3-14; Figure 3-27) which are typical of alkali basalts; the basanites have higher La/Yb ratios (Figure 3-28) as well as higher incompatible element abundances than the tholeiites. Thus, abundances of incompatible elements such as Rb, K, Ba, and Sr, correlate positively with La/Yb ratio (Figure 3-29, Table 3-14); in contrast Sc decreases slightly as La/Yb ratio increases while Cr and Co appear to vary independently of La/Yb ratio (Table 3-14). On plots of incompatible versus incompatible elements, the tholeiites and basanites form single, linear arrays (Figure 3-30).

In general, the trace element data for the Nunivak basalts are similar to the data for other alkali basalt suites (Table 3-15). Relative to normal MORBs, the alkali basalts have high alkali and alkaline earth element abundances, high Th abundances, low K/Rb, high Ba/Sr, and La/Yb ratios and low K/Ba ratios and Sc contents (Table 3-15). The Nunivak basalts are similar in all respects to other alkali basalts (Table 3-15) with the exception of having higher K contents and K/Ba ratios than most other suites.

The isotopic ratios of the basalts (Table 3-9) lie within the mantle array (Figure 3-11) and are similar to some MORBs and to some oceanic islands (Figure 3-11). The $^{143}Nd/^{144}Nd$ ratios of the Nunivak basalts are among the highest found in oceanic island basalts. A second important observation is that the range of isotopic compositions of the basalts overlaps the range for the CE, CT, ACE, and ACT

Table 3-14. Trace element abundances (ppm) in the Nunivak basalts.

| rock type | B-1 ol thol | B-5 ol thol | B-12 ol thol | B-6 bas | B-7 bas |
|---|---|---|---|---|---|
| K | 6990 | 8640 | 7600 | 14850 | 12990 |
| Sc | 22.6 | 22.1 | 23.5 | 18.0 | 20.9 |
| Cr | 312 | 276 | 327 | 203 | 358 |
| Co | 53.3 | 50.1 | 51.3 | 48.8 | 59.6 |
| Rb | 10.9 | 14.2 | 12.3 | 27.9 | 26.7 |
| Sr | 469 | 524 | 526 | 785 | 700 |
| Cs | 0.12 | 0.20 | 0.14 | 0.32 | 0.35 |
| Ba | 190 | 209 | 187 | 353 | 386 |
| La | 15.3 | 17.4 | 13.1 | 29.2 | 32.9 |
| Ce | 33.5 | 38.0 | 30.1 | 63.7 | 62.8 |
| Nd | 16.8 | 19.6 | 16.5 | 27.5 | 27.1 |
| Sm | 4.27 | 4.86 | 4.21 | 6.34 | 6.11 |
| Eu | 1.60 | 1.76 | 1.60 | 2.22 | 2.06 |
| Tb | 0.75 | 0.81 | 0.73 | 0.88 | 0.84 |
| Ho | 0.83 | 0.82 | 0.74 | 0.69 | 0.83 |
| Yb | 1.58 | 1.70 | 1.66 | 1.59 | 1.65 |
| Lu | 0.26 | 0.24 | 0.24 | 0.23 | 0.22 |
| Th | 1.9 | 2.0 | 1.3 | 3.6 | 4.3 |

Table 3-14. Trace element abundances (ppm) in the Nunivak basalts, continued.

| rock type | B-9 bas | B-10 bas | B-13 bas |
|---|---|---|---|
| K | 20990 | 18790 | 11400 |
| Sc | 15.6 | 19.7 | 25.4 |
| Cr | 281 | 292 | 348 |
| Co | 41.1 | 49.4 | 58.2 |
| Rb | 45.7 | 37.5 | 21.1 |
| Sr | 1046 | 897 | 639 |
| Cs | 0.49 | 0.49 | 0.32 |
| Ba | 541 | 492 | 310 |
| La | 55.6 | 43.3 | 27.1 |
| Ce | 101 | 90.0 | 58.0 |
| Nd | 38.8 | 34.1 | 23.8 |
| Sm | 7.40 | 7.23 | 5.30 |
| Eu | 2.46 | 2.61 | 2.09 |
| Tb | 1.02 | 1.08 | 0.74 |
| Ho | 1.05 | 0.90 | 0.63 |
| Yb | 2.28 | 2.22 | 1.82 |
| Lu | 0.33 | 0.34 | 0.29 |
| Th | 7.1 | 5.7 | 3.3 |

Table 3-15. Geochemical characteristics of alkali basalts* and MORBs.

| Location | Environs | $Mg/Mg+Fe^{2+}$ | %ne/hy | Sc ppm | Cr ppm | K ppm | Rb ppm | Ba ppm |
|---|---|---|---|---|---|---|---|---|
| Nunivak | ocean island (?) | | | | | | | |
| basanites | | 64-70 | 8-14 ne | 16-25 | 203-358 | 11403-20988 | 21-46 | 310-541 |
| tholeiites | | 67 | 10-12 hy | 22-24 | 276-327 | 6988-8640 | 11-14 | 187-209 |
| Normal MORBs | ocean ridge | | - | 33-55 | 35-510 | 430-2154 | 0.7-3.9 | 7-46 |
| Southern Highlands Australia | continental | 38-73 | 2-23 ne | - | 201-685 | 7470-16600 | 19-33 | 390-740 |
| Monaro Australia | continental | 60-70 | - | - | 110-280 | 8632-14270 | 18-33 | 296-827 |
| Tasmania, Victoria Australia | continental | | | | | | | |
| alkali basalts & basanites | | 66-75 | 1-20 ne | 14-23 | 219-520 | 9800-18430 | 24-45 | 350-590 |
| olivine tholeiites | | 60-75 | 3-20 hy | 22-26 | 240-312 | 4480-9547 | 9-24 | 125-1200 |
| Ross Island | continental (?) | 63-74 | - | - | 328-581 | 9000-16000 | 26-56 | 328-581 |
| Honolulu Volcanic Series alkali basalts | ocean island | 52-71 | 1-18 ne | 18-29 | 395-555 | 4150-9047 | - | 325-880 |
| Grenada | island arc | 69-75 | 5 hy-13 ne | - | - | 2739-12118 | 5-54 | 108-500 |
| basanites and alkali basalts | | | | | | | | |

Table 3-14. Trace element abundances (ppm) in the Nunivak basalts, continued.

| rock type | B-9 bas | B-10 bas | B-13 bas |
|---|---|---|---|
| K | 20990 | 18790 | 11400 |
| Sc | 15.6 | 19.7 | 25.4 |
| Cr | 281 | 292 | 348 |
| Co | 41.1 | 49.4 | 58.2 |
| Rb | 45.7 | 37.5 | 21.1 |
| Sr | 1046 | 897 | 639 |
| Cs | 0.49 | 0.49 | 0.32 |
| Ba | 541 | 492 | 310 |
| La | 55.6 | 43.3 | 27.1 |
| Ce | 101 | 90.0 | 58.0 |
| Nd | 38.8 | 34.1 | 23.8 |
| Sm | 7.40 | 7.23 | 5.30 |
| Eu | 2.46 | 2.61 | 2.09 |
| Tb | 1.02 | 1.08 | 0.74 |
| Ho | 1.05 | 0.90 | 0.63 |
| Yb | 2.28 | 2.22 | 1.82 |
| Lu | 0.33 | 0.34 | 0.29 |
| Th | 7.1 | 5.7 | 3.3 |

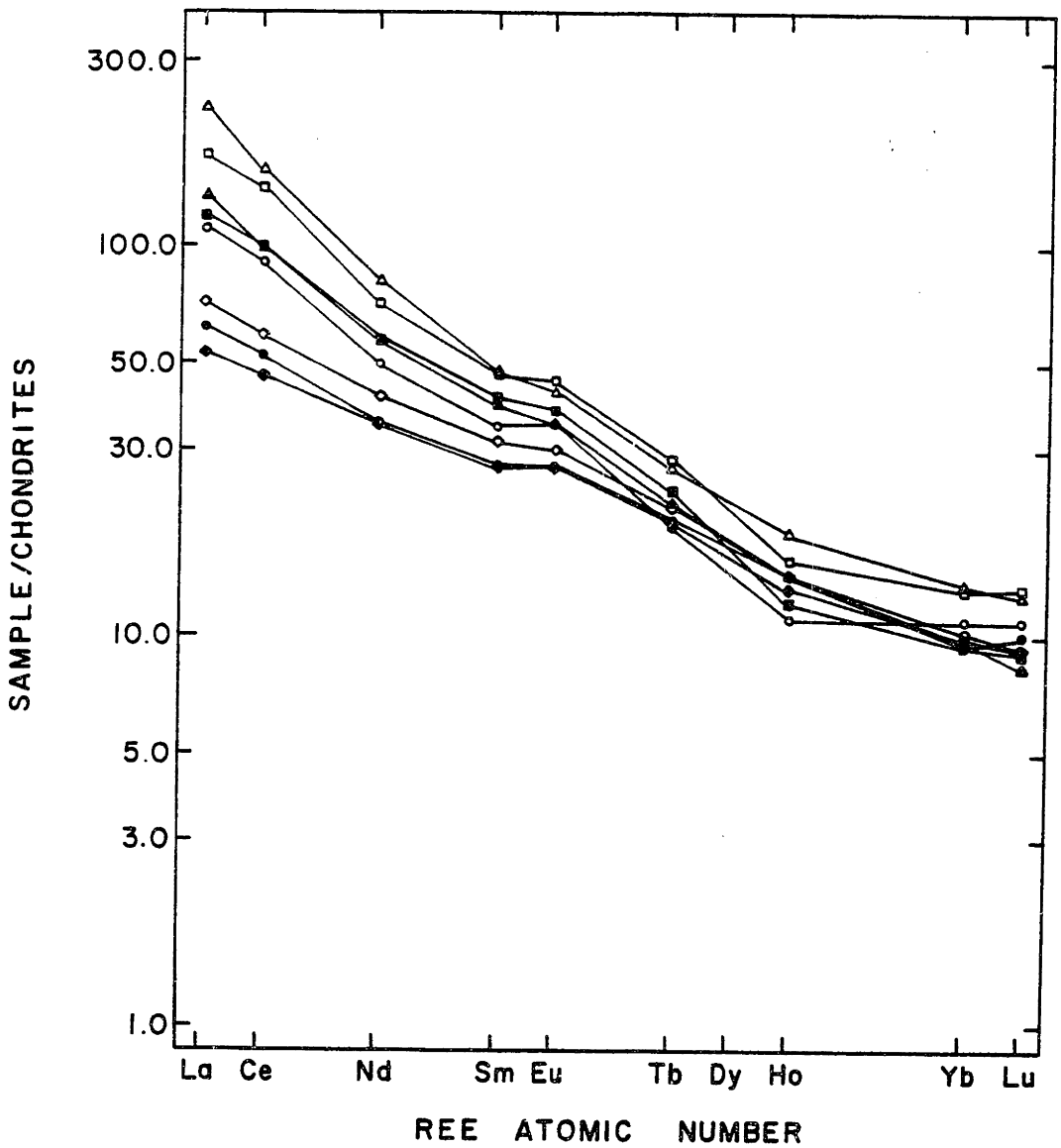
300.0
100.0
50.0
30.0
10.0
5.0
3.0
1.0
SAMPLE/CHONDRITES
La
Ce
Nd
Sm
Eu
Tb
Dy
Ho
Yb
Lu
REE ATOMIC NUMBER

Figure 3-27. Chondrite-normalized REE patterns for the Nunivak basalts.

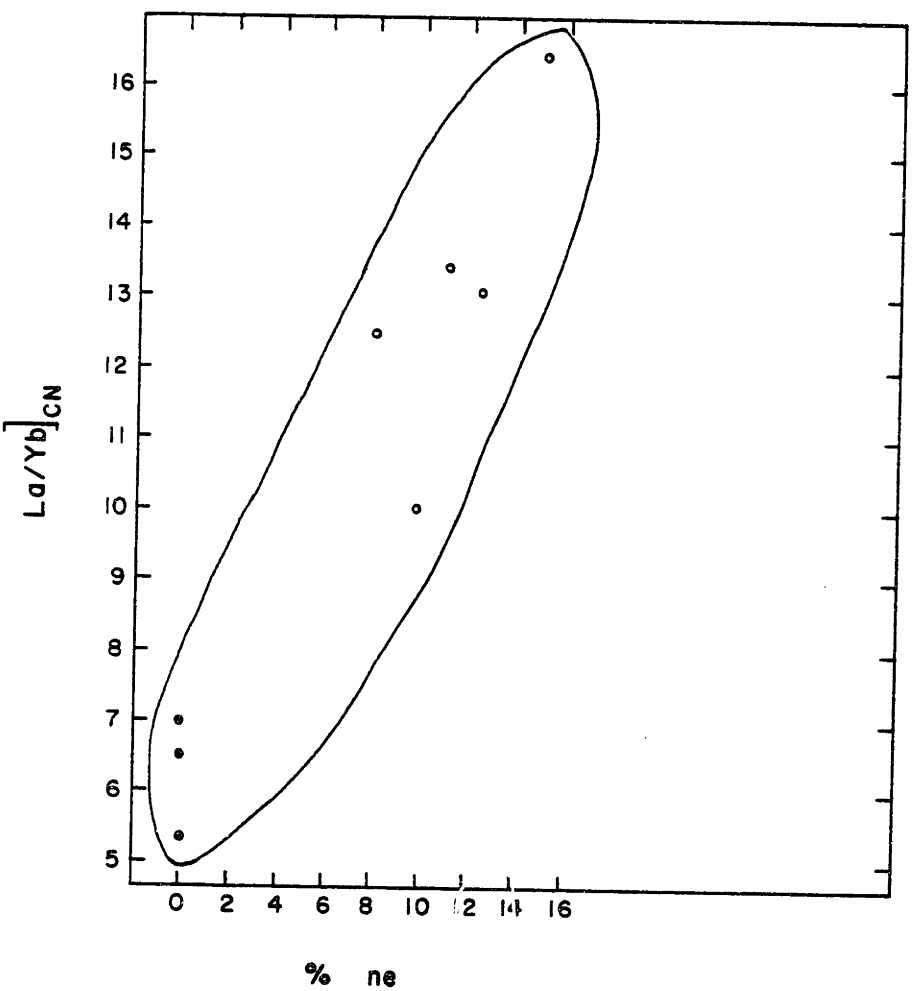
16
15
14
13
12
11
10
9
8
7
6
5
La/Yb]CN
0
2
4
6
8
10
12
14
16
% ne

Figure 3-28. Chondrite-normalized La/Yb ratio plotted versus percent normative nepheline for the Nunivak tholeiites (●) and basanites (o).

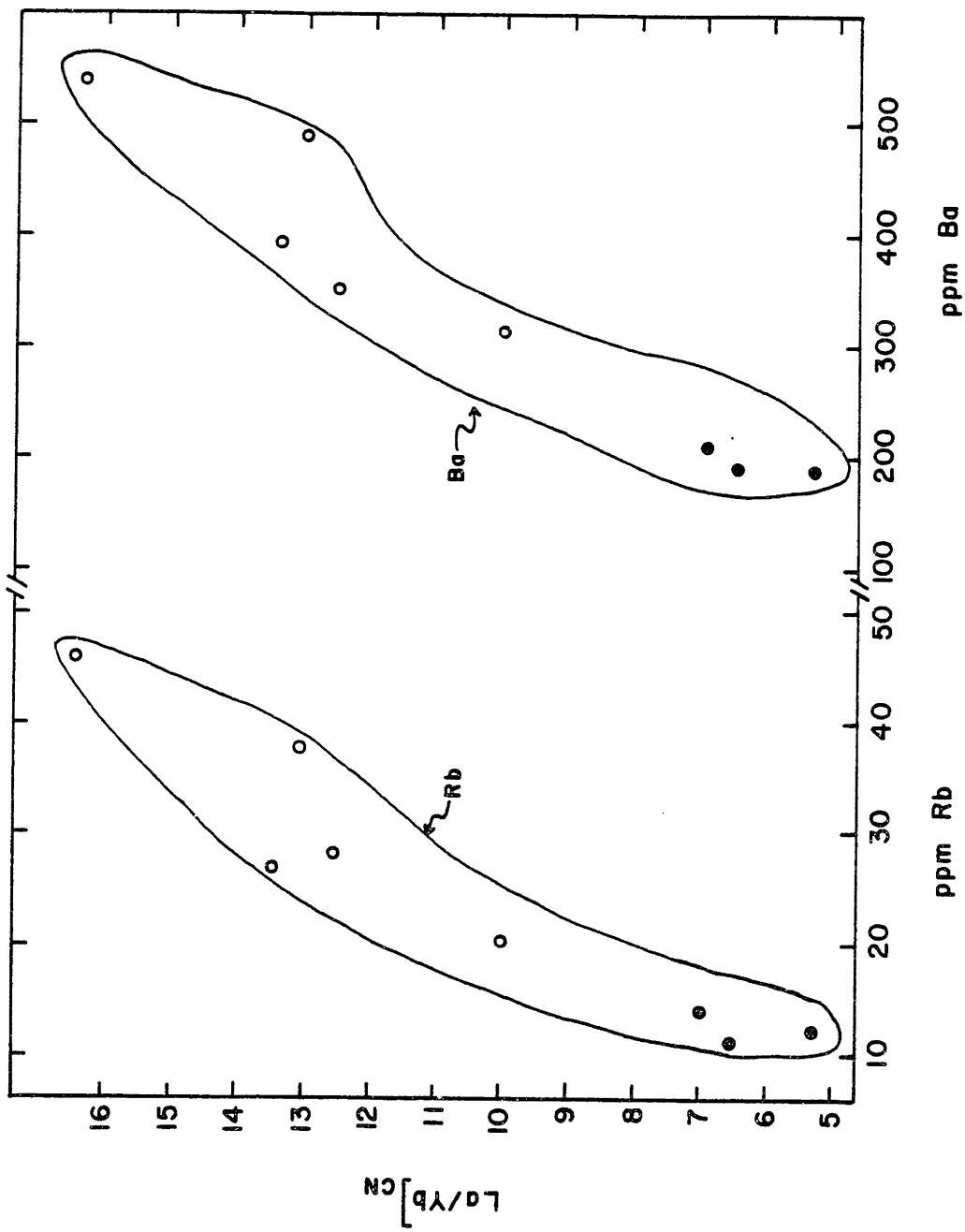
[La/Yb]CN
16
15
14
13
12
11
10
9
8
7
6
5
Rb
Ba
10
20
30
40
50
100
200
300
400
500
ppm Rb
ppm Ba

Figure 3-29. $(La/Yb)_{cn}$ plotted versus Rb and Ba for the Nunivak tholeiites (●) and basanites (o).

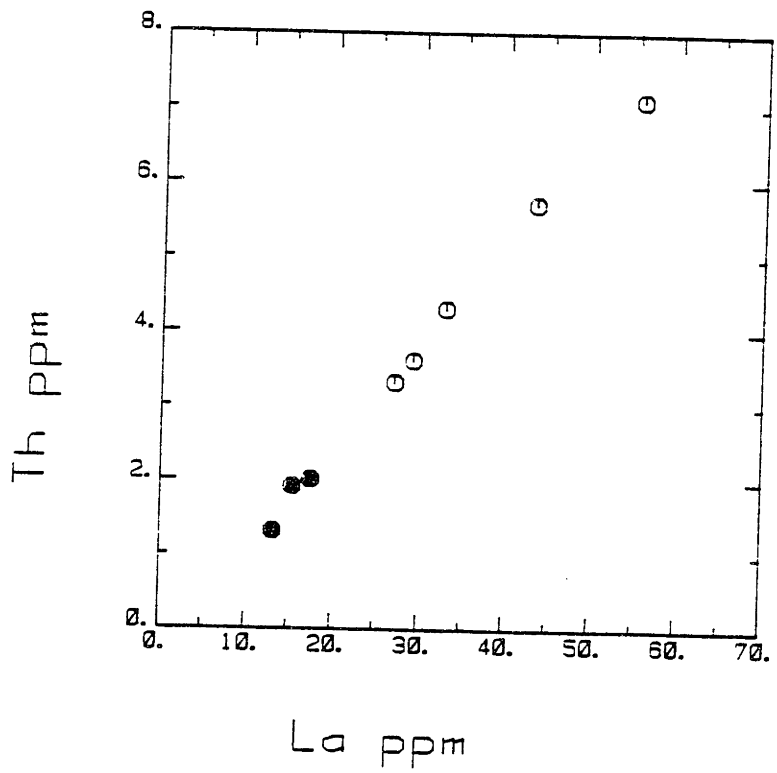
8.
6.
4.
2.
0.
0.
10.
20.
30.
40.
50.
60.
70.
Th ppm
La ppm

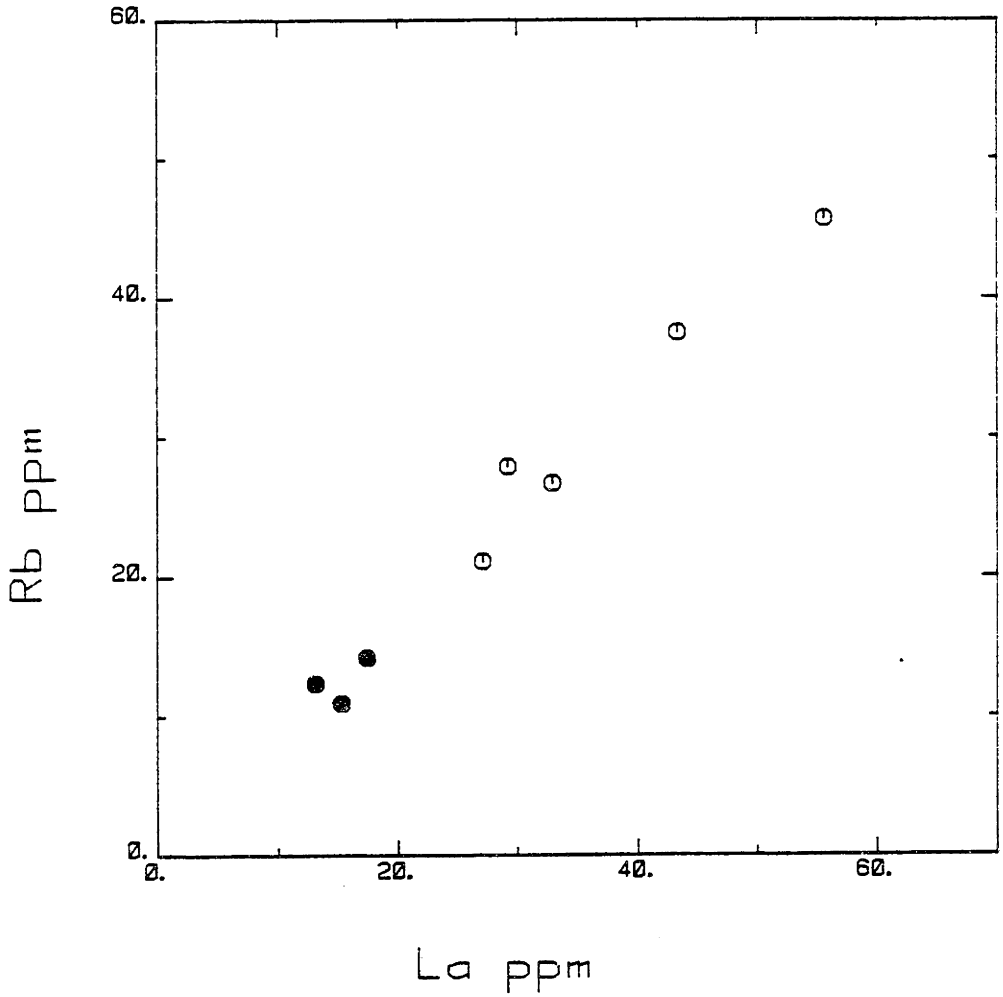
60.
40.
20.
0.
0.
20.
40.
60.
Rb ppm
La ppm

Figure 3-30. Plots of Th(A) and Rb(B) versus La for the Nunivak basalts (this study). Solid symbols indicate tholeiites, open symbols indicate basanites.

inclusions while the GE inclusions have significantly lower $^{87}Sr/^{86}Sr$ and higher $^{143}Nd/^{144}Nd$ ratios than the basalts (Figures 3-12, 3-13). The isotopic ratios of the ACE and ACT inclusions lie within the range of these ratios for the Nunivak basalts (Figures 3-12, 3-13).

When the basalts data are considered along with the other Nunivak data two trends are visible on the $(La/Yb)_{cn}$ versus $^{87}Sr/^{86}Sr$ plot (Figure 3-10) which involve the basalts, the pyroxenites, and the CE, CT, ACE, and ACT inclusions. Firstly, there is a vertical trend of variable $(La/Yb)_{cn}$ and essentially constant $^{87}Sr/^{86}Sr$ which involves some basalts, the ACE and ACT inclusions, and the pyroxenites. A second trend is approximately hyperbolic in form and involves some ACE and ACT inclusions, the basalts, and the CE and CT inclusions (Figure 3-10).

When the data of Mark (1971) are considered along with the present data it becomes apparent that the basanites have lower $^{87}Sr/^{86}Sr$ than the tholeiites, and thus, an inverse correlation exists between $^{87}Sr/^{86}Sr$ ratios and incompatible element abundances, e.g., Rb (Figure 3-31). Furthermore, there is an inverse correlation between $^{87}Sr/^{86}Sr$ and Rb/Sr (Figure 3-32). This relationship is of particular interest because of the parent-daughter relationship between $^{87}Rb$ and $^{87}Sr$. In contrast, based on our limited data, the $^{143}Nd/^{144}Nd$ ratios of the basalts do not exhibit consistent trends relative to elemental ratios or concentrations (Figure 3-33).

An interesting parallel exists between the Nunivak basalts and at least two Hawaiian shield volcanoes, Haleakala on East Maui Is. and

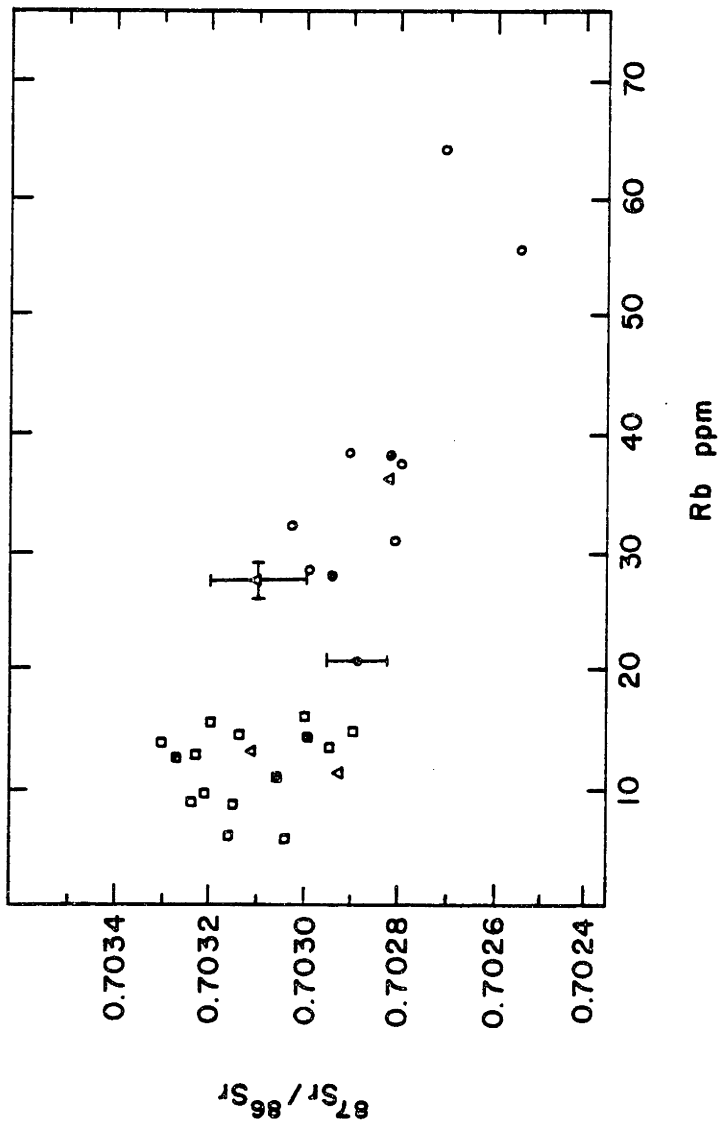
0.7034
0.7032
0.7030
0.7028
0.7026
0.7024
$^{87}Sr/^{86}Sr$
10
20
30
40
50
60
70
Rb ppm

Figure 3-31. $^{87}Sr/^{86}Sr$ plotted versus Rb ppm for Nunivak tholeiites (□, ■), transitional basalts (△), and basanites (○, ●). Open symbols indicate data from Mark (1971); filled symbols indicate data from this study. Typical errors for the two data sets are shown by error bars.

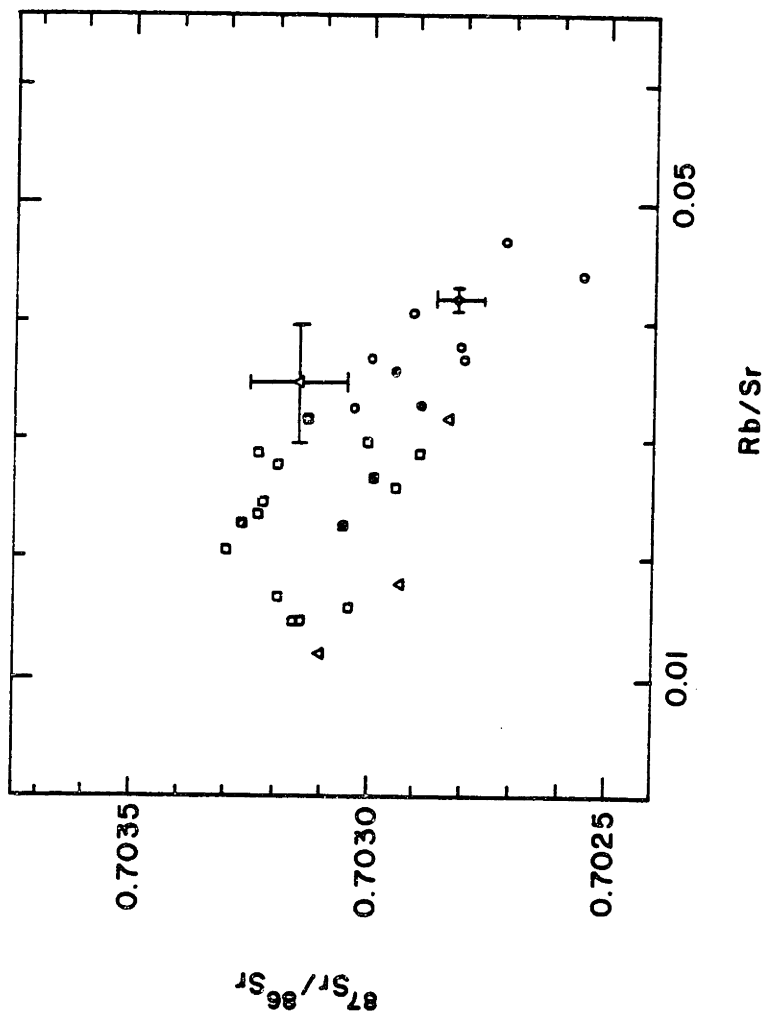
0.7035
0.7030
0.7025
$^{87}Sr/^{86}Sr$
0.01
0.05
Rb/Sr

Figure 3-32. $^{87}Sr/^{86}Sr$ plotted versus Rb/Sr for Nunivak tholeiites (□, ■), transitional basalts (△), and basanites (○, ●). Open symbols indicate data from Mark (1971); filled symbols indicate data from this study.

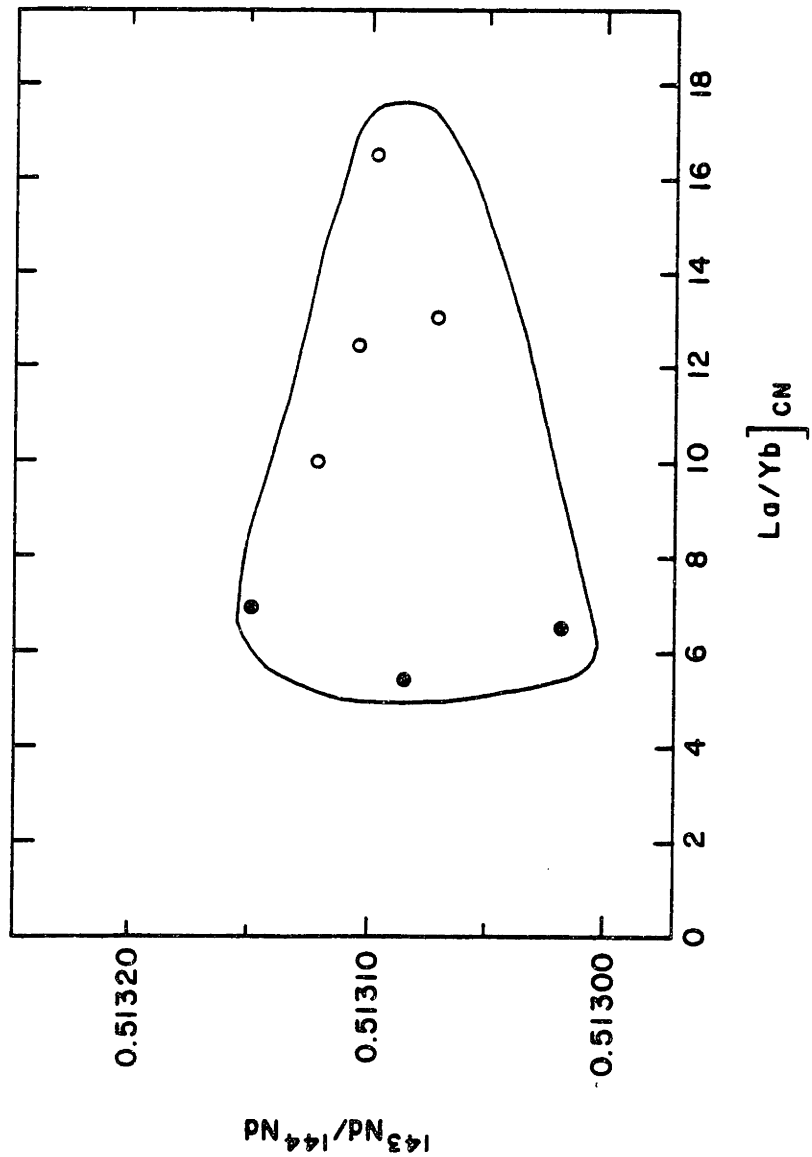
0.51320
0.51310
0.51300
$^{143}Nd/^{144}Nd$
0
2
4
6
8
10
12
14
16
18
$[La/Yb]_{CN}$

Figure 3-33. $^{143}Nd/^{144}Nd$ plotted versus chondrite-normalized La/Yb ratio for Nunivak tholeiites (●) and basanites (⊙).

Koolau on Oahu. In all these cases, the younger, more alkalic basalts have lower $^{87}Sr/^{86}Sr$ ratios than the older and more voluminous tholeiites (Chen et al., 1981; Lanphere and Dalrymple, 1980). In the two Hawaiian cases, $^{143}Nd/^{144}Nd$ ratios are also higher in the alkali basalts than in the tholeiites (Chen et al., 1981; Roden et al., 1981 and unpublished data). Although the inverse correlation of incompatible element contents and $^{87}Sr/^{86}Sr$ ratios is not a general pattern in oceanic island volcanism (Carmichael et al., 1974) it appears to be a fundamental feature of both the cited Hawaiian examples and of the Nunivak basalts.

## VI. DISCUSSION

### (A) Mass balance

In order to pursue the problem of mantle metasomatism it is important to establish where the incompatible elements are concentrated in the peridotite inclusions. Previous studies have shown that clinopyroxene and hydrous phases from metasomatized peridotite inclusions commonly have La/Sm ratios greater than chondrites (e.g., Figure 3-6; Varne and Graham, 1971; Frey and Green, 1974; Frey and Prinz, 1978). Hydrous phases are important sinks for other incompatible elements such as K, Rb, Sr, and Ba (e.g., Menzies and Murthy, 1980b; Delaney et al., 1980). Significant amounts of the LREE and other incompatible elements may also be concentrated along grain boundaries, or in unusual accessory phases (e.g., Kurat et al.,

1980; Ottonello, 1980; Erlank and Rickard, 1977). Recent studies (e.g., Zindler and Jagoutz, 1980) showed that fluid inclusions may be another important sink for incompatible elements in metasomatized inclusions.

For the Nunivak inclusions 10070, 10068, 10004, and 10002 mass balance calculations were performed to determine where the LREE and other incompatible elements were concentrated. These calculations are based on the partition coefficients in Table 3-16, modal analyses, and mineral and bulk rock trace element abundances from Tables 3-3, 3-5. Equilibrium between clinopyroxene, orthopyroxene, and olivine was assumed and the contribution from spinel was ignored.

For the two GE inclusions, 10068 and 10070, the bulk of the whole rock content of the heavy REE (HREE) and Sr are contained in the constituent silicates (Table 3-7, 3-8). The high calculated bulk rock abundances of the HREE in 10068 relative to the observed abundances is probably due to the overestimation of clinopyroxene in the modal analyses. In the GE inclusions, clinopyroxene and olivine were difficult to distinguish because much of the olivine is unstrained and the clinopyroxene lacks visible exsolution lamellae. Thus, the amount of clinopyroxene in 10068 could easily have been overestimated by as much as one-third.

K, Rb, Ba, and the LREE appear to be decoupled from the HREE because the observed bulk rock abundances are significantly greater than the calculated bulk rock abundances (Tables 3-17, 3-18). These elements are probably concentrated along grain boundaries or possibly

Table 3-16. Partition coefficients.

| | opx / cpx | ol / cpx |
|---|---|---|
| K | 0.11[1] | 0.045[2] |
| Rb | 0.58[1] | 0.53[2] |
| Sr | 0.0027[1] | 0.00081[2] |
| Ba | 0.32[1] | 0.049[3] |
| La | 0.0070[4] | 0.0008[4] |
| Ce | 0.0085[4] | 0.0008[4] |
| Nd | 0.013[4] | 0.0007[4] |
| Sm | 0.028[4] | 0.0006[4] |
| Eu | 0.034[4] | 0.0007[4] |
| Tb | 0.057[4] | 0.0020[4] |
| Yb | 0.20[4] | 0.019[4] |
| Lu | 0.25[4] | 0.028[4] |

1. average, precise values, Zindler (1980)
2. average, sample P39, Hart and Brooks (1974) and precise values, Zindler (1980).
3. average, sample P39, Hart and Brooks (1974).
4. average, Dreiser Weiher inclusions, Stosch (1982).

Table 3-17. 10070 mass balance (ppm).

| | CPX | OPX | oliv | calc. BR | meas. BR |
|---|---|---|---|---|---|
| mode % | 12.6 | 27.2 | 57.3 | | |
| K | 28.8 | 3.17 | 1.30 | 5.2 | 9.01 |
| Rb | 0.021 | 0.012 | 0.011 | 0.012 | 0.011 |
| Sr | 93.2 | 0.252 | 0.075 | 12 | 16 |
| La | 1.37 | 0.00959 | 0.0011 | 0.18 | 0.267 |
| Ce | 5.49 | 0.0467 | 0.00439 | 0.71 | 0.99 |
| Nd | 6.1 | 0.0793 | 0.00427 | 0.79 | 0.99 |
| Sm | 2.07 | 0.0580 | 0.00124 | 0.28 | 0.35 |
| Eu | 0.859 | 0.0292 | 0.00060 | 0.12 | 0.15 |
| Tb | 0.558 | 0.0318 | 0.00112 | 0.080 | 0.099 |
| Yb | 2.26 | 0.452 | 0.0429 | 0.43 | 0.43 |
| Lu | 0.35 | 0.088 | 0.0099 | 0.074 | 0.074 |

---

CPX = measured clinopyroxene abundances; OPX = calculated orthopyroxene abundances; oliv = calculated olivine abundances; BR = calculated bulk rock abundances; meas. BR = measured bulk rock abundances.

Table 3-18. 10068 mass balance (ppm).

| | CPX | OPX | oliv | calc. BR | meas. BR |
|---|---|---|---|---|---|
| mode (%) | 14.2 | 37.4 | 46.1 | | |
| K | 22.0 | 2.42 | 0.99 | 4.49 | 16.5 |
| Rb | 0.0603 | 0.035 | 0.032 | 0.036 | 0.11 |
| Sr | 72.2 | 0.19 | 0.058 | 10.4 | 12.9 |
| Ba | 0.366 | 0.12 | 0.018 | 0.11 | 0.56 |
| La | 0.918 | 0.0064 | 0.00073 | 0.13 | 0.26 |
| Ce | 3.80 | 0.032 | 0.0030 | 0.55 | 1.1 |
| Nd | 4.00 | 0.052 | 0.0028 | 0.59 | 0.76 |
| Sm | 2.05 | 0.057 | 0.0012 | 0.31 | 0.29 |
| Eu | 0.823 | 0.028 | 0.00058 | 0.13 | 0.12 |
| Tb | 0.541 | 0.031 | 0.0011 | 0.089 | 0.080 |
| Yb | 2.46 | 0.49 | 0.047 | 0.55 | 0.39 |
| Lu | 0.362 | 0.091 | 0.010 | 0.090 | 0.061 |

---

column headings as in Table 3-16

in fluid inclusions. The only other mineral phase present, spinel, is known to have very low concentrations of the LREE relative to coexisting silicates in ultramafic inclusions (Stosch, 1982). The partitioning of the other elements into spinel is unknown, but spinel is unlikely to be a satisfactory host for LIL elements because of its small crystallographic sites (e.g., Jensen, 1973). If these incompatible elements are concentrated along grain boundaries, then their distribution could have resulted from either contamination by the host basalt, surface alteration, or a mantle process. Thus, in these GE inclusions the measured bulk rock concentrations of K, Rb, Ba, and the LREE represent upper limits to actual mantle concentrations.

The CT inclusion 10004 appears to have a more complex incompatible element distribution than the GE inclusions. The mass balance calculations for the REE are in reasonable agreement with bulk rock concentrations in clinopyroxene (Table 3-19). In contrast, measured K, Rb, and Ba abundances are much higher in the whole rock samples than in the calculated bulk rocks. These alkali and alkaline earth elements may be concentrated in fluid inclusions; Zindler and Jagoutz (1980) noted a correlation between fluid inclusions and high alkali contents of mineral separates from San Carlos inclusions. However, the low alkali contents of 10004 clinopyroxene are inconsistent with this supposition because the fluid inclusions are more concentrated in the clinopyroxene than the other silicates. Perhaps a more reasonable explanation is that K, Rb, and Ba are concentrated along grain boundaries. As above, this concentration could be the result of contamination by the host

Table 3-19. 10004 mass balance (ppm).

| | CPX | OPX | oliv | calc. BR | meas. BR |
|---|---|---|---|---|---|
| mode (%) | 8.7 | 21.3 | 68.6 | | |
| K | 28.6 | 3.15 | 1.29 | 4.04 | 172 |
| Rb | 0.0639 | 0.037 | 0.034 | 0.037 | 0.419 |
| Sr | 285 | 0.77 | 0.23 | 25.1 | 31.1 |
| Ba | 4.08 | 1.31 | 0.20 | 0.77 | 8.05 |
| La | 9.26 | 0.065 | 0.0074 | 0.825 | 0.910 |
| Ce | 25.0 | 0.213 | 0.02 | 2.23 | 2.5 |
| Nd | 12.6 | 0.16 | 0.0088 | 1.14 | 1.12 |
| Sm | 2.36 | 0.066 | 0.0014 | 0.22 | 0.18 |
| Eu | 0.815 | 0.028 | 0.00057 | 0.077 | 0.060 |
| Tb | 0.362 | 0.021 | 0.00072 | 0.036 | 0.036 |
| Yb | 1.34 | 0.27 | 0.12 | 0.26 | 0.19 |
| Lu | 0.209 | 0.052 | 0.0059 | 0.033 | 0.031 |

---

column headings as in Table 3-16

basalt, surface alteration, or the result of a mantle enrichment event. However, contamination by host basalt cannot explain the relatively high $^{87}Sr/^{86}Sr$ ratio of the bulk rock compared to the ratio of 10004 clinopyroxene (Table 3-9) because the $^{87}Sr/^{86}Sr$ ratios of the Nunivak basalts are lower than 10004 clinopyroxene (Table 3-9). Groundwater contamination is also an unlikely explanation because it does not provide an adequate explanation of the $^{87}Sr/^{86}Sr$ ratio of 10004 clinopyroxene which is higher than $^{87}Sr/^{86}Sr$ ratios of the other Nunivak inclusions and basalts (Table 3-9). We prefer the interpretation that the relatively high $^{87}Sr/^{86}Sr$ ratios of 10004 bulk rock and clinopyroxene are the result of a mantle metasomatic event characterized by an initial $^{87}Sr/^{86}Sr$ ratio of approximately 0.70343. We propose that this event is the cause of the apparent concentration of alkali elements along grain boundaries in this inclusion. The relationship between bulk rock and clinopyroxene in 10004 (Figure 3-12) is consistent with an age of 580 million years for the enrichment event.

For the ACE inclusion 10002, the bulk rock concentrations of K, Rb, and Sr were calculated using the analysis of a pargasite (Menzies and Murthy, 1980b) from Nunivak peridotite UM1 because we did not analyze the 10002 glass for these elements. Although it is unlikely that UM1 pargasite has the same concentrations of K, Rb, and Sr as 10002 glass, we can nevertheless qualitatively decide whether the calculated bulk rock abundances are consistent with the measured bulk rock abundances. The calculations show that in contrast to the inclusions described above, all the incompatible elements appear to be

concentrated in mineral phases (Table 3-20). The REE and Sr appear to be more or less equally distributed between clinopyroxene and amphibole/glass; note that apatite inclusions in the clinopyroxene were observed in this section. The K and Rb calculations indicate that K and Rb must be concentrated in the amphibole/glass phase although the high calculated bulk rock abundances of K and Rb compared to the measured bulk rock abundances show that UM1 pargasite has higher K and Rb abundances than the original amphibole in 10002. We also suspect that Ba is concentrated in the amphibole/glass because amphiboles from other mantle-derived inclusions typically have Ba contents in the range 110-370 ppm (Basaltic Volcanism Study Project, 1981).

In the absence of further data it is uncertain whether the above results can be extrapolated to other inclusions from Nunivak. It seems clear, however, based on the mass balance calculations (Table 3-20) above and on the data of Menzies and Murthy (1980b) that in the ACE and ACT inclusions the incompatible elements are concentrated in clinopyroxene, apatite, fluid inclusions, and hydrous phases. For the GE, CT, and CE inclusions the HREE and Sr are concentrated in clinopyroxene; however, in the case of the 3 GE and CT inclusions studied above, a significant amount of K, Rb, and Ba and for the GE inclusions, LREE, appear to be concentrated along grain boundaries. The isotopic data for 10004 indicate that this phase or phases is not related to the host basalts; thus, the grain boundary phase(s) is a consequence of either surface alteration or a mantle process.

Table 3-20. 10002 mass balance (ppm).

| | cpx | cpx | oliv | gl | calc. BR | meas. BR |
|---|---|---|---|---|---|---|
| mode (%) | 6.8 | 13.1 | 70.4 | 8.9 | | |
| K | 11.3 | 1.24 | 0.51 | 5260[1] | 469 | 206 |
| Rb | 0.00983 | 0.0057 | 0.0052 | 4.37[1] | 0.39 | 0.23 |
| Sr | 676 | 1.83 | 0.55 | 806 | 118 | 82.2 |
| Ba | 1.04 | 0.33 | 0.051 | - | 0.15[2] | 7.03 |
| La | 18.8 | 0.13 | 0.015 | 23.9 | 3.44 | 3.65 |
| Ce | 42.1 | 0.36 | 0.034 | 44.2 | 6.86 | 6.53 |
| Nd | 15.0 | 1.5 | 0.011 | 13.9 | 2.33 | 2.06 |
| Sm | 1.80 | 0.050 | 0.0011 | 1.83 | 0.29 | 0.25 |
| Eu | 0.628 | 0.021 | 0.00044 | 0.648 | 0.097 | 0.084 |
| Tb | 0.188 | 0.011 | 0.00038 | 0.204 | 0.033 | 0.030 |
| Yb | 1.11 | 0.22 | 0.021 | 0.76 | 0.19 | 0.15 |
| Lu | 0.19 | 0.048 | 0.0053 | 0.127 | 0.034 | 0.024 |

column headings as in Table 3-16 except gl = glass

1. K, Rb abundances from UM1 pargasite, Nunivak Island peridotite inclusion, Menzies and Murthy (1980a).

2. without glass contribution.

# GEOCHEMISTRY OF THE EARTH'S MANTLE, NUNIVAK ISLAND, ALASKA AND OTHER AREAS: EVIDENCE FROM XENOLITH STUDIES

(Vol. II)

by

MICHAEL FRANK RODEN

A.B., Hamilton College
(1972)

M.A., University of Texas
(1977)

SUBMITTED TO THE DEPARTMENT OF EARTH AND PLANETARY SCIENCES IN PARTIAL FULFILLMENT OF THE REQUIREMENTS FOR THE DEGREE OF

DOCTOR OF PHILOSOPHY

at the

MASSACHUSETTS INSTITUTE OF TECHNOLOGY

September, 1982

Signature of Author Michael F. Roden
Department of Earth and Planetary Sciences
May 28, 1982

Certified by Frederick A. Frey
Frederick A. Frey
Thesis Supervisor

Accepted by Theodore R. Madden
Theodore R. Madden
Chairman, Departmental Committee on Graduate Students

(B) Mantle Metasomatism: constraints from Nunivak

(1) Definition of mantle metasomatism

"If the chemical composition of a rock is altered when its minerals are replaced by others, the processes are said to be metasomatic" (Korzhinsky, 1970). In the CE, CT, ACE, and ACT inclusions, the concentrations of incompatible elements, K, Rb, Ba, Sr, and LREE, in the minerals clinopyroxene, amphibole, and apatite which appear to be replacing other silicates indicate that "metasomatic" is an appropriate word to apply to these inclusions. In the following discussion, "metasomatism" will be used to refer to the event which caused the precipitation of amphibole, clinopyroxene, and apatite, and which resulted in the relatively high incompatible element concentrations in the ACE and ACT inclusions. The CE and CT inclusions which lack hydrous phases but have relatively high incompatible element concentrations (Figure 3-9) may be recrystallized material related to an earlier metasomatic event. Alternatively, the CE and CT inclusions may have been metasomatized at the same time as the ACE and ACT inclusions but under conditions where amphibole was not stable.

In the last decade, it has been recognized that portions of the upper mantle are metasomatized, and that this metasomatism may have important ramifications for the petrogenesis of alkali basalts. For example, a number of inclusion suites from alkali basalts contain peridotites with high incompatible element concentrations and with La/Yb ratios greater than chondrites. These inclusions commonly contain amphibole or other volatile-bearing phases (Frey and Green,

1974; Frey and Prinz, 1978; Stosch and Seck, 1980; Wass and Rogers, 1980; Ottonello, 1980; Kurat et al., 1980; among others). In general, the high incompatible element concentrations in these inclusions cannot be simply related to partial melting or fractional crystallization processes and most workers have been forced to argue that a metasomatic event caused the influx of incompatible elements and the precipitation of amphibole and associated phases (e.g., Frey and Prinz, 1978; Stosch and Seck, 1980). Isotopic studies of selected metasomatized inclusions from Nunivak Island (Menzies and Murthy, 1980a), San Carlos (Zindler and Jagoutz, 1980), and Dreiser Weiher (Stosch et al., 1980) have shown in each case that metasomatism occurred recently, most likely in the last 200 million years. Amphibole-bearing peridotites also occur in alpine peridotites such as Etang de Lherz (e.g., Wilshire et al., 1980) and in two ultramafic massifs in the ocean basins, St. Paul's Rocks (Melson et al., 1972) and Zabargad Island (Bonatti et al., 1980). In the latter two occurrences, amphibole-bearing peridotites have La/Yb ratios greater than chondrites (Frey, 1970; Bonatti et al., 1981), and thus, are geochemically similar to metasomatized inclusions in alkali basalts.

(2) Unsolved problems regarding mantle metasomatism

A fundamental question with regard to metasomatism in the upper mantle is whether the metasomatic event is a precursor to alkaline basalt magmatism, i.e., is the source of alkali basalts metasomatized? (e.g., Frey et al., 1978; Menzies and Murthy, 1980b; Boettcher and O'Neill, 1980; Wass and Rogers, 1980), or whether metasomatism is a

consequence of the crystallization of basaltic magma in the upper mantle. In the latter case, the metasomatizing agent could be either a residual silicate melt (Wilshire et al., 1980) or a H2O- and CO2-rich fluid which exsolved from a crystallizing basaltic melt (Wyllie, 1980). We call the former model the "precursory model" of mantle metasomatism, and the latter model the "consequent model" of mantle metasomatism in the ensuing discussion.

Evidence supporting the precursory model of metasomatism lies principally in quantitative trace element modelling of alkali basalt suites (e.g., Sun and Hanson, 1975; Frey et al., 1978; Clague and Frey, 1982). These studies indicate that the source rocks for the basalts had La/Yb ratios greater than condrites, and were enriched in incompatible elements relative to primitive mantle. Note, however, that isotopic data (Lanphere and Dalrymple, 1980; Roden et al., 1981) for the Honolulu Volcanic Series (HVS) studied by Clague and Frey (1982) indicates that the source of the HVS had a history of depletion in incompatible elements relative to the bulk earth. Thus, if the source of the HVS was metasomatized, then the metasomatism occurred less than 500 million years ago (Roden, unpub. data). Further evidence of the existence of metasomatized mantle is the inference that some portions of subcontinental mantle have been enriched in incompatible elements relative to primitive mantle for a long time based on the isotopic compositions of diopsides from kimberlite xenoliths (Menzies and Murthy, 1980c).

The principle evidence for the consequent model of metasomatism

is the observation that amphibole-phlogopite veins in alpine peridotites have structural relations consistent with an origin by precipitation from a residual silicate melt filter pressed from adjacent pyroxenite dikes (Wilshire et al., 1980). Also consistent with the consequent model of metasomatism is a recent synthesis of phase equilibria for the system peridotite-$H_2O$-$CO_2$ (Wyllie, 1980) in which no carbonate is stable on the peridotite solidus at pressures less than approximately 25 kb. Thus, any basalt which crystallized in this system at pressures less than 25 kb will eventually exsolve a fluid phase if the magma contains any $CO_2$. That basalts fractionate in the mantle is evidenced by the presence of lherzolite inclusions in phonolites (e.g., Irving and Price, 1981).

A second fundamental question for both the precursory and consequent models of mantle metasomatism is whether the metasomatizing agent is a silicate melt or a $H_2O$- and $CO_2$-rich fluid or both. Residual silicate melts contain the required high abundances of incompatible elements based on the bulk composition of lherzolite-bearing phonolites and differentiated minettes (Irving and Price, 1981; Roden, 1981). Recent experimental evidence (summarized in Spera, 1981) indicates that $H_2O$- and $CO_2$-rich fluids are also effective solvents of incompatible elements at upper mantle pressures. In particular, at 20 kb a $CO_2$ or a $H_2O$ vapor in equilibrium with a silicate melt will be enriched in most of the REE relative to that melt (Wendlandt and Harrison, 1979; Mysen, 1979) and will have LREE/HREE ratios greater than the coexisting melt. At lower pressures, i.e., 5 kb, a $CO_2$ vapor

in equilibrium with a silicate melt is still enriched in the REE relative to the melt although a $H_2O$ vapor is not (Wendlandt and Harrison, 1979; Mysen, 1979). One complication in applying these data to inclusions is the uncertain speciation of C at the low and uncertain oxygen fugacities prevalent in the upper mantle (Arculus and Delano, 1981).

It seems inevitable that both silicate melts and volatile-rich fluids will be metasomatizing agents in the earth's mantle because a basaltic magma crystallizing in the upper mantle will eventually yield a residual melt which will become saturated with a fluid phase as it crystallizes as long as a C-bearing solid phase is not in equilibrium with the melt.

(3) Nunivak metasomatism: constraints mineralogy

The aim of ensuing discussion is to answer the two questions posed above for the Nunivak metasomatism. The initial strategy is to describe the constraints imposed on the metasomatism at Nunivak by features of the metasomatized inclusions beginning with their petrography and culminating with their isotopic and trace element characteristics.

The incompatible elements which are the signature of metasomatism are concentrated in the phases: amphibole, clinopyroxene, apatite, and phlogopite (Table 3-5, 3-11; Menzies and Murthy, 1980b). Clinopyroxenes with La/Yb ratios greater than chondrites from the ACE, ACT, and one CT inclusion contain the large Type II (Figure 3-20) fluid inclusions which are absent from clinopyroxenes of the unmetasomatized

GE inclusions. This spatial association indicates a fluid phase was associated with the metasomatism. Hence, a metasomatic assemblage can be defined which consists of amphibole + clinopyroxene ± phlogopite ± apatite ± fluid. Based on what is known of volatiles in the mantle (e.g., Roedder, 1965; Murck et al., 1978; Anderson, 1975), $CO_2$ or a more reduced form of C was an important component of the fluid phase. If true, the absence of an observable carbonate phase in the Nunivak inclusions and other metasomatized inclusions has important implications for the conditions of metasomatism. In the more oxidized system where $CO_2$ is the dominant C-bearing gas, the lack of a carbonate implies temperatures in excess of approximately 700°-800°C at 8 kb and 900°-1000°C at 18 kb, depending on vapor composition (Wyllie, 1978). Only at lower temperatures is peridotite carbonated.

Alternatively, the lack of a carbonate may be due to the low oxygen fugacity in the upper mantle (Arculus and Delano, 1981). Indeed, submicroscopic graphite has been inferred to occur in some xenoliths (Sato, 1977) and was identified optically in some fluid inclusions of peridotite xenoliths (Mathez and Delaney, 1981). In that case, the lack of a carbonate phase does not necessarily reflect high temperatures, but Arculus and Delano (1981) suggested that oxidation may accompany metasomatism. Consequently, our present understanding of phase relations does not lead to an unequivocal interpretation, however, the lack of a carbonate in the metasomatized Nunivak peridotites is consistent with a relatively high temperature of metasomatism.

Another feature which is consistent with relatively high

temperatures prevailing at the time of metasomatism is the sequence of assemblages present in the ACE and ACT inclusions. Sample 10055 contains no hydrous phases (Figure 3-15A), 10051 and 10075 contain amphibole and phlogopite (Figure 3-15B), and the other inclusions contain amphibole or glass after amphibole only. In particular, textures in 10051 (Figure 3-17) indicate that amphibole reacted with and replaced phlogopite. The assemblages can be explained if the inclusions equilibrated in different stability fields in the peridotite-$H_2O$-$CO_2$ system as follows: 10055, peridotite + vapor; 10051 and 10075, initially phlogopite + peridotite + vapor, then amphibole + peridotite + vapor; the other inclusions, amphibole + peridotite + vapor. Just this sequence, peridotite + vapor, phlogopite + peridotite + vapor, amphibole + peridotite + vapor occurs with decreasing temperature in the system peridotite-$CO_2$-$H_2O$ at relatively low pressures (8-11 kb) and high $CO_2/(CO_2 + H_2O)$ ratios in the vapor (Figure 3-34; Wyllie, 1980). The vapor composition is important because with high $CO_2/(CO_2 + H_2O)$ ratios in the vapor, the amphibole stability field shrinks so that it no longer intersects the solidus (Wyllie, 1979). Thus, with falling temperature phlogopite precipitates before amphibole (Figure 3-34). The inferences drawn above are based on a synthesis of available experimental data in the peridotite-$CO_2$-$H_2O$ system (Wyllie, 1980), and much of this synthesis needs to be experimentally verified. Furthermore, the above discussion was based on the assumption of constant bulk composition; the introduction of alkalies during metasomatism may have an effect on the stabilities of the hydrous

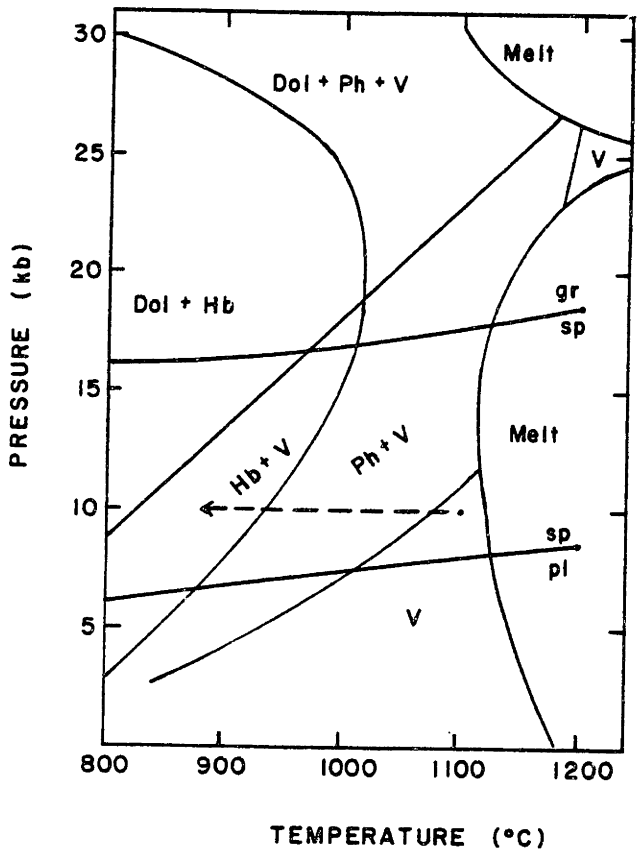
30
25
20
15
10
5
PRESSURE (kb)
Dol + Ph + V
Melt
V
Dol + Hb
gr
sp
Hb + V
Ph + V
Melt
sp
pl
V
800
900
1000
1100
1200
TEMPERATURE (°C)

Figure 3-34. Possible isobaric cooling path (dashed line) in the system peridotite-$CO_2$-$H_2$ (after Figure 2, Wyllie, 1980) to explain phase assemblages in Nunivak peridotites (Dol = dolomite, Ph = phlogopite, V = vapor, Hb = hornblende). This synthesis was constructed by assuming a closed system, $CO_2/(CO_2 + H_2O) = 0.8$ and $CO_2$ less than 5 wt.% and $H_2O$ less than 0.4 wt.%. Also shown are the stability fields of plagioclase, spinel, and garnet lherzolite (Herzberg, 1978). Possible cooling paths for the Nunivak metasomatized peridotites are limited to the spinel peridotite field where the sequence upon isobaric cooling is: vapor + anhydrous peridotite, vapor + phlogopite + peridotite, vapor + amphibole + peridotite.

phases. Nevertheless, the phase relations in the ACE and ACT inclusions are consistent with (1) the temperatures of metasomatism being close to the solidus in the peridotite-$CO_2$-$H_{20}$ system at pressures in the range of 8-18 kb, and (2) the modal variation of the metasomatic assemblage resulting from falling temperature at 8-11 kb in the presence of vapor rich in $CO_2$. The geothermometric calculations of Francis (1978) are consistent with the first inference above: using two methods he inferred temperatures greater than or equal to 900°C for the inclusions studied here (D.M. Francis, written communication).

(4) Nunivak metasomatism: constraints from isotopic data

As recognized by Menzies and Murthy (1980a), the isotopic data for the peridotites, pyroxenites, and basalts from Nunivak Island provide important constraints on the metasomatism. The Sr and Nd isotopic ratios for both the ACE and ACT peridotites, and the amphibole-pyroxenites lie within the range of these ratios for the Nunivak basalts (Table 3-9, Figures 3-12, 3-13; also see Menzies and Murthy, 1980a). This result is not due to contamination of inclusions by host basalt because the $^{87}Sr/^{86}Sr$ ratio of an acid-washed clinopyroxene from ACE inclusion 10002 lies within error of the bulk rock value (Table 3-9), and both the $^{87}Sr/^{86}Sr$ and $^{143}Nd/^{144}Nd$ ratios of this clinopyroxene lie within range of these ratios for the basalts (Figures 3-12, 3-13). Furthermore, Menzies and Murthy (1980a) found that pargasite, diopside, and mica separated from two lherzolite

inclusions had $^{87}Sr/^{86}Sr$ and $^{143}Nd/^{144}Nd$ ratios within the range of Nunivak basalts as did 2 pargasites from amphibole-pyroxenite inclusions. Because of the overlapping range of $^{87}Sr/^{86}Sr$ and $^{143}Nd/^{144}Nd$ ratios of the ACE and ACT inclusions, the pyroxenites, and the basalts these rock types may be petrogenetically related.

Zartman and Tera (1973) reported that a Nunivak basalt and an amphibole-bearing peridotite (probably an ACT inclusion) were distinct in terms of Pb isotopic ratios. This observation is not necessarily in conflict with the data presented here or by Menzies and Murthy (1980a). Although the strontium and neodymium isotopic ratios of the ACE and ACT inclusions lie within the range of the isotopic ratios of the Nunivak basalts (e.g., Figure 3-10), some individual basalts are isotopically distinct from some ACE and ACT inclusions. For example, compare the $^{87}Sr/^{86}Sr$ ratio of basalt B-10 to the $^{87}Sr/^{86}Sr$ ratio of ACT inclusion 10075 (Table 3-9). Nonetheless, measurement of the Pb isotopic ratios of ACE and ACT inclusions and basalts would be one critical test of the model we develop below in which the Nunivak metasomatism is petrogenetically related to the basaltic volcanism.

Francis (1976c) showed that the amphibole of the amphibole-pyroxenites probably formed during the metasomatic event which caused the precipitation of amphibole and phlogopite in the associated ACE and ACT peridotites. The overlapping isotopic ratios of the ACE, ACT, and pyroxenite inclusions are consistent with his conclusion. Thus, it is likely that the pyroxenites either formed contemporaneously with the metasomatism, or predated the metasomatism. Provided that

the metasomatism was the last event to affect the isotopic systems in the pyroxenites and ACE and ACT peridotites then consideration of the $^{87}Sr/^{86}Sr$ and $^{143}Nd/^{144}Nd$ data for these rocks can yield information on the timing of metasomatism. For example, on a Nd evolution diagram (Figure 3-35), the growth curves for pyroxenites 13002 and 13004 diverge, indicating that if the isotopic ratios of the pyroxenites were homogenized at the time of metasomatism then the age of metasomatism must be relatively recent, i.e., less than 450 million years ago when the uncertainties in the position of the growth curves are considered (Figure 3-35).

The $^{87}Sr/^{86}Sr$ data provide similar constraints. In a Sr evolution diagram, error envelopes around the growth curves of ACE peridotite 10051 and pyroxenite 13002 intersect the estimated growth curve for the most depleted MORB source between 250 and 500 million years ago (Figure 3-36). Because at greater ages, these growth curves lie in regions where we have no evidence for terrestrial mantle occurring (e.g., Basaltic Volcanism Study Project, 1981), the metasomatism must have occurred less than 500 million years ago. In fact, if the metasomatic event homogenized the $^{87}Sr/^{86}Sr$ ratios of the ACE and ACT peridotites and the pyroxenites, then the divergence of the growth curves of 10051 and 13002 from the growth curves of the other inclusions (Figure 3-31) indicates that metasomatism must have occurred less than 100 million years ago.

Finally, 10002 clinopyroxene has a low Sm/Nd ratio relative to chondrites (Figure 3-6); this low Sm/Nd ratio is a consequence of the

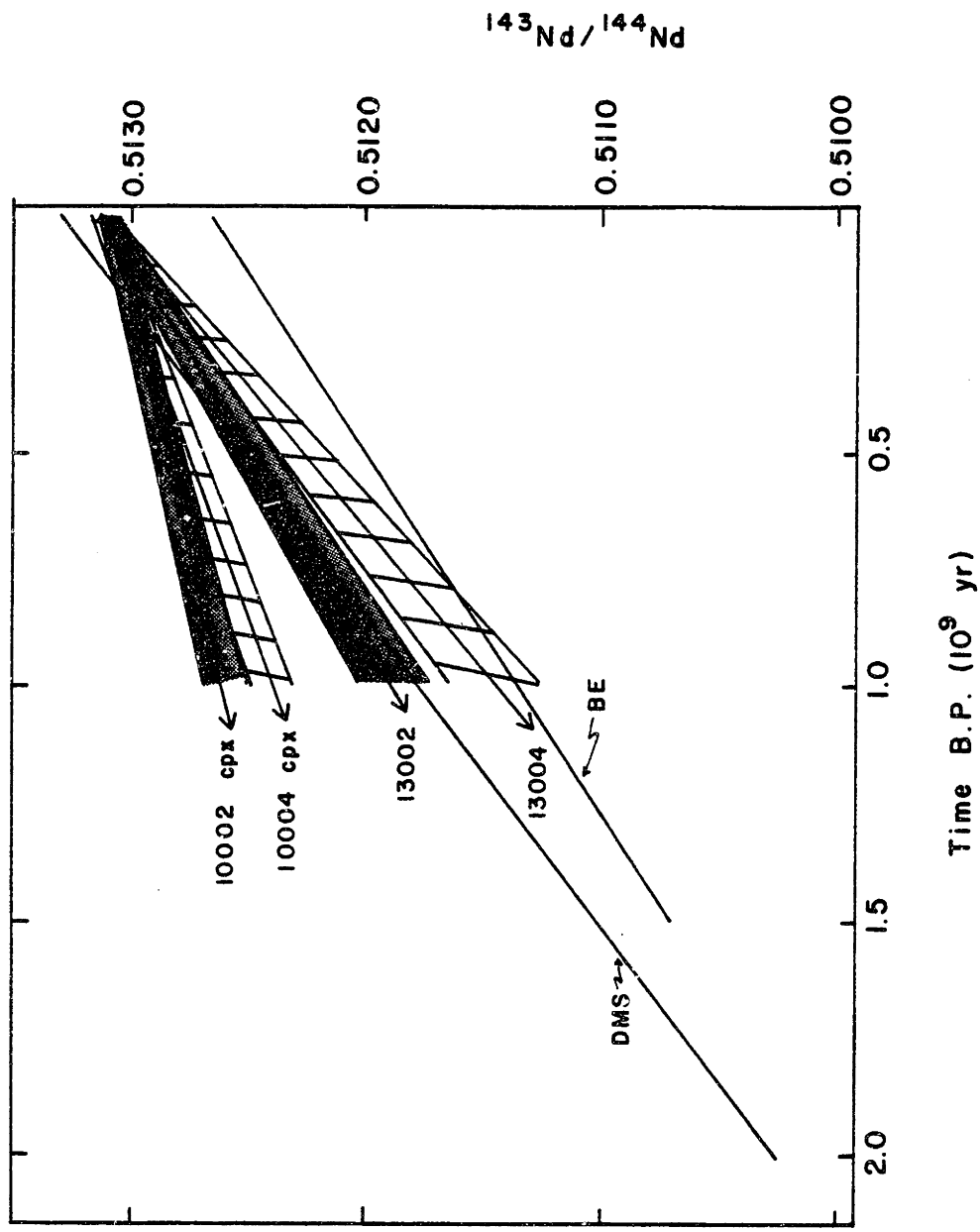
$^{143}Nd/^{144}Nd$
0.5130
0.5120
0.5110
0.5100
0.5
1.0
1.5
2.0
Time B.P. ($10^9$ yr)
10002 cpx
10004 cpx
13002
13004
BE
DMS

Figure 3-35. $^{143}Nd/^{144}Nd$ evolution diagram for pyroxenites 13002 and 13004 and 10004 and 10002 clinopyroxenes. Curve BE is the bulk earth curve assuming that bulk earth $^{143}Nd/^{144}Nd = 0.51264$ and $^{147}Sm/^{144}Nd = 0.1967$ (Jacobsen and Wasserburg, 1980; Wasserburg et al., 1981). Curve DMS is an estimate of the most radiogenic MORB source based on a first order transport model after Zindler et al. (1981) in which $^{143}Nd/^{144}Nd)_0 = 0.5133$, $^{143}Nd/^{144}Nd)_{4.6} = 0.50663$, $K = -4.5 \times 10^{-11}$ yr$^{-1}$, and the age of the earth is assumed to be $4.6 \times 10$ yr$^{9}$. Shaded and lined regions are error envelopes calculated by assuming a 10% uncertainty in the $^{147}Sm/^{144}Nd$ ratio (determined by RNAA) and the 2$\sigma$ error in the measured $^{143}Nd/^{144}Nd$ ratio.

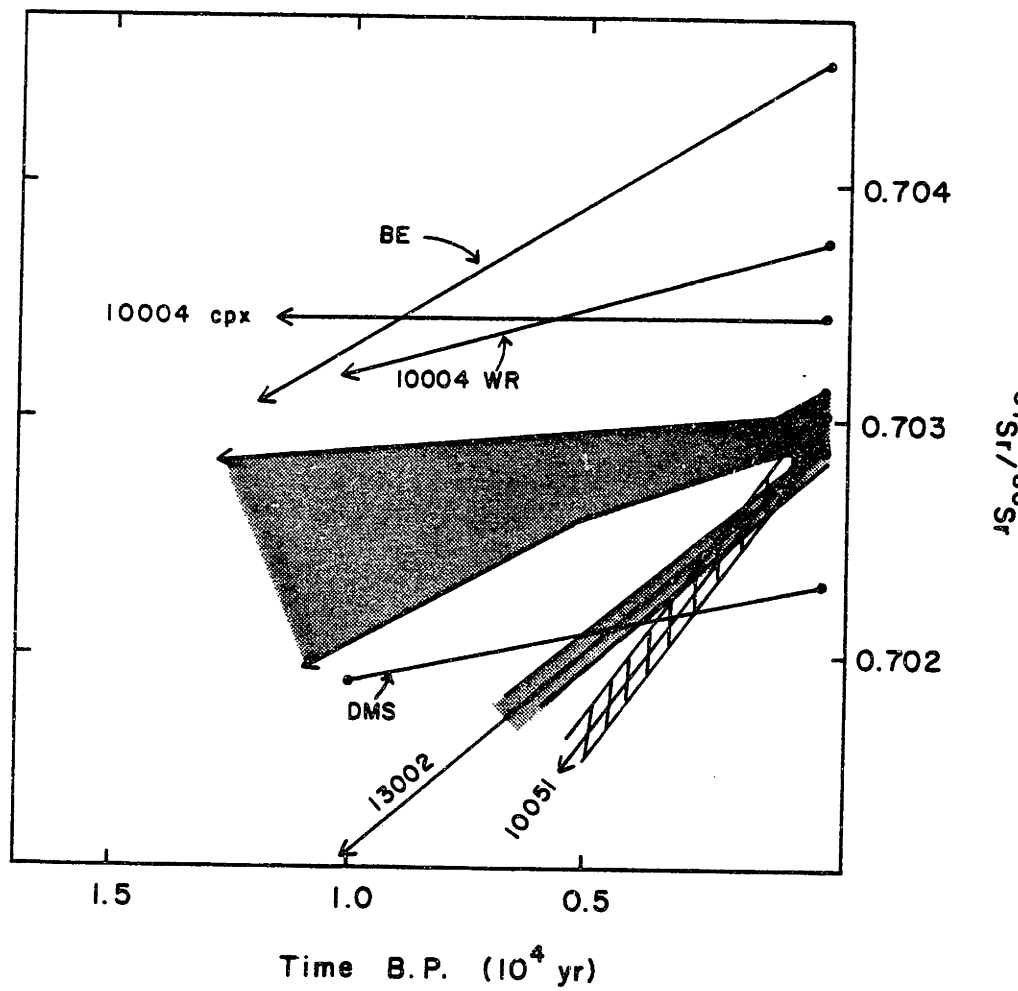
0.704
0.703
0.702
$^{87}Sr/^{86}Sr$
BE
10004 cpx
10004 WR
DMS
13002
10051
1.5
1.0
0.5
Time B.P. ($10^4$ yr)

Figure 3-36. $^{87}Sr/^{86}Sr$ evolution diagram of Nunivak ACE, ACT, CE, and CT peridotites and amphibole-pyroxenites (shaded region except individual growth curves of 10004 whole rock (WR), 10004 clinopyroxene (CPX), 13002, 10051 are indicated). Bulk earth curve (BE) is constrained by $^{87}Sr/^{86}Sr)_0 = 0.7045$ (DePaolo and Wasserburg, 1976a) and $^{87}Sr/^{86}Sr)_i = 0.699$. Curve DMS is an estimate of the evolution of the least radiogenic MORB source based on a first order rate equation after Zindler et al. (1981) where $^{87}Sr/^{86}Sr)_0 = 0.7023$, $^{87}Sr/^{86}Sr)_{4.6} = 0.699$, $K = 2.5 \times 10^{-11}$ $yr^{-1}$, and the age of the earth is assumed to be $4.6 \times 10^9$ yr. Error envelopes around the growth curves of 13002 and 10051 were calculated assuming a 2% uncertainty in $^{87}Rb/^{86}Sr$ and the measured uncertainty in the $^{87}Sr/^{86}Sr$ ratio.

metasomatism. An upper limit to the age of this metasomatism is given by the intersection of the growth curve for 10002 clinopyroxene with the estimated growth curve for the most depleted MORB source (Figure 3-35) because at ages greater than this intersection age, the growth curve for the clinopyroxene traverses regions where no known terrestrial examples occur (e.g., Basaltic Volcanism Study Project, 1981). In Figure 3-35 the growth curve for the most depleted MORB source is based on a first-order transport model (Zindler et al., 1981) and the specified variables (Figure 3-35). This particular model was chosen because it provides an older age for the intersection (thus, an older "maximum age of metasomatism") of the clinopyroxene growth curve and the MORB source growth curves than two stage, "catastrophic" models for the MORB source (e.g., Basaltic Volcanism Study Project, 1981). The ages of intersection of the error envelope around 10002 clinopyroxene growth curve and the estimated curve for the most depleted MORB source range from 250 to 150 million years (Figure 3-35).

Thus, we concur with the conclusion of Menzies and Murthy (1980a) that the metasomatism which affected the ACE, ACT, and pyroxenite inclusions probably occurred less than 200 million years ago, and we emphasize that the data are consistent with the metasomatism occurring immediately prior to eruption. Furthermore, based on the overlapping isotopic ratios of the basalts, and ACE, ACT, and pyroxenite inclusions, it is likely that the metasomatism is petrogenetically related to the host basalts.

Two of the three CE and CT inclusions have $^{87}Sr/^{86}Sr$ ratios

within error of both the ACE and ACT inclusions and the basalts (Figure 3-12), but the third sample, 10004, has significantly more radiogenic Sr than the host basalts and the ACE and ACT inclusions (Table 3-9). The clinopyroxene separated from 10004 has an $^{87}Sr/^{86}Sr$ ratio (Table 3-9) within error of the most radiogenic tholeiite reported by Mark (1971). The petrogenetic relationship of the CE and CT inclusions to the metasomatism which affected the ACE and ACT inclusions is uncertain because even though the CE and CT inclusions are enriched in the same incompatible elements as the ACE and ACT inclusions (Figure 3-9), 10004 is isotopically distinct from the ACE and ACT inclusions, and all three CE and CT inclusions lack the amphibole or glass after amphibole and the amoeboid spinels typical of the ACE and ACT inclusions. The CE and CT inclusions may represent recrystallized and dehydrated wall rock affected by an earlier metasomatism, possibly one related to the older, more tholeiitic volcanism on Nunivak. On a $^{143}Nd/^{144}Nd$ evolution diagram (Figure 3-35), the error envelope around the growth curve of 10004 clinopyroxene intersects the most depleted MORB source between 150 and 250 million years ago. Thus, the metasomatism which affected this inclusion occurred less than 250 million years ago. The 580 million year internal isochron (Figure 3-12) for this inclusion cannot simply be related to the age of metasomatism.

The remainder of this discussion will focus on the ACE and ACT peridotites and the pyroxenites because a reasonable model can be developed to explain the metasomatism which involved the Nunivak basalts, amphibole-pyroxenites, and the ACE and ACT peridotites.

(5) Nunivak metasomatism: constraints from the amphibole pyroxenites

The geochemistry and petrography of the amphibole pyroxenites is a key to understanding whether the metasomatism at Nunivak is a precursor to or a consequence of basaltic magmatism. Two features of the amphibole pyroxenites indicate that Nunivak metasomatism may be the consequence of the intrusion and crystallization of the parental magma to the pyroxenites. Firstly, the trace element data indicate that the pyroxenites formed by "accumulation" (e.g., Frey, 1980) from a silicate melt, and secondly, the pyroxenites contain amphibole which is spatially and compositionally related to the amphibole in the lherzolites (Francis, 1976c).

Evidence for an accumulate origin

Frey and Prinz (1978) described a suite of pyroxenites, their Group II inclusions, from San Carlos which are remarkably similar to the Nunivak pyroxenites in terms of mineralogy, texture, and trace element geochemistry. They concluded that the Group II inclusions were cumulates from an alkali basalt for several reasons including the textures, the wide variation in compatible trace element concentrations, and the similarity of the chondrite-normalized REE patterns of these pyroxenites to the REE patterns expected for clinopyroxene-amphibole cumulates. Primarily to avoid the connotation of gravity acting on crystals in an upper mantle magma chamber, processes such as filter pressing of basaltic dikes (Wilshire et al., 1980) and crystal plating

on conduit walls (Irving, 1980) have been invoked to explain the geochemistry of similar inclusions. However, all of these processes are described by "crystal accumulates" (e.g., Frey, 1980).

The overall similarity of the geochemistry of the Nunivak amphibole-pyroxenites to the Group II inclusions from San Carlos indicates that the Nunivak inclusions are also crystal accumulates. For example, in Figure 3-37 the REE abundances of one fine-grained pyroxenite, 13007, and one coarse-grained pyroxenite, 13002 are compared to the REE abundances of model crystal accumulates composed of amphibole and clinopyroxene in equilibrium with Nunivak basalts. Also for comparison, the range of REE abundances in the Group II inclusions is shown (Figure 3-37). The convex-upward chondrite-normalized REE pattern of the fine-grained Nunivak pyroxenites is particularly significant because it is a signature of amphibole- or clinopyroxene-dominated accumulates from relatively LREE-enriched melts similar to the Nunivak basalts. This feature results from amphibole and clinopyroxene having higher partition coefficients for the HREE than the LREE (see discussion in Frey and Prinz, 1978). The presence of poikilitic amphibole and subhedral to euhedral spinel enclosed in amphibole and clinopyroxene are also consistent with an origin as accumulates. Thus, we infer, based on the textures and the similarity in terms of geochemistry between the Nunivak pyroxenites and other Group II inclusions, that the Nunivak fine-grained pyroxenites originated as crystal accumulates from melts similar in REE geochemistry to the Nunivak basalts.

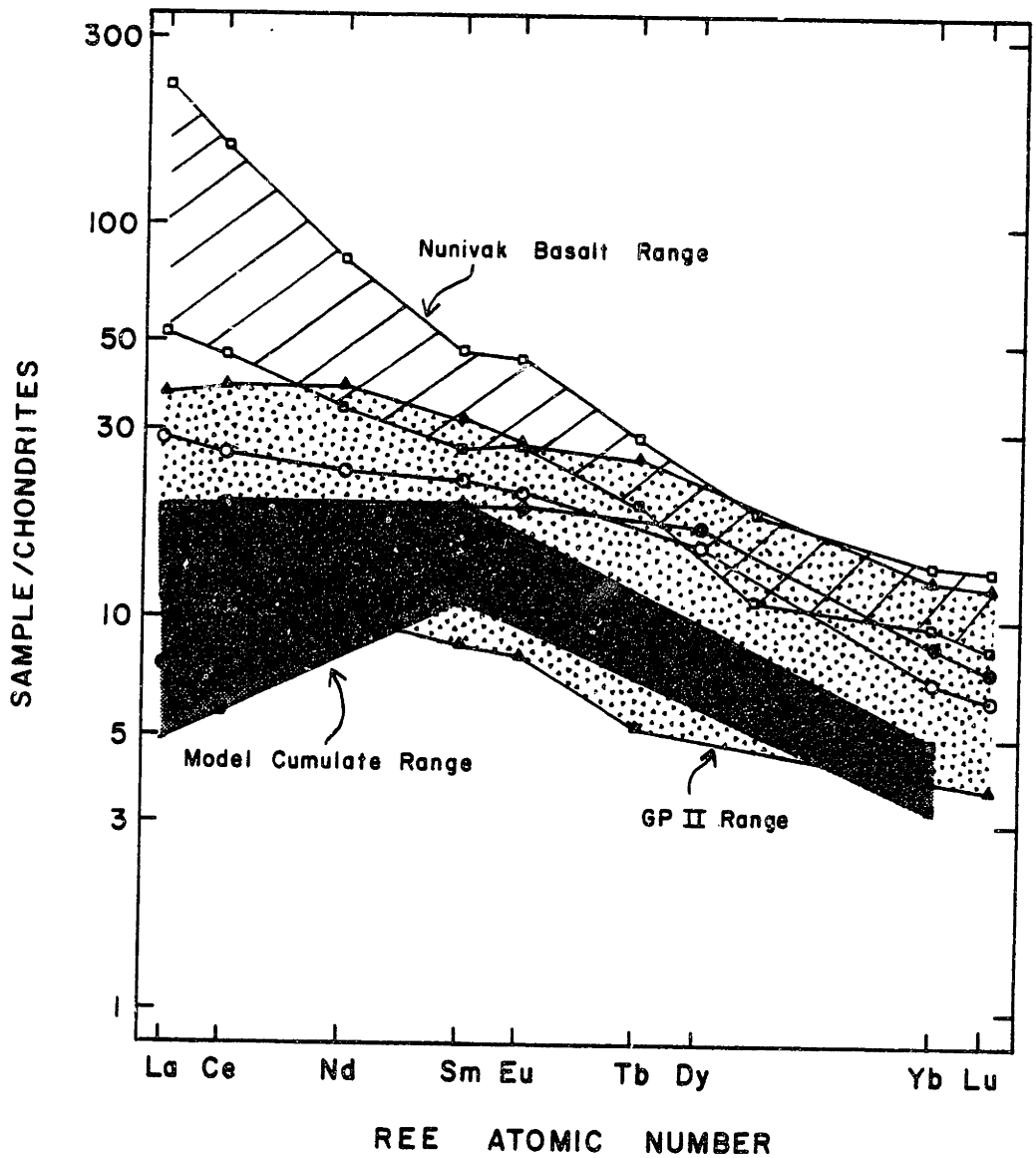
300
100
50
30
10
5
3
1
SAMPLE/CHONDRITES
Nunivak Basalt Range
Model Cumulate Range
GP II Range
La Ce Nd Sm Eu Tb Dy Yb Lu
REE ATOMIC NUMBER

Figure 3-37. Chondrite-normalized REE patterns of fine-grained pyroxenite 13007 (●) and coarse-grained pyroxenite 13002 (o) compared to the range of REE concentrations in a calculated amphibole-clinopyroxene cumulate in equilibrium with the Nunivak basalts (Table 3-14). Also plotted is the range of REE abundances in the Group II inclusions from San Carlos (Frey and Prinz, 1978). The REE abundances of the model cumulate were calculated using the REE partition coefficients of Frey et al. (Set 1, 1978) for clinopyroxene and Irving and Price (1981) for amphibole. The mode of the crystal accumulate was set at 40% amphibole and 60% clinopyroxene which is similar to the actual modes of the pyroxenites.

The coarse-grained pyroxenites, 13002 and 13005, which are relatively LREE-enriched (Figure 3-32), probably have a more complex origin than the fine-grained pyroxenites. The coarse-grained pyroxenites have higher incompatible element concentrations, e.g., La and Rb (Table 3-12), and higher Cr concentrations (Table 3-12) than the fine-grained pyroxenites. The higher incompatible element concentrations could result from crystallization from a more differentiated melt than the fine-grained pyroxenites, however, the high Cr content of the coarse-grained pyroxenites mitigates against this explanation. For example, using the amphibole and clinopyroxene partition coefficients for Cr from Irving and Price (1981) we calculate that the magma in equilibrium with 13002 had more than 500 ppm Cr based on the present mode. Although the actual crystallization history was probably more complex than the simple equilibrium model, the relatively high Cr content of these pyroxenites, and the relatively low crystal/melt partition coefficients, less than 2, for Cr of the constituent minerals (Irving and Price, 1981; Irving, 1978) indicates that the parental magma for these pyroxenites was relatively primitive. Indeed, the high spinel content and low Cr content of the fine-grained pyroxenites relative to the coarse-grained pyroxenites further substantiates this inference. Also consistent with this inference is the higher $Mg/(Mg + Fe^{2+})$, 0.79 to 0.80, of clinopyroxene from coarse-grained pyroxenite 13002 compared to that, 0.75, from fine-grained pyroxenite 13004 (D.M. Francis, unpublished data).

Thus, the relatively high La and Rb contents of the coarse-grained pyroxenites are most likely not the result of crystallization from a differentiated melt, however, the rather porous nature of these coarse-grained pyroxenites indicates that contamination by host basalt, or trapped residual melt may explain the relatively high incompatible element concentrations of the coarse-grained pyroxenites. Without knowing the initial incompatible element abundances in the coarse-grained pyroxenites it is difficult to evaluate which possibility is responsible for their geochemistry. For example, if the uncontaminated pyroxenites had a La/Rb ratio similar to that of the fine-grained pyroxenites then the La/Rb ratios of the coarse-grained pyroxenites can be explained by contamination by host basalt (Figure 3-38). Although one coarse-grained pyroxenite lies off the calculated mixing curve (Figure 3-38), given the inherent uncertainties in endmember compositions, this discrepancy is probably not significant. However, the data can as well be explained by contamination by a residual melt with an appropriate La/Rb ratio prior to incorporation in the basalts. Our data do not allow us to distinguish between these possibilities.

Timing of pyroxenite emplacement relative to metasomatism

If the emplacement of the pyroxenites had predated the metasomatism then a metasomatic signature should have been superimposed over their original geochemistry.

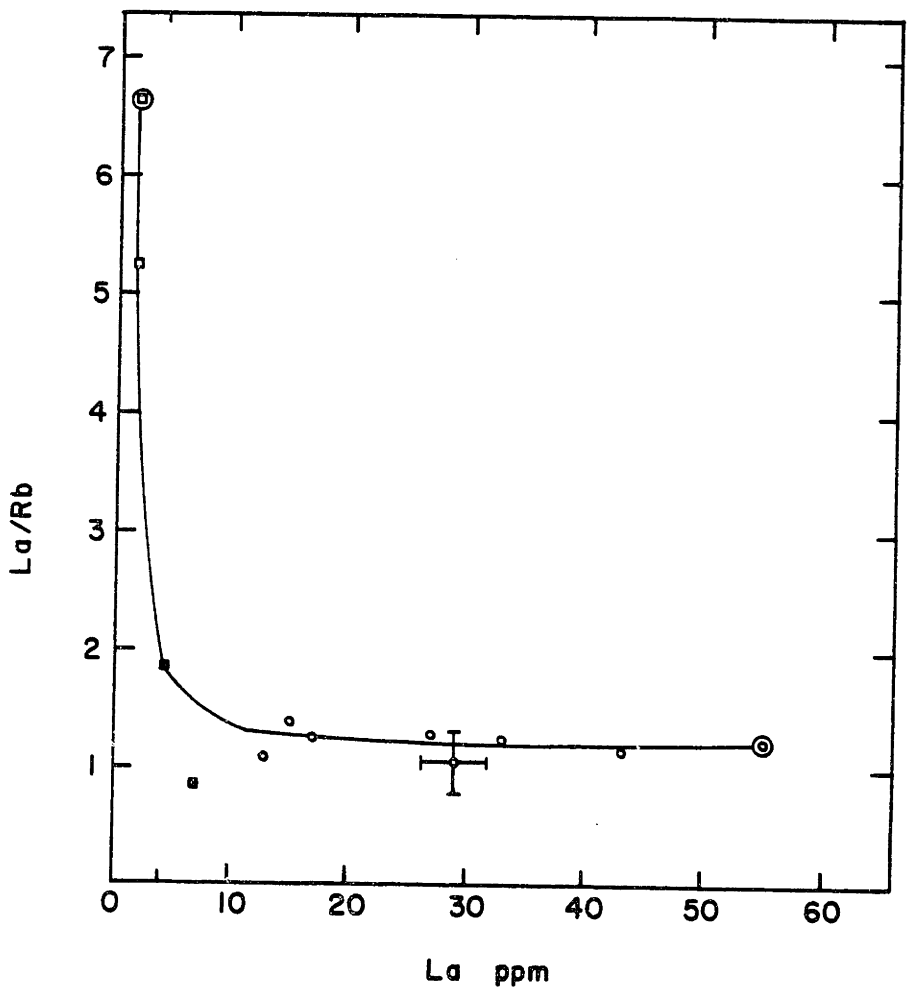
La/Rb
7
6
5
4
3
2
1
0
10
20
30
40
50
60
La ppm

Figure 3-38. La/Rb plotted versus La for Numivak fine-grained (□) and coarse-grained (■) pyroxenites and basalts (○). The solid line indicates a calculated mixing curve (Langmuir et al., 1978) based on the circled data points.

For example, the REE abundances of 10056 clinopyroxenite clinopyroxene (10056c cpx) can be interpreted to be the result of metasomatism of a clinopyroxene accumulate. From Sm to Lu, 10056c cpx has a chondrite-normalized REE pattern similar to clinopyroxenes in equilibrium with a normal MORB (Figure 3-39). However, the chondrite-normalized REE pattern of 10056c cpx has an inflection at Sm and a La/Yb ratio greater than chondrites unlike REE patterns of clinopyroxenes in equilibrium with basaltic melts (Figure 3-39). Furthermore, a calculated silicate melt in equilibrium with 10056c cpx has a chondrite-normalized REE pattern with an inflection at Sm unlike any geologically common silicate melt. The REE pattern of 10056c cpx can be explained by a two stage model: an initial stage of accumulation from a basalt similar to present day MORBs and a second stage in which the accumulate reacted with a metasomatic fluid with a very high La/Yb ratio. Thus, we infer that the emplacement of 10056c cpx predated the metasomatism at Nunivak. The lack of complex REE patterns in the amphibole-pyroxenites and the fact that their REE abundances can be interpreted as the result of accumulation from an alkali basalt, leads us to conclude that the emplacement of these pyroxenites was either contemporaneous with or postdated the metasomatism.

## Relationship of amphibole in pyroxenites and peridotites

A fundamental feature of the amphibole-pyroxenites which must be reconciled with any model to explain the metasomatism at Nunivak

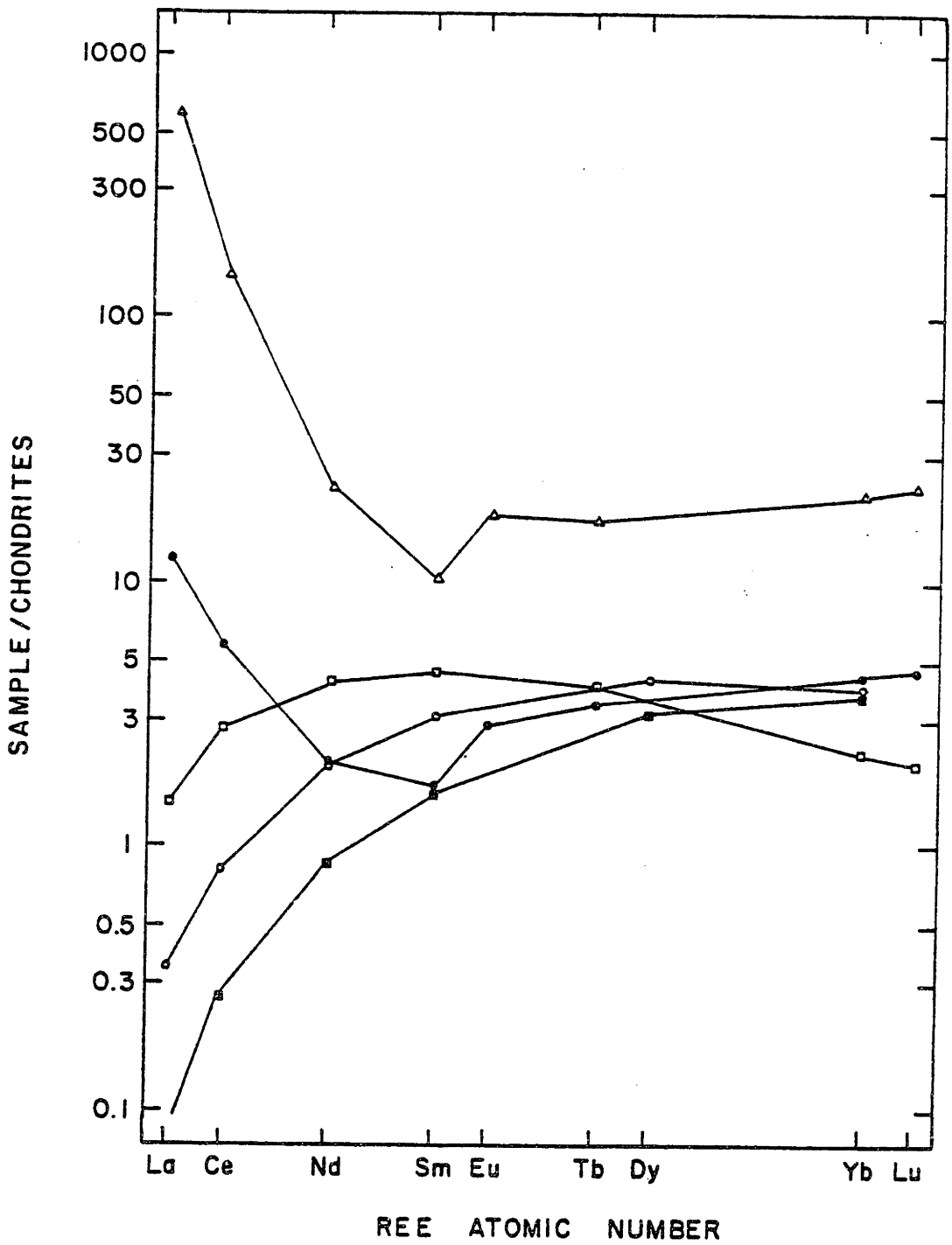
1000
500
300
100
50
30
10
5
3
1
0.5
0.3
0.1
SAMPLE/CHONDRITES
La
Ce
Nd
Sm
Eu
Tb
Dy
Yb
Lu
REE ATOMIC NUMBER

Figure 3-39. 10056 clinopyroxenite clinopyroxene (●) compared to clinopyroxenes in equilibrium with continental tholeiite T-14 (□) (Frey et al., 1978), and normal MORBs 482/3 (■) and 482/4 (○) (Sun et al., 1979). Clinopyroxene partition coefficients were from Frey et al. (Set 1, 1978). Also shown is a calculated melt (△) in equilibrium with 10056 clinopyroxenite clinopyroxene.

Island is that the pyroxenites contain amphibole which appears to be related to the amphibole in the peridotites. In a composite Nunivak inclusion Francis (1976c) observed veins of amphibole and minor phlogopite which appeared to originate in a pyroxenite vein and pierce the adjacent lherzolite. Furthermore, the amphibole composition varied as a function of lithology: ranging from kaersutite in the pyroxenite to pargasite in the lherzolite. We interpret the occurrence of amphibole in adjacent lherzolite and pyroxenite to indicate that the amphibole in the lherzolite and pyroxenite of this inclusion formed in the same event as Francis (1976c) suggested. The amphiboles in this composite inclusion are typical in terms of habit and composition of the amphiboles in the discreet spinel lherzolites, i.e., ACE, ACT inclusions, and the amphibole pyroxenites; because of this similarity, we believe that the amphiboles in the ACE, ACT, and the amphibole pyroxenite inclusions formed contemporaneously.

The observation that the amphibole compositions vary as a function of lithology indicates that the precipitation of amphibole was an equilibrium or near-equilibrium process. That is, the amphibole compositions appears to have been defined by the bulk composition of the system whether it was peridotite + volatiles (ACE, ACT inclusions) or basalt + volatiles (amphibole pyroxenites). Francis (1976c) interpreted this relationship to indicate that the amphibole formed by replacement of anhydrous minerals in both the lherzolites and the pyroxenites by an alkali-bearing, aqueous fluid, i.e., both the lherzolites and the pyroxenites were metasomatized. However, unlike

the ACT and ACE inclusions, the trace element abundances of the pyroxenites can be interpreted as the result of accumulation from a basaltic melt, i.e., the pyroxenites do not appear to be metasomatized. Therefore, we prefer an alternative hypothesis in which metasomatism of adjacent lherzolite wallrock (ACE, ACT inclusions) is the consequence of the partial crystallization of basalts in the form of amphibole pyroxenites and the migration of residual silicate melts and possibly C-H-O rich fluids into adjacent lherzolite wallrock. Just as in the replacement model of Francis (1976c), the composition of the amphibole will be defined to some extent by the bulk composition of the system. Our interpretation is essentially indistinguishable from the interpretation of Wilshire et al. (1980) regarding the origin of lherzite veins at Etang de Lherz. The relationship between lherzite (amphibole + mica rock), pyroxenite, and lherzolite at Etang de Lherz is remarkably similar to the textures in the composite Nunivak inclusion described by Francis (1976c); Wilshire et al. (1980) argued that the lherzite veins, which invade lherzolite wallrock, were residual melts derived from adjacent pyroxenite dikes by filter pressing. Although we do not necessarily argue for filter pressing, we invoke a very similar model to explain the metasomatism of ACE and ACT peridotites at Nunivak.

Because we interpret the pyroxenites to be the result of accumulation of clinopyroxene and amphibole from an alkali basalt, we infer that the amphibole in the pyroxenites formed by crystallization from the parental basalt. Therefore, we interpret the textural relations

Figure 3-42. Calculated, chondrite-normalized REE abundances in $H_{20}$ vapor in equilibrium with 10051 clinopyroxene (51), 10067 clinopyroxene (67), 10002 clinopyroxene (02), and a 10% and 3% residual melt (labelled) from Nunivak basalts . Regions are plotted instead of lines for 10002 and 10067 clinopyroxenes because of uncertain amount of included apatite. $H_2O$ vapor/ silicate melt partition coefficients are from Mysen (1979); clinopyroxene/silicate melt partition coefficients are from Frey et al. (Set 1; 1978).

Table 3-21. Calculated equilibrium melts or fluids.

| | La/Sm | La/Dy | La/Lu |
|---|---|---|---|
| residual melts from Nunivak basalts | | | |
| F = 0.10 | 6.7-16 | 7.1-16 | 103-282 |
| F = 0.03 | 10-25 | 11-32 | 134-377 |
| F = 0.01 | 15-36 | 17-48 | 173-482 |
| melts in equilibrium with clinopyroxenes | | | |
| 10002 | 40-73 | 69-136 | 428-940 |
| 10067 | 8.9-16 | 12-23 | 157-348 |
| 10051 | 9.2 | 18 | 270 |

| | Ce/Sm | Ce/Tm |
|---|---|---|
| $CO_2$ vapor (20 kb) in equilibrium with: | | |
| residual melt F = 0.10 | 66-163 | 68-2044 |
| F = 0.03 | 189-362 | 1823-4075 |
| F = 0.01 | 257-491 | 2500-5780 |
| 10002 clinopyroxene | 409-816 | 4170-9840 |
| 10067 clinopyroxene | 121-234 | 1520-3650 |
| 10051 clinopyroxene | 160 | 3600 |
| $H_2O$ vapor (20 kb) in equilibrium with: | | |
| residual melt F = 0.10 | 8.3-16 | 53-123 |
| F = 0.03 | 12-22 | 69-154 |
| F = 0.01 | 16-30 | 96-217 |
| 10002 clinopyroxene | 25-51 | 154-364 |
| 10067 clinopyroxene | 7.5-15 | 57-137 |
| 10051 clinopyroxene | 9.9 | 135 |

be less sensitive to pressure than absolute values of partition coefficients (Wendlandt and Harrison, 1979) and thus, we emphasize elemental ratios in evaluating the model.

The most significant result of the model calculations is that 10002 clinopyroxene probably did not precipitate from a residual silicate melt derived from a Nunivak basalt because the La/Dy ratios of melts calculated to be in equilibrium with 10002 clinopyroxene are significantly higher than the La/Dy ratios of model residual melts (Figure 3-40; Table 3-21). In contrast, residual melts in equilibrium with 10051 and 10067 clinopyroxenes have elemental ratios within the range of these ratios for model residual melts derived from the Nunivak basalts (Figure 3-40; Table 3-21). Thus, these clinopyroxenes may have precipitated from a residual melt. Indeed, the relative REE abundances in these two clinopyroxenes are similar to the relative REE abundances in the Group II pyroxenites from San Carlos (compare Figures 3-6 and 3-37). These latter pyroxenites are thought to have precipitated from a silicate melt (Frey and Prinz, 1978).

The calculated elemental ratios of $CO_2$- and $H_2O$-vapors in equilibrium with the 3 clinopyroxenes all fall in the range of these ratios in model $CO_2$- and $H_2O$-vapors in equilibrium with residual melts derived from the Nunivak basalts (Table 3-21). Hence, the model calculations are consistent with all of the clinopyroxenes having precipitated from either a $CO_2$- or $H_2O$-vapor. However, in both cases, 10002 clinopyroxene appears to have precipitated from a vapor

with a more fractionated REE pattern than the other two clinopyroxenes (Figures 3-41, 3-42). An alternative also consistent with the model calculations is that 10051 and 10067 clinopyroxenes crystallized from a residual silicate melt while 10002 clinopyroxene precipitated from a $H_2O$- or $CO_2$-rich vapor derived from a residual melt. The model calculations are consistent with basalts similar in REE geochemistry to the Nunivak basalts being the ultimate source of the metasomatizing fluid. There are some discrepancies in terms of absolute abundances (e.g., Figures 3-41, 3-42) but in view of the uncertain values of the partition coefficients, these discrepancies are probably not significant.

In summary, REE modelling indicates that clinopyroxenes with relatively high La/Yb ratios such as 10002 could have equilibrated with a $H_2O$-rich or $CO_2$-rich vapor phase derived from basalts similar in REE geochemistry to the Nunivak basalts. In contrast, REE modelling for 10051 clinopyroxene and 10067 clinopyroxene indicates that these pyroxenes could have equilibrated with any of the three fluids modelled.

This modelling does not provide conclusive evidence as to the nature of the metasomatic fluid for the following reasons: (1) the assumption of equilibrium was not satisfactorily justified, and (2) the partition coefficients are poorly known in terms of their pressure and temperature dependence. In principle, modelling such as that pursued above should provide information as to the nature of the metasomatic fluid once a well constrained set of partition coefficients is available.

(7) Major element effects of metasomatism

Francis (1976b; 1978) described major element variations as a function of texture in the Nunivak peridotites. The effects of metasomatism on major elements in the ACE and ACT inclusions is reflected mainly in elements normally present in low amounts in peridotites. The major element compositions of the metasomatic phases, phlogopite, pargasite, and apatite, shows that the metasomatic fluid introduced $K_2O$, $TiO_2$, $P_2O_5$, $H_2O$, and possibly $Na_2O$ (Francis, 1976b; Tables 3-10, 3-11) into wallrock, provided that the protolith was a typical, anhydrous peridotite. Associated fluid inclusions indicate that $CO_2$ was probably also introduced.

However, besides the presence of metasomatic phases, the only distinguishing features of the ACE, and ACT inclusions related to major elements are the jadeitic nature of the clinopyroxenes and the slightly lower $Mg/(Mg + Fe^{2+})$ of clinopyroxene and olivine (Francis, 1978) relative to the CE, CT, and GE inclusions. Francis (1978) argued that the jadeitic nature of the clinopyroxenes in the ACE and ACT inclusions predated the formation of the amphibole, although his argument is unclear. We have found no evidence inconsistent with the jadeitic nature of the clinopyroxene being the consequence of metasomatism.

The lower $Mg/(Mg + Fe^{2+})$ ratios may not be related to the metasomatism because the olivine as well as the clinopyroxene is relatively Fe-rich. Thus, if the slightly lower $Mg/(Mg + Fe^{2+})$ ratios are the result of metasomatism, then the olivine must have

equilibrated with the metasomatic fluid. Textural evidence relevant to this possibility is equivocal: metasomatic clinopyroxene appears to replace olivine in 10006 (Figure 3-14b), but in 10051 olivine contains phlogopite inclusions (Figure 3-16). This latter texture may indicate that the host olivine equilibrated with the fluid that precipitated the phlogopite, but another possibility is that the fluid penetrated along a crack which is either not visible due to the orientation of the thin section or is annealed.

Consideration of the major elements indicates that metasomatism at Nunivak introduced elements, e.g., $K_2O$, $TiO_2$, $P_2O_5$, $H_2O$, $CO_2$, normally present in low abundances in anhydrous peridotites. Thus, the Nunivak metasomatism is typical of many other described examples of mantle metasomatism (e.g., Boettcher and O'Neill, 1980). If the lower $Mg/(Mg + Fe^{2+})$ ratios and the higher jadeite component in the clinopyroxene is a consequence of metasomatism then these data imply that the metasomatic fluid had a lower $Mg/(Mg + Fe^{2+})$ ratio and possibly higher $Na_2O$ and $Al_2O_3$ than a basaltic melt of a typical anhydrous peridotite. This inference is consistent with our model for the Nunivak metasomatism.

(8) Nunivak metasomatism: implications for other metasomatized inclusion suites

An important question is whether the above model in which metasomatism is a consequence of the intrusion and crystallization of alkali basalt magma in the upper mantle is applicable to other metasomatized inclusion suites. Isotopic data are unavailable for pyroxenites from other suites. Thus, there are insufficient data to evaluate whether a petrogenetic link between pyroxenites and metasomatized peridotites exists at other localities. However, there are important geochemical similarities between the Nunivak suite and several other inclusion suites:

San Carlos, Arizona

Both metasomatized peridotites with La/Yb ratios greater than chondrites and amphibole-bearing pyroxenites which formed by crystal segregation occur at San Carlos (Frey and Prinz, 1978). Zindler and Jagoutz (1980) reported a $^{143}Nd/^{144}Nd$ ratio of 0.51308 for a relatively LREE enriched Group I inclusion from San Carlos. Thus, if metasomatism is responsible for the Sm/Nd ratio being less than chondrites then this metasomatism must have occurred recently, i.e., less than 180 million years ago (Zindler and Jagoutz, 1980). Therefore the age of the San Carlos' metasomatism relative to the associated volcanism is similar to that which we inferred at Nunivak.

Dreiser Weiher, Germany

The xenolith suite from the Dreiser Weiher maar is remarkably

similar to the Nunivak suite. At Dreiser Weiher inclusions with La/Yb ratios less than chondrites (Group Ib of Stosch and Seck, 1980) as well as amphibole-bearing, metasomatized inclusions with La/Yb ratios greater than chondrites (Group Ia) occur. Two clinopyroxenes from metasomatized inclusions have $^{143}Nd/^{144}Nd$ ratios of 0.51264 and 0.51280 (Stosch et al., 1980) and thus, are closer to the ratio for the bulk earth than the examples from Nunivak and San Carlos. Consideration of the evolution of $^{143}Nd/^{144}Nd$ in these Group Ia inclusions led Stosch et al. (1980) to conclude that the metasomatism at Dreiser Weiher occurred recently, i.e., less than 200 million years ago. Although pyroxenite inclusions occur at Dreiser Weiher, geochemical data for these inclusions have not been reported, hence, their relationship, if any, to the metasomatism is uncertain.

Kilbourne Hole, New Mexico

In a study of composite lherzolite-pyroxenite inclusions from Kilbourne Hole and several other localities, Irving (1980) found that both amphibole-bearing and amphibole-free pyroxenites have REE patterns which are similar to the Nunivak pyroxenites. A particularly interesting observation is that a spinel lherzolite wallrock (sample KH77-20L) adjacent to pyroxenite dikes has higher concentrations of incompatible elements than discrete spinel lherzolite inclusions from Kilbourne Hole. KH77-20L has a convex upward, chondrite-normalized REE pattern similar to that of Nunivak sample 10051 although the REE

concentrations of KH77-20L are lower than in 10051. These data are consistent with wallrock being metasomatized by a phase related to the pyroxenites. However, Irving (1980) argued that this interaction occurred early in the crystallization history of the basaltic magma in contrast to our model in which metasomatism occurs as residual melt infiltrates lherzolite wallrock.

Kiami dike, Australia and Western U.S.

The metasomatized peridotites and amphibole pyroxenites from Nunivak have important features in common with apatite-bearing inclusions from eastern Australia (Wass et al., 1980; Wass and Rogers, 1980) and western U.S. (Wilshire et al., 1980). Amphibole-mica-apatite assemblages occur at all three localities. At Nunivak these minerals occur as interstitial grains and in veins; the latter habit is similar to the selvages cutting lherzolite from Dish Hill and Deadman Lake (Wilshire et al., 1980). In the Kiama dike (Wass et al., 1980) discrete amphibole-apatite inclusions have extremely high concentrations of the LREE (La = 10 to 2000 x chondrites, Wass and Rogers, 1980). Both Wilshire et al. (1980) and Wass and Rogers (1980) concluded that these amphibole-apatite veins and inclusions formed as the result of the crystallization of a melt in the upper mantle, a model similar to the one postulated here.

Apparently, the Nunivak peridotites and pyroxenites are geochemically and mineralogically similar to metasomatized inclusions from other localities. If the model proposed here to explain the Nunivak metasomatism is generally applicable then pyroxenites

associated with metasomatized peridotites from other localities should have geochemical features consistent with crystal accumulation, and should be isotopically indistinguishable from the associated metasomatized peridotites. Detail companion studies on massif-type peridotites where the geochemical relationship between pyroxenites, interstitial amphibole, vein amphibole, and peridotitic wallrock can be studied in situ may provide the most convincing evidence as to whether or not metasomatism is a local effect related to the intrusion and crystallization of basaltic magma in the upper mantle.

(C) Petrogeneisis of the Nunivak basalts

(1) The primitive nature of the basalts

In order to relate the geochemistry of the basalts to source characteristics it is necessary to sort out the effects of crystal fractionation from characteristics reflecting the geochemistry of the source material. The basalts studied here are relatively primitive with $Mg/(Mg + Fe^{2+})$ = 65 to 71 (Table 3-13). Olivines inferred (Roeder and Emslie, 1970) to be in equilibrium with melts having $Mg/(Mg + Fe^{2+})$ of 65 to 71 range from $Fo_{86}$ to $Fo_{89}$ and thus overlap the Fe-rich end of the range of olivine compositions ($Fo_{88-94}$) believed to be present in the source regions of basalts (e.g., Ringwood, 1975). However, the oxygen fugacity in the upper mantle is uncertain, and the $Fe^{2+}/Fe^{3+}$ ratios of basalts may not reflect the oxygen fugacity at the site of generation (e.g., Arculus and Delano, 1981). Even if all the Fe of the basalts is reduced, the calculated equilibrium olivines are still relatively Fo-rich, ranging from $Fo_{82}$ to $Fo_{86}$. These olivines are slightly more Fe-rich than olivined inferred for the source of basaltic magmas.

Another difficulty in the calculation of equilibrium olivines is contamination of the basalts with xenolithic debris which is rare to common in all of the basanites and one tholeiite (Table 3-1). This debris occurs as fragments as small as a millimeter in diameter, and thus, it was impossible to completely separate this material from the basalts during sample preparation. The amount of xenolithic contamination can be monitored by using an elemental ratio between two

compatible elements, e.g., Cr/Sc. Sc concentrations are relatively constant in the basalts while the inclusions have relatively low Sc concentrations (7.5 to 16 ppm Sc in the peridotites, 16 to 25 ppm in the basalts). In contrast, Cr occurs in very high concentrations in the xenoliths (2300 to 3200 ppm Cr) relative to the basalts (200 to 350 ppm Cr). Consequently, Cr/Sc ranges from 11 to 18 in the basalts and 149 to 363 in the peridotites which are the most common xenolith type (Francis, 1978). Two of the basalts, B-7 and B-9, have Cr/Sc ratios (17.1 - 18.0) significantly higher than the Cr/Sc ratios of the other basalts (11-15). These two basalts also contain abundant xenolithic debris in thin section (Table 3-1). The amount of contamination of these basalts can be calculated by mass balance, assuming a Cr/Sc ratio of 13.8 for uncontaminated basalts (xenolith-free tholeiites B-1 and B-12 have Cr/Sc ratios of 13.8 to 13.9), and assuming a Cr content of 2700 ppm in the contaminating xenoliths (a representative Cr concentration for the Nunivak peridotites, Table 3-8). For basalt B-9 we calculate that 3% contamination by weight of the basalt with peridotite debris could account for the observed Cr/Sc ratio of 18. Assuming that the contaminant had an average MgO content of 40 wt.% (range in Nunivak peridotites: 38.7 to 42.0% MgO; D.M. Francis, unpublished data) and a $Mg/(Mg + Fe^{2+})$ ratio of 0.9, the net effect of this contamination would be to raise the $Mg/(Mg + Fe^{2+})$ ratio of the basalt by approximately 0.025 and the Fo content of the calculated equilibrium olivine by one Fo unit.

The above complexities do not strongly affect calculation of

(Francis, 1976c) in the pyroxenites which indicate a reaction relationship between amphibole and clinopyroxene and probably spinel to be the consequence of closed system crystallization of alkali basalt magma. We suggest that the residual, volatile-rich melt was not in equilibrium with the anhydrous phases precipitated earlier in the history of crystallization as suggested by Best (1974) to explain similar textures in amphibole-bearing inclusions from the Grand Canyon.

The occurrence of a reaction rim of orthopyroxene between olivine and amphibole in a fragment of spinel lherzolite sandwiched between pyroxenite dikes (Francis, 1976c) is apparently in conflict with the accumulate model because it indicates the presence of a fluid with a high $SiO_2$ activity. It was just this observation which led Francis to conclude that the amphibole forming event could not be related to a residual melt from an initially undersaturated basalt. We suggest that the reaction occurred when a small pocket of initially undersaturated melt or fluid underwent closed system fractionation and became more silica-rich by separation of $SiO_2$-poor amphibole until the fluid was no longer in equilibrium with olivine.

In summary, the isotopic data presented earlier are consistent with the existence of a petrogenetic relationship between the Nunivak basalts and the amphibole-pyroxenites. We suggest that the amphibole-pyroxenites crystallized from a magma related to the recent volcanism on Nunivak Island. Our interpretation of the REE abundances of the pyroxenites indicates that metasomatism of adjacent wallrock

lherzolites was contemporaneous with the crystallization of the pyroxenites. However, in contrast to Francis (1976c) we infer that the metasomatizing agent originated in the pyroxenites as a residual silicate melt or a H-C-O fluid phase which exsolved from the melt. Note that at shallow depths in the upper mantle, $CO_2$ or CO saturation of a crystallizing melt which initially contained some $CO_2$ with a $CO_2$-rich phase is inevitable if no C-bearing phase occurs on the solidus. In essence, our model to explain the metasomatism is indistinguishable from the model of Wilshire et al. (1980), and thus, we believe that the metasomatism at Nunivak to be an example of consequent metasomatism.

One of the puzzling aspects of the amphibole-pyroxenites is that some of the textures present, such as the exsolution lamellae in amphibole and clinopyroxene, require a period of cooling following crytallization. If the pyroxenites are genetically related to the Nunivak volcanism then the textures indicate that the influx of magma into shallow depths of the upper mantle was more likely episodic rather than continuous.

(6) Nunivak metasomatism: composition of metasomatizing fluid as inferred from REE modelling

One of the puzzling aspects of the metasomatized Nunivak peridotites is the range in relative REE abundances in the ACE and ACT inclusions and their constituent clinopyroxenes (Figure 3-6); for example, chondrite-normalized La/Ce ratios range from 0.74 to 1.2 and chondrite-normalized Ce/Nd ratios range from 0.86 to 2.1 in separated clinopyroxenes (Figure 3-6 ). Because the relative partition coefficients for the REE between clinopyroxene and silicate melt do not vary greatly with melt composition, e.g., $K_D^{Ce}/K_D^{Nd} = 0.53$ for basalts, $K_d^{Ce}/K_D^{Nd} = 0.51$ for rhyolites (e.g., Arth, 1976), it seems likely that the variation in the relative REE abundances in the ACE and ACT inclusions is the result of varying REE abundances in the metasomatic fluid. It is possible that the fluid composition, in terms of REE abundances, $(CO_2 + H_2O/SiO_2$, and $CO_2/(CO_2 + H_2O)$, was variable.

We attempted to determine whether the metasomatizing agent was a residual silicate melt or a $CO_2$- or $H_2O$-rich vapor and to infer its REE abundances by calculating the REE contents of residual melts and $CO_2$- or $H_2O$- rich vapors in equilibrium with various phases. Specifically, we calculated and compared the following:

1. Melts and vapors in equilibrium with 10051, 10002 and 10067 clinopyroxenes whose REE abundance span the range in ACE and ACT inclusions.

2. Residual melts formed from the Nunivak basalts by closed

system Rayleigh fractionation of amphibole and clinopyroxene.

3. $H_2O$- and $CO_2$-rich fluids in equilibrium with the residual melts calculated in step 2.

In order to calculate melts and vapors in equilibrium with clinopyroxenes in the ACE and ACT inclusions (step 1), we assumed equilibrium between clinopyroxene and the metasomatizing fluid. This assumption is open to question because mantle metasomatism may be a disequilibrium process. However, limited data from inclusion 10006 indicate that the clinopyroxene equilibrated with the metasomatic fluid. For example, reconnaissance ion probe analysis of 10006 clinopyroxene detected no Sr zoning (Figure 3-23). Thus, we can infer the Sr contents of silicate melts in equilibrium with this clinopyroxene. A basaltic melt in equilibrium with this clinopyroxene would contain approximately 3900 ppm Sr based on a clinopyroxene/basalt partition coefficient of 0.1 (e.g., Hart and Brooks, 1974) and the concentration of 390 ppm Sr in this pyroxene. Such a Sr content is well in excess of that in typical basaltic magmas, and thus, we infer that this clinopyroxene equilibrated with the metasomatic phase whether it was a residual silicate melt or C-H-O fluid. Furthermore, 10006 clinopyroxene appears to be in equilibrium with another phase, apatite, which we infer was precipitated by the metasomatic fluid. For example, the relative La/Y ratios in host 10006 clinopyroxene and apatite are consistent with equilibrium partitioning (see Chapter 3, V-(B)-(3)). Furthermore, the lack of trace element or major element zoning in 10006 clinopyroxene near apatite inclusions (Figure 3-23, 3-24) is consistent with these

two minerals being in equilibrium. Thus, because the 10006 clinopyroxene is rich in Sr, unzoned with respect to Sr, and appears to be in equilibrium with apatite, we infer that this clinopyroxene equilibrated with the metasomatic fluid.

However, we lack information on trace element zoning in other ACT and ACE clinopyroxenes and thus, we cannot demonstrate that equilibrium calculations are valid for these clinopyroxenes. The high La/Yb ratios of leached clinopyroxenes from ACT and ACE inclusions (Figure 3-6), however, indicates that these clinopyroxenes either equilibrated with or precipitated from the metasomatic fluid. Indeed, some textures indicate that some clinopyroxene formed during metasomatism (Figures 3-14A, 3-15A, 3-18), although other textures (Figure 3-14B) indicates the presence of two generations of clinopyroxene. Also, Francis (1976b) noted strong zoning at spinel-host amphibole grain boundaries in some ACE and ACT inclusions. These last two textures indicate that total equilibrium was not attained in all cases. Therefore, our equilibrium calculations may not be justified in all cases.

A second problem is whether the clinopyroxene REE abundances were altered during transport to the surface. The lack of significant grain boundary zoning in amphibole-rich inclusion 10067 (Figure 3-25) indicates that mineral compositions in this inclusion were probably not strongly affected by transport to the surface. By analogy with 10067, mineral compositions in 10051 were probably not strongly affected during transport to the surface because this inclusion also

retains most of its hydrous phases. However, mineral compositions may have been affected in inclusions which were subjected to greater thermal stress, such as those where the amphibole broke down to glass during transport to the surface. Thus, for 10002 where all the amphibole is broken down, the measured REE abundances of 10002 clinopyroxene may only approximate the abundances present prior to incorporation in the basalt.

A further complication is that both 10067 clinopyroxene and 10002 clinopyroxene contain apatite, thus, the REE concentrations in the host clinopyroxenes were estimated using the apatite partition coefficients of Watson and Green (20 kb, basanite, 1981) and by assuming that the weight percent of apatite in clinopyroxene is between 0 and 1%. This estimate is reasonable based on optical examination of the clinopyroxenes.

The residual melts (Step 2) were modelled by closed system fractionation of amphibole and clinopyroxene in the ratio 40:60 (i.e., representative of the mode of the pyroxenites) from the alkali basalts according to a Rayleigh fractionation model $C_l^i/C_o^i = F^{D^i-1}$ where $C_l^i$ is the concentration of trace element of i in the fractionated liquid, $C_o^i$ is the concentration of i initially in the system, F is the mass fraction of liquid remaining, and $D^i$ is the bulk distribution coefficient for i. Initial concentrations of the REE were specified by the range of REE abundances in the alkali basalts (Table 3-14). Partition coefficients are from Frey et al. (Set 1, 1978) for clinopyroxene, and Irving and Price (1981) for amphibole.

If a Nunivak basalt underwent closed system fractionation in the upper mantle, then other phases, e.g., olivine and spinel, would probably fractionate in addition to amphibole and clinopyroxene. Thus, the percentages of residual melt in our model are not applicable to the real system. However, because amphibole and clinopyroxene are the most important REE-bearing phases in the fractionation of a basalt in the upper mantle, the change of relative REE abundances with crystal fractionation should be applicable to the real case.

The results of the model calculations are shown in Figures 3-40, 3-41, 3-42, and Table 3-21. In evaluating the model calculations, we compare fluids/melts calculated to be in equilibrium with the clinopyroxenes to fluids/melts petrogenetically related to the Nunivak basalts either as residual melts or as $CO_2$ or $H_2O$ vapors in equilibrium with the residual melts. If the absolute abundances and more importantly, the elemental ratios (Table 3-2 ) of the two fluids overlap, then we conclude that the calculations are consistent with that particular fluid/melt (i.e., either the calculated residual melt or the fluid in equilibrium with that residual melt) being the metasomatic fluid which equilibrated with that particular clinopyroxene.

The data of Mysen (1979) and Wendlandt and Harrison (1979) show that there is a large pressure dependence of REE partitioning between $CO_2$ and $H_2O$ vapors and silicate melt. Experiments in the appropriate pressure range for the Nunivak peridotites (8-18 kb) have not been performed; in the present model we used 20 kb data (Mysen, 1979; Wendlandt and Harrison, 1979). Relative REE partitioning appears to

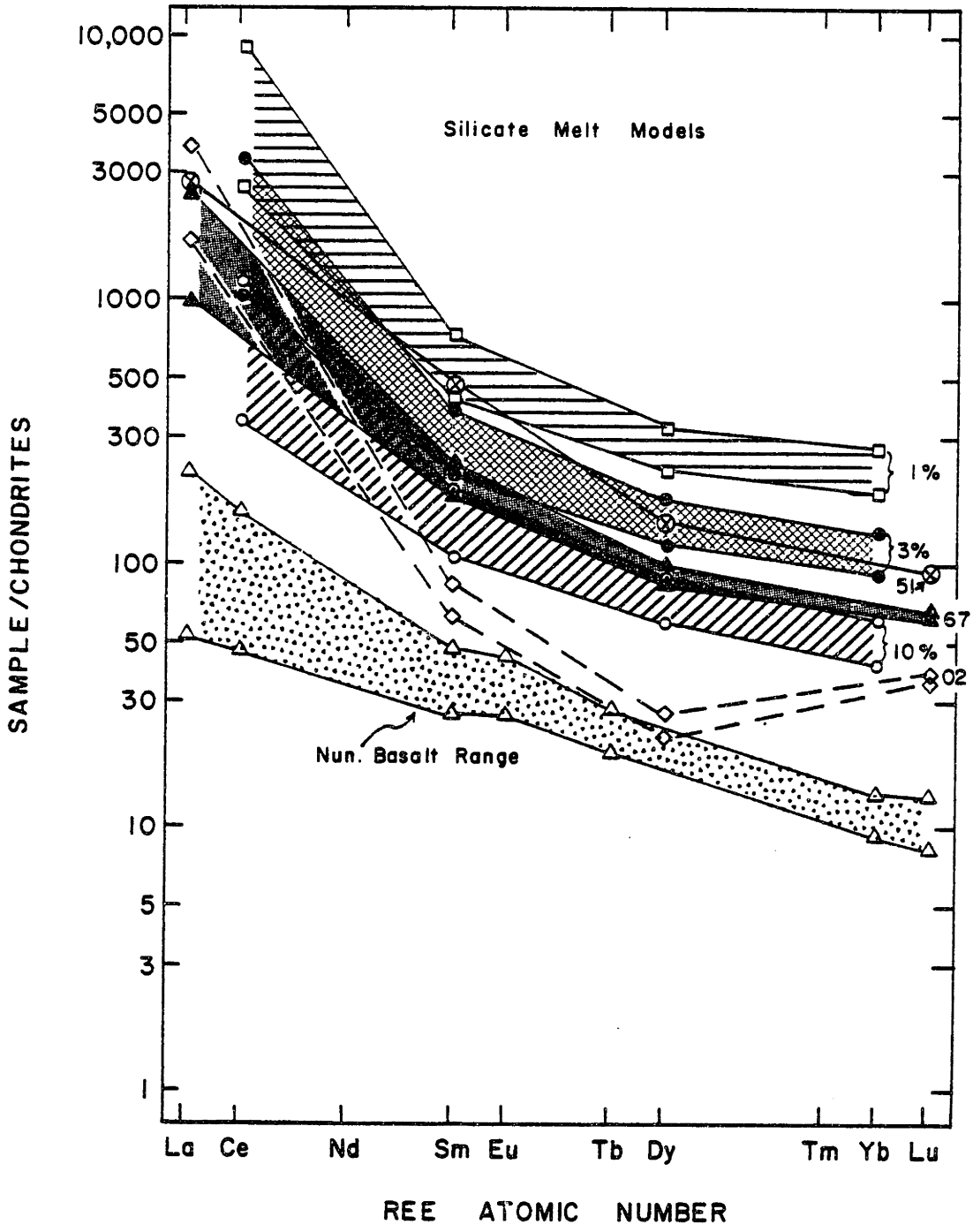
10,000
5000
3000
1000
500
300
100
50
30
10
5
3
1
SAMPLE/CHONDRITES
Silicate Melt Models
1%
3%
5%
10%
67
02
Nun. Basalt Range
La Ce Nd Sm Eu Tb Dy Tm Yb Lu
REE ATOMIC NUMBER

Figure 3-40. Closed system, crystal fractionation model for Nunivak basalts showing chondrite-normalized REE abundances in basalts from Table 3-14 and 10%, 3%, and 1%, residual melts. Also plotted are calculated REE abundances in melts in equilibrium with 10051 (51), 10067 (67), and 10002 (02) clinopyroxenes. Regions are plotted for 10067 and 10002 clinopyroxenes because of the uncertain amount of apatite in these clinopyroxenes. Partition coefficients for clinopyroxene are from Frey et al. (Set 1; 1978) and for amphibole are from Irving and Price (1981).

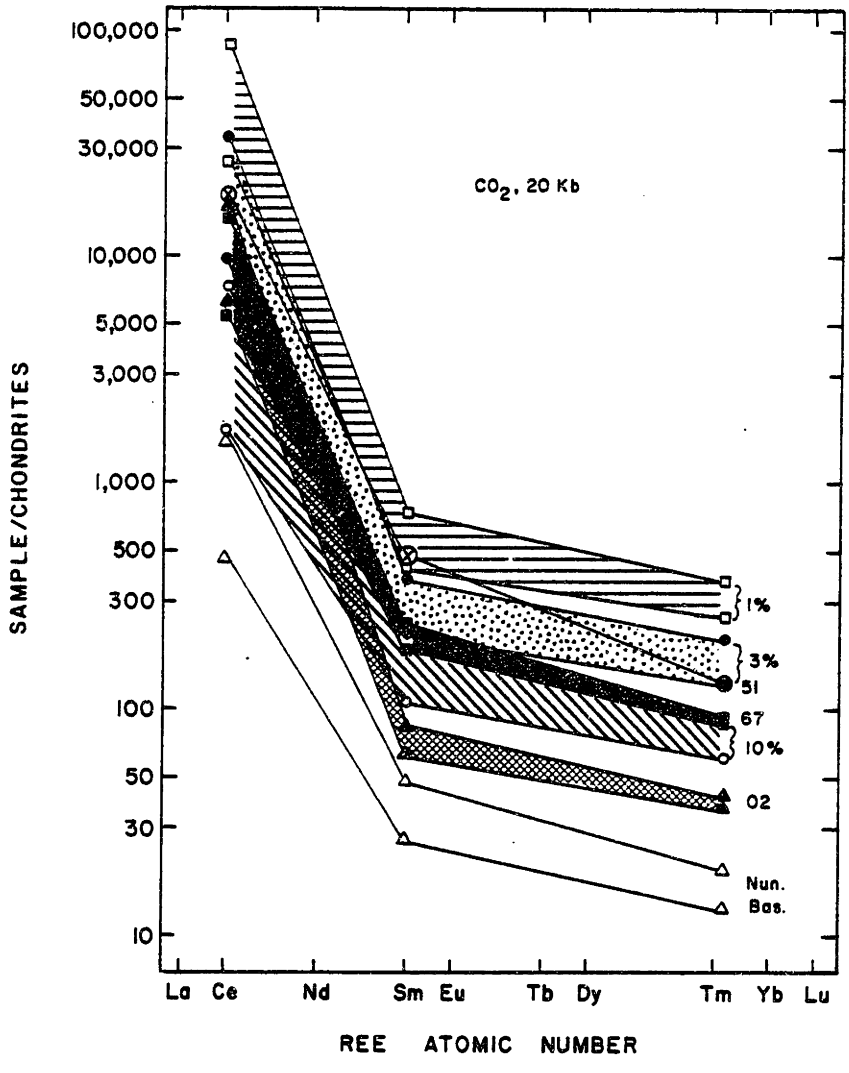
100,000
50,000
30,000
10,000
5,000
3,000
1,000
500
300
100
50
30
10
SAMPLE/CHONDRITES
$CO_2$, 20 Kb
1%
3%
51
67
10%
02
Nun.
Bas.
La Ce Nd Sm Eu Tb Dy Tm Yb Lu
REE ATOMIC NUMBER

Figure 3-41. Calculated, chondrite-normalized REE abundances in $CO_2$ vapor (20 kb) in equilibrium with 10051 clinopyroxene (51), 10067 clinopyroxene (67), 10002 clinopyroxene (02), Nunivak basalts (Nun. bas.), and 1%, 3%, and 10% residual melts (labelled) from Nunivak basalts. $CO_2$ vapor/silicate melt partition coefficients are from Wendlandt and Harrison (1979); clinopyroxene/silicate melt partition coefficients are from Frey et al. (Set 1; 1978). Regions are plotted for 10067 and 10002 clinopyroxenes because of uncertain amounts of included apatite.

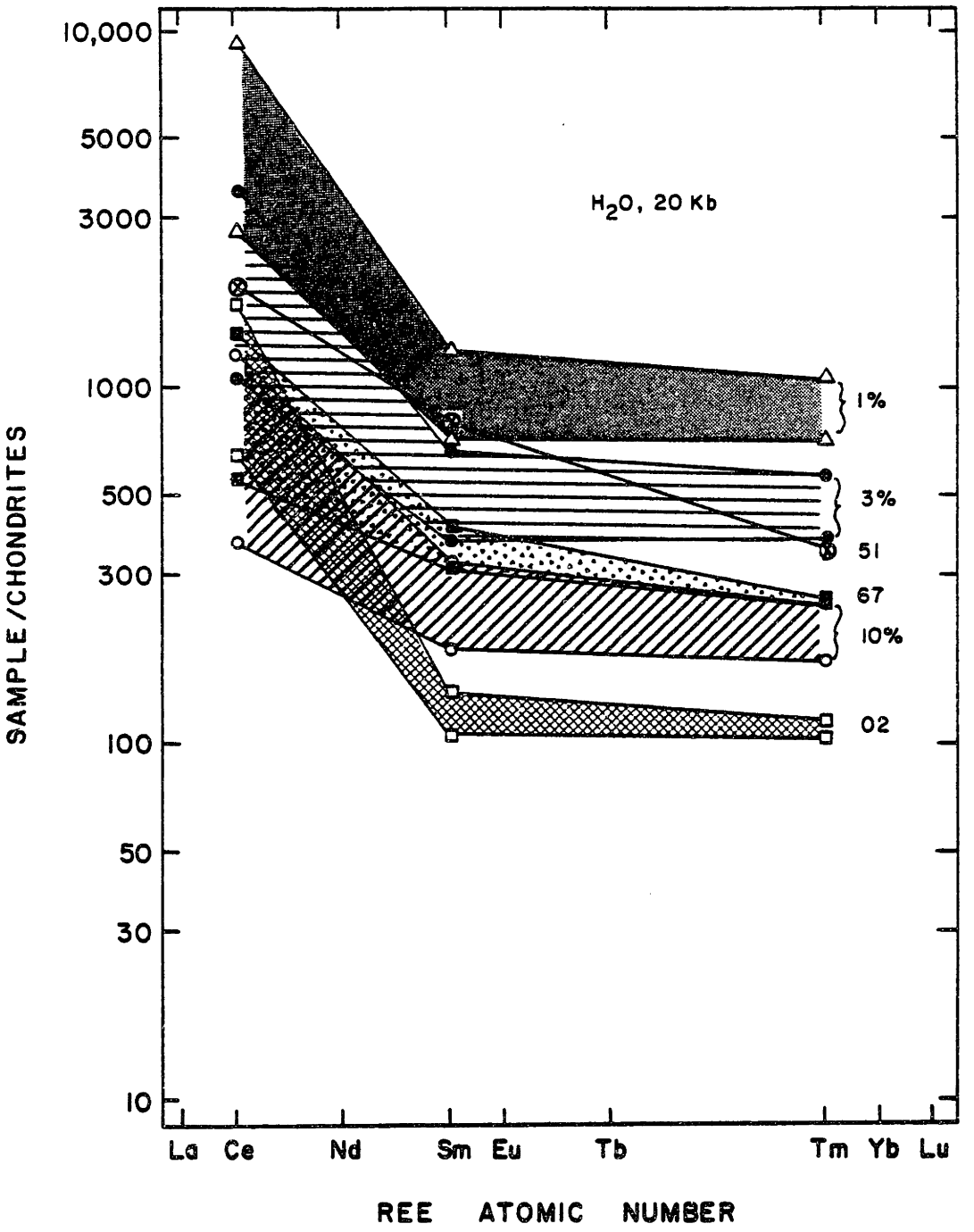
10,000
5000
3000
1000
500
300
100
50
30
10
SAMPLE/CHONDRITES
$H_2O$, 20 Kb
1%
3%
51
67
10%
02
La
Ce
Nd
Sm
Eu
Tb
Tm
Yb
Lu
REE ATOMIC NUMBER

equilibrium olivine composition. Therefore, the Nunivak basalts studied are relatively primitive in the sense that olivines calculated to be in equilibrium with these basalts are either in the range of or are slightly more Fe-rich than olivines presumed to be in the source regions of the basalts. The latter observation indicates that it is likely that many of the basalts have undergone small amounts of crystal fractionation. Based on petrographic evidence (Table 3-1), the most likely fractionating phases are olivine and chromite, and in some cases clinopyroxene. In general, plagioclase is not a phenocryst and thus, does not appear to have been an important fractionating phase. In addition to the phenocryst phases, kaersutite, anorthoclase, and clinopyroxene occur as megacrysts in many Nunivak basalts (Francis, 1974) and Menzies and Murthy (1980a) found that a kaersutite megacryst was isotopically indistinguishable from the host basalts. Thus, it is possible that megacrysts are high pressure, cognate phases. However, anorthoclase is generally not encountered in experiments involving the crystallization of alkali basalts at high pressures (e.g., Allen et al., 1975; Brey and Green, 1975; Green and Ringwood, 1967). Amphibole does occur on the liquidus of some $H_2O$-rich alkali basalts (e.g., Allen et al., 1975). Hence, this latter mineral as well as the phenocryst phases may have fractionated from the Nunivak basalts.

Olivine, chromite, clinopyroxene, and possible amphibole appear to be the dominant phases involved during fractionation of the Nunivak basalts. In the ensuing discussion of basalt petrogenesis, we focus on the incompatible elements, K, Rb, Sr, Ba, Th, La, and Ce because the

fractionating phases, with the exception of amphibole, have partition coefficients less than 0.2 (e.g., Frey et al., 1978) for these elements. Amphibole fractionation, however, may have an important effect on several of these trace elements, e.g., Sr and Ba. Therefore, in the ensuing discussion, we indicate the calculated effect of amphibole fractionation where this effect may be significant, i.e., where Sr or Ba are involved.

During crystal fractionation, the concentrations of these incompatible elements will increase but ratios between two incompatible elements will remain nearly constant. Provided reasonable models can be constructed, consideration of these incompatible element ratios will yield information on the processes responsible for the geochemistry of the basalts.

(2) Evidence for two-component mixing

Any model to explain the petrogenesis of the Nunivak basalts must explain two fundamental geochemical features of the basalts: (1) on plots involving incompatible elements or ratios of incompatible elements, the basalts form coherent trends (Figures 3-43, 3-44) regardless of whether they are nepheline normative or not, and (2) the basalts are markedly heterogeneous with respect to $^{87}Sr/^{86}Sr$ ratios (Figure 3-45). Furthermore, the $^{87}Sr/^{86}Sr$ ratios of the basalts vary systematically with respect to some trace element abundances or ratios (Figures 3-45, 3-46).

The Nunivak basalts resemble the Honolulu Volcanic Series (HVS)

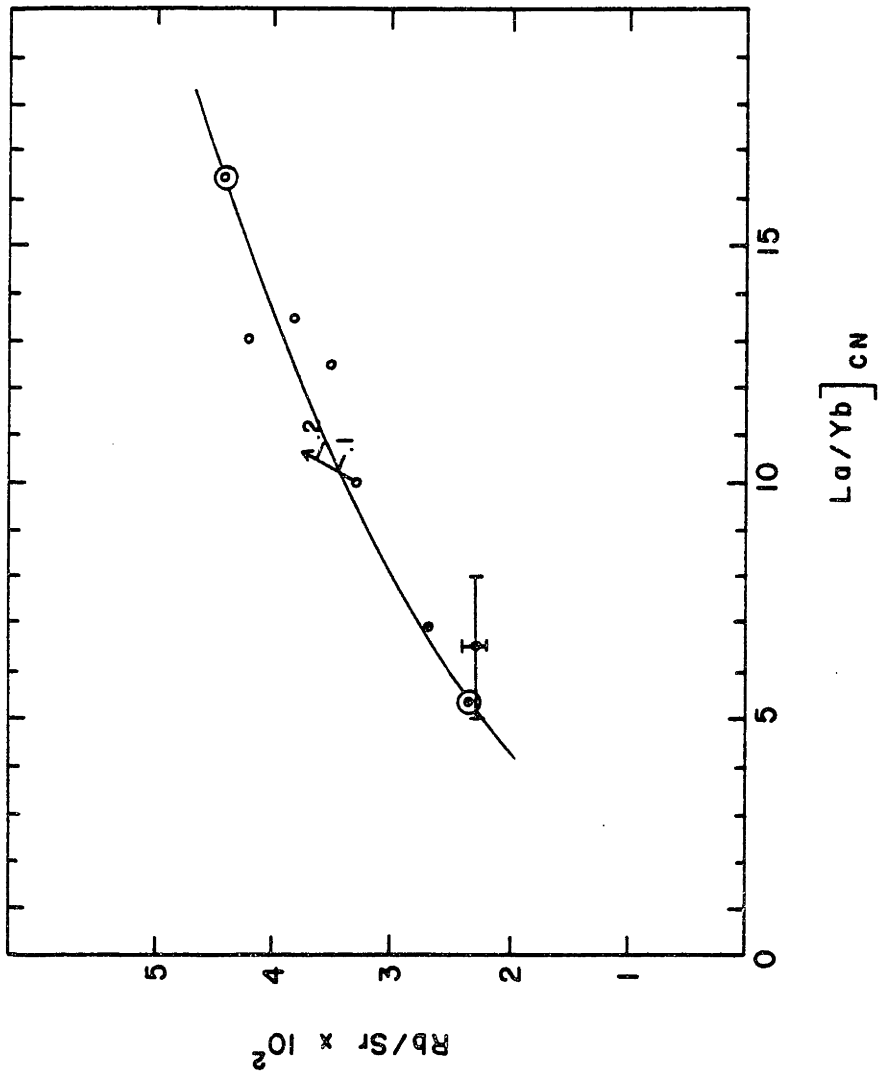
Rb/Sr x 10²
0
1
2
3
4
5
0
5
10
15
La/Yb]CN
1.2
.1

Figure 3-43. Rb/Sr ratio versus chondrite-normalized La/Yb ratio for the 8 Nunivak basalts from Table 3-14. Tholeiites are indicated by solid symbols, basanites by open symbols. The solid line is a two-component miking curve calculated using the two circled data points. The vector indicates the effect of amphibole fractionation; the tic marks and numbers along this vector refer to the amount (mass fraction of system) of amphibole fractionation.

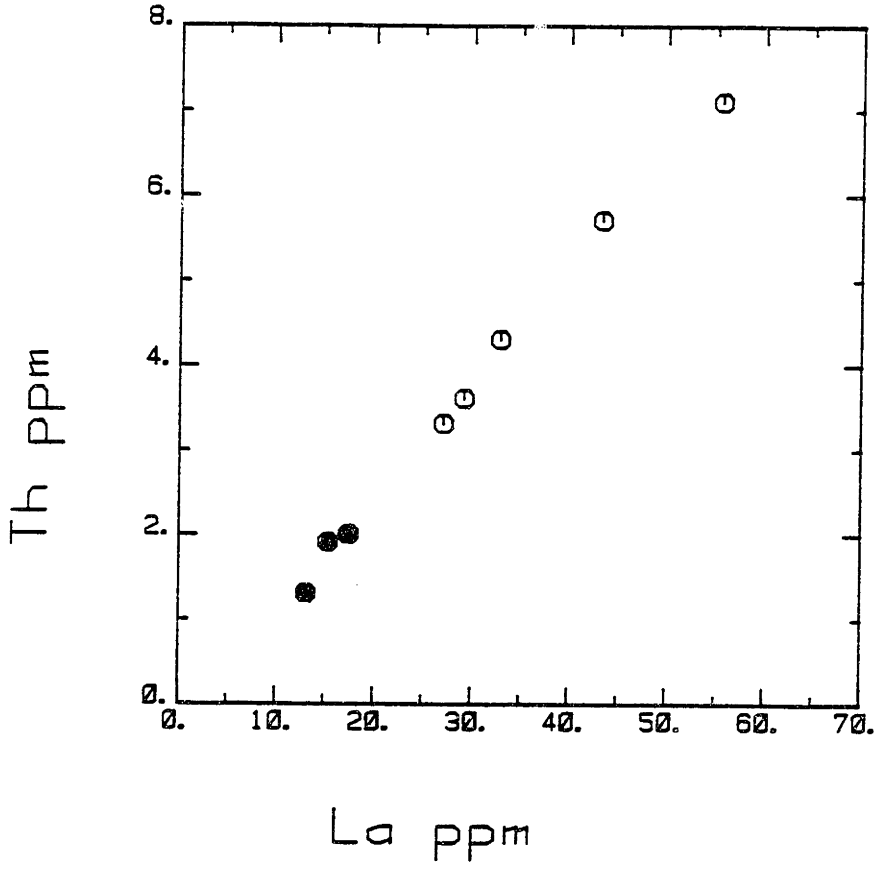
8.
6.
4.
2.
0.
0.
10.
20.
30.
40.
50.
60.
70.
Th ppm
La ppm

Figure 3-44. Th abundances plotted versus La abundances for Nunivak basalts from Table 3-14. Filled symbols indicate tholeiites; open symbols indicate basanites.

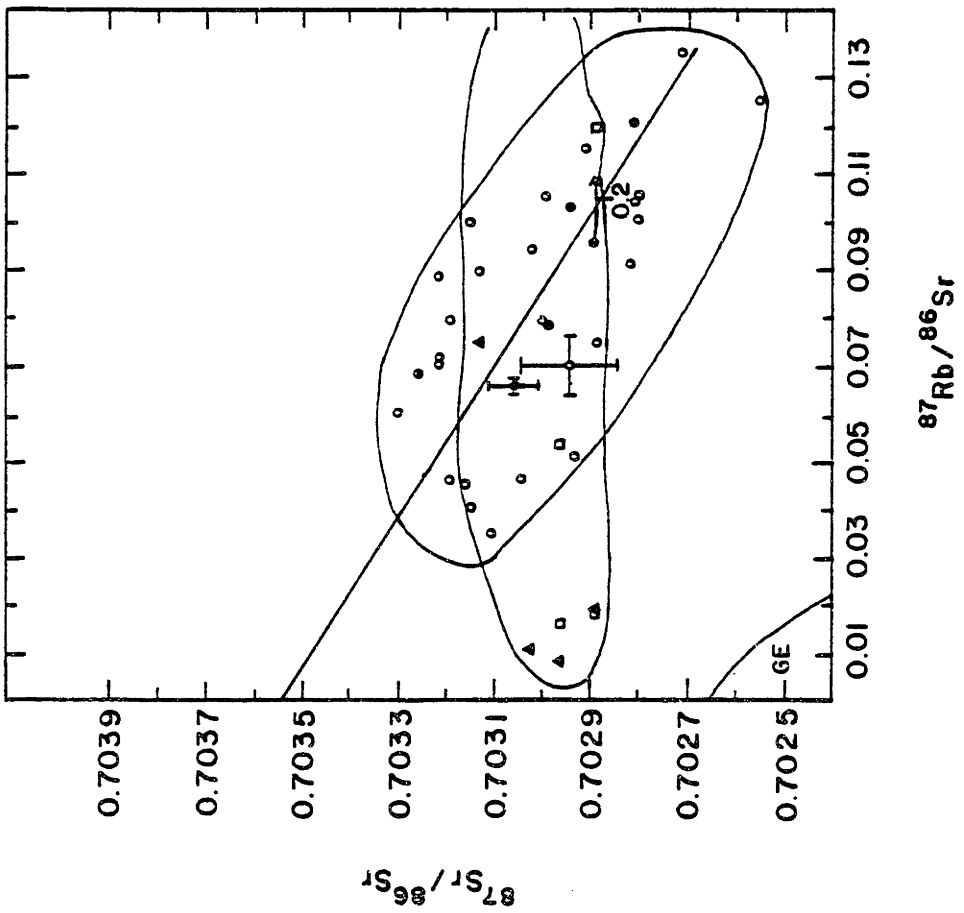
0.7039
0.7037
0.7035
0.7033
0.7031
0.7029
0.7027
0.7025
$^{87}Sr/^{86}Sr$
0.01
0.03
0.05
0.07
0.09
0.11
0.13
$^{87}Rb/^{86}Sr$
GE

Figure 3-45. $^{87}Sr/^{86}Sr$ versus $^{87}Rb/^{86}Sr$ for Nunivak basalts, [(○), Mark, 1971; (●) Table 3-14], ACT and ACE inclusions (△) and amphibole pyroxenites (□). The line is regressed to the 6 basalt data points from Table 3-14. The vector shows the effect of amphibole fractionation as in Figure 3-43.

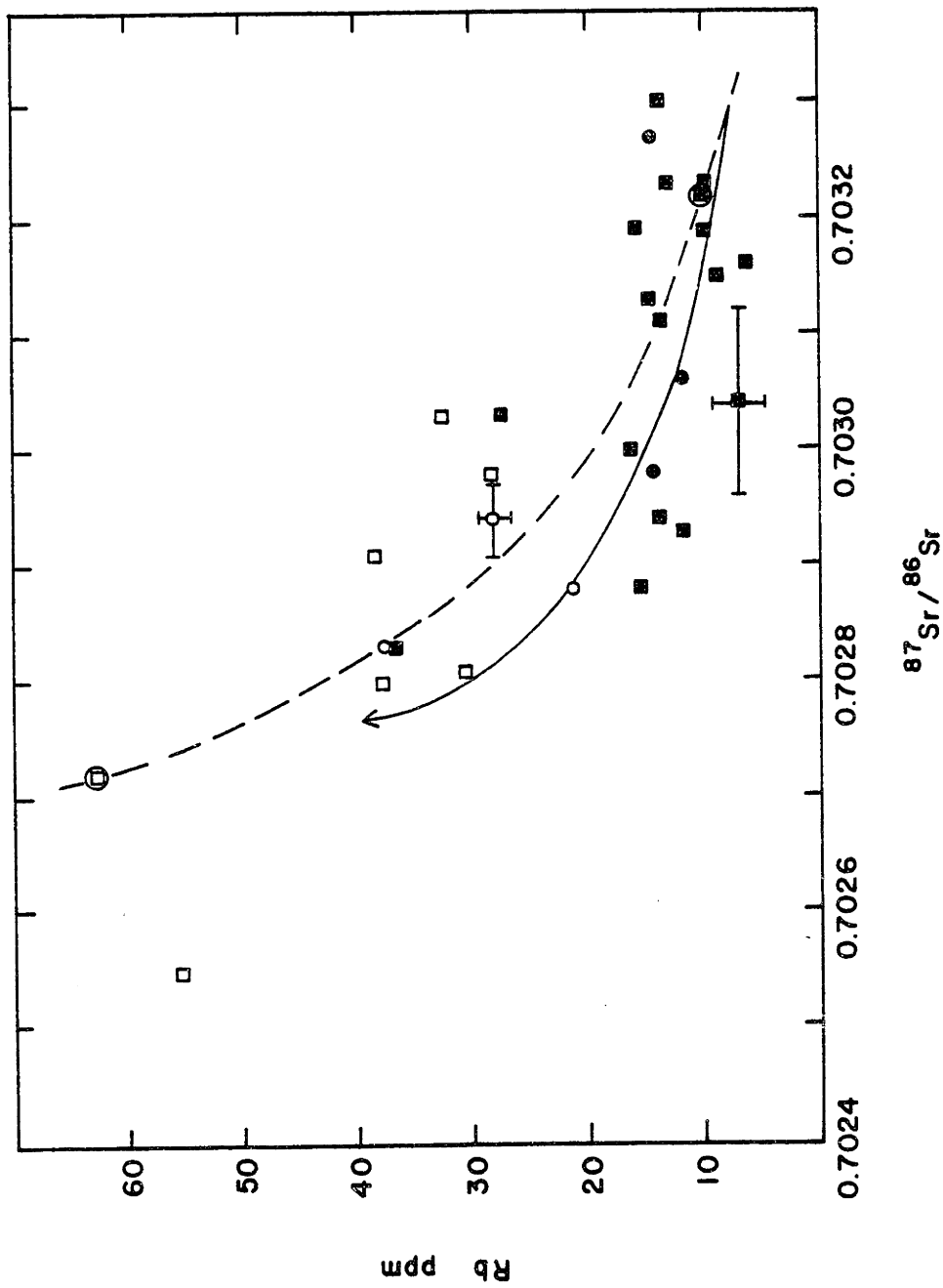
Rb ppm
60
50
40
30
20
10
0.7024
0.7026
0.7028
0.7030
0.7032
$^{87}Sr/^{86}Sr$

Figure 3-46. Rb abundances versus plotted $^{87}Sr/^{86}Sr$ for Nunivak basalts. Solid symbols (■, Mark, 1971; ●, Table 3-14) indicate tholeiites; open symbols (□, Mark, 1971; ○, Table 3-14) indicate basanites. Representative errors for both data sets are shown. Solid curve indicates wallrock reaction model described in the text; dashed line is a mixing curve calculated using the two circled data points.

in having coherent trends on plots of incompatible elements versus incompatible elements. Clague and Frey (1982) argued that the HVS originated by partial melting of a homogeneous source. As predicted from their model, the HVS is homogeneous or nearly so in terms of Pb, Sr, and Nd isotopic ratios (Sun, 1980; Lanphere and Dalrymple, 1980; Roden et al., 1981). Unlike the HVS, the Nunivak basalts are isotopically heterogeneous (Figure 3-45) in terms of Sr isotopic ratios, and thus their geochemistry cannot be explained simply by melting of a homogeneous source unless the Sr isotopic system was decoupled from the trace elements. This possibility is unlikey in view of the correlation between $^{87}Sr/^{86}Sr$ ratio and some trace element ratios and abundances (Figure 3-45, 3-46).

Of particular significance to the problem of the petrogenesis of the basalts is the inverse correlation between $^{87}Sr/^{86}Sr$ and $^{87}Rb/^{86}Sr$ because of the parent-daughter relationship between $^{87}Rb$ and $^{87}Sr$. When the data of Mark (1971) and that from Table 3-9 are considered, the data form a distinctly linear cloud with a negative slope on a $^{87}Sr/^{86}Sr$ versus $^{87}Rb/^{86}Sr$ plot (Figure 3-8). However, when only the more precise isotope dilution data from Table 3-9 are considered, the data points form a distinctly linear trend, although not all the points plot within error of the regressed line. On $^{87}Sr/^{86}Sr$ versus $^{87}Rb/^{86}Sr$ plots, linear trends with positive slopes could be explained by ageing of source materials (e.g., Brooks et al., 1976), disequilibrium melting of an old, Rb-rich phase (e.g., Flower et al., 1975), or by two component mixing (e.g., Langmuir et al., 1978). However, the

only simple explanation of a linear trend with a negative slope on such a plot is two component mixing.

In order to test the hypothesis that the geochemistry of the basalts was controlled by two component mixing, we have calculated mixing curves (Langmuir et al., 1978) for plots of incompatible element and/or isotopic ratios (Figures 3-43, 3-45 to 3-53). On such plots, unless the denominators of the two ratios are the same, mixing curves will be hyperbolas. If the denominators are the same, then mixing curves will be straight lines.

Where amphibole fractionation may have significantly affected one or both ratios, i.e., where Sr, Ba, or Yb are involved, amphibole fractionation vectors have been calculated. In these latter calculations we used a Rayleigh fractionation equation and the amphibole partition coefficients of Irving and Price (1981). These vectors were calculated for up to 20% mass fractionation of amphibole which is a plausible upper limit to the amount of amphibole fractionation. Fractionation of amphibole would likely have been accompanied by fractionation of olivine and possibly other phases; and thus, it is unlikely that the basalts would have retained their primitive geochemical character after large amounts of amphibole fractionation.

The calculated mixing trends are similar to the observed trends for many of the trace element ratios and for $^{87}Sr/^{86}Sr$ ratios (Figures 3-43, 3-45, 3-46, 3-48 to 50, 3-52, 3-53); thus the observed trends in these cases can be explained by two-component mixing. In other examples (Figures 3-47, 3-51) the agreement between the calculated

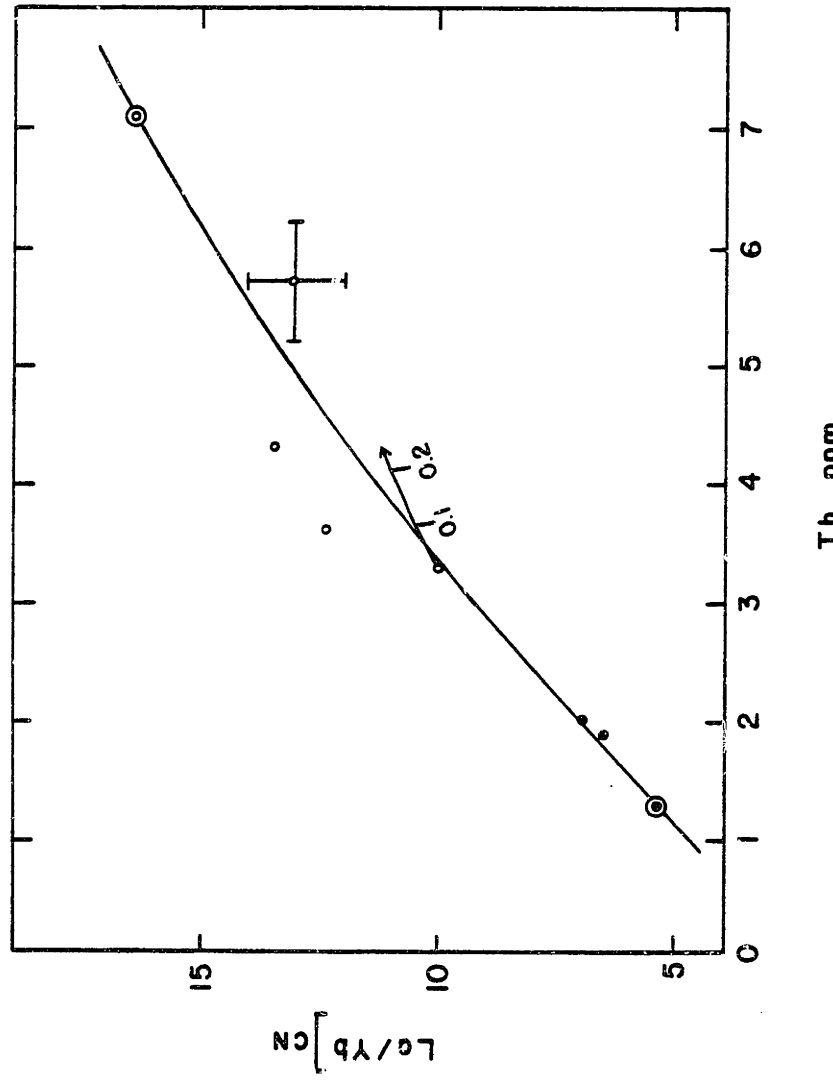
La/Yb]CN
15
10
5
0
1
2
3
4
5
6
7
Th ppm
0.2
0.1

Figure 3-47. Chondrite-normalized La/Yb ratio plotted versus Th ppm for Nunivak basalts from Table 3-14. Solid circles indicate tholeiites, open circles indicate basanites. Mixing curve (solid line) calculated using circled data points. The vector indicates the effect of amphibole fractionation; the numbers along the vector indicates the amount (mass fraction of system) of amphibole fractionated.

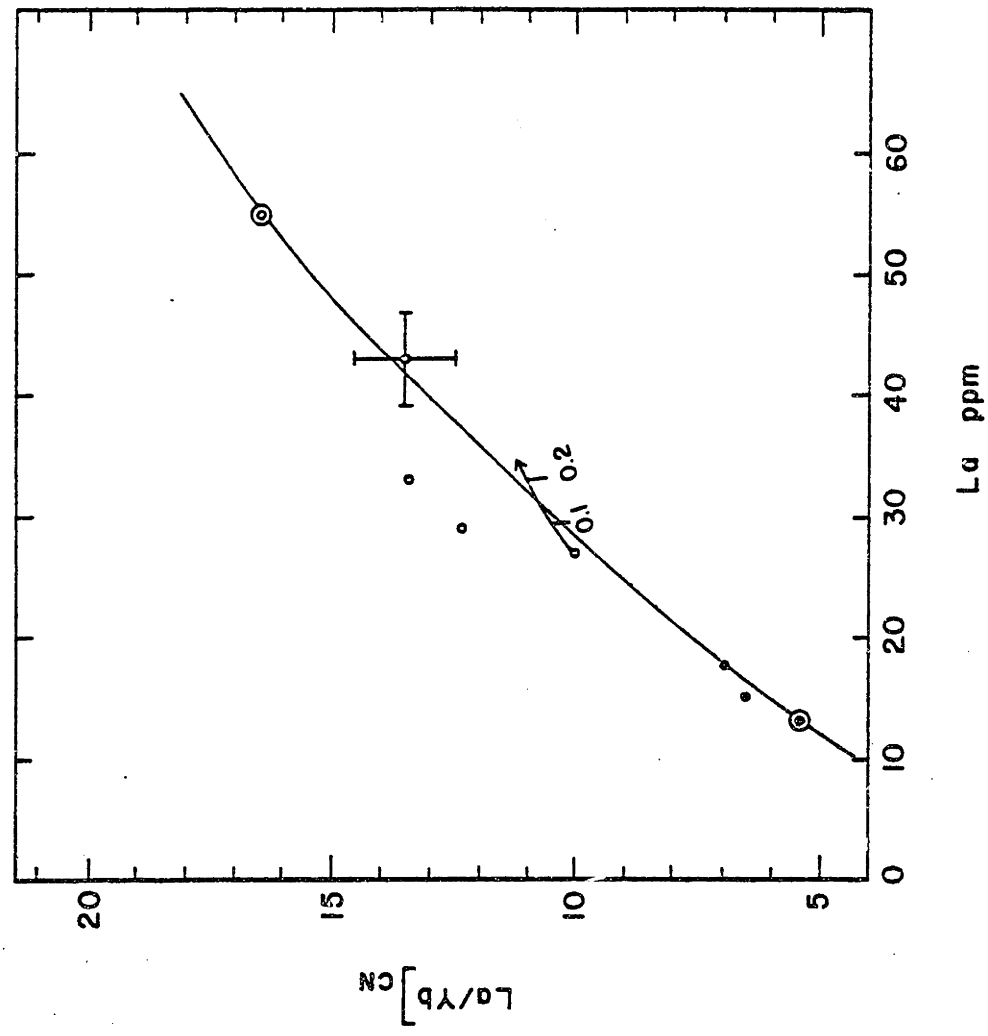
La/Yb]CN
20
15
10
5
0
10
20
30
40
50
60
La ppm
0.2
1.0

Figure 3-48. Chondrite-normalized La/Yb ratio plotted versus La ppm for basalts from Table 3-14. Solid symbols indicate tholeiites; open symbols indicate basanites. Solid curve is a mixing curve calculated by using circled data points. Vector shows the effect of amphibole fractionation; the numbers along the vector indicates the amount (mass fraction of the system) of amphibole fractionated.

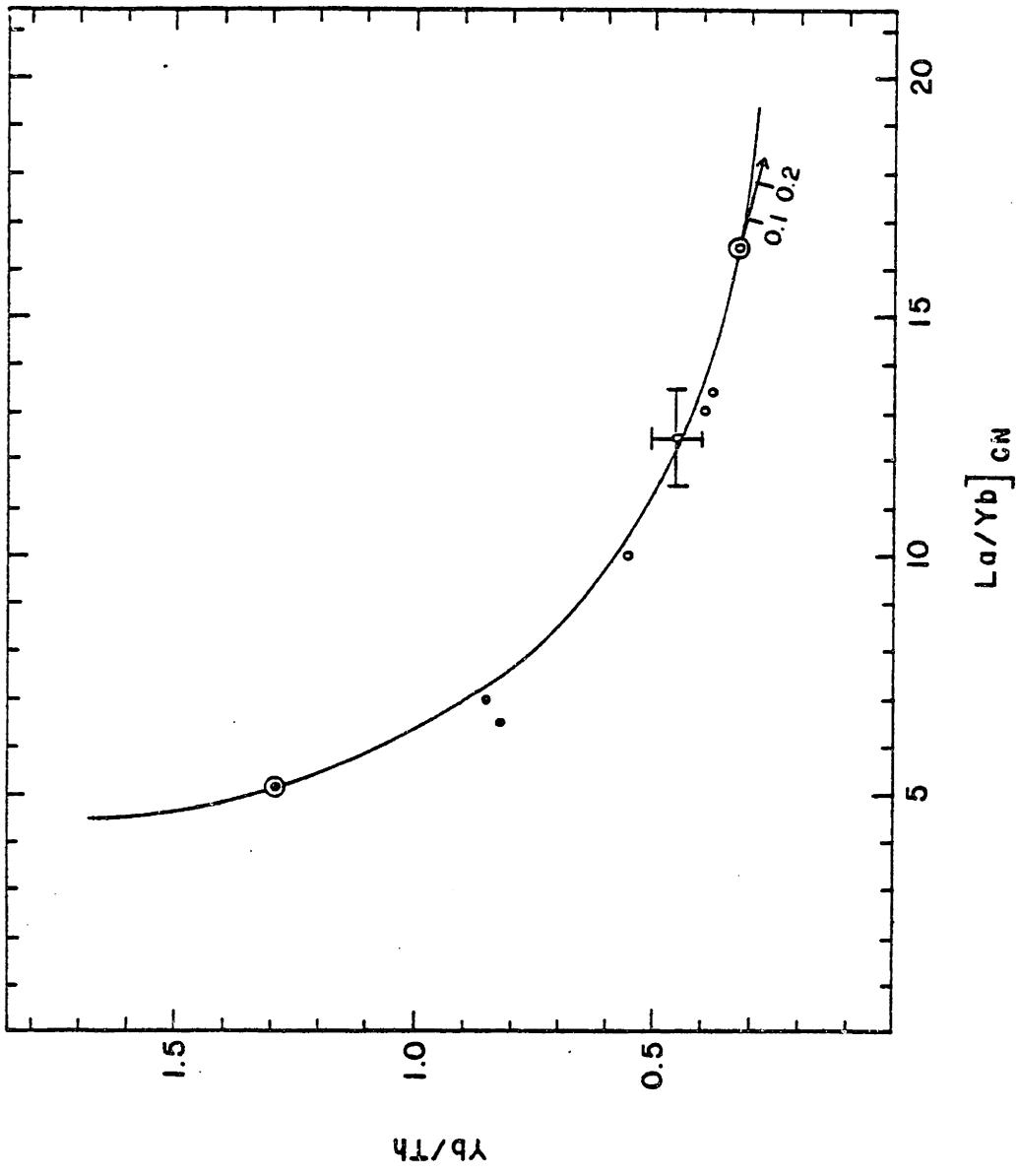
Yb/Th
1.5
1.0
0.5
La/Yb]CN
5
10
15
20
0.1 0.2

Figure 3-49. Yb/Th plotted versus chondrite-normalized La/Yb ratio for tholeiites (●) and basanites (⊙) from Table 3-14. Mixing curve (solid line) calculated using circled data points. Vector indicates the effect of amphibole fractionation; the numbers along this vector indicate the amount (mass fraction of system) of amphibole fractionated.

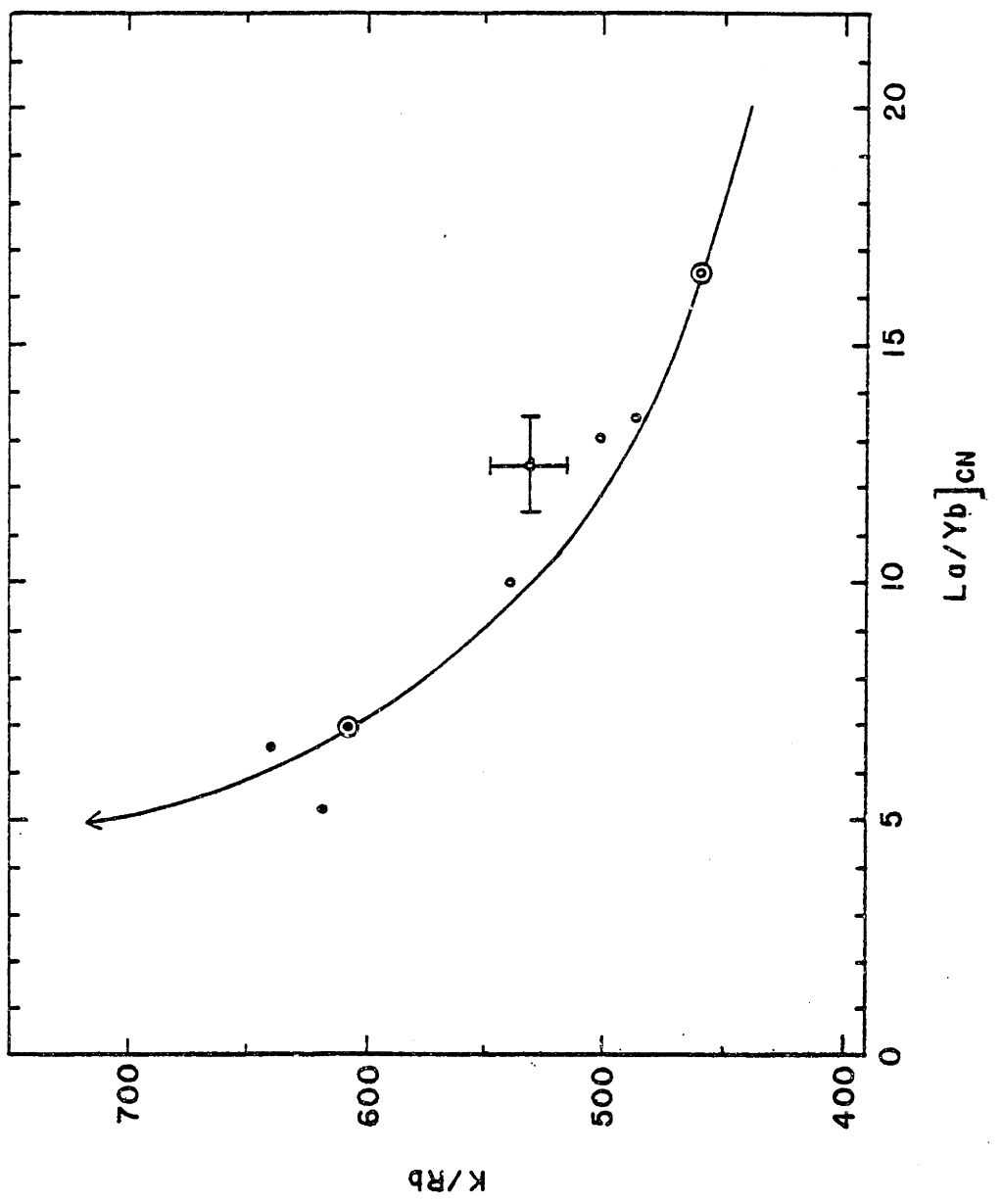
K/Rb
700
600
500
400
0
5
10
15
20
La/Yb]CN

Figure 3-50. K/Rb plotted versus chondrite-normalized La/Yb ratio for Nunivak tholeiites (●) and basanites (⊙) from Table 3-14. Mixing curve (solid line) calculated using the circled data points.

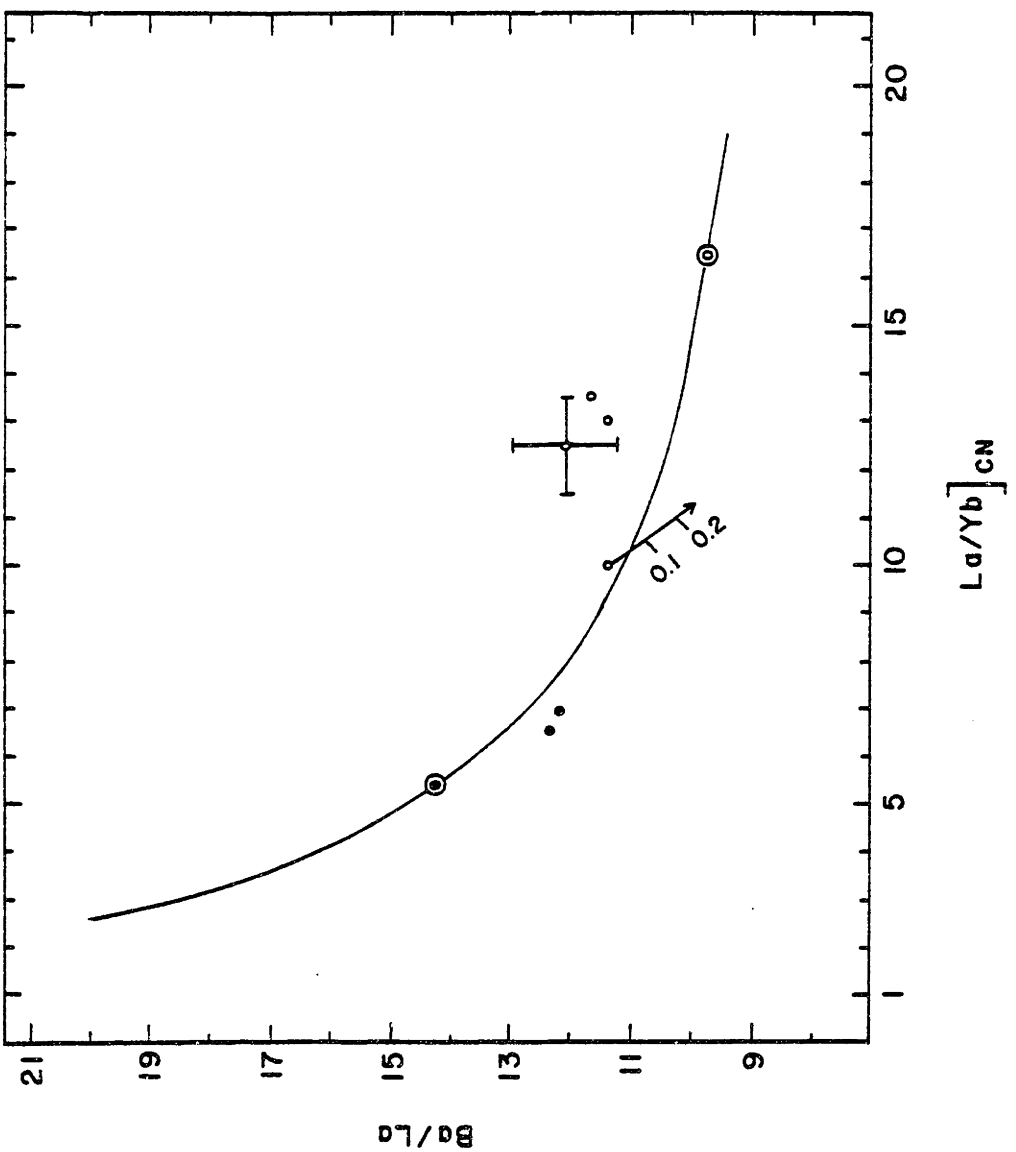
Ba/La
21
19
17
15
13
11
9
1
5
10
15
20
[La/Yb]CN
0.1
0.2

Figure 3-51. Ba/La plotted versus chondrite-normalized La/Yb ratio for Nunivak tholeiites (●) and basanites (○) from Table 3-14. Mixing curve (solid line) was calculated using the two circled data points. The vector shows the effect of amphibole fractionation; the numbers along this vector indicate the amount (mass fraction of system) of amphibole fractionated.

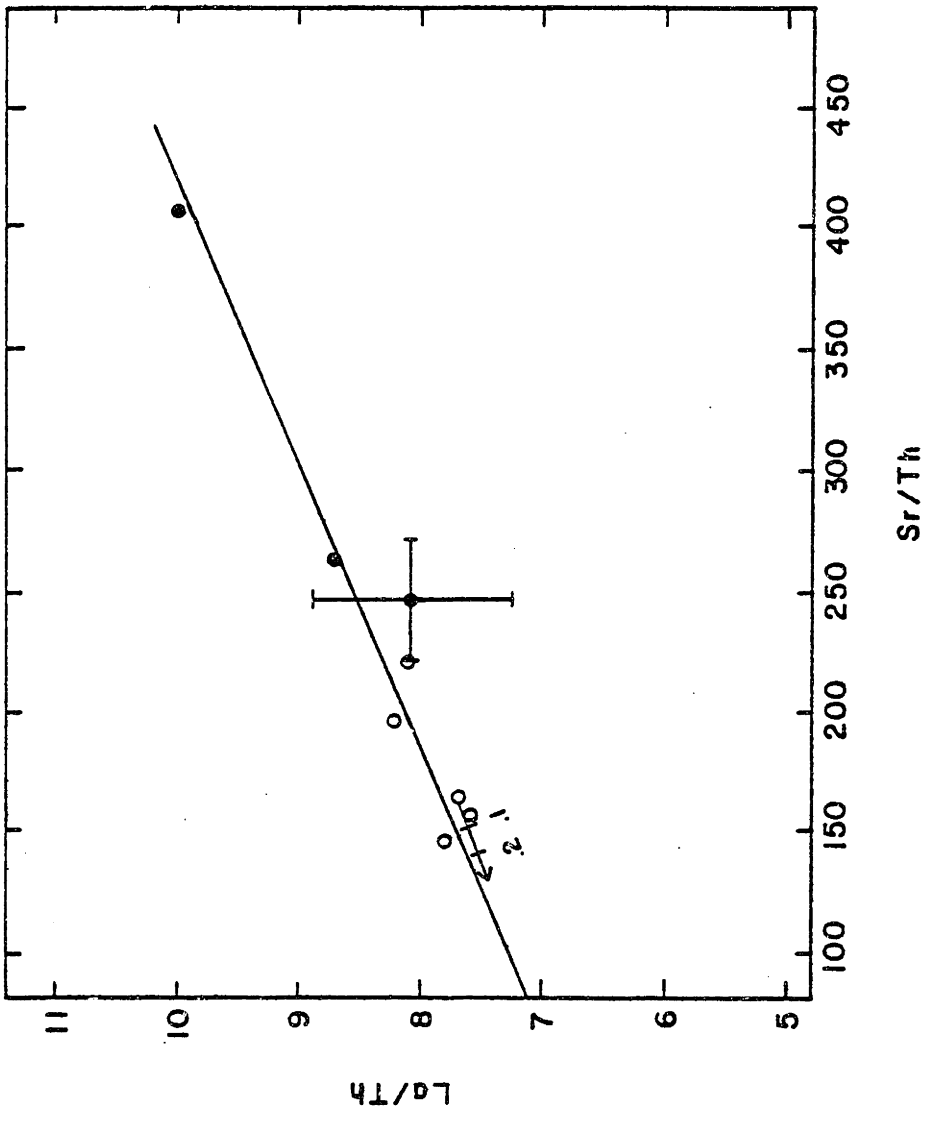
La/Th
Sr/Th
11
10
9
8
7
6
5
100
150
200
250
300
350
400
450
1
2

Figure 3-52. La/Th plotted versus Sr/Th for Nunivak tholeiites (●) and basanites (o) from Table 3-14. On this plot a mixing curve is a straight line (e.g., Langmuir et al., 1978); the line is a linear regression of La/Th on Sr/Th. The vector indicates the effect of amphibole fractionation; the numbers along the vector indicate the amount (mass fraction of system) of amphibole fractionated.

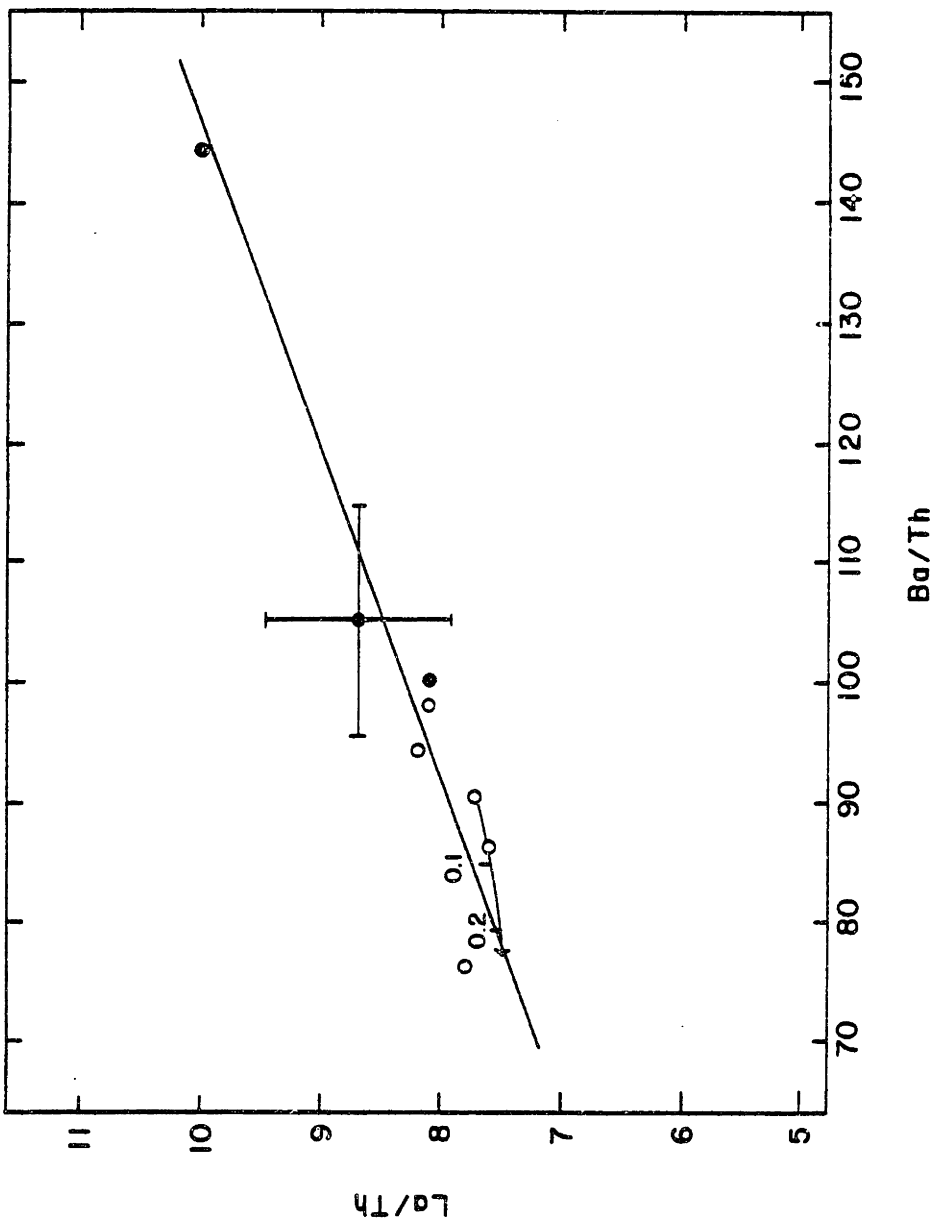
La/Th
Ba/Th
11
10
9
8
7
6
5
70
80
90
100
110
120
130
140
150
0.1
0.2

Figure 3-53. La/Th plotted versus Ba/Th for Nunivak tholeiites (●) and basanites (○) from Table 3-14. On this plot a mixing curve is a straight line (e.g., Langmuir et al., 1978); the line is a linear regression of La/Th on Ba/Th. The vector indicates the effect of amphibole fractionation; the numbers along the vector indicate the amount (mass function of system) of amphibole fractionated.

mixing curves and the observed trends is not as good, and K/Ba and $^{143}Nd/^{144}Nd$ ratios show no consistent variation with other trace element ratios (Figures 3-54, 3-55). The majority of the examples are consistent with two component mixing as an explanation of the data, and we find the variation of $^{87}Sr/^{86}Sr$ with Rb/Sr to be particularly compelling evidence for mixing. Thus, we conclude that two component mixing is the simplest explanation of the observed trends.

One consequence of our interpretation is that the two components are not distinguishable on the basis of $^{143}Nd/^{144}Nd$ or K/Ba ratios. Apparently, the two end members had similar $^{143}Nd/^{144}Nd$ and K/Ba ratios, or these ratios were affected by another process. A second consequence of our interpretation is that the ACT and ACE inclusions are not similar to either component in terms of their $^{87}Sr/^{86}Sr$ and $^{87}Rb/^{86}Sr$ ratios (Figure 3-45). Hence, it is unlikely that these inclusions could be representative of the source for the Nunivak basalts as suggested by Menzies and Murthy (1980a); however, these inclusions could have metasomatized by fluids or residual melts related to the basaltic volcanism on Nunivak as we suggested previously.

We estimated the trace element and isotopic ratios of the two components by calculating asymptotes to the mixing curves in favorable cases, i.e., where the curvature of the mixing curve is such that realistic limits can be placed on the two components. In unfavorable cases we used basalt compositions to set limits. The results are shown in Table 3-22. One component is characterized by low $^{87}Sr/^{86}Sr$, K/Rb, Ba/Th, Sr/Th, La/Th, Ba/Th, and Yb/Th ratios and high La/Yb,

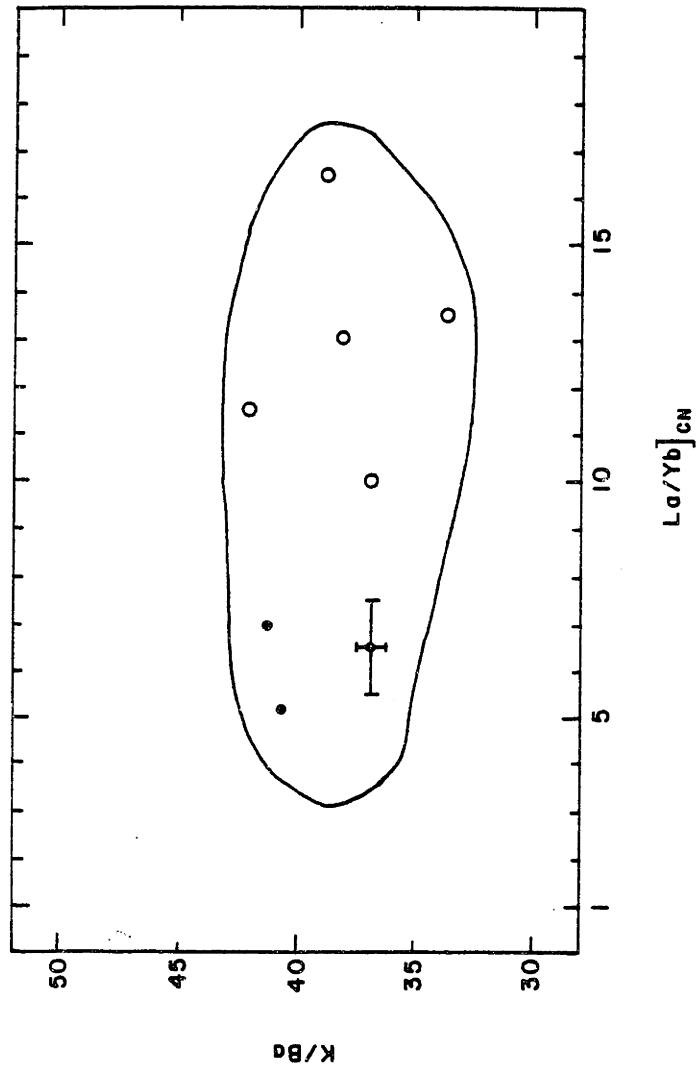
K/Ba
50
45
40
35
30
1
5
10
15
La/Yb]CN

Figure 3-54. K/Ba plotted versus chondrite-normalized La/Yb ratio for Nunivak tholeiites (●) and basanites (O) from Table 3-14.

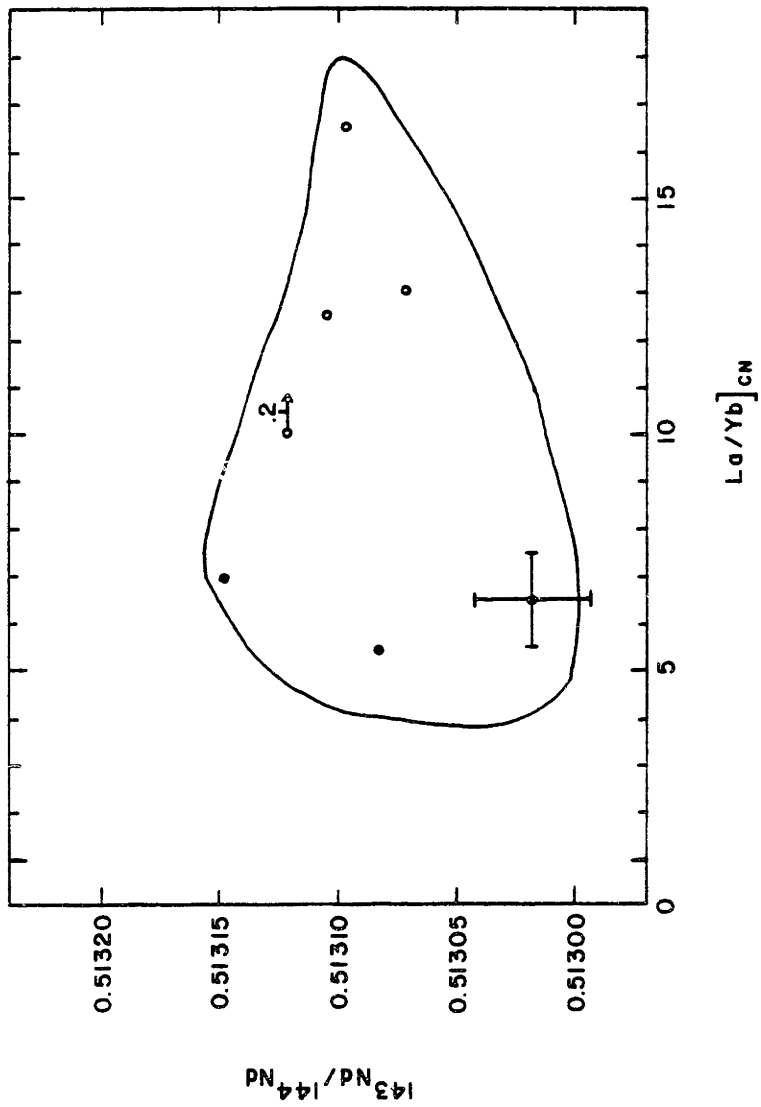
0.51320
0.51315
0.51310
0.51305
0.51300
$^{143}Nd/^{144}Nd$
0
5
10
15
$La/Yb]_{CN}$
.2

Figure 3-55. $^{143}Nd/^{144}Nd$ plotted versus chondrite-normalized La/Yb ratio for Nunivak tholeiites (●) and basanites (○) from Tables 3-9 and 3-14. Vector indicates the effect of amphibole fractionation; the number along the vector indicates the amount (mass fraction of system) of amphibole fractionated.

Table 3-22. Geochemistry of Nunivak mixing components.

| | Component 1 | Component 2 |
|---|---|---|
| K/Rb | 350-460 | >640 |
| $La/Yb]_{cn}$ | >16 | 1.6-5.3 |
| Ba/Th | <85 | >140 |
| Rb/Sr | >0.045 | <0.014 |
| Sr/Th | <150 | >400 |
| La/Th | < 7.6 | > 10 |
| Ba/La | 7.5-9.9 | > 14 |
| Yb/Th | <0.4 | > 1.3 |
| K/Ba | ~ 40 | ~ 40 |
| $^{87}Sr/^{86}Sr$ | <0.7026 | 0.7033-0.7035 |
| $^{143}Nd/^{144}Nd$ | ~0.5131 | ~ 0.5131 |

and Rb/Sr ratios relative to the second component. In the ensuing discussion we refer to the former component as "component 1" and the latter component as "component 2".

The endmember $^{87}Sr/^{86}Sr$ and $^{87}Rb/^{86}Sr$ ratios require a complex history for both components. For example, integrated over the history of the earth ($\sim 4.6 \times 10^9$ yr; $^{87}Sr/^{86}Sr]_i = 0.699$) the Rb/Sr ratio of component 1 would yield a present-day $^{87}Sr/^{86}Sr$ ratio of greater than or equal to 0.7078 while the Rb/Sr ratio of component 2 would yield a present-day $^{87}Sr/^{86}Sr$ ratio of less than or equal to 0.7017. Thus, the data require two-stage models for both components: a relatively recent increase in Rb/Sr ratio in the case of component 1 and a relatively recent decrease in Rb/Sr ratio in the case of component 2. One obvious explanation of a change in Rb/Sr ratio is that both components have been involved in melting events; however, in view of the lack of knowledge about the possible mineralogy of the residual solids, we will not propose a specific model.

(3) Towards a physical model

Relating the two component mixing model to a physical process is a difficult problem. Firstly, the basalts lack textures which can be attributed to mixing. Thus, it appears that the mixing cannot be a shallow phenomena related to the transport of the basalts through the crust, or else some textural evidence would be expected to remain.

Secondly, the evaluation of the mixing process is hampered by the lack of data; specifically, our interpretation of mixing is based on only 8 data points, except in the cases of $^{87}Sr/^{86}Sr$, Rb, and Sr. Thus, in some cases where no mixing relationship was observed, e.g.,

$^{143}Nd/^{144}Nd$ versus La/Yb (Figure 3-55), it is possible that more data would show a mixing relationship. Indeed, the converse is equally possible: in examples where a satisfactory mixing relationship exists, more data might make the relationship less convincing. However, we find the well documented inverse correlation between $^{87}Sr/^{86}Sr$ and $^{87}Rb/^{86}Sr$ to be convincing evidence for mixing of at least two components.

There are at least 3 physical processes which could explain the data for the Nunivak basalts: (1) magma mixing, (2) contamination by altered oceanic crust, or (3) reaction with refractory mantle wallrock. The first hypothesis is plausible at Nunivak although without textural evidence for magma mixing there is no way to prove this model. The existence of the mixing relationship shows that mixing of two magmas with endmember compositions can explain the data. One consequence of this model is that the two magmas differ in $^{87}Sr/^{86}Sr$ ratios, but the limited $^{143}Nd/^{144}Nd$ data are consistent with the two components being nearly indistinguishable in terms of $^{143}Nd/^{144}Nd$ ratios. In that case, component 2 is displaced from component 1 on a $^{143}Nd/^{144}Nd$ versus $^{87}Sr/^{86}Sr$ diagram towards higher $^{87}Sr/^{86}Sr$ ratios (Figure 3-56). This displacement is in the same sense as that produced by basalt-seawater interaction (e.g., McCulloch et al., 1981). Hence, it is possible that component 2 is either altered, recycled (?) oceanic crust or a melt derived from this crust.

A second plausible physical model for the Nunivak mixing is contamination of the older tholeiites by altered oceanic crust. Such contamination could explain the elevated $^{87}Sr/^{86}Sr$ ratios of the

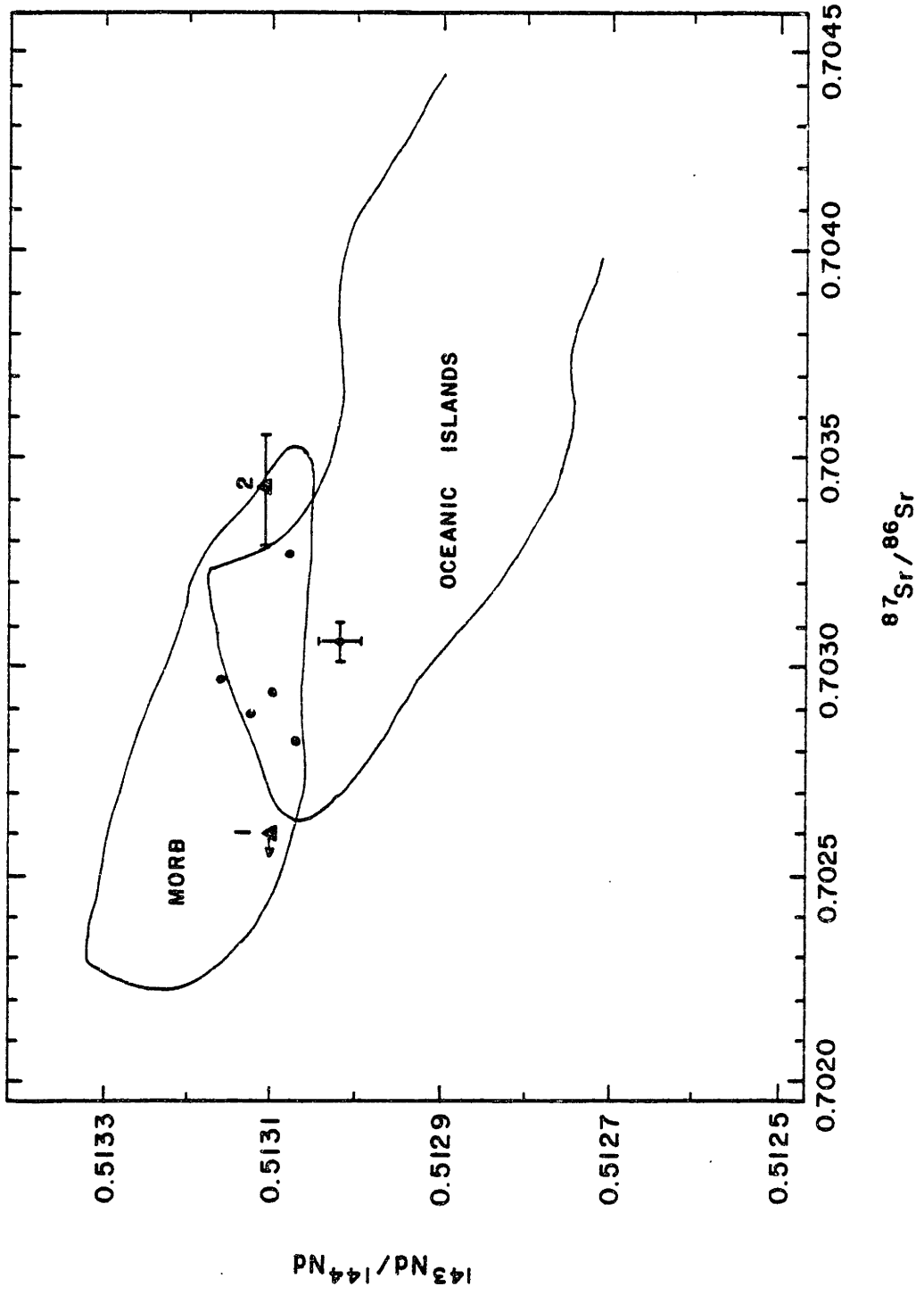
MORB
OCEANIC ISLANDS
1
2
0.5133
0.5131
0.5129
0.5127
0.5125
0.7020
0.7025
0.7030
0.7035
0.7040
0.7045
$^{143}Nd/^{144}Nd$
$^{87}Sr/^{86}Sr$

Figure 3-56. $^{143}Nd/^{144}Nd$ versus $^{87}Sr/^{86}Sr$ showing the inferred positions of the two mixing components (▲). MORB and ocean island fields are from Figure 3-11. Six Nunivak basalts (●) from Table 3-9 are also shown.

tholeiites and similar $^{143}Nd/^{144}Nd$ ratios relative to the basanites (e.g., McCulloch et al., 1981). An important question in evaluating this hypothesis is whether the Nunivak trace element $^{87}Sr/^{86}Sr$ correlations are the same phenomena as the correlations in Hawaiian lavas where younger, more alkalic basalts have lower $^{87}Sr/^{86}Sr$ ratios and higher $^{143}Nd/^{144}Nd$ ratios than the underlying tholeiites (e.g., Chen et al., 1981). The most extreme example of this phenomena occurs on Oahu where the Koolau shield tholeiites have $^{87}Sr/^{86}Sr$ = 0.7036-0.7046 and $^{143}Nd/^{144}Nd$ = 0.51267-0.51288 while the overlying post-erosional Honolulu Volcanic Series has $^{87}Sr/^{86}/Sr$ = 0.7030-0.7034 and $^{143}Nd/^{144}Nd$ = 0.51302-0.51306 (Lanphere and Dalrymple, 1980; Roden et al., 1981; Roden, unpublished data). It is unlikely that crystal contamination can explain these observations because the Koolau data lie within the mantle array while contamination by altered oceanic crust would most likely result in higher $^{87}Sr/^{86}Sr$ ratios without changing $^{143}Nd/^{144}Nd$ ratios (e.g., McCulloch et al., 1981). If the ultimate cause of both the Hawaiian and Nunivak phenomena is the same, then contamination by altered oceanic crust is not a satisfactory physical model for the Nunivak data. At present, we lack sufficient data to demonstrate whether or not $^{143}Nd/^{144}Nd$ is correlated with incompatible trace element abudances as in the Hawaiian lavas.

We evaluated the third model, melt-wallrock reaction, in some detail because reaction between orthopyroxene-bearing wallrock and alkalic basalts probably occurs at shallow depths in the mantle. This inference follows from the observation that orthopyroxene is absent

from the liquidi of alkali basalts and many olivine tholeiites at pressures less than approximately 8 kb (e.g., Green and Ringwood, 1967; Thompson, 1974). Even if the basalt is in equilibrium with the major phases in the wallrock, the magma will tend to scavenge incompatible elements from the wallrock according to the relation $c_i^s/c_i^l = D^i$, and to equilibrate isotopically, with the wallrock if its passage through the wallrock is slow enough. Thus, melt-wallrock reaction must occur, the question is whether or not this process is important in determining the geochemistry of the basalts.

The model which we evaluated is a variant of the zone refining model described by Harris (1957) and very similar to the models which Green and Ringwood (1967) and Bultitude and Green (1968) proposed to explain the origin of alkali basalts. In this model, the tholeiites represent an initial melt which reacted with refractory wallrock to form the basanites. The model was constructed as follows: an initial melt similar to the tholeiites with Rb = 6 ppm, Sr = 400 ppm, and $^{87}Sr/^{86}Sr = 0.7034$ percolates through and equilibrates with more refractory wallrock with Rb = 0.3 ppm, Sr = 15 ppm, and $^{87}Sr/^{86}Sr = 0.7027$. The wallrock is isotopically similar to the basanites. The wallrock Sr concentration is similar to that of the GE inclusions and within the range of the primitive inclusions of Jagoutz et al. (1979). The wallrock Rb concentration is somewhat higher than the Rb concentrations of the GE peridotites (0.01-0.11 ppm) but within the range of Rb concentrations in the primitive inclusions of Jagoutz et al. (1979). Both of these concentrations were chosen to be consistent with probable

mantle concentrations and to provide good fits to the data because our primary objective was to show that the model could explain the inverse correlation between $^{87}Sr/^{86}Sr$ and Rb (Figure 3-46).

We did not evaluate the behavior of $^{143}Nd/^{144}Nd$ ratios in this model because our data is limited and we have not demonstrated that two-component mixing explains the $^{143}Nd/^{144}Nd$ ratios of the basalts. We note parenthetically, that based on the mantle array, mantle wallrock with an $^{87}Sr/^{86}Sr$ ratio of 0.7027 should have a $^{143}Nd/^{144}Nd$ ratio of approximately 0.5132 (e.g., Figure 3-56). We use this number later to illustrate a problem with the model.

We quantified the above model as a step function by (1) using the initial melt and wallrock compositions specified above, (2) assuming that $D^{Rb} = 0.002$ based on olivine and clinopyroxene data from Hart and Brooks (1974), orthopyroxene data of Zindler (1980), and by assuming that $K^{Rb}_{cpx} = K^{Rb}_{gt}$, (3) $D^{Sr} = 0.01$, a value consistent with partition coefficients in the literature (e.g., Hart and Brooks, 1974; Clague and Frey, 1982), (4) assuming a wallrock mode of 60% olivine, 20% orthopyroxene, 10% clinopyroxene, 10% garnet, or 60% olivine, 20% orthopyroxene, 20% clinopyroxene, and (4) assuming a solid to liquid ratio of 3:7 in each equilibration step. The bulk solid-liquid distribution coefficient, $D^{Rb}$, is poorly constrained; however, because $D^{Rb}$ is very small, the model results are not very sensitive to this parameter. We chose a small solid: liquid ratio because it is unlikely that a small amount of melt could equilibrate with a relatively large amount of wallrock without freezing.

For convenience we modelled this process as a series of steps; in each step, the isotopic ratios of the melt are calculated by mass balance assuming total equilibrium between wallrock and melt. Rb concentrations are defined by mass balance and the relation, $C_s^{Rb}/C_1^{Rb} = D^{Rb}$. Note that the ultimate limit of concentration for a trace element is $C_s^i/D^i$ as in zone-refining (Harris, 1957).

The results of the model calculations are shown in Figure 3-46. On a Rb versus $^{87}Sr/^{86}Sr$ plot the model liquid follows a curving trajectory characterized by an initial period of rapid approach to isotopic equilibrium with the wallrock combined with a slow increase in Rb concentration. This initial stage is followed by a period in which the isotopic composition of the liquid is buffered by the small difference in the isotopic composition between liquid and wallrock while the Rb concentration continues to increase. The trajectory of the model liquid is similar to the trend of the Nunivak data on a Rb versus $^{87}Sr/^{86}Sr$ diagram (Figure 3-46).

The wallrock-melt reaction model accounts for increasing Rb concentration with decreasing $^{87}Sr/^{86}Sr$, but several considerations indicate that this model does not present an accurate physical model. The most important difficulty is the heat budget of the melt. For example, in order for the melt to reach a composition of Rb = 20 ppm and $^{87}Sr/^{86}Sr = 0.7029$, 120 steps of equilibration in the mass ratio 3 wallrock: 7 liquid are required. Simple heat budget calculations after Yoder (1976) in which a melt rises adiabatically from 250 km and reacts with wallrock at 50 km, indicates that neither superheat due to the

adiabatic rise of the melt, nor latent heat of crystallization can supply the heat required to equilibrate wallrock with melt. For example, if the wallrock was initially at 900°C, a temperature consistent with the mid-cell oceanic geothermal gradient of Solomon (1976), and the melt at 1200°C, a temperature consistent with the mantle solidus and adiabatic calculations of Wyllie (1980), the melt does not contain enough heat to raise the wallrock temperature to 1200°C. The heat required to raise 360 gm (specified by 7 gm of melt, 7:3 melt to solid ratio, and 120 steps) of wallrock from 900°C to 1200°C is 30,240 calories assuming that the heat capacity of the wallrock is approximately 0.28 cal/gm-deg (Yoder, 1976). In contrast, superheat of 7 gm of melt supplies only 196 calories per 100°C of cooling (assuming that the heat capacity of the melt is approximately equal to that of the wallrock (e.g., Carmichael et al., 1974). The latent heat of crystallization of all 7 gm is 840 calories (assuming that 120 cal/gm is an appropriate value for the heat of fusion, Yoder, 1976). Thus, the process requires a heat input greatly in excess of that contained in the initial batch of melt. Possibly this heat could be supplied by repeated pulses of magma injected into warming wallrock. Then, eruption might be triggered by a final pulse of melt which does not completely freeze and which attains a high volatile content (Spera, 1981).

However, a further important problem in the wallrock-melt reaction model as we formulated it, is that the model does not satisfactorily explain the trend of the basalt data on a La-Ce plot. In a one stage

model, in order for the REE data to be consistent with the inferred $^{143}Nd/^{144}Nd$ ratio, 0.5132, the wallrock, the La/Ce ratio of the wallrock should be less than chondrites. To model the behavior of the La/Ce ratio we chose as two endmembers the La/Ce ratio in B-12, the tholeiite with the lowest La and Ce concentration, and the average La/Ce ratio of the GE inclusions. The results (Figure 3-57) show that as the melt continuously reacts with wallrock, La and Ce concentrations increase in the melt, but the La/Ce ratio decreases. The model trend is significantly different from that observed in the basalts.

Fractionation of clinopyroxene or garnet will increase the La/Ce ratio in the melt because $K_D^{La} < K_D^{Ce}$ for both minerals; both these minerals are common liquidus or near-liquidus phases in alkali basalts at high pressures (e.g., Thompson, 1974; Green and Ringwood, 1967). Furthermore, crystallization of these phases would liberate heat to fuel further reaction with wallrock (e.g. Taylor, 1980). However, modelling of clinopyroxene and garnet crystal fractionation reveal that La and Ce are too incompatible for crystallization of these phases to increase the La/Ce ratios of the melts sufficiently to conform with the observed La/Ce ratios in the basalts (Figure 3-57). This is the case even if partition coefficients (Frey et al., 1978) most favorable to La/Ce fractionation are used. If the La/Ce ratio in the wallrock was similar to or greater than chondrites, then trends generated by wallrock-melt reaction would be consistent with the observed trends. However, in that case the simplicity of the model is lost and a two stage model would be necessary to explain the La/Ce ratio and the

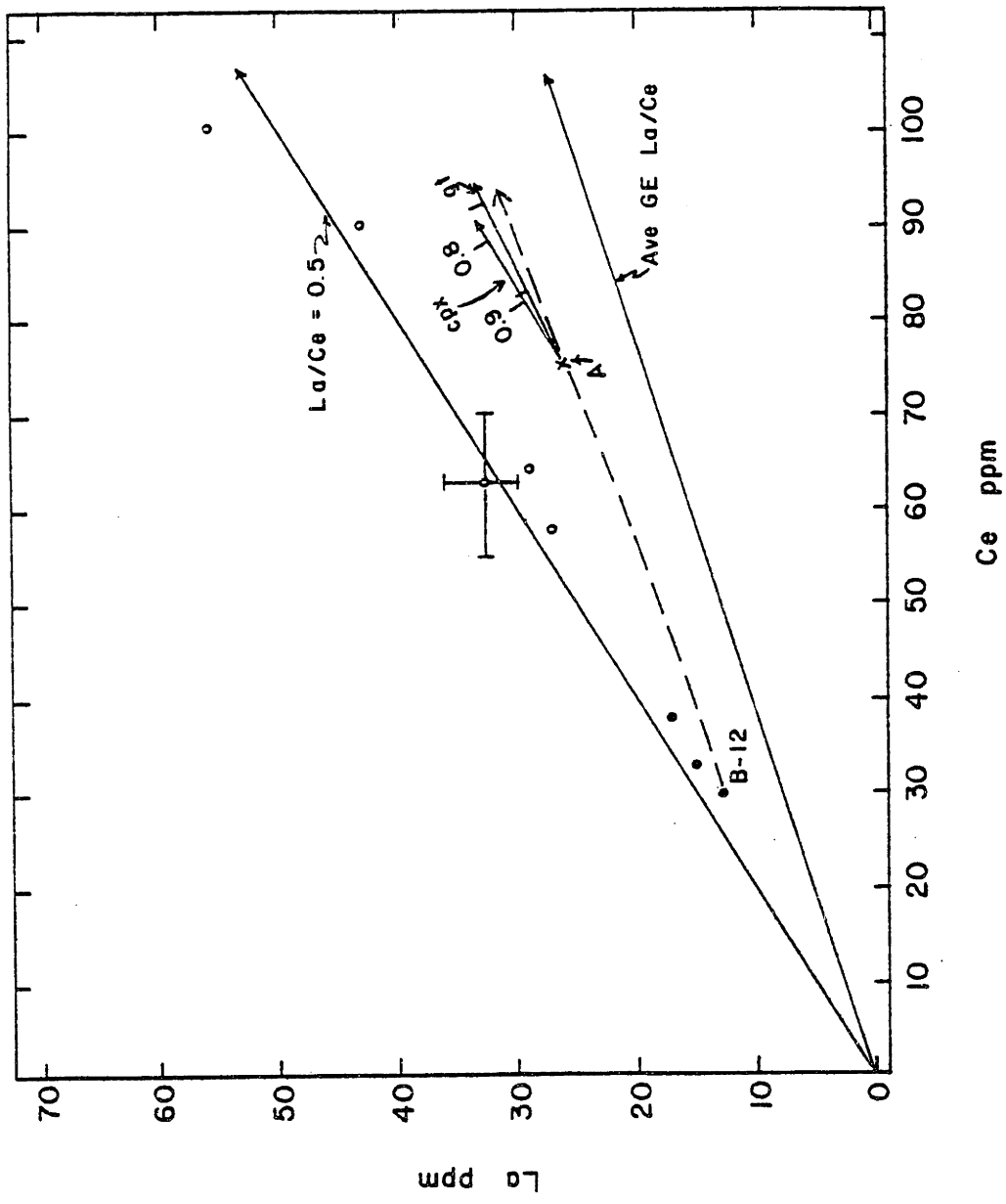
La/Ce = 0.5
Ave GE La/Ce
1.0
0.8
0.6
cpx
A
B-12
La ppm
Ce ppm
0
10
20
30
40
50
60
70
80
90
100

Figure 3-57. La versus Ce plot for Nunivak tholeiites (●) and basanites (○) from Table 3-14. Dashed vector indicates the trend of an initially tholeiitic melt which reacts with wallrock with a La/Ce ratio similar to the GE inclusions. Solid vectors indicate the effect of clinopyroxene and garnet fractionation from liquid A; tick marks indicate amount of fractionation (mass fraction of system).

inferred $^{143}Nd/^{144}Nd$, 0.5132, ratio of the wallrock.

In summary, we reach no firm conclusions as to the best physical model to explain the mixing relationships in the Nunivak basalts. The wallrock reaction model can explain the inverse correlation of Rb concentration and $^{87}Sr/^{86}Sr$ but it has heat budget problems, and is inconsistent with the nearly constant La/Ce ratio (0.44 to 0.55) of the basalts. Both magma mixing and contamination of the tholeiites are consistent with the available trace element and isotopic data. However, we lack sufficient $^{143}Nd/^{144}Nd$ data to determine whether this ratio as well as $^{87}Sr/^{86}Sr$ correlates with trace element ratios and abundances. Whether or not this correlation exists is crucial evidence in evaluating the physical models for mixing. For example, in wallrock reaction a positive correlation between $^{143}Nd/^{144}Nd$ and incompatible trace element abundances should exist, but in the contamination by altered oceanic crust model, no such correlation should exist. In order to satisfactorily evaluate the mixing relationships at Nunivak, both additional trace element data, and $^{143}Nd/^{144}Nd$ ratios should be determined on a well constrained sample suite, preferably the suite collected by Hoare et al. (1968), and studied by Mark (1971).

(D) Petrogenesis of GE Nodules

(1) Relationship to normal MORBs

Three important geochemical features of the GE nodules are: (1) their low $^{87}Sr/^{86}Sr$ ratios relative to other Recent terrestrial samples (Figure 3-58), (2) their high $^{143}Nd/^{144}Nd$ ratios relative to other young terrestrial samples (Figure 3-58), and (3) their low La/Yb ratios relative to chondrites (Figure 3-4). Many orogenic or alpine lherzolites have similar REE patterns (e.g., Loubet et al., 1975; Frey and Suen, ms) and separated clinopyroxenes also have low $^{87}Sr/^{86}Sr$ and high $^{143}Nd/^{144}Nd$ ratios (Richard and Allegre, 1980; Polve and Allegre, 1980; Menzies and Murthy, 1978). Some lherzolite inclusions in alkali basalts from widely scattered continental diatremes such as Dreiser Weiher (Stosch and Seck, 1980), Kapfenstein (Kurat et al., 1980; Jagoutz et al., 1979), Kilbourne Hole (Jagoutz et al., 1979) and Green Knobs (Chapter 4) also have REE patterns with La/Yb ratios less than chondrites. The Dreiser Weiher locality is remarkably similar to the Nunivak locality because both metasomatized inclusions with La/Yb ratios greater than chondrites (Group Ia of Stosch and Seck, 1980) and anhydrous peridotites (Group Ib of Stosch and Seck, 1980) with La/Yb ratios less than chondrites occur at both localities. Only limited isotopic data for these inclusions exist, but clinopyroxenes from the Dreiser Weiher and Kilbourne Hole inclusions have $^{87}Sr/^{86}Sr$ and $^{143}Nd/^{144}Nd$ ratios (Stosch et al., 1980; Jagoutz et al., 1980) similar to the GE nodules (Figure 3-58).

Normal MORBs share with the GE peridotites relatively low $^{87}Sr/^{86}Sr$

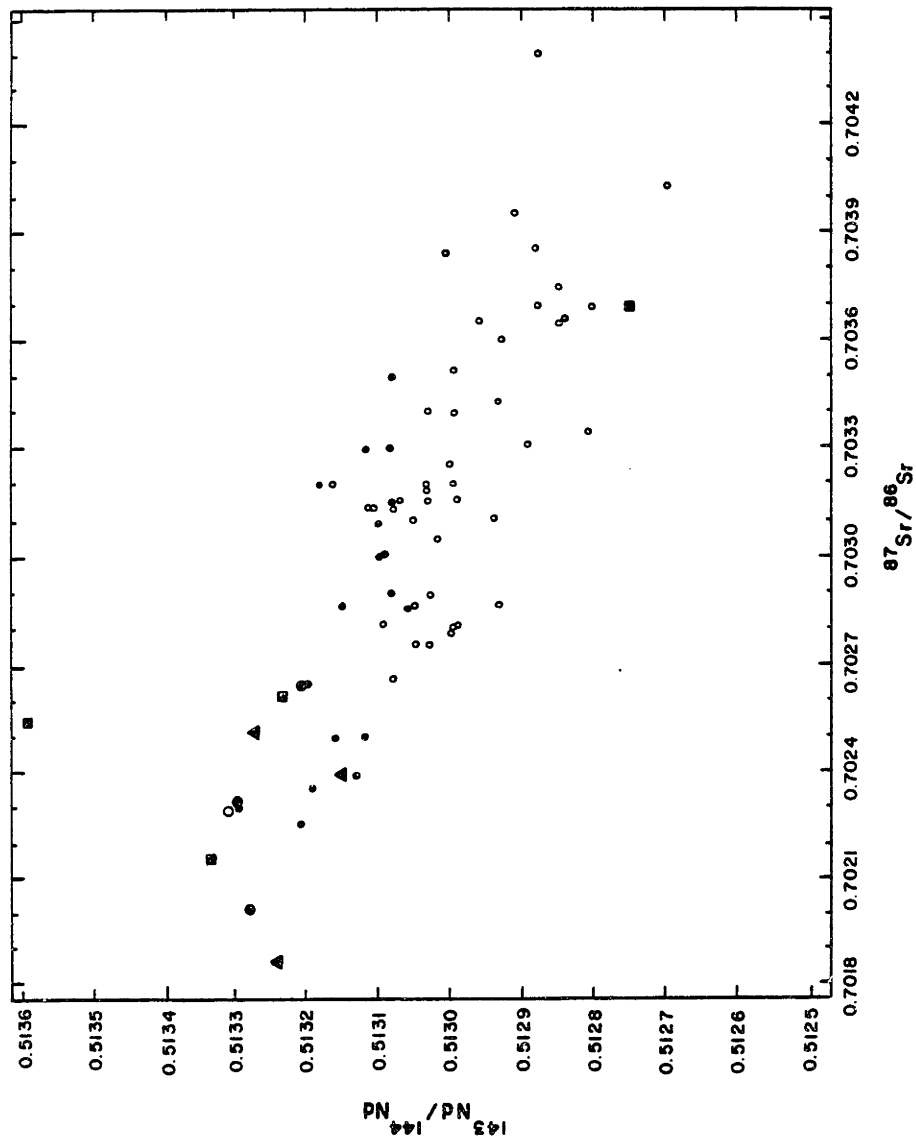
0.5136
0.5135
0.5134
0.5133
0.5132
0.5131
0.5130
0.5129
0.5128
0.5127
0.5126
0.5125
$^{143}Nd/^{144}Nd$
0.7018
0.7021
0.7024
0.7027
0.7030
0.7033
0.7036
0.7039
0.7042
$^{87}Sr/^{86}Sr$

Figure 3-58. $^{87}Sr/^{86}Sr$ and $^{143}Nd/^{144}Nd$ ratios of clinopyroxenes from the GE nodules (●) compared to these ratios in clinopyroxenes from primitive Kilbourne Hole nodule KH1 (○) of Jagoutz et al. (1980), clinopyroxenes from Group Ib nodules (▲) from Dreiser Weiher of Stosch et al. (1980), orogenic lherzolites (■) of Richard and Allegre (1980), MORBs (●) of DePaolo and Wasserburg (1976a, b), O'Nions et al. (1977), Richard et al. (1976), Carlson et al. (1978), and oceanic islands (⊙) (Hawaii, Iceland, Galapagos, St. Pauls Rocks) of DePaolo and Wasserburg (1976a, b), Zindler et al. (1979), O'Nions et al. (1977), White and Hofmann (1978). All data plotted relative to BCR-1 = 0.51264.

and relatively high $^{143}Nd/^{144}Nd$ ratios (Figure 3-58). These basalts also have La/Yb ratios less than chondrites, and their chondrite-normalized REE patterns are qualitatively similar to the REE patterns of clinopyroxenes separated from the GE inclusions (Figure 3-59). No other common basaltic magma type has all three of these geochemical features; consequently, we conclude that the GE nodules are petrogenetically related to normal MORBs.

The high clinopyroxene content (Figure 3-3) of the GE inclusions indicates that these inclusions may be potential source rocks for MORBs. A 20% melt of a lherzolite source with initial REE concentrations equal to that of the average GE nodules is similar in relative REE abundances to normal MORBs (Figure 3-60). This model liquid was calculated by mass balance assuming a harzbugite residue (70% olivine, 30% orthopyroxene) and using the average Dreiser Weiher partition coefficients of Stosch (1982) for olivine/clinopyroxene and orthopyroxene/clinopyroxene, and Set 1 of Frey et al. (1978) for clinopyroxene/liquid. This model is consistent with recent models for the petrogenesis of MORBs (Green et al., 1979; Stolper, 1981) based on experimental evidence in which the parental magma for MORBs equilibrated with a harzburgite residue. The similarity of the REE element data for the GE nodules to the REE abundances inferred for the source material of MORBs is further illustrated in Figure 3-61. Average Sr, and REE abundances for the GE nodules, when normalized to the source models for MORBs of White and Schilling (1978) and Wood (1979) plot near 1. However, note that Ba, Rb, and especially K concentrations are significantly lower in the GE

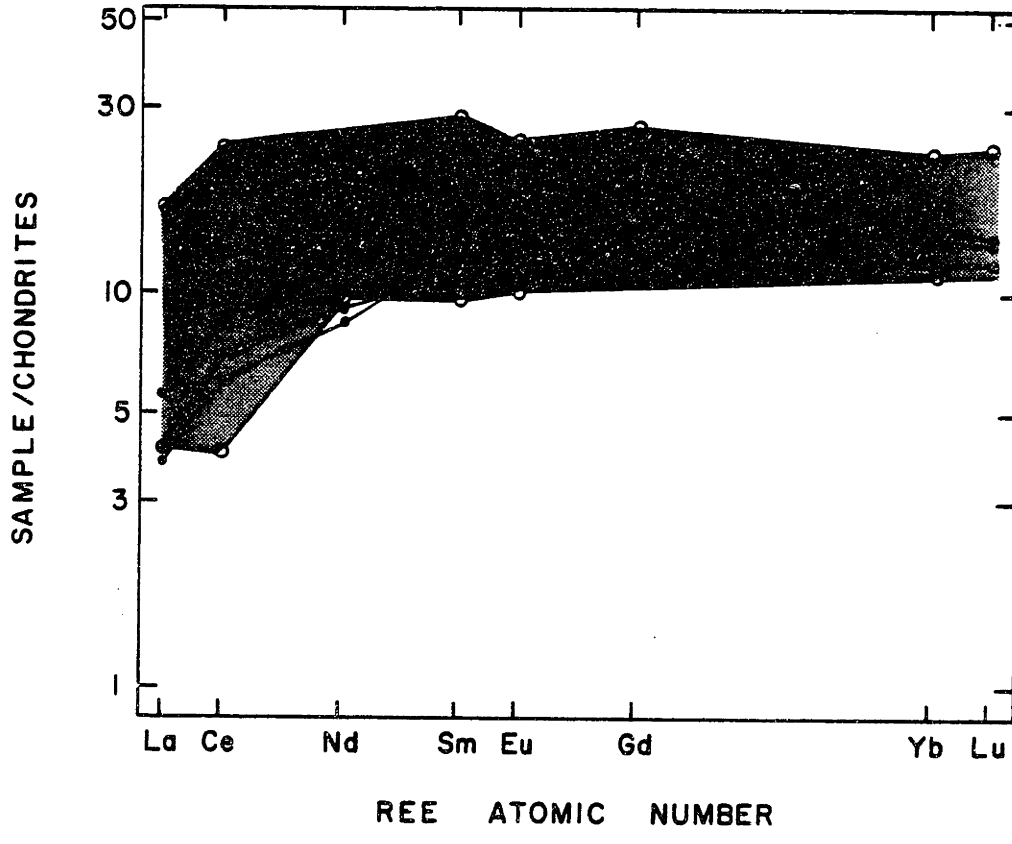
50
30
10
5
3
1
SAMPLE/CHONDRITES
La
Ce
Nd
Sm
Eu
Gd
Yb
Lu
REE ATOMIC NUMBER

Figure 3-59. Chondrite-normalized REE patterns of GE clinopyroxenes (●) compared to typical MORBs (shaded region) with La/Yb ratios less than chondrites (Frey et al., 1974; Sun et al., 1979).

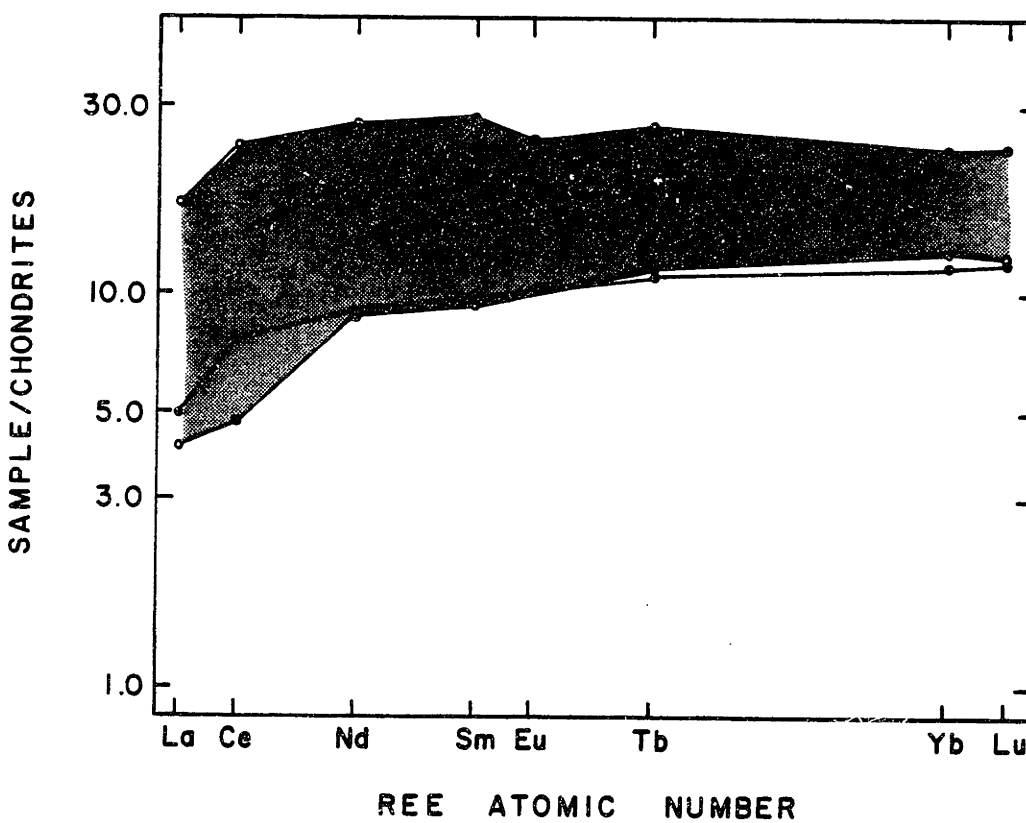
30.0
10.0
5.0
3.0
1.0
SAMPLE/CHONDRITES
La
Ce
Nd
Sm
Eu
Tb
Yb
Lu
REE ATOMIC NUMBER

Figure 3-60. 20% melt ( ● ) of average GE nodule compared to the range (shaded region) of normal MORBs from Figure 3-B. See text for discussion.

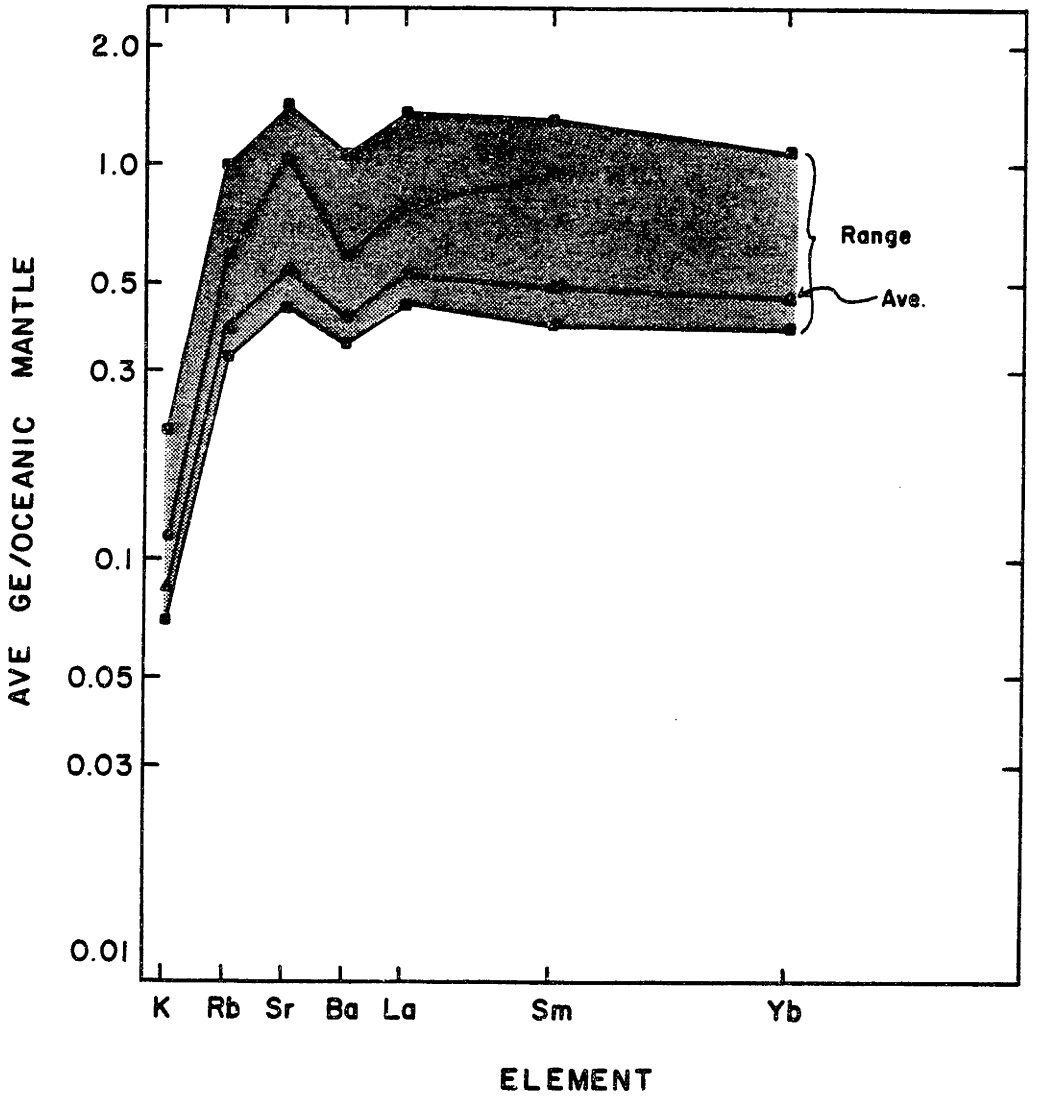
2.0
1.0
0.5
0.3
0.1
0.05
0.03
0.01
AVE GE/OCEANIC MANTLE
Range
Ave.
K
Rb
Sr
Ba
La
Sm
Yb
ELEMENT

Figure 3-61. Average GE nodule compared to two models for the source material for normal MORBs. The limits for the model of White and Schilling (1978) are indicated by the shaded region with their preferred values indicated by the line (▲) within the shaded region. The model of Wood (1979) is indicated by the filled circles (●).

inclusions than in the inferred source for normal MORBS.

Murthy and coworkers (Griffin and Murthy, 1969; Basu and Murthy, 1977; Menzies and Murthy, 1980b) have repeatedly pointed out the difficulty in generating basaltic liquids from anhydrous lherzolites with low alkali and alkaline earth element contents. Even normal MORBs, which have low K contents, typically contain more than 500 ppm K (Figure 3-62). Very small amounts of melting, less than 3%, are required to yield a melt with 500 ppm K if the source had an initial K content of 12.8 ppm, the average K concentration in the GE inclusions. In recent models (Green et al., 1979; Stolper, 1981) for the petrogenesis of MORBs, it has been proposed that basalts erupted on the surface have undergone substantial amounts of olivine fractionation. Therefore, to some extent, the problem of the low K content in the model melts can be circumvented by arguing that the K content in MORBs has been increased by crystal fractionation. However, the real key to the alkali problem is the K/La ratio as illustrated in Figure 3-62. Both these elements are nearly perfectly incompatible during the MORB melting process because olivine, orthopyroxene, and clinopyroxene have partition coefficients much less than 0.1 (Hart and Brooks, 1974; Frey et al., 1978; Zindler, 1980; Stosch, 1982) for these elements. The most reasonable partial melting model (Figure 3-62) indicates that K and La will not be fractionated during melting, and that K/La ratios of melts derived from source rocks geochemically similar to the GE nodules will be significantly lower than the K/La ratios of MORBs. Similar problems (Figure 3-62) exist for the two primitive inclusions from Dreiser Weiher and

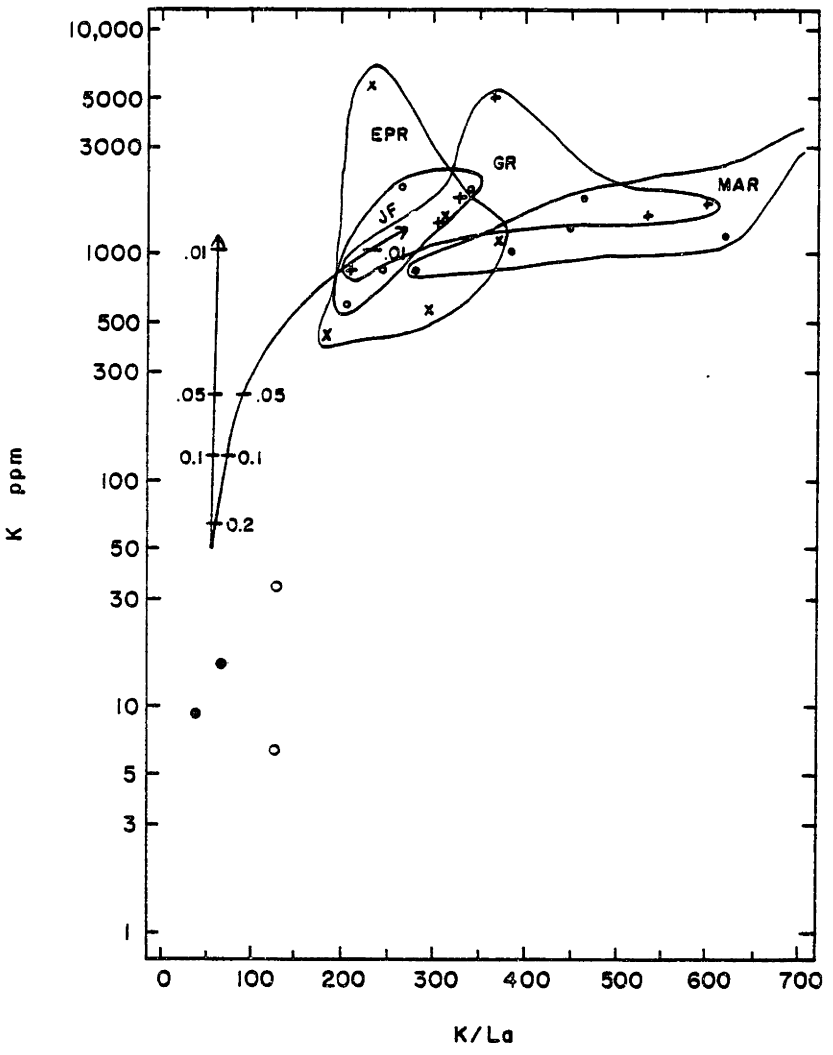
10,000
5000
3000
1000
500
300
100
50
30
10
5
3
1
K ppm
0
100
200
300
400
500
600
700
K/La
EPR
GR
MAR
JF
.01
.01
.05
.05
0.1
0.1
0.2

Figure 3-62. K concentrations and K/La ratios of GE nodules (●) and two primitive nodules (○) from Jagoutz et al. (1979) which have $^{87}Sr/^{86}Sr$ and $^{143}Nd/^{144}Nd$ ratios in the range of MORBs (Jagoutz et al., 1980). MORB data are all isotopic dilution data from Kay et al. (1970). MORB samples are from various geographic regions: Gorda Ridge (+), East Pacific Rise (×), Mid-Atlantic Ridge (●), and Juan de Fuca Ridge (○). The curves show the trajectories of melts derived by various amounts of melting from a source with K content and K/La ratio the same as that of the average GE nodule. Numbers along the curves indicate percent melting. The curve which shows no fractionation of La from K is the preferred model for which partition coefficients (Hart and Brooks, 1974; Zindler, 1980; Set 1 of Frey et al., 1978) appropriate for MORB genesis were used. The model in which K/La ratio of the melt is greater than the K/La ratio of the source, partition coefficients were deliberately chosen to maximize the fractionation of K from La. However, the La partition coefficients (same as above for K, but Set 7 of Frey et al., 1978, for La) used are probably too large to be applicable to the petrogenesis of MORBs.

Kilbourne Hole (Jagoutz et al., 1979) which have REE patterns similar to the GE nodules, and $^{87}Sr/^{86}Sr$ and $^{143}Nd/^{144}Nd$ ratios within the range of normal MORBs (Figure 3-62 ; Stosch et al., 1980; Jagoutz et al., 1980).

Because most MORBs appear to be fractionated (e.g. Stolper, 1981), it is possible that the K and La are fractionated following the melting event. To satisfy the data (Figure 3-62), some phase preferentially incorporating La relative to K must fractionate. Phases which may have fractionated are olivine ± clinopyroxene ± plagioclase ± chromite (e.g., Green et al., 1979 and references cited therein). Neither olivine nor clinopyroxene are capable of fractionating La from K as described above. The partition coefficients for spinel are poorly known, but it is unlikely that this phase has a large partition coefficient for La (Kay and Gast, 1973; Stosch, 1982). Plagioclase is the only fractionating phase which has $K_D^K$ , and $K_D^{La}$ greater than 0.1. The data obtained to date indicate that $K_D^K \cong 0.2 \geq K_D^{La}$ (Hart and Brooks, 1974; Drake and Weill, 1975; Shih, 1972; Dickey et al., 1977; McKay and Weill, 1976). We conclude that plagioclase is probably not capable of fractionating K from La in the desired direction.

The low K/La ratio in the GE nodules is indeed a formidable objection to directly relating the GE nodules as source rocks for MORBs. Nevertheless, the isotopic and REE abundance similarities to source models for MORBs (Figures 3-58, 3-59, 3-61) are compelling evidence that the GE nodules are indeed potential source rocks for MORBs. Thus, we infer that the behavior of K is altered by some process not accounted for in simple partial melting models. One possibility is the amphibole-

addition hypothesis of Basu and Murthy (1977). Note, however, that this amphibole-precipitating component must be geochemically distinct from the Nunivak metasomatic component which precipitated amphibole. Specifically, the Nunivak metasomatic component is characterized by high La/Yb ratios unlike MORBs. Most examples of amphibole-bearing inclusions also have high La/Yb ratios (e.g., Frey and Prinz, 1978; Stosch and Seck, 1980; Wass and Rogers, 1980) as do amphibole-bearing peroditite massifs (Frey, 1970; Bonatti et al., 1981) in the ocean basins. However, there are some examples of mantle-derived amphibole-bearing inclusions which have La/Yb ratios less than chondrites: Nunivak pyroxenites 13007, 13004 (Figure 3-26), Victoria peridotite inclusion 2642 of Frey and Green (1974) and several amphibole-bearing inclusions from Kapfenstein (Kurat et al., 1980). These inclusions provide evidence that fluids or melts can precipitate amphibole in mantle materials without causing a significant increase in the La/Yb ratio of the host material. If the precipitation of this amphibole is associated with an increase in the abundance of K, Rb, and Ba in the host rock then a similar amphibole-forming event in the source of MORB's could explain the discrepancy between K/La ratios in anhydrous lherzolites and MORBs.

(2) Model ages

Model ages corresponding to the intersection of the growth curve for clinopyroxenes from 10026, 10068, and 10070 with the growth curve of the bulk earth can be calculated from the measured $^{143}Nd/^{144}Nd$ ratios and Sm/Nd ratios. The more precise isotope dilution Sm/Nd

ratios (Table 3-9) were used for this calculation. The three clinopyroxenes have model ages ranging from $1.6 \times 10^9$ to $1.8 \times 10^9$ yr (Figure 3-63, Table 3-23). Consideration of the propagation of errors back through time assuming that Sm and Nd are known to ± 1% and that the present day $^{143}Nd/^{144}Nd$ ratio is known to ± 0.000025 indicates that these ages are <u>not</u> distinguishable (Figure 3-63, Table 3-23).

In a similar manner Rb-Sr model ages can be calculated for the three GE clinopyroxenes relative to the bulk earth. We calculate model ages ranging from $1.6 \times 10^9$ to $2.1 \times 10^9$ yr. for the three clinopyroxenes (Figure 3-64, Table 3-23). Consideration of error propagation with time assuming errors of ± 5% for Rb, ± 1% for Sr and ± 0.00005 for $^{87}Sr/^{86}Sr$ indicates that the Rb-Sr model ages are distinguishable. In spite of the low analytical precision for Rb due to low Rb concentrations, the Rb-Sr model ages for the clinopyroxenes are relatively precise because of the very low $^{87}Rb/^{86}Sr$ ratios of the clinopyroxenes (Table 3-9) and the relatively high angle of intersection between the growth curves of the clinopyroxenes and that of the Bulk earth (Figure 3-64). The Rb-Sr model ages are distinct from the Sm-Nd model ages for 2 of the 3 clinopyroxenes (Table 3-23); all the Sm-Nd model ages lie within the range defined by the Rb-Sr model ages.

In interpreting the model ages we chose to emphasize the conformity of the Sm-Nd model ages rather than the unconformity of the Rb-Sr model ages. Jagoutz et al. (1980) showed that in primitive inclusion KH1, which is similar to the GE nodules both in terms of its REE and isotopic geochemistry, the bulk rock Sm/Nd and $^{143}Nd/^{144}Nd$ ratios were

Table 3-23. Calculated[1] model ages relative to the bulk earth.

| Sample | Rb-Sr Age ($10^9$ yr) | Sm-Nd Age ($10^9$ yr) |
|---|---|---|
| 10068 clinopyroxene | 1.92 ± 0.05 | 1.6 ± 0.2 |
| 10070 clinopyroxene | 1.62 | 1.8 |
| 10026 clinopyroxene | 1.73 | 1.7 |

1. Calculated as in DePaolo & Wasserburg (1976a).

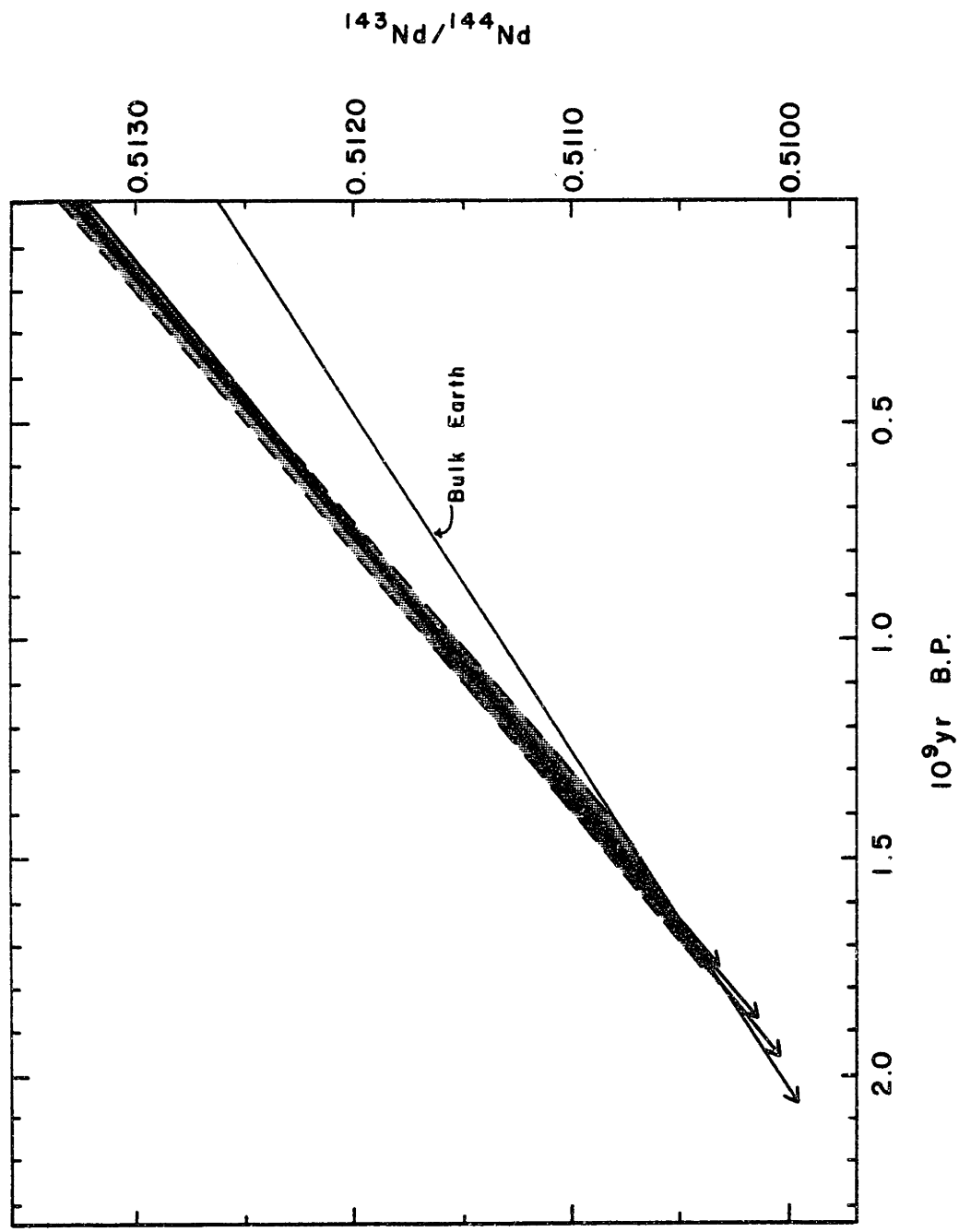
$^{143}Nd/^{144}Nd$
0.5130
0.5120
0.5110
0.5100
Bulk Earth
0.5
1.0
1.5
2.0
$10^9$yr B.P.

Figure 3.63. Nd evolution diagram for clinopyroxenes from GE nodules 10070, 10068, and 10026. Bulk earth curve calculated by assuming present day $^{143}Nd/^{144}Nd = 0.51264$ and $^{147}Sm/^{144}Nd = 0.1967$ (Jacobsen and Wasserburg, 1980). Growth curves for clinopyroxenes indicated by solid lines; shaded region is the error envelope around the growth curve for 10068 clinopyroxene.

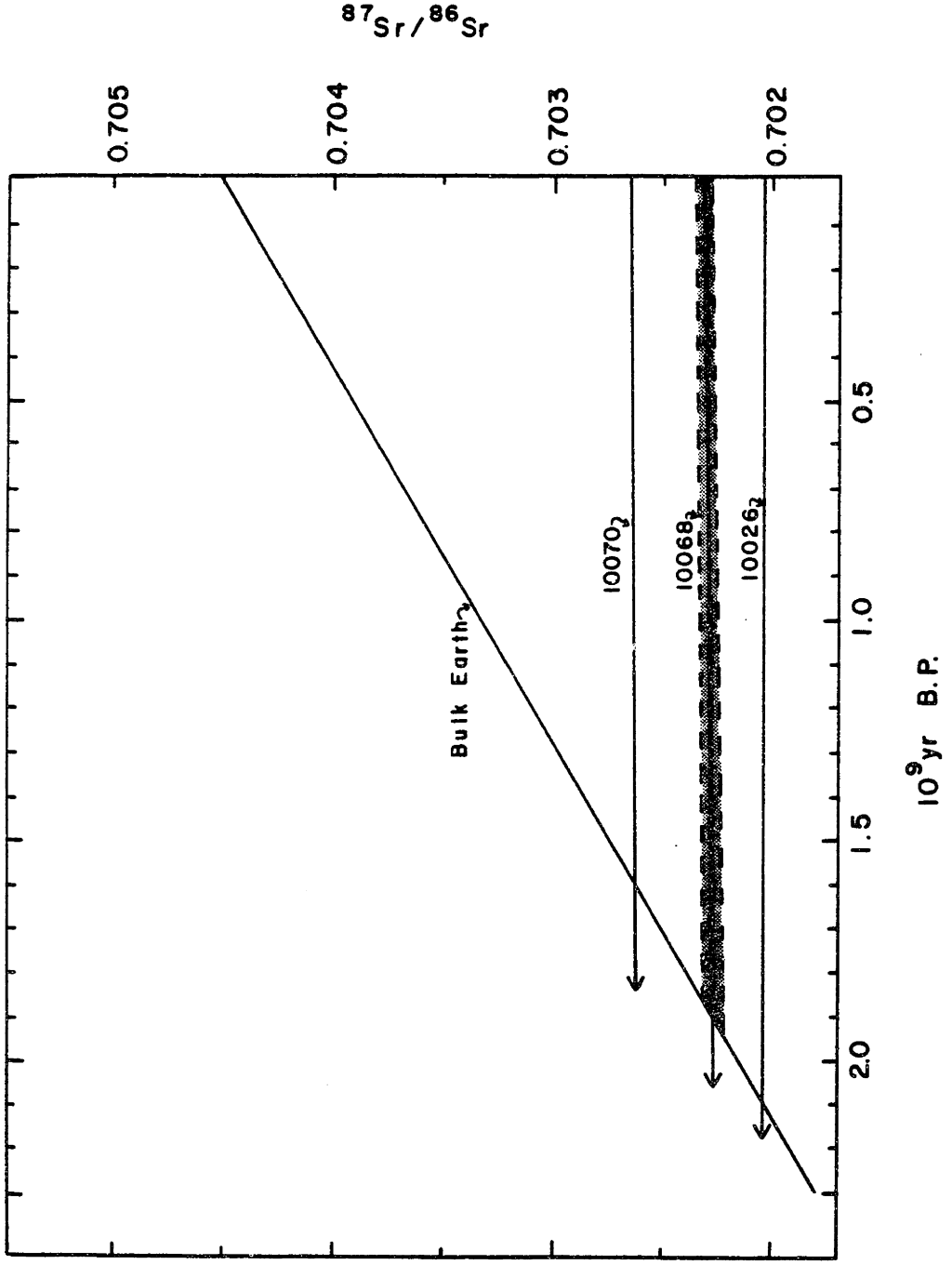
$^{87}Sr/^{86}Sr$
0.705
0.704
0.703
0.702
Bulk Earth
10070
10068
10026
0.5
1.0
1.5
2.0
$10^9$yr B.P.

Figure 3-64. Sr evolution diagram for clinopyroxenes from GE nodules 10070, 10068, and 10026. Bulk earth curve calculated by assuming present day $^{87}Sr/^{86}Sr = 0.7045$ (DePaolo and Wasserburg, 1976b) and and initial $^{87}Sr/^{86}Sr$ ratio of 0.699 at $4.6 \times 10^9$ yr. ago (Papanastassiou and Wasserburg, 1969). Growth curves for clinopyroxenes indicated by solid lines; shaded region is the error envelope around the growth curve for 10068 clinopyroxene.

indistinguishable from these ratios in the clinopyroxenes. Also, orthopyroxene and clinopyroxene were in isotopic equilibrium with respect to neodymium. In contrast, clinopyroxene was not in isotopic equilibrium with coexisting orthopyroxene with respect to strontium; and there was apparently a radiogenic grain boundary phase present. In the GE peridotites more than 74% of the bulk rock Sr, Sm, and Nd contents reside in clinopyroxene (Table 3-17, 3-18); however, only 8-25% of the bulk rock Rb is contained in the clinopyroxenes. The bulk rock $^{147}Sm/^{144}Nd$ ratios for 10068 and 10070, 0.229 and 0.210 respectively, are within error of the isotope dilution $^{147}Sm/^{144}Nd$ ratios of the clinopyroxenes given the inherent lower precision of the neutron activation data. In contrast, the $^{87}Rb/^{86}Sr$ ratios of bulk rocks 10070 and 10026 are significantly higher than these ratios in the clinopyroxenes (Table 3-9). All these data indicate that the Rb-Sr systematics of spinel-bearing peridotites are inherently more complex than the Sm-Nd systematics because Rb is fractionated from Sr. We attribute the spread in Rb-Sr model ages for the GE nodules to this inherent greater complexity.

In spite of the spread of the Rb-Sr model ages, all of the Sm-Nd model ages and two of the three Rb-Sr model ages fall in the range $1.6 \times 10^9$ to $1.9 \times 10^9$ yr. These model ages may have an age significance if (1) clinopyroxene acted as a closed system for this length of time, or (2) the parent/daughter and isotopic ratios of clinopyroxene is representative of the bulk system. Based on the data presented in the previous paragraph, proposition (2) is probably true for the Sm-Nd

system insofar as the bulk nodule is representative of the bulk system. However, proposition (2) is definitely not true for the Rb-Sr system. The Rb-Sr model ages may still have an age significance if proposition (1) is true. This proposition can be evaluated using temperatures estimated from clinopyroxene geothermometry and the diffusion coefficients for Sr in clinopyroxene of Sneeringer (1981). For the GE inclusions, Francis (1978) estimated temperatures of approximately 800°C using the two-pyroxene solvus of Lindsley and Dixon (1976). When the Ca content of clinopyroxene was corrected for Al, Ti, and Cr (after Mysen, 1976), Francis (1978) estimated temperatures for the three GE nodules of approximately 1100°C. Based on his study of natural diopsides, Sneeringer (1981) estimated a diffusion coefficient for Sr of $2 \times 10^{-14}$ $cm^2/sec$ at 1100°C. His data, extrapolated to lower temperatures, indicates a diffusion coefficient for Sr of approximately $10^{-18}$ $cm^2/sec$ at 800°C. Using the relation $x = \sqrt{Dt}$ (Hofmann and Hart, 1978), we calculate characteristic transport distances of 31 cm for $1.5 \times 10^9$ yr. at 1100°C, and 2.2 mm for $1.5 \times 10^9$ yr at 800°C. These distances are upper limits to diffusive transport in a dry mantle because clinopyroxene is surrounded by Sr-poor olivine and orthopyroxene which will inhibit equilibration (Hofmann and Hart, 1978). The implication of these calculations is that whether proposition (1) is valid or not is extremely sensitive to temperature. With characteristic transport distances of 30 cm it appears unlikely that clinopyroxene grains 1 mm in diameter (approximate upper limit to grain size in GE nodules,

Francis, 1978) behaved as closed systems. However if the lower inferred temperature is correct, then it seems possible that 1 mm clinopyroxene grains surrounded by orthopyroxene and olivine could have behaved as closed or nearly closed systems. Which temperature is appropriate is uncertain; however, we note that the lower temperature is consistent with the oceanic mid-cell geotherm of Solomon (1976) at pressures appropriate for the stability of spinel.

Returning to the Sm-Nd data, one possible explanation for the model ages is that they have age significance. Then, in a two stage model the model age is related to an increase in the Sm/Nd ratio relative to the bulk earth, if the parental peridotite had chondrite relative to REE abundances. One way to increase the Sm/Nd ratio is by extracting a melt because Nd is more incompatible than Sm in a spinel or garnet peridotite-melt system. REE concentrations in this hypothetical melt can be calculated using the REE concentrations in the GE clinopyroxenes and the partition coefficients of Frey et al. (1973). The REE contents of the hypothetical melts are shown in Figure 3-65; these model melts have chondrite-normalized REE patterns similar to many alkali basalts and continental tholeiites (e.g., Kay and Gast, 1973; Leeman, 1976).

We conclude that the Sm-Nd data can be explained by a model in which the model ages data a melting event in which the Sm/Nd ratio in the system changed from chondritic to that presently measured in the GE nodules. The GE nodules are the residuum from this melting event; the extracted melt had REE characteristics similar to many alkali

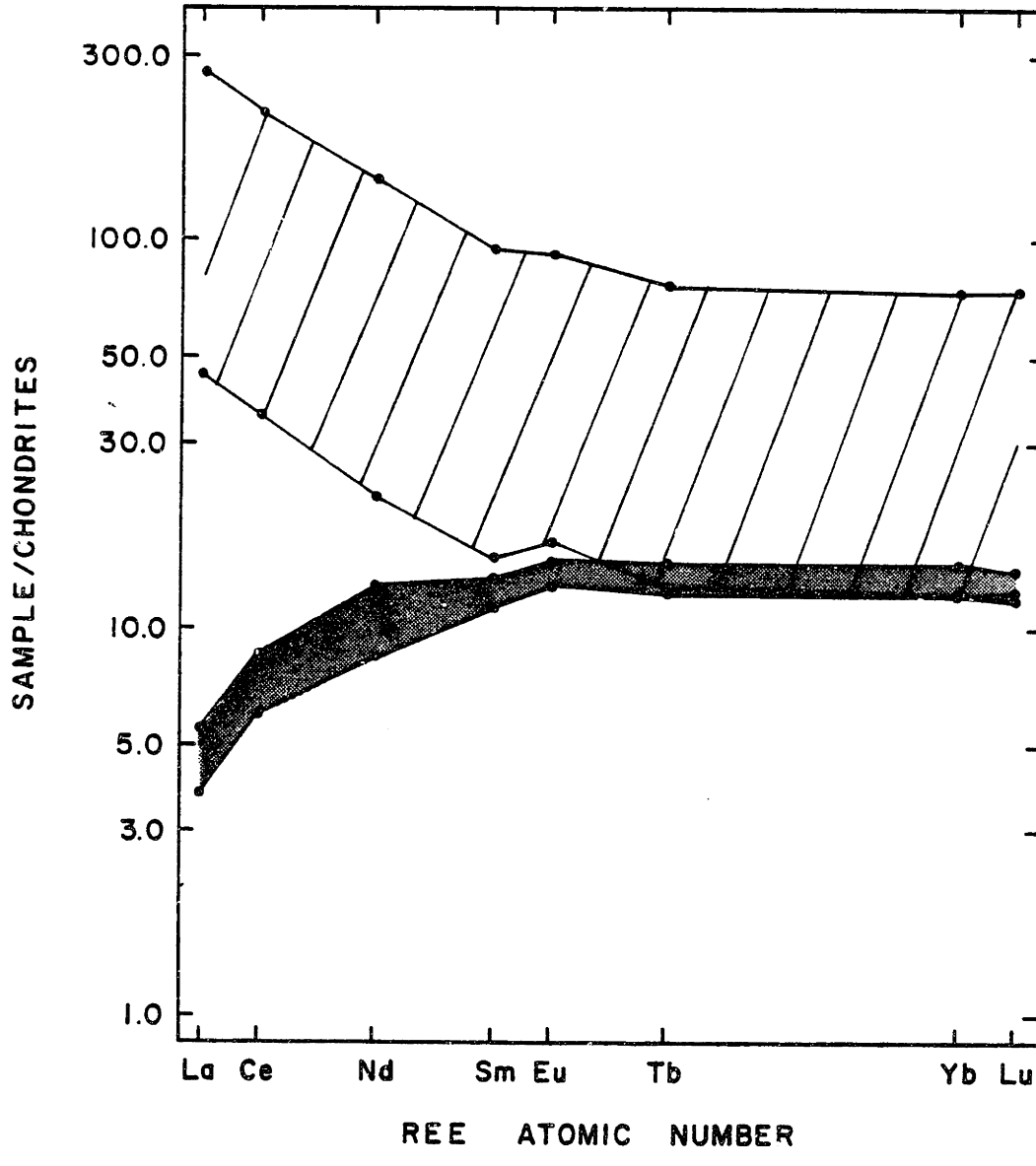
300.0
100.0
50.0
30.0
10.0
5.0
3.0
1.0
SAMPLE/CHONDRITES
La
Ce
Nd
Sm
Eu
Tb
Yb
Lu
REE ATOMIC NUMBER

Figure 3-65. Chondrite-normalized REE patterns of silicate melts (lined region) in equilibrium with GE clinopyroxenes (shaded region). Upper limit to silicate melt region calculated using partition coefficients of Set 1 (Frey et al., 1978); lower limit calculated using partition coefficients of Set 2, Frey et al. (1978).

basalts and continental tholeiites.

(E) Summary and Synthesis

In this section we present two models, or perhaps more realistically, two cartoons which illustrate two possible sequences of lithologies in the pressure range 9-18 kb (Figure 3-66) beneath Nunivak Island. These two models were designed to be consistent with the petrogenesis of the various rock types as inferred from their geochemistry and with the phase equilibria as inferred from mineral chemistry (Francis, 1976a; 1978).

The pressure-temperature conditions of equilibration of the pyroxene granulites are the best constrained because their mineralogy records the reaction of olivine with plagioclase. Francis (1976a) inferred that these inclusions equilibrated at approximately 950°C and 9 kb near the base of the crust. Both their geochemistry and their inferred igneous mineralogy (Francis, 1976a) indicates that the protoliths for these rocks were troctolite cumulates. The parental magma was an oceanic basalt, most likely a normal MORB. A two point, whole rock isochron provides somewhat equivocal evidence that the troctolites formed approximately $2 \times 10^8$ yr. ago.

A second group of inclusions which appears to be petrogenetically related to MORBs are the GE peridotites. These are four phase, anhydrous lherzolites which equilibrated in the spinel peridotite field at approximately 800°C based on the Lindsley and Dixon (1976) pyroxene solvus. If the CaO content of the diopsides is corrected

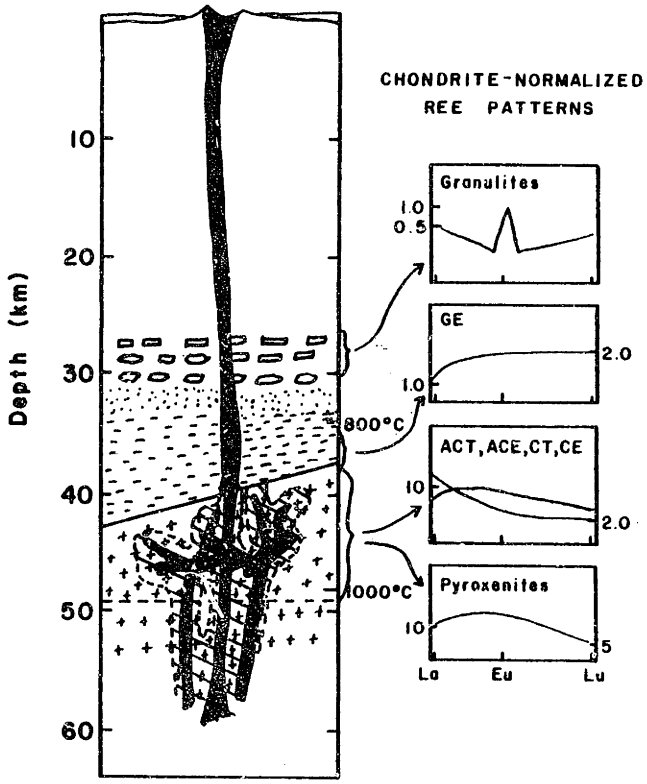


| | $^{87}Sr/^{86}Sr$ | $^{143}Nd/^{144}Nd$ |
|---|---|---|
| Granulites | 0.70242-0.70255 | 0.51305-0.51311 |
| GE | 0.70203-0.70264 | 0.51321-0.51330 |
| ACT, ACE, CT, CE | 0.70289-0.70343 | 0.51309-0.51314 |
| Pyroxenites | 0.70288-0.70297 | 0.51310 |

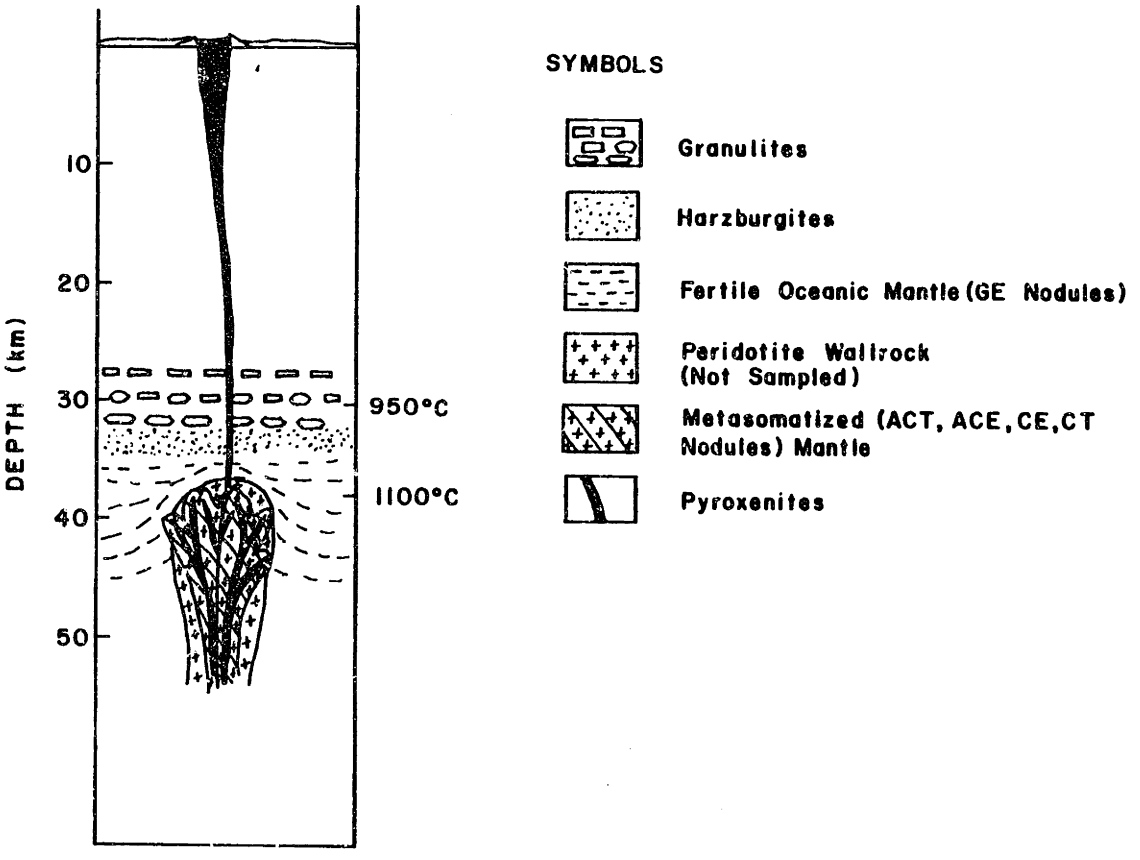
DEPTH (km)
10
20
30
40
50
950°C
1100°C
SYMBOLS
Granulites
Harzburgites
Fertile Oceanic Mantle (GE Nodules)
Peridotite Wallrock (Not Sampled)
Metasomatized (ACT, ACE, CE, CT Nodules) Mantle
Pyroxenites

Figure 3-66. A. Static or layered model for the upper mantle beneath Nunivak Island. Essential geochemical features of various rock types are also shown. Symbols defined in Figure 3-66B.

B. Dynamic or diapiric model for the upper mantle beneath Nunivak Island. Refer to Figure 3-66A for essential geochemical features of various rocktypes.

for $Al_2O_3$ content, higher temperatures, 1100°C-1150°C, are inferred (Francis, 1978). No precise pressure estimates are presently possible but the pressures at which these inclusions equilibrated are limited by the stability of aluminous spinel in the peridotite system to 6-16 kb at 800°C and 8-17 kb at 1100°C (Herzberg, 1978). These GE inclusions have La/Yb ratios less than chondrites, and $^{87}Sr/^{86}Sr$ and $^{143}Nd/^{144}Nd$ ratios in the range of normal MORBs (Figure 3-58); we propose that these inclusions are potential source material for normal MORBs. Based on Sm-Nd model ages, the GE peridotites apparently attained their present geochemical characteristics in the vicinity of $1.6 \times 10^9$ to $1.8 \times 10^9$ yr. ago.

The granulites and the GE nodules are linked by their petrogenetic relationship to normal MORBs. We propose that these inclusions are samples of an oceanic terrane present in the uppermost mantle beneath Nunivak Island. This terrane became a geochemical entity approximately $1.6 \times 10^9$ to $1.8 \times 10^9$ yr. ago and underwent a significant melting event approximately $2 \times 10^8$ yr. ago, possibly at an ocean ridge crest. The GE lherzolites did not participate in this melting event. It seems likely that this oceanic terrane is part of the Yukon-Koyukuk terrane accreted to Alaska during the Cretaceous (Churkin et al., 1980).

The CT, CE, ACE, and ACT peridotites and the amphibole pyroxenites appear to be derived from a terrane geochemically distinct from the oceanic terrane described above. The pyroxenites appear to be spatially associated with the amphibole-bearing peridotites in the

mantle because they occur together in composite nodules (Francis, 1976a) and because they are isotopically indistinguishable from many of the ACT and ACE nodules (Figures 3-12, 3-13). The pyroxenites probably formed by segregation from a silicate melt (Figure 3-37). The peridotites have high concentrations of incompatible elements attributed to metasomatism (Figures 3-5, 3-6); the agent of this metasomatism was most likely a residual melt or a H-C-O rich fluid which evolved from the pyroxenites. Calculated temperatures for the peridotites (Francis, 1978) show a significant range, from 800° to 1000°C (Lindsley and Dixon, 1976) or 900° to 1150°C with an $Al_2O_3$ correction (Francis, 1978).

Several lines of somewhat equivocal evidence indicate that the CE, CT, ACE, ACT, and amphibole pyroxenites originated from deeper levels than the inclusions from the oceanic terrane. Firstly, if the Lindsley and Dixon (1976) solvus is applicable then the CE, CT, ACE, and ACT nodules record higher temperatures than the GE nodules. Thus if the geotherm was unperturbed, then the CE, CT, ACT, and ACE nodules must be from deeper levels than the GE nodules. Secondly, Francis (1974) noted that the ACE and ACT nodules were concentrated at the more explosive eruption centers on Nunivak. If the more explosive eruptions are related to more rapid magma ascent velocities through the crust and upper mantle, then the concentration of ACE and ACT nodules at maars on Nunivak is consistent with these inclusions being derived from greater depths than the GE nodules. Finally, with one exception the isotopic ratios of the CE, CT, ACE, and ACT nodules

and the amphibole pyroxenites lie within the range of isotopic ratios of the basalts (Figures 3-12, 3-13). This relationship implies that either (1) these nodules represent source materials for the basalts, or (2) the alternative which we favor, these inclusions represent segregations from and wallrock which reacted with magmas related to the host basalts. In either case, these inclusions were most likely derived from greater depths than the GE inclusions which did not reside in the basalts long enough to show any evidence of reaction. In the following discussion we refer to the CE, CT, ACE, and ACT peridotites and the amphibole pyroxenites as part of an "oceanic island" terrane. We use this phrase which implies an oceanic environment because the $^{87}Sr/^{86}Sr$ and $^{143}Nd/^{144}Nd$ ratios of these peridotites, pyroxenites, and basalts are similar to oceanic island basalts.

The first model is shown in Fig. 55A and is a static or layered model. In this model the isotherms are unperturbed and horizontal; we have used the temperatures calculated from the Lindsley and Dixon (1976) solvus without an $Al_2O_3$ correction because (1) they are reasonably consistent with the oceanic mid-cell geotherm of Solomon (1976) and (2) they are consistent with an increase in temperature with depth. The temperatures calculated for the granulites, approximately 950°C, are anomalously high relative to the temperatures calculated for the GE nodules. This high temperature may be related to more rapid cooling relative to the GE inclusions (Hart, 1981), or to the use of the Lindsley and Dixon (1976) solvus without correcting for the $Al_2O_3$ content of the GE clinopyroxenes. In addition to the

granulites and GE inclusions, the oceanic terrane as illustrated contains harzburgites which occupy a level between the granulites and the GE lherzolites; harzburgites were not studied here, but are known to occur on Nunivak (Francis, 1978). Thus, the oceanic terrane in the layered model and for that matter in the dynamic model (Figure 3-66B) is structurally similar to some ophiolites and to the structure inferred for oceanic crust.

In the layered model (Figure 3-66A) the boundary between the overlying oceanic terrane and the oceanic island terrane is shown as thin and sharp, i.e. a fault, because there is no textural, mineralogical, or geochemical evidence for rocks transitional in character between the GE peridotites and the metasomatized peridotites (Francis, 1978; this study). In view of the large number of accreted terranes (e.g., Churkin et al., 1980) in the area, it is tempting to speculate that the boundary between the two terranes is a fossil subduction zone. However, the geometry illustrated (Figure 3-66A) is inconsistent with modern subduction zones because in the model the oceanic plate has overridden the oceanic island plate.

Within the oceanic island terrane, the metasomatized peridotites appear as hydrothermal aureoles around intrusive pyroxenites. This relationship is consistent with our conclusions derived previously. The unmetasomatized wallrock from this terrane is never observed at the surface because magmatic flow in this region was such that all wallrock was metasomatized. Thus, we invoke Heisenberg's Uncertainty Principle as formulated by Irving (1976) to explain the lack of

unmetasomatized CE and CT nodules at Nunivak. We also speculate (for both models) that as the magma crossed the boundary between the two terranes there was a significant increase in the magma ascent velocity. This speculation is consistent with the essentially pristine nature of the GE lherzolites and the granulites. Rapid transport of these inclusions to the surface and a relatively short residence time in the host basalts is a reasonable explanation of their apparent lack of contamination by the basalts.

The second model is a dynamic or diapiric model similar to the one originally proposed by Francis (1978). In this model the oceanic terrane is similar lithologically to that in the layered model. However, the isotherms are no longer horizontal; they have been perturbed by the intrusion of a diapir of oceanic island terrane from below. This diapir is in effect being autometasomatized by the intrusion of basalts derived from lower in the diapir and their partial crystallization as pyroxenites. The metasomatizing agents are envisioned as residual silicate melts or C-H-O-rich fluids derived from the pyroxenites. Eventual eruption of basalts on the surface is probably triggered by a combination of factors including gradual warming of wallrock and concentration of volatiles in the upper portion of the diapir.

The models described are clearly nonunique. It is conceivable that the models are accurate representations of the physical distributions of rock types, but the primary value of such models is that they summarize the essential geochemical information on the various

rocktypes and relate it to a reasonable physical distriubtion of lithologies.

# 4. MANTLE WITH OCEANIC AFFINITIES BENEATH THE COLORADO PLATEAU: REE EVIDENCE

## I. Introduction

The 25-30 million year old Navajo volcanic field (Figure 4-1; Roden and Smith, 1979, and references therein) of the Four Corners region of the Colorado Plateau provides a unique opportunity to determine the geochemical and petrological variations of the uppermost mantle because of the occurrence of closely spaced xenolith-bearing diatremes over a rather large area (approximately 34000 $km^2$). Both minette and serpentinized ultramafic microbreccia (SUM) contain garnet- and spinel-bearing ultramafic inclusions which are probably samples of the uppermost mantle.

Most previous studies on inclusion suites from the Navajo field focussed on mineral chemistry and petrography. McGetchin and Silver (1972) in a study of the inclusion suite from the Moses Rock SUM (Figure 4-1) found that many of the peridotite xenoliths contain volatile-bearing minerals including titanoclinohumite and antigorite. They suggested that partially hydrated spinel lherzolite may be an important constituent of the uppermost mantle beneath the Colorado Plateau. Recently, Hunter and Smith (1981) reported observations consistent with this hypothesis: they identified amphibole, chlorite, apatite, and dolomite inclusions within garnet xenocrysts from the Red Mesa and Garnet Ridge SUM diatremes (Figure 4-1). Smith and Levy (1976) and Smith (1979) studied a suite of spinel peridotites and

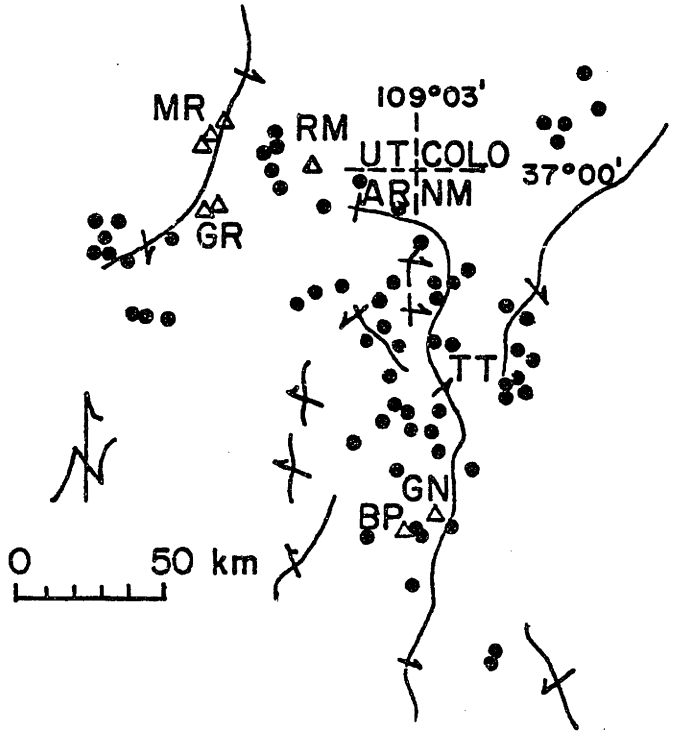
MR
RM
109°03'
UT
COLO
AR
NM
37°00'
GR
TT
GN
BP
0
50 km

Figure 4-1. Sketch map of the Navajo volcanic field. Localities mentioned in the text are indicated by letters: GN, Green Knobs, GR, Garnet Ridge, TT, The Thumb, MR, Moses Rock, BP, Buell Park, RM, Red Mesa.

pyroxenites from a southerly SUM diatreme, Green Knobs (Figure 4-1). These inclusions share an important feature in common with the Moses Rock suite, namely, the presence of the volatile-bearing phases, chlorite, titanoclinohumite, pargasite, magnesite, and antigorite. Smith (1979) concluded that the hydration of the peridotite inclusions occurred prior to the incorporation of the peridotites in the SUM and at depths of 45-60 km. Thus, the evidence from Moses Rock and Green Knobs suggests that hydrated spinel lherzolite is an important rock type in the upper mantle beneath the Colorado Plateau.

McGetchin and Silver (1972) also suggested that eclogites may be an important albeit volumetrically subordinate rock type in the lower crust and upper mantle. These eclogites are particularly enigmatic rocks whose mineralogy resembles that of some eclogites in high-pressure, low-temperature metamorphic belts rather than eclogite xenoliths in kimberlites. Eclogites appear to be absent from or rare in the more southerly Navajo diatremes (Roden, Smith, unpublished data). There is considerable controversy about the origin of the Navajo eclogites; in particular Helmstaedt and Doig (1975) and Helmstaedt and Schultze (1979) suggested that the eclogites are samples of subducted oceanic crust now present under the Colorado Plateau (recent review of the problem in Hunter and Smith, 1981).

The only inclusion suite from a minette diatreme to receive detailed attention is the garnet peridotite and pyroxenite inclusions from The Thumb (Figure 4-1) studied by Ehrenberg (1979). These inclusions are compositionally and texturally diverse, and appear to

have last equilibrated over a narrow depth range, 100-120 km or 130-150 km, depending on the method employed to estimate pressure (Ehrenberg, 1982). Recently, Ehrenberg (1982) found that lherzolites relatively rich in CaO and $Al_2O_3$ (high Ca-Al lherzolites) have La/Yb ratios slightly greater than chondrites. Lherzolites more depleted in basaltic components (low Ca-Al lherzolites) have significantly higher La/Yb ratios than the high Ca-Al lherzolites.

This paper presents REE abundances for eight spinel peridotite inclusions from the Green Knobs diatreme. These same inclusions were studied by Smith and Levy (1976), Smith (1979), and Smith and Zientek (1980). Our major objectives were to understand the petrogenesis of the peridotites and eclogites, and to infer the geochemical nature of the upper mantle as represented by these inclusions. REE abundances when normalized to chondritic REE abundances have proven to be particularly useful in understanding the petrogenesis of ultramafic rocks because of the systematic way these elements behave during igneous processes. For example, primitive mantle is expected to have relative REE abundances similar to chondrites (e.g., Ringwood, 1979) whereas peridotites residual from small amounts of partial melting are expected to be relatively depleted in the light REE, i.e., to have La/Sm ratios less than chondrites. Indeed, lherzolites from alpine peridotites and some oceanic fracture zones, and some inclusions in basalts are characterized by La/Sm ratios less than chondrites with Yb abundances greater than or equal to chondrites. Some uncommon lherzolite inclusions have nearly chondritic REE abundances; these

inclusions may be samples of primitive mantle.

Many peridotites have more complex chondrite-normalized REE patterns than the examples cited above. For example, harzburgites from ophiolites, some inclusion suites, and some oceanic fracture zones appear to be residual from large degrees of melting and are depleted in all REE relative to chondrites but they commonly have La/Sm ratios greater than chondrites. Also, metasomatized peridotites with high La/Yb ratios relative to chondrites and commonly containing amphibole or phlogopite are common in many inclusion suites and are found as massifs at two localities in the ocean basins, St. Paul's Rocks (Frey, 1970) and Zabargad Island, Red Sea (Bonatti et al., 1981). In general, these peridotites cannot be explained by simple two stage models if the peridotite initially had chondritic relative REE abundances. A recent review of the application of REE to the problem of the petrogenesis of ultramafic rocks was given by Frey (in press).

Our third objective was to compare the REE geochemistry of the hydrated peridotites of the Green Knobs suite to metasomatized inclusions (e.g., Boettcher and O'Neill, 1980) from alkali basalts. The latter inclusions commonly contain amphibole and/or phlogopite in constrast to the amphibole + chlorite + antigorite assemblage of the Green Knobs suite. A probable implication of the differing phase equilibria is that the Green Knobs assemblage equilibrated at relatively lower temperatures (Smith, 1979; see also recent discussion in Jenkins, 1981). By comparing the hydrated Green Knobs suite to metasomatized suites we hoped to learn whether the variation in intensive parameters

between the Green Knobs and alkali basalt inclusion suites was reflected in the REE geochemistry.

## II. Sample Description

Eight spinel peridotites from Green Knobs were chosen to be representative of the variation in mineral chemistry and texture present in the suite. The peridotite samples are listed in Table 4-1, referenced to the classification systems of Smith and Levy (1976) and Smith (1979). Briefly, Smith and Levy (1976) divided the inclusions into two major groups: Group I with fabrics which do not display strong deformation and Group II with fabrics which display strong deformation. These groups were further subdivided on the basis of mode, mineralogy, and texture. Later, Smith (1979) divided the assemblages with primary hydrous phrases into the following groups: Group A: assemblages with some aluminous spinel preserved; Group B: assemblages with amphibole and chlorite and without spinel; and Group C: rocks with abundant antigorite. It is important to note that even the peridotites labelled as anhydrous in Table 4-1 contain secondary veinlets of serpentine along grain boundaries and cutting olivine. Details on the petrography and mineral chemistry of these inclusions are contained in Smith and Levy (1976) and Smith (1979).

Only one eclogite has been reported (O'Hara and Mercy, 1966) from the southern Navajo diatremes including Green Knobs, thus the two eclogites are from one of the northernNavajo SUM diatremes, Garnet Ridge (Figure 4-1). These eclogites are described in detail by Smith and Zientek (1979). Sample N371 is a lineated rock containing pyroxene

Table 4-1. Peridotite sample description.

| | Classification | | |
|---|---|---|---|
| | Smith & Levy (1976) | Smith (1979) | Description |
| N16 | IC | Anhydrous | clinopyroxene-rich lherzolite; antigorite veins cut olivine |
| N61 | IC | Anhydrous | Lherzolite with abundant shear zones composed of very fine (<0.01 mm diam.) silicates. Only minor secondary antigorite |
| N17 | IB | A | Harzburgite (?) Abundant Amphibole and chlorite |
| N23 | IA | B | Lherzolite with abudant chlorite, antigorite amphibole, titanoclino-humite & magnesite |
| N71 | IIA | B | Lherzolite, extensively sheared; chlorite & amphibole show strain features along with anhydrous silicates |
| N51 | IA | C | Harzburgite cut by numerous, subparallel cracks abundant primary antigorite, chlorite, common titanoclinohumite |
| N147 | IIA | B (?) | Sheared pharzburgite, sheared lines of hydrous phases (chlorite, antigorite) in matrix of sheared anhydrous silicates |
| N138 | IIC | - | Harzburgite mylonite. |

(70%), garnet (26%), altered lawsonite (1.5%), rutile (3%), and pyrite (trace). N350 is a poorly layered rock with pyroxene (80%), garnet (13%), lawsonite (2.5%), phengite (1.5%), rutile (2%), and sulphides (0.5%). Major element data (Table 4-2) show that N371 is broadly basaltic in composition except for its $Na_2O/K_2O$ ratio, its very low $K_2O$ content, and its somewhat high $Na_2O$ content. N350 differs significantly from most basalts, primarily in its extremely high $Na_2O$ content (Table 4-2).

## III. Analytical Methods

Rock powders were produced by hand crushing on a steel plate, followed by grinding in a tungsten carbide shatterbox. Mineral separates were obtained by handpicking a coarse 16-40 mesh size after crushing in a steel percusion mortar. This rough separate was crushed in a steel percussion mortar and a final separate obtained by hand-picking the 40-60 mesh size. The final separates were essentially 100% pure with the following qualification: the mineral separate from N23 is a composite separate consisting predominantly of chlorite and tremolite with minor diopside. The N61 clinopyroxene separate was leached for 10 minutes in 2.5 N HCl at 50°C and then in 5% HF at 50°C for 20 minutes; whereas the composite separate from N23 was leached in 2.5 N HCl only. All reagents used in leaching were doubly distilled.

Major elements (Table 4-2) were determined by G.K. Hoops at the University of Texas using standard wet chemical techniques. The REE abundances were determined using a radiochemical neutron activation

Table 4-2. Major element analyses.

| rock type | N16[1] lherz | N61[1] lherz | N17[1] harz | N23[2] lherz | N71[2] lherz |
|---|---|---|---|---|---|
| $SiO_2$ | 42.31 | 45.34 | 45.40 | 44.05 | 43.05 |
| $Al_2O_3$ | 1.94 | 2.34 | 1.97 | 2.91 | 3.40 |
| $Fe_2O_3$ | 1.90 | 2.67 | 1.04 | 1.36 | 1.70 |
| FeO | 7.17 | 5.37 | 6.12 | 6.35 | 5.77 |
| CaO | 3.02 | 2.24 | 1.68 | 3.12 | 2.42 |
| MgO | 39.11 | 39.66 | 40.47 | 35.98 | 37.84 |
| $Na_2O$ | 0.20 | 0.36 | 0.18 | 0.49 | 0.44 |
| $K_2O$ | 0.01 | 0.01 | 0.01 | 0.05 | 0.03 |
| $H_2O+$ | 1.63 | 0.89 | 1.17 | 3.50 | 4.17 |
| $H_2O-$ | 0.13 | 0.09 | 0.09 | 0.10 | 0.13 |
| $CO_2$ | 0.17 | 0.07 | 0.19 | 0.56 | 0.23 |
| $TiO_2$ | 0.11 | 0.11 | 0.02 | 0.11 | 0.06 |
| $P_2O_5$ | - | - | - | - | - |
| MnO | 0.12 | 0.12 | 0.08 | 0.10 | 0.10 |
| Total | 97.89 | 99.19 | 98.48 | 98.68 | 99.34 |

1. From Smith and Levy (1976)

2. From Smith (1979)

Table 4-2. Continued.

| rock type | N51[2] harz | N147[2] harz | N138 harz | N350[3] eclog | N371[3] eclog |
|---|---|---|---|---|---|
| $SiO_2$ | 40.63 | 40.88 | 34.27 | 52.16 | 48.66 |
| $Al_2O_3$ | 1.13 | 0.59 | 2.08 | 16.92 | 15.13 |
| $Fe_2O_3$ | 2.01 | 2.09 | 3.60 | 3.54 | 3.37 |
| FeO | 6.28 | 4.61 | 5.79 | 5.24 | 9.58 |
| CaO | 0.61 | 0.33 | 0.03 | 6.64 | 8.57 |
| MgO | 43.77 | 45.60 | 41.93 | 4.89 | 7.50 |
| $Na_2O$ | 0.00 | 0.03 | 0.02 | 8.00 | 4.74 |
| $K_2O$ | 0.00 | 0.00 | 0.01 | 0.35 | 0.01 |
| $H_2O+$ | 4.10 | 4.14 | 5.78 | 0.55 | 0.22 |
| $H_2O-$ | 0.16 | 0.30 | 0.32 | 0.13 | 0.16 |
| $CO_2$ | 0.48 | 0.16 | 1.32 | 0.00 | 0.00 |
| $TiO_2$ | 0.04 | 0.01 | 0.13 | 0.93 | 1.29 |
| $P_2O_5$ | - | - | - | 0.07 | 0.11 |
| MnO | 0.12 | 0.09 | 0.11 | 0.16 | 0.22 |
| Total | 99.33 | 98.24 | 95.39 | 99.58 | 99.56 |

3. From Smith and Zientek (1979)

technique described in Hickey and Frey (1982). U.S. Geological Survey standard rock BCR-1 was used as the primary standard; thus, the REE abundances are reported relative to the values for BCR-1 in Table 4-3. There are no significant differences between the average of 5 instrumental neutron activation analyses in the MIT lab of mid-ocean ridge basalt standard A II 92-29-1 and 5 radiochemical neutron activation analyses of the same standard performed during the course of this and a companion study (Table 4-3), even though the instrumental analyses are reported relative to a synthetic standard. The absolute REE abundances for A II 92-29-1 in Table 4-3 compare well with published values for this rock (Staudigel, 1980). Precision for the lherzolites analyzed here can be estimated from the precision for 4 replicate radiochemical analyses of Nunivak Island peridotite 10070 (Table 4-3). At the 95% confidence level, the data indicate precisions of 10-20% for La, Ce, Nd, and Tb, and less than 10% for Sm, Eu, Yb, and Lu. For rocks with very low REE concentrations such as the harzburgites, precision is considerably worse. Based on duplicate analyses of U.S. Geological Survey standard PCC-1 (Table 4-3) precision at these low concentration levels is on the order of 50% for La, Sm, and Eu, and 20% for Yb and Lu.

## IV. Results

The essential features of the data are illustrated in Figures 4-2, 4-3, and 4-4. For the peridotites there is a correlation between heavy REE (HREE) abundances as represented by Yb and bulk rock CaO, while the light REE (LREE) as represented by La show no correlation with bulk rock

Table 4-3. Trace element abundances (ppm).

| | N16 wr | N61 wr | N61 cpx | N17 wr | N23 wr |
|---|---|---|---|---|---|
| La | 0.15 | 0.22 | 0.75 | 0.21 | 0.29 |
| Ce | - | 0.79 | 3.1 | 0.44 | 0.52 |
| Nd | - | - | 4.2 | - | - |
| Sm | 0.15 | 0.22 | 1.61 | 0.011 | 0.12 |
| Eu | 0.063 | 0.090 | 0.65 | 0.0022 | 0.054 |
| Tb | 0.058 | 0.039 | 0.33 | 0.007 | 0.046 |
| Yb | 0.40 | 0.20 | 1.29 | 0.11 | 0.27 |
| Lu | 0.062 | 0.033 | 0.19 | 0.022 | 0.042 |

| | N23 chl/amp | N71 wr | N51 wr | N147 wr | N138 wr |
|---|---|---|---|---|---|
| La | 0.13 | 0.11 | 0.22 | 0.26 | 0.11 |
| Ce | - | - | - | - | - |
| Nd | - | - | - | - | - |
| Sm | 0.13 | 0.079 | 0.046 | 0.015 | 0.003 |
| Eu | 0.067 | 0.039 | 0.017 | 0.008 | 0.007 |
| Tb | 0.046 | 0.041 | 0.009 | 0.008 | - |
| Yb | 0.27 | 0.31 | 0.041 | 0.026 | 0.014 |
| Lu | 0.042 | 0.051 | 0.011 | 0.0059 | 0.004 |

---

wr = whole rock; cpx - clinopyroxene separate; chl/amp = composite chlorite-ampmibole + minor clinopyroxene separate

Table 4-3. Continued.

| | N350[1] wr | N371 wr | A II 92-[2] 29-1 | A II 92-[3] 29-1 | 10070[4] |
|---|---|---|---|---|---|
| La | 4.48 | 2.05 | 4.00 ±0.30 | 3.97 ±0.34 | 0.27 ±0.05 |
| Ce | 10.5 | 5.9 | 13.1 ±0.8 | 13.7 ±1.0 | 0.99 ±0.18 |
| Nd | 5.3 | 5.4 | 12.1 ±1.2 | 11.6 ±0.6 | 0.99 ±0.14 |
| Sm | 1.51 | 2.02 | 4.20 ±0.24 | 4.05 ±0.24 | 0.345 ±0.024 |
| Eu | 0.51 | 0.72 | 1.47 ±0.12 | 1.51 ±0.06 | 0.146 ±0.010 |
| Tb | 0.44 | 0.79 | 1.01 ±0.18 | 0.99 ±0.26 | 0.099 ±0.012 |
| Yb | 3.20 | 3.97 | 3.95 ±0.32 | 3.90 ±0.32 | 0.46 ±0.03 |
| Lu | 0.50 | 0.62 | 0.62 ±0.04 | 0.60 ±0.04 | 0.074 ±0.006 |

1. Instrumental neutron activation analysis

2. Error of 2σ. Average of five analyses (Roden) by radiochemical neutron activation analysis.

3. Error is 2σ. Average of five analyses (2 by Roden, 3 by S. Roy and F. Frey) by instrumental neutron activation analysis.

4. Error is 2σ. Mean of 4 analyses by radiochemical neutron activation analysis.

Table 4-3. Continued

| | PCC-1[5] | BCR-1[6] |
|---|---|---|
| La | 0.035 ±0.004 | 25.1 |
| Ca | - | 54.1 |
| Nd | - | 28.7 |
| Sm | 0.007 ±0.002 | 6.63 |
| Eu | 0.003 ±0.001 | 1.97 |
| Tb | - | 1.03 |
| Yb | 0.025 ±0.003 | 3.46 |
| Lu | 0.006 ±0.001 | 0.54 |

5. Average of two analyses; error quoted is the deviation from the mean.

6. Average of isotope dilution analyses (except for Tb) from the literature (F.A. Frey, written communication, 1981). Tb value is average of INAA analyses from literature (F.A. Frey, written communication, 1981).

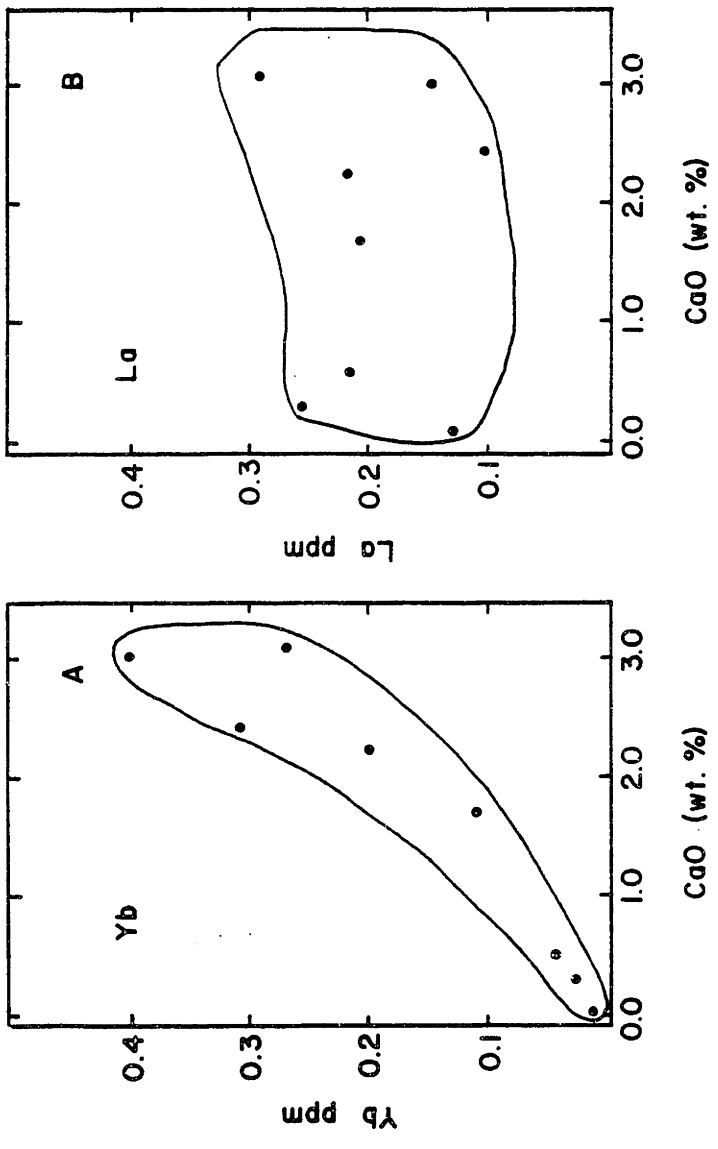
A
Yb
Yb ppm
0.4
0.3
0.2
0.1
0.0
1.0
2.0
3.0
CaO (wt. %)
B
La
La ppm
0.4
0.3
0.2
0.1
0.0
1.0
2.0
3.0
CaO (wt. %)

Figure 4-2. Yb (A) and La (B) concentrations plotted versus bulk rock CaO content for the Green Knobs peridotites.

CaO content (Figure 4-2). The correlation of CaO with Yb is consistent with clinopyroxene being the main host for the HREE in peridotites. The harzburgites are depleted in the heavy and middle REE relative to chondrites (Figure 4-3) but have La/Sm ratios greater than chondrites. One of the lherzolites, N23, also has a La/Sm ratio greater than chondrites, although the N23 chlorite/amphibole separate does not (Figure 4-3). The high La/Sm ratios relative to chondrites correlate with the presence of at least one primary hydrous phase (Table 4-1) such as chlorite, amphibole, titanoclinohumite, or antigorite in thin section. The only exception is lherzolite N71 which contains chlorite and amphibole has a La/Sm ratio less than chondrites (Figure 4-3).

The four lherzolites (N16, N71, N61, N23) have La/Yb ratios less than chondrites with Yb = 1.2 to 2.5 x chondrites (Figure 4-3). N61 has a nearly flat REE pattern with a peculiar positive hump relative to chondrites in the vicinity of Sm and Eu. Clinopyroxene separated from this inclusion also has the same hump in the vicinity of Sm and Eu, but has a significantly lower La/Yb ratio than the whole rock (Figure 4-4, Table 4-3). As a group the lherzolites have chondrite-normalized REE patterns similar to the REE patterns of lherzolites from alpine peridotites (e.g., Loubet et al., 1975), some ocean fracture zones (e.g., Coish et al., 1979), and to some lherzolite inclusions in alkali basalts (e.g., Jagoutz et al., 1979).

The two eclogites have quite distinct REE patterns relative to chondrites (Figure 4-4). The eclogite, N371, with a major element composition most nearly basaltic in composition has a La/Yb ratio less

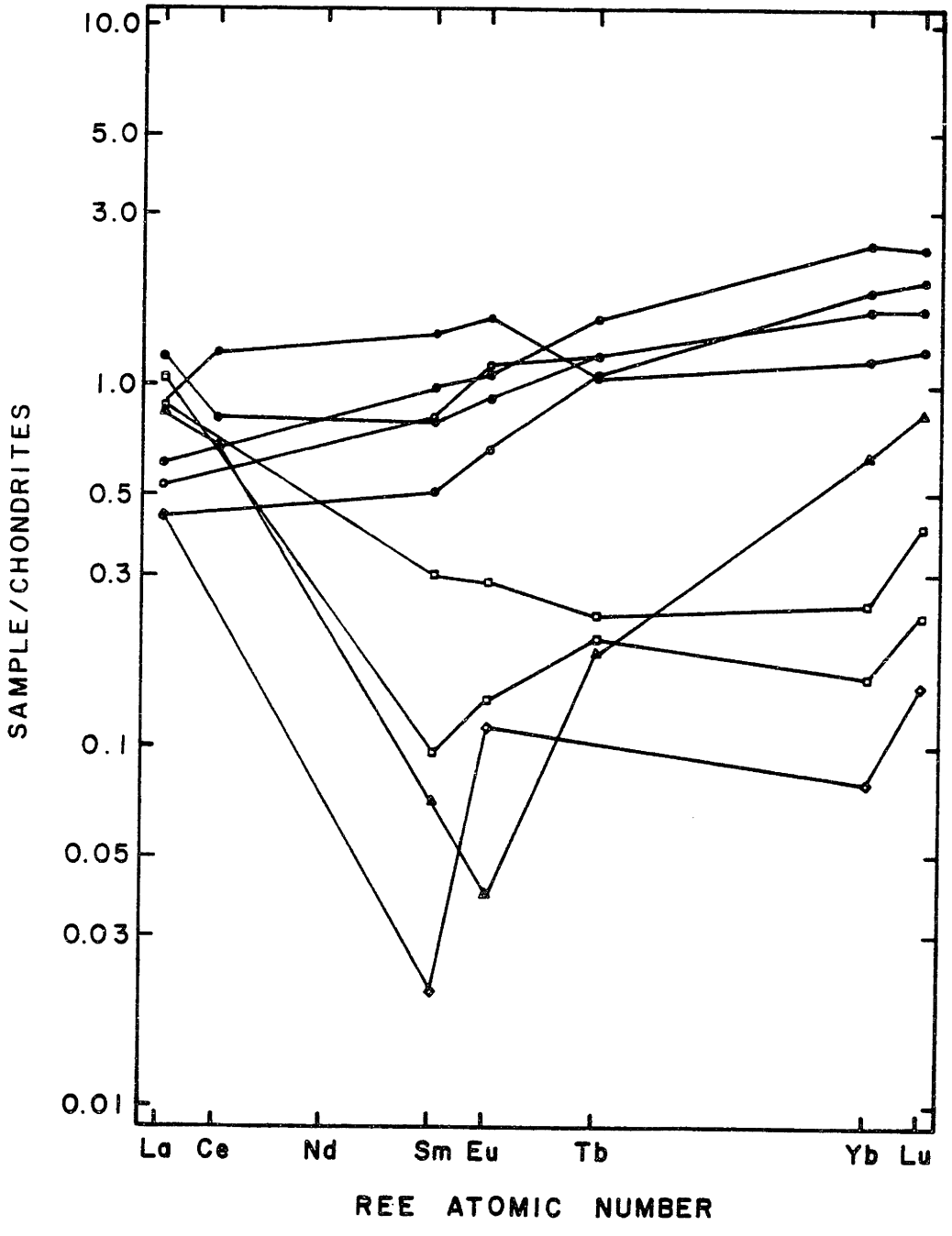
10.0
5.0
3.0
1.0
0.5
0.3
0.1
0.05
0.03
0.01
SAMPLE/CHONDRITES
La
Ce
Nd
Sm
Eu
Tb
Yb
Lu
REE ATOMIC NUMBER

Figure 4-3. Chondrite-normalized REE abundances for Green Knobs lherzolites (●), harzburgites (□,◇,▲), and N23 chlorite/amphibole separate (○). Chondrite concentrations from Evensen et al. (Table 3, "CI Average", 1978).

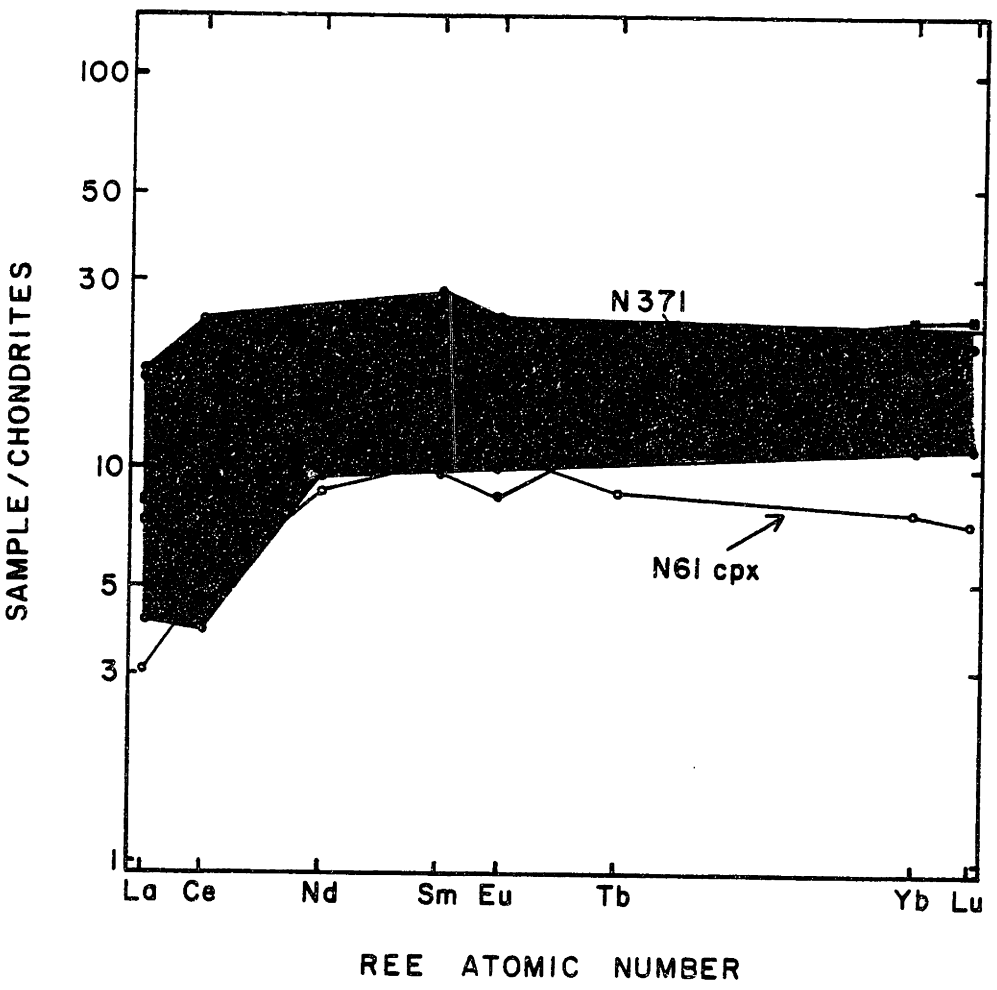
100
50
30
10
5
3
1
SAMPLE/CHONDRITES
N371
N61 cpx
La
Ce
Nd
Sm
Eu
Tb
Yb
Lu
REE ATOMIC NUMBER

Figure 4-4. Chondrite-normalized REE abundances for 2 eclogites (●, ■) from Garnet Ridge, and clinopyroxene (○) from N61 lherzolite from Green Knobs. Also shown is the average, normal MORB (□) from White and Schilling (1978), and the range (shaded region) of normal MORBs from Frey et al. (1974) and Sun et al. (1979).

than chondrites with Yb = 23 x chondrites (Figure 4-4). This elcogite also has a small negative Eu anomaly. Thus, the chondrite-normalized REE pattern of N371 is similar to many mid-ocean ridge basalts (MORBs). In contrast, the more alkali-rich eclogite, N350, has a "V-shaped" REE pattern relative to chondrites. This REE pattern is somewhat similar to the REE patterns of the Green Knobs harzburgites but displaced to much higher concentrations.

## V. Discussion

### (A) High La/Sm ratios relative to chondrites and mantle metasomatism

All of the harzburgites, one of the lherzolites, and one of the eclogites (Figures 4-3, 4-4) have La/Sm ratios greater than chondrites, and these relatively high La/Sm ratios correlate with the presence of primary hydrous phases (Smith, 1979). Similar high La/Sm ratios in relatively depleted peridotites (e.g., Frey and Prinz, 1978) have led to a two component model to explain the data. Component A is a partial melt residue while component B, the metasomatic component, is considered to be either a silicate melt or a mixed $CO_2$-$H_2O$ volatile phase (e.g., Frey and Prinz, 1978; Boettcher and O'Neill, 1980).

The hyperbolic relationship between La/Sm and Yb (Figure 4-5) for the Green Knobs peridotites is consistent with mixing (Langmuir et al., 1978) between a relatively high La/Sm, low Yb endmember (analogous to component B) and a relatively low La/Sm, high Yb endmember (analogous to component A). An alternative explanation of contamination by the host SUM to explain the relatively high La/Sm ratios of the Green Knobs

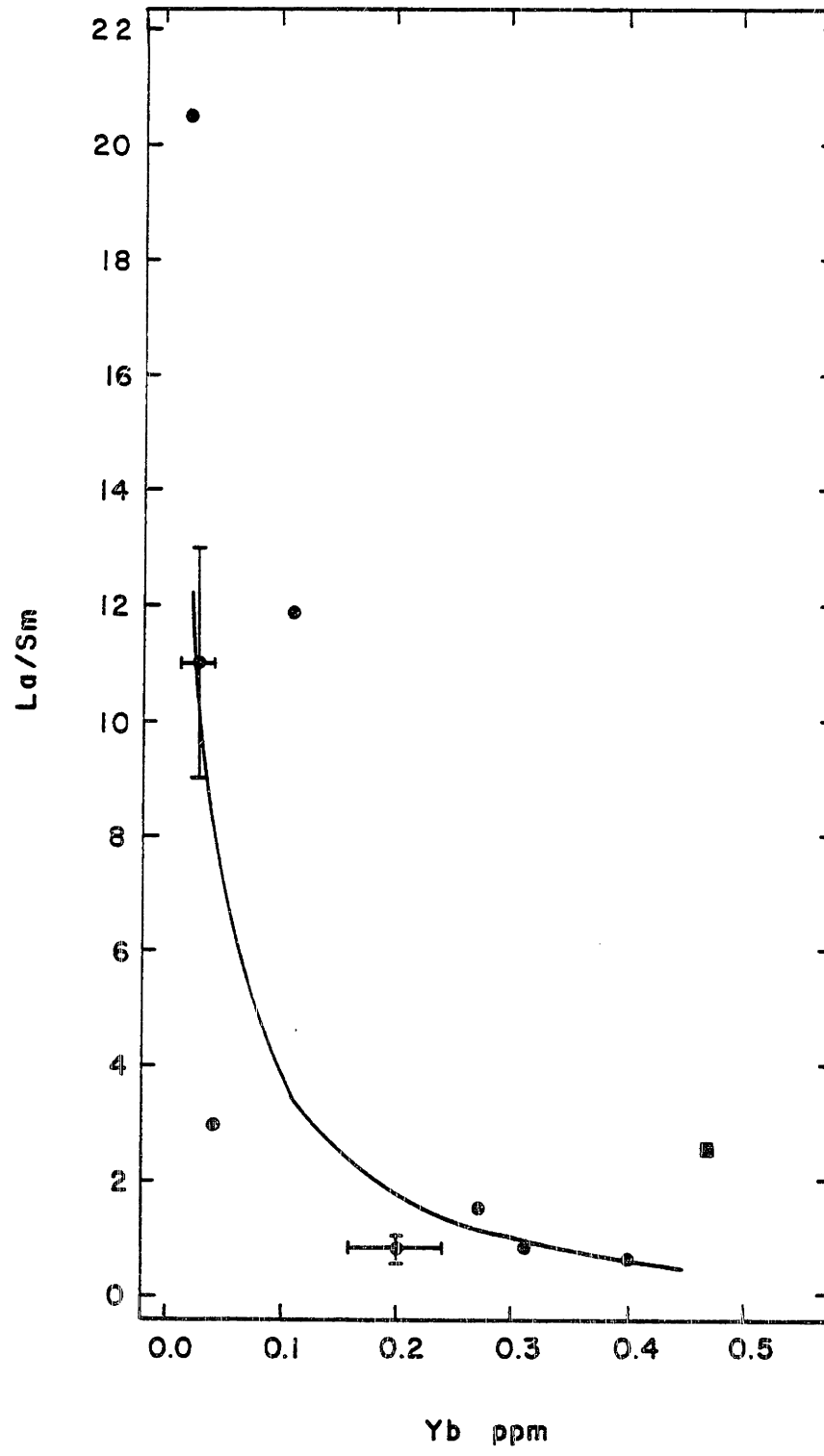
22
20
18
16
14
12
10
8
6
4
2
0
La/Sm
0.0
0.1
0.2
0.3
0.4
0.5
Yb ppm

Figure 4-5. Chondrite-normalized La/Sm plotted versus Yb concentration for the Green Knobs peridotites (●). Also shown is the La/Sm ratio and Yb concentration for SUM (■) from the Buell Park diatreme (Roden, 1981). The solid line is a mixing curve calculated using the circled data points.

inclusions is unlikely because some of the lherzolites such as N16 and N61 show no evidence of this LREE enrichment. Furthermore, the La/Sm ratio and Yb abundances of SUM from the neighboring Buell Park diatreme is inconsistent with a two component mixing relationship (Langmuir et al., 1978) because the La/Sm ratio and Yb abundances of the Buell Park SUM do not lie along a calculated mixing curve (Figure 4-5).

We attribute the relative light REE enrichment in the harzburgites and N23 lherzolite to the hydration event which formed the primary hydrous phases because all but one of the inclusions which contain primary hydrous phases also have La/Sm ratios greater than chondrites. In contrast, the two anhydrous (except for serpentine veinlets) lherzolites have La/Sm ratios less than chondrites. However, the data for the N23 amphibole/chlorite mineral separate (Figure 4-3) show that the LREE are not concentrated in the primary hydrous phases, amphibole and chlorite. We infer that the LREE may be concentrated either along grain boundaries or in primary magnesite or titanoclinohumite. Our data do not allow us to discriminate between these two alternatives, however, we favor the first alternative because the major cations in magnesite, Mg, $Fe^{2+}$ and titanoclinohumite, Mg, Ti, $Fe^{2+}$, all have small ionic radii relative to the REE. Typically, trace elements with ionic radii similar to the major cations are preferentially incorporated into mineral structures (e.g., Jensen, 1973). Thus, we do not expect either magnesite nor titanoclinohumite to have high concentrations of the LREE. Indeed, most published analyses of these minerals show low concentrations

of major elements, e.g., Ca, Na, with ionic radii similar to the REE (Deer et al., 1962). A grain boundary phase rich in the LREE is apparently present in lherzolites from The Thumb diatreme (Ehrenberg, 1982).

Smith (1979) summarized textural and mineralogical evidence which indicated that the hydrous phases in the Green Knobs peridotites formed in the upper mantle prior to eruption. The occurrence of titanoclinohumite, chlorite, amphibole, and dolomite (McGetchin et al., 1970; Hunter and Smith, 1981) as inclusions in garnet probably derived from garnet peridotite is consistent with the arguments of Smith (1979). Smith (1979) and Smith and Levy (1976) suggested that hydration occurred at temperatures less than 700°C and at pressures of 15-20 kb based on phase equilibrium and geothermometry. Such conditions eliminate the possibility that the metasomatizing agent was a silicate melt (e.g., Wyllie, 1979), and Smith (1979) suggested that the fluid phase was water-rich. This hypothesis is consistent with the REE data because water-rich fluids may contain significant amounts of the LREE at mantle pressures (Mysen, 1979).

An instructive comparison can be made between the Green Knobs suite and an amphibole-bearing, metasomatized suite such as the lherzolites from Nunivak Island (Figure 4-6). Many of the metasomatized Nunivak inclusions have La/Sm ratios greater than chondrites as do most of the Green Knobs peridotites which contain primary hydrous phases. However, the Nunivak inclusions contain significantly higher LREE concentrations than the Green Knobs peridotites. A second important

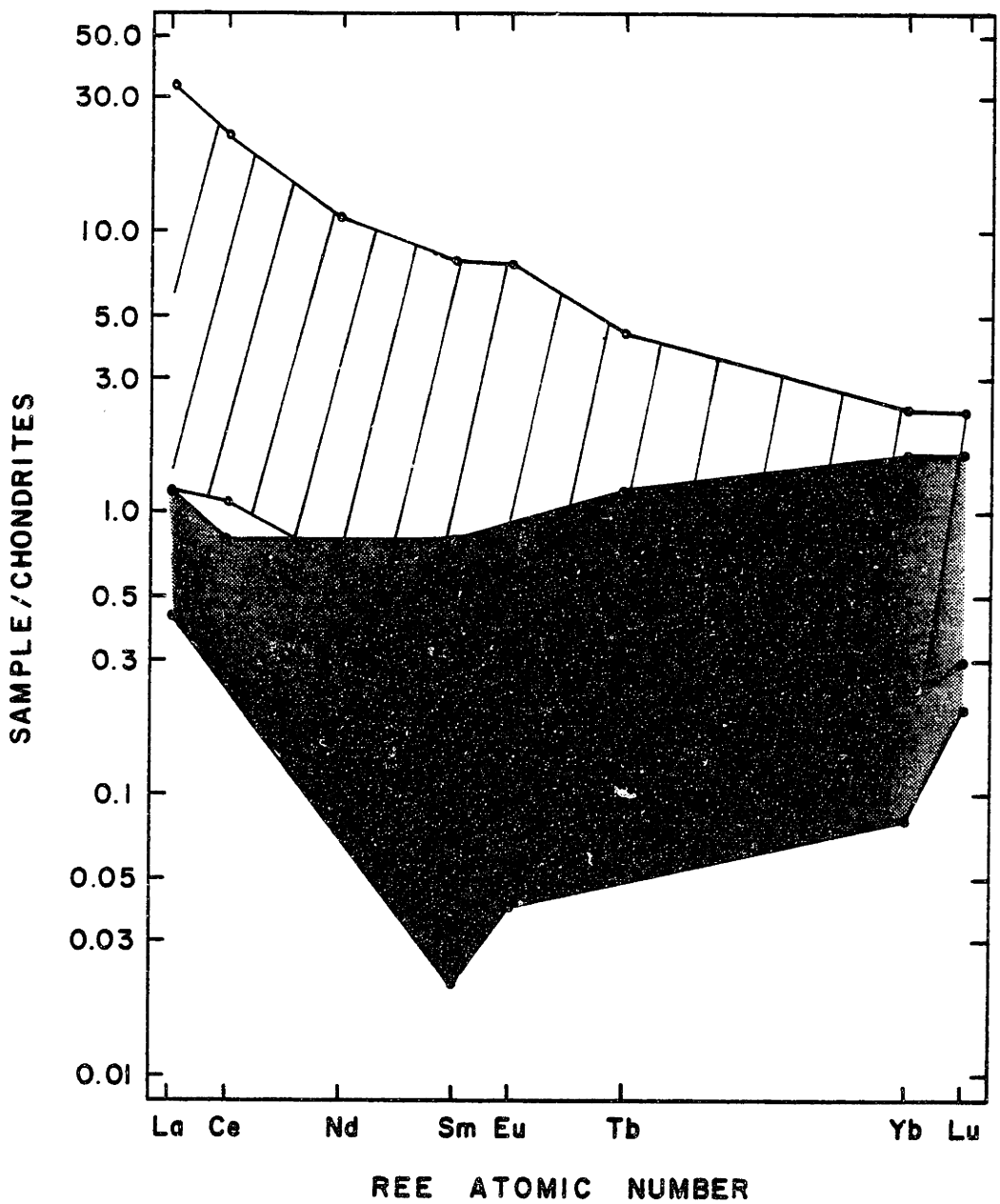
50.0
30.0
10.0
5.0
3.0
1.0
0.5
0.3
0.1
0.05
0.03
0.01
SAMPLE/CHONDRITES
La
Ce
Nd
Sm
Eu
Tb
Yb
Lu
REE ATOMIC NUMBER

Figure 4-6. Range of chondrite-normalized REE abundances for Green Knobs peridotites (shaded region) with La/Sm greater than chondrites compared to the range of REE abundances in metasomatized peridotite inclusions (lined region) from Nunivak Island, Alaska (Chapter 3).

difference between the two suites lies in the phase assemblage, amphibole + clinopyroxene ± phlogopite ± apatite ± $CO_2$(?) fluid inclusions, present at Nunivak (Francis, 1976b; Chapter 3) compared to the hydrous assemblage at Green Knobs. The only phase in common between the two suites is amphibole. Assuming that the protoliths for both suites were anhydrous lherzolites then the ultimate cause of the mineralogic differences between the two suites must lie in the variation of the intensive variables pressure, temperature, and fluid composition.

It seems clear that the temperature of the hydration event at Green Knobs was lower than the temperature of the metasomatism at Nunivak. Geothermometric calculations for the Green Knobs inclusions suggest temperatures of 700°C or less immediately prior to eruption (Smith and Levy, 1976) while similar calculations for the Nunivak suite suggest temperatures of 800-1150°C (Francis, 1978) prior to eruption. Furthermore, phase relations in the model CMAS-$H_2O$ system (Jenkins, 1981) suggest that chlorite-amphibole peridotite is stable at lower temperatures than amphibole peridotite in the pressure range 4 to 10 kb. The absence of a carbonate in the Nunivak suite and the presence of magnesite in the Green Knobs suite may also be related to temperature differences between the two suites. Both Eggler (1978) and Wyllie (1979) show a field of amphibole and mixed $CO_2$-$H_2O$ vapor at temperatures in the vicinity of 1000°C at 15 kb. At lower temperatures the vapor will react with peridotite to form a carbonate (dolomite, however instead of magnesite) in addition to amphibole.

A further difference between the two suites may be related to the

composition of the fluid phase: the Green Knobs suite may be an example of the interaction of a $H_2O$-rich fluid with peridotite (Smith, 1979) while the Nunivak suite may be an example of the interaction of a $Co_2$-rich fluid with peridotite. The worldwide association of undersaturated basalts with metasomatized xenoliths and the observation that silica-poor melts are generated in the presence of high $CO_2/CO_2$ + $H_2O$ vapor (e.g., Eggler, 1978) provides a link between the metasomatized inclusion suites and $CO_2$-rich fluids. Any undersaturated basalt which contains some $CO_2$ and crystallizes at shallow depth, i.e., less than approximately 20 kb, will eventually exsolve a $CO_2$-bearing fluid because carbonates are not stable on the solidus (Eggler, 1978; Wyllie, 1979). With cooling this fluid will be buffered by equilibration with amphibole to higher $CO_2/CO_2$ + $H_2O$ ratios (e.g., Wyllie, 1979), and this fluid is likely to contain high REE and other incompatible element abundances (Wendlandt and Harrison, 1979). The record of this $CO_2$-rich fluid may be preserved in the abundant fluid inclusions that occur in some metasomatized suites such as Nunivak Island (Chapter 3), San Carlos (Zindler and Jagoutz, 1980), and Dreiser Weiher (Stosch, 1982). At all these localities, abundant fluid inclusions correlate with relatively high incompatible element abundances.

(B) Oceanic affinities of the Green Knobs lherzolites

La/Yb ratios less than chondrites and Sm/Nd ratios greater than chondrites are fundamental features of MORBs (e.g., White and Schilling, 1978), many peridotites dredged from oceanic fracture zones (Figure 4-7),

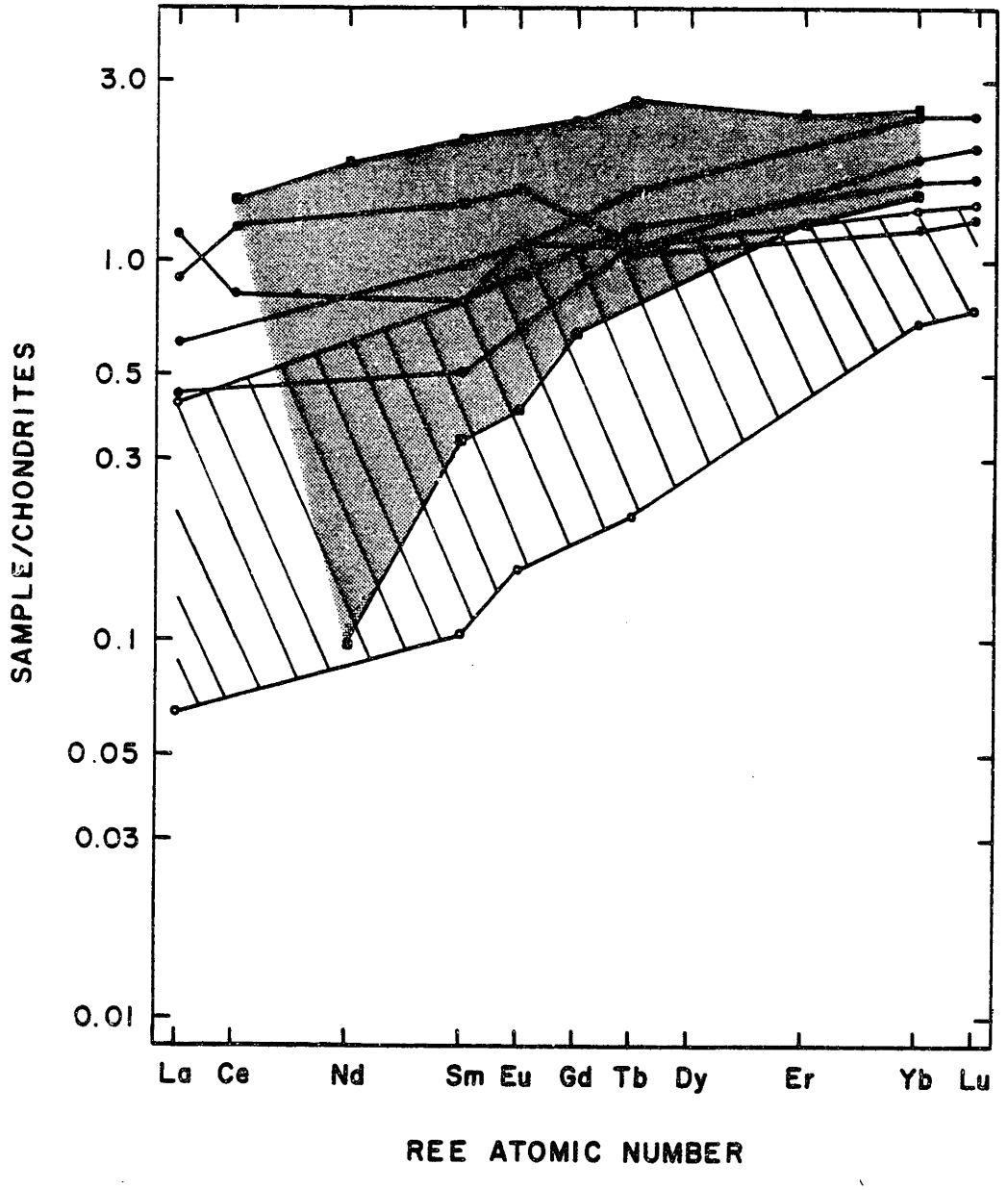
3.0
1.0
0.5
0.3
0.1
0.05
0.03
0.01
SAMPLE/CHONDRITES
La Ce Nd Sm Eu Gd Tb Dy Er Yb Lu
REE ATOMIC NUMBER

Figure 4-7. Chondrite-normalized REE abundances for Green Knobs lherzolites (●) compared to the range of REE abundances for 10 peridotites (lined region) dredged from the Islas Orcadas Fracture Zone, South Atlantic (Coish et al., 1979) and 17 European alpine peridotites (shaded region, Loubet et al., 1975; Frey, 1969).

and lherzolites from many alpine peridotites (Figure 4-7). Integrated over time, these Sm/Nd ratios result in high $^{143}Nd/^{144}Nd$ ratios relative to the bulk earth. Richard et al. (1976) and DePaolo and Wasserburg (1976a, 1976b) noted an empirical correlation between high $^{143}Nd/^{144}Nd$ ratios and low $^{87}Sr/^{86}Sr$ ratios in modern basalts. Normal MORBs have the highest $^{143}Nd/^{144}Nd$ and lowest $^{87}Sr/^{86}Sr$ ratios of any modern volcanic rocks (e.g., O'Nions et al., 1977). These three fundamental geochemical features of MORBs, La/Yb ratios less than chondrites, high $^{143}Nd/^{144}Nd$ ratios, and low $^{87}Sr/^{86}Sr$ ratios are found only in basalts erupted in oceanic environments; to the writers' knowledge, no basalts with all three of these characteristics have been erupted in a continental environment.

Trace element models for the petrogenesis of MORBs have led to the conclusion that their source rocks also have La/Yb ratios less than and Sm/Nd ratios greater than chondrites (Figure 4-8). This conclusion is consistent with the isotopic data for MORBs which implies that averaged over the history of the earth, source rocks for MORBs have been depleted in incompatible elements relative to the bulk earth and chondrites. The inferred REE abundances in the model sources for MORBs is similar to the measured REE abundances in lherzolites from alpine peridotites and some peridotites from oceanic fracture zones (Figures 4-7, 4-8). Furthermore, clinopyroxenes from alpine peridotites have $^{87}Sr/^{86}Sr$ and $^{143}Nd/^{144}Nd$ ratios similar to these ratios in MORBs (Menzies and Murthy, 1978; Richard and Allegre, 1980; Polve and Allegre, 1980). Hence, lherzolites from some alpine peridotites are

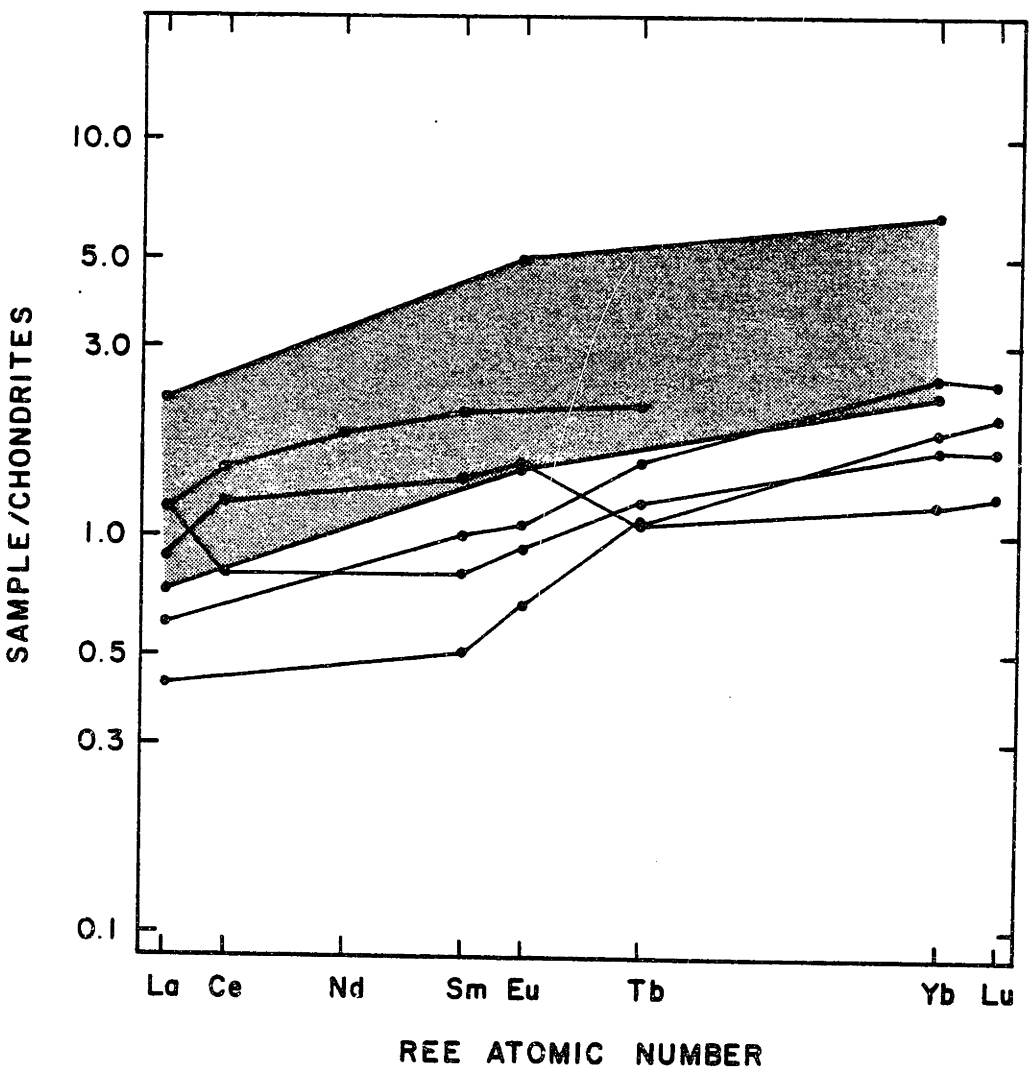
10.0
5.0
3.0
1.0
0.5
0.3
0.1
SAMPLE/CHONDRITES
La
Ce
Nd
Sm
Eu
Tb
Yb
Lu
REE ATOMIC NUMBER

Figure 4-8. Chondrite-normalized REE abundances of Green Knobs lherzolites ( ● ) compared to two models of the source for normal MORBs. The shaded region indicates the possible range of REE abundances in the source for normal MORBs calculated by White and Schilling (1978) while the line is the source for normal MORBs as calculated by Wood (1979).

potential source rocks for basalts with REE abundances, $^{87}Sr/^{86}Sr$ ratios, and $^{143}Nd/^{144}Nd$ ratios similar to MORBs.

The similarity between the chondrite-normalized REE patterns of the Green Knobs lherzolites, and the REE patterns of model sources for MORBs and of alpine lherzolites is the fundamental reason for stating that the Green Knobs xenoliths have oceanic affinities. Also, note that the REE pattern of eclogite N371 is similar to the REE patterns of normal MORBs (Figure 4-4), and the REE pattern of the harzburgites is similar to the REE patterns of harzburgites from ophiolites (Figure 4-9). We emphasize the lherzolite REE patterns, however, because of the uncertain effect of metamorphic events on the REE patterns of the eclogites and harzburgites.

Alkali basalts from continental regions such as Kilbourne Hole, Dreiser Weiher, and Nunivak Island also contain spinel lherzolite inclusions with relatively LREE depleted chondrite-normalized REE patterns similar to the REE patterns of the Green Knobs lherzolites (Figure 4-10). Clinopyroxenes from these xenoliths have $^{87}Sr/^{86}Sr$ and $^{143}Nd/^{144}Nd$ ratios similar to these ratios in MORBs (Chapter 3; Jagoutz et al., 1980; Stosch et al., 1980). Apparently, "oceanic mantle" characterized by relative depletion in the LREE occurs at shallow depths in many places under the continental crust (see also Stosch et al., 1980; Jagoutz et al., 1980). This mantle may be of regional extent in the southwestern U.S. based on the occurrence of inclusions with La/Yb ratios less than chondrites at Kilbourne Hole (Jagoutz et al., 1979; Basaltic Volcanism Study Project, 1981) as well

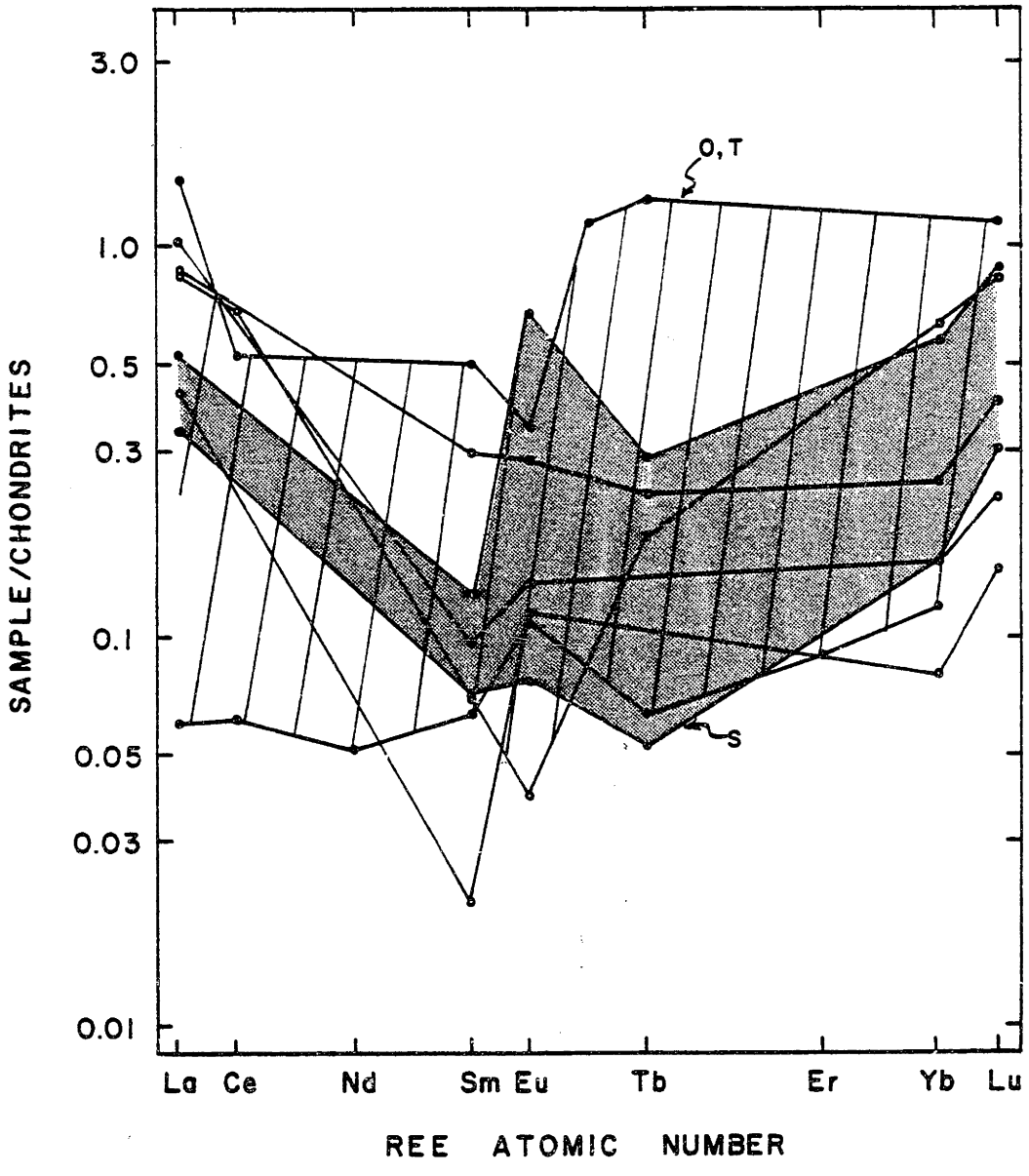
3.0
1.0
0.5
0.3
0.1
0.05
0.03
0.01
SAMPLE/CHONDRITES
O, T
S
La
Ce
Nd
Sm
Eu
Tb
Er
Yb
Lu
REE ATOMIC NUMBER

Figure 4-9. Chondrite-normalized REE abundances of Green Knobs harzburgites (o) compared to range of REE abundances for 3 harzburgites and 1 dunite (S) from the Samail ophiolite (Pallister and Knight, 1981) and 5 peridotites (O,T) from the Othris and Troodos ophiolites (Kay and Senechal, 1976; Menzies, 1976).

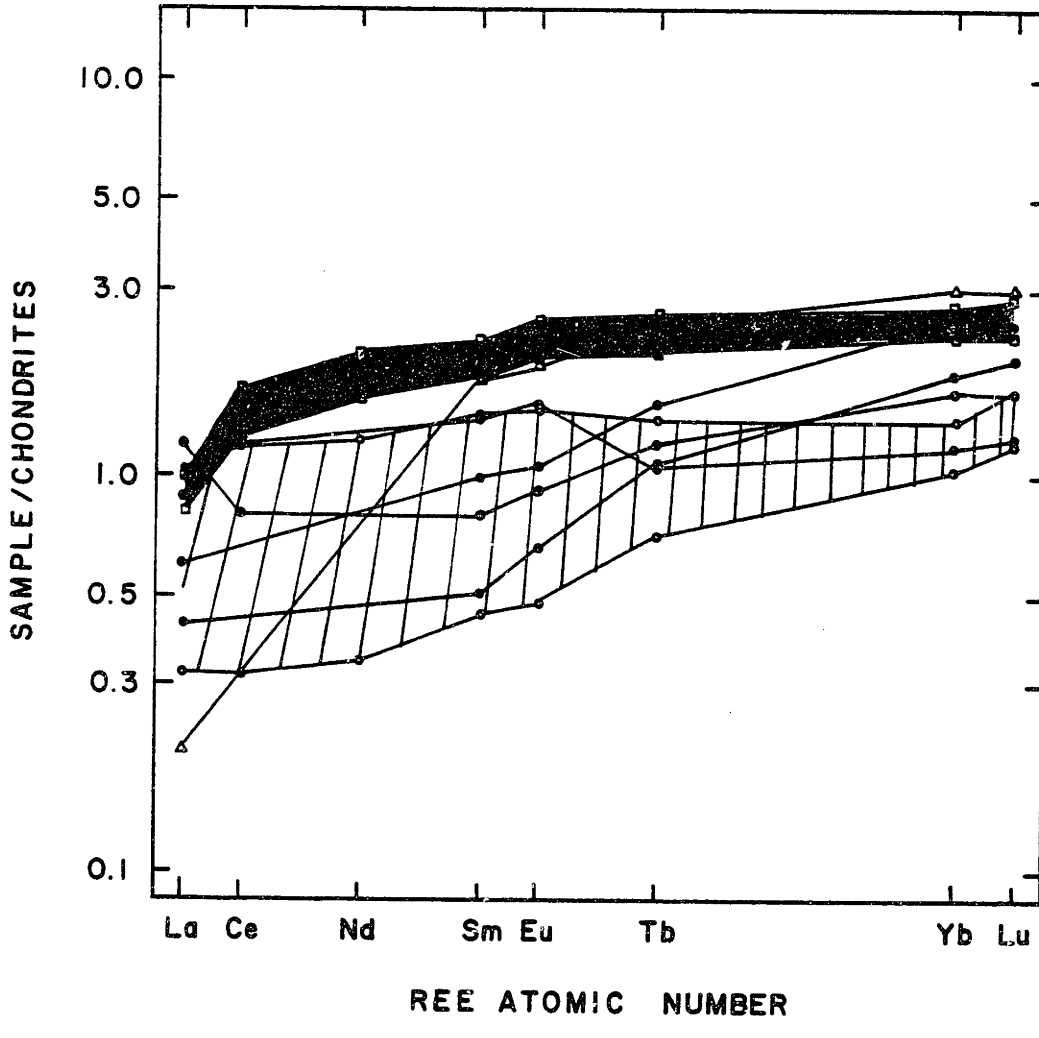
10.0
5.0
3.0
1.0
0.5
0.3
0.1
SAMPLE/CHONDRITES
La
Ce
Nd
Sm
Eu
Tb
Yb
Lu
REE ATOMIC NUMBER

Figure 4-10. Chondrite-normalized REE abundances of Green Knobs lherzolites (●) compared to the range of REE abundances in relatively light REE depleted inclusions from Nunivak Island (shaded region, Chapter 3), and Dreiser Weiher (lined region, IB inclusions with La/Sm ratios less than chondrites, Stosch and Seck, 1980), and to the Kilbourne Hole inclusion (Δ) studied by Jagoutz et al. (1979, 1980).

as Green Knobs. In order to further substantiate the oceanic affinities of this mantle, the writer will attempt to obtain $^{87}Sr/^{86}Sr$ and $^{143}Nd/^{144}Nd$ ratios on clinopyroxenes from the four lherzolites studied here in collaboration with V.R. Murthy at the University of Minnesota.

Our data is consistent with the model of Helmstaedt and Doig (1975) and Helmstaedt and Schulze (1979) in which the Plateau eclogites are samples of subducted oceanic lithosphere. However, one of the underlying premises of their argument is the uniqueness of the mineralogy of the Plateau eclogites relative to eclogite inclusions in kimberlite diatremes. Although our peridotite data show the intrinsically oceanic nature of the uppermost mantle beneath Green Knobs, these inclusions are not unique relative to other continental diatremes. Hence, the geochemistry of the Green Knobs inclusions probably reflect the occurrence of substantial amounts of "oceanic mantle" beneath continental areas rather than the specific occurrence of subducted oceanic lithosphere beneath the Colorado Plateau.

Ehrenberg (1982) studied garnet peridotite inclusions from The Thumb, a minette diatreme (Figure 4-1). These garnet peridotites are derived from deeper (100 to 150 km, Ehrenberg, 1982) portions of the mantle beneath the Colorado Plateau than the Green Knobs inclusions which last equilibrated at 45 to 60 km depth (Smith and Levy, 1976). The Thumb suite consists of high Ca-Al lherzolites which are relatively fertile with respect to basaltic components, low Ca-Al lherzolites which are relatively depleted in basaltic components, and megacrystal rocks which will not be discussed here.

Average REE patterns for the first two groups are compared to the REE patterns of the Green Knobs lherzolites in Figure 4-11. The low Ca-Al lherzolites have La/Yb ratios greater than chondrites but have low absolute concentrations of the REE relative to chondrites. Sample N51 is the only Green Knobs sample with a similar REE pattern. The most interesting comparison is between the high Ca-Al lherzolites from The Thumb and the Green Knobs lherzolites. The calculated, average REE abundances in the former lherzolites are quite different from Green Knobs lherzolites N16, N71, and N23, but bear a remarkable resemblance to N61 (Figure 4-11). In particular, on the chondrite-normalized plot (Figure 4-11) the peculiar positive hump in the vincinity of Sm and Nd occurs in the REE pattern for the calculated average REE abundance of the high Ca-Al lherzolites as well as in the curve for N61 clinopyroxene.

However, there is a discrepancy between calculated bulk rock LREE abundances and measured bulk rock LREE abundances (Figure 4-11) for the high Ca-Al lherzolites; apparently the LREE are concentrated to some degree along grain boundaries (Ehrenberg, 1982). It is uncertain whether this LREE enrichment predates the incorporation of the xenoliths in the minette host or not. If the discrepancy between calculated and observed bulk rock REE abundances in the high Ca-Al lherzolites is the consequence of a recent event related to the minette magmatism then the average, calculated REE abundances of the high Ca-Al lherzolites may be a more accurate indicator of the geochemistry of the mantle. In that case the similarity in chondrite-normalized REE patterns

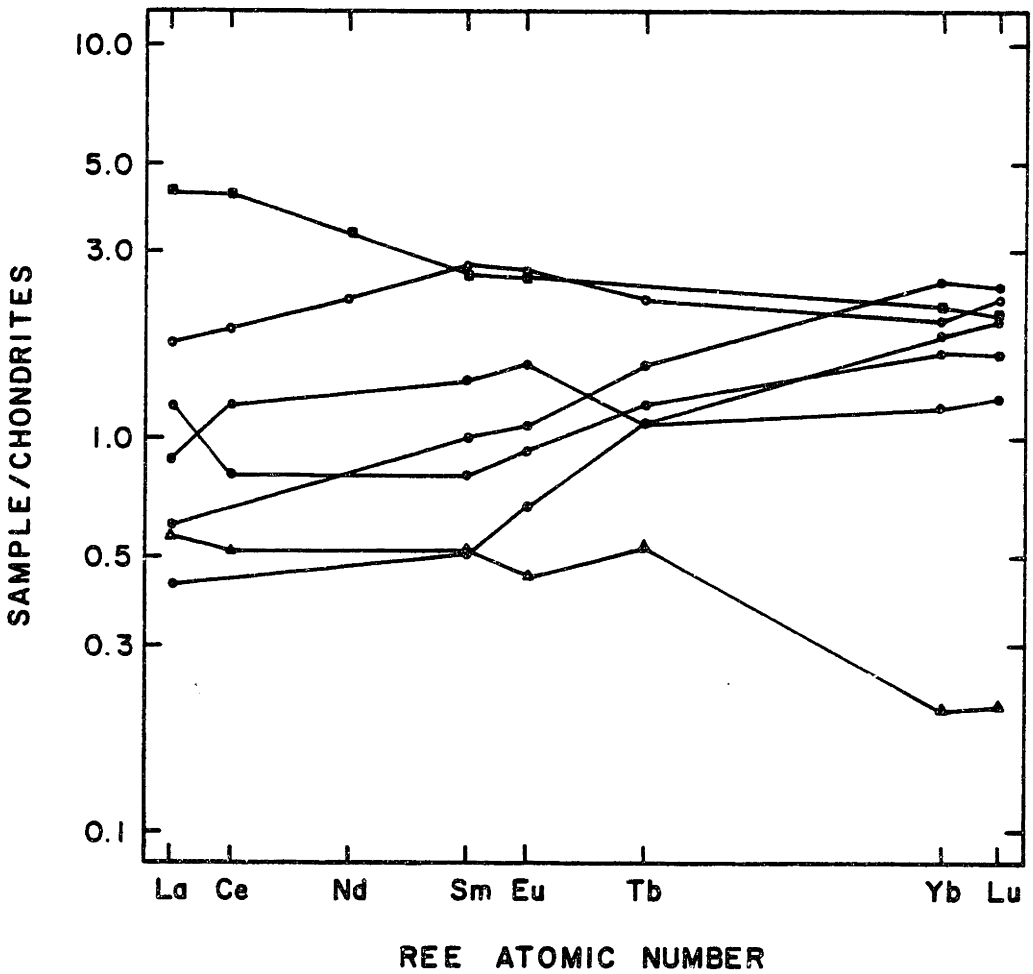
10.0
5.0
3.0
1.0
0.5
0.3
0.1
SAMPLE/CHONDRITES
La
Ce
Nd
Sm
Eu
Tb
Yb
Lu
REE ATOMIC NUMBER

Figure 4-11. Chondrite-normalized REE abundances of Green Knobs lherzolites (●) compared to calculated, average low Ca-Al garnet peridotites (△) and to calculated, average high Ca-Al garnet peridotites (○) from The Thumb (Ehrenberg, 1982). Measured REE abundances (■) in the high Ca-Al peridotites are also shown. Calculated REE patterns are based on mineral analyses and modal abundances.

of N61 and the calculated, average REE pattern of the high Ca-Al lherzolites indicate that clinopyroxene-rich mantle with slight relative LREE depletion may be a feature of regional extent beneath the Colorado Plateau.

The harzburgites and the lherzolites N16, N71, and N23 from Green Knobs have no counterpart in The Thumb suite studied by Ehrenberg (1982). These Green Knobs inclusions represent mantle strongly depleted in incompatible elements which occurs at shallower depths than the garnet peridotite xenoliths from The Thumb.

If The Thumb and the Green Knobs diatremes sampled geochemically similar mantle, then the data from the two diatremes can be combined in a single geochemical model for this region of the Colorado Plateau. In Figure 4-12 we present one possible model which shows the average La/Yb ratio increasing with depth. The proof or disproof of this model awaits further studies of Navajo inclusion suites to determine (1) if the inclusion of xenolith suites from diatremes 70 km apart in a single model of the mantle is valid, (2) if inclusions geochemically similar to the Green Knobs and Thumb inclusions are present at other diatremes, and (3) if estimates of pressures and temperatures of equilibration of such inclusions is consistent with the model.

(C) Partial melting model

If the relatively high La/Sm ratios of the harzburgites, N23 lherzolite, and N350 eclogite are due to a hydration event as we suggest, and if the igneous protoliths for these rocks were relatively

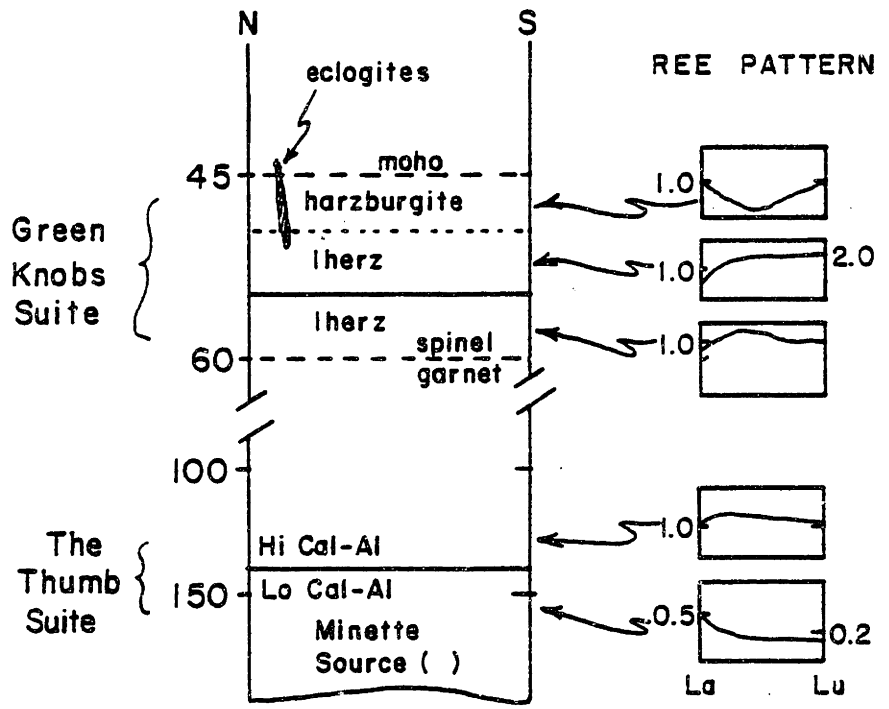
N
S
REE PATTERN
eclogites
45
moho
harzburgite
lherz
Green
Knobs
Suite
lherz
spinel
garnet
60
100
Hi Cal-Al
The
Thumb
Suite
150
Lo Cal-Al
Minette
Source ( )
1.0
1.0
2.0
1.0
1.0
0.5
0.2
La
Lu

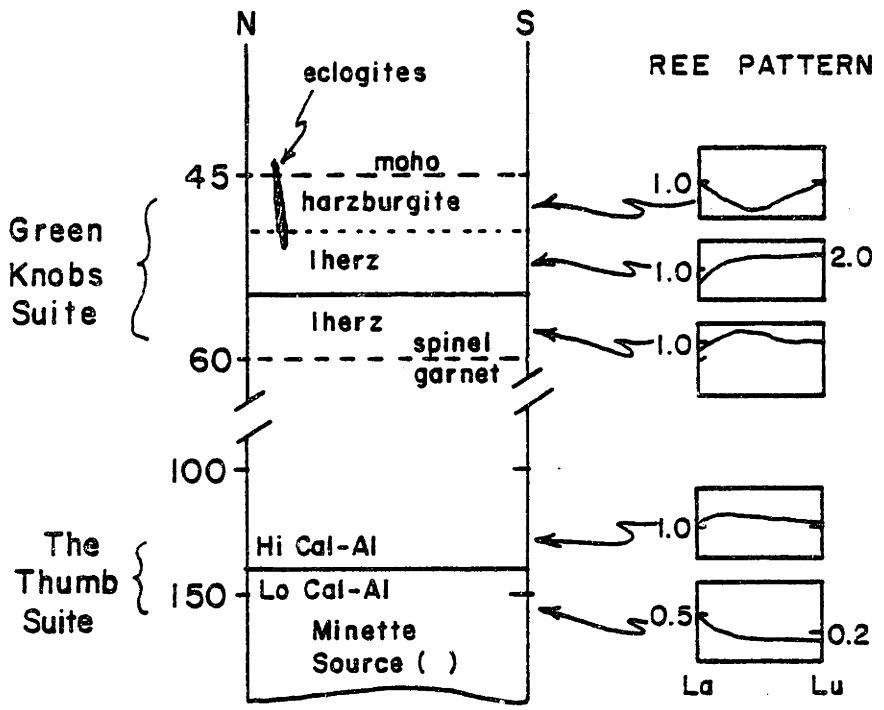
N
S
eclogites
REE PATTERN
45
moho
harzburgite
Green
Knobs
Suite
lherz
1.0
1.0
2.0
lherz
spinel
garnet
60
1.0
100
The
Thumb
Suite
Hi Cal-Al
1.0
150
Lo Cal-Al
Minette
Source ( )
0.5
0.2
La
Lu

Figure 4-12. Cartoon illustrating one possible distribution of rock types in the upper mantle beneath the Colorado Plateau. Xenolith data are from Ehrenberg (1982) and this paper. Position of Moho and transition from spinel to garnet peridotite from Smith and Levy (1976).

LREE depleted as are the other lherzolites and N371 eclogite, then the pre-hydration REE geochemistry of the Green Knobs harzburgites and the two Garnet Ridge eclogites can be explained by a single equilibrium melting event in which the source rock has REE abundance similar to the Green Knobs lherzolites. The eclogites and harzburgites correspond to basaltic melts and melt residues respectively. To illustrate this model we used the expression for equilibrium, non-modal melting (equation 15, Shaw, 1970) and assumed an initial source composition, 70% olivine, 20% orthopyroxene, and 10% clinopyroxene, representative of the lherzolites (Smith and Levy, 1976). Melting was assumed to occur in the proportions 20% olivine, 20% orthopyroxene, and 60% clinopyroxene. Spinel was ignored in this model because it is present in small amounts and because of its very low partition coefficients for the REE relative to coexisting minerals in lherzolites (Stosch, 1982). Partition coefficients used were those of Set 1, Frey et al. (1978) for clinopyroxene, and Stosch (average Dreiser Weiher, 1982) for orthopyroxene and olivine. The melting equation used is almost certainly an inaccurate representation of the true melting reaction; however, in the case of REE, the model results are rather insensitive to the melting equation used because all the minerals have partition coefficients much smaller than 1. Furthermore, it is clear that clinopyroxene is a major contributor to basaltic melts simply from the bulk composition of basalts, their high pressure phase equilibria, and the sequence lherzolite-harzburgite which can be most easily understood to be the result of an increasing amount of basaltic melt being extracted from mantle source rocks.

The model is illustrated in Figure 4-13. Basalts with REE abundances similar to the eclogites could result from approximately 7% melting of source rocks similar to the lherzolites. Note that we assumed that the igneous protoliths of these rocks all had La/Sm ratios less than chondrites. The model residues have similar Sm/Yb ratios as the harzburgites but generally higher REE concentrations. By increasing the amount of melt extraction or increasing the amount of clinopyroxene contributing to the melt, the model residues would become more like the harzburgites in absolute REE abundances.

Thus, the REE data for the harzburgites and eclogites are consistent with models in which the protoliths for these rocks are considered to be residues from partial melting and basaltic melts respectively. In particular, the REE data for the eclogites are consistent with previous models for their petrogenesis in which these rocks were viewed as metasomatized basaltic dikes (Smith and Zientek, 1979) or as fragments of subducted oceanic lithosphere (Helmstaedt and Doig, 1975). The REE modelling (Figure 4-12) shows that the igneous protolith for the eclogites could have been a relatively light REE depleted basalt which was similar to modern MORBs in REE geochemistry.

## VI. Conclusions

Based on the REE data we conclude that:

(1) The high La/Sm ratios of the harzburgites, one lherzolite, and one eclogite is the result reaction with a hydrous fluid. The Green Knobs suite may reflect the interaction of a relatively cool, $H_2O$-rich

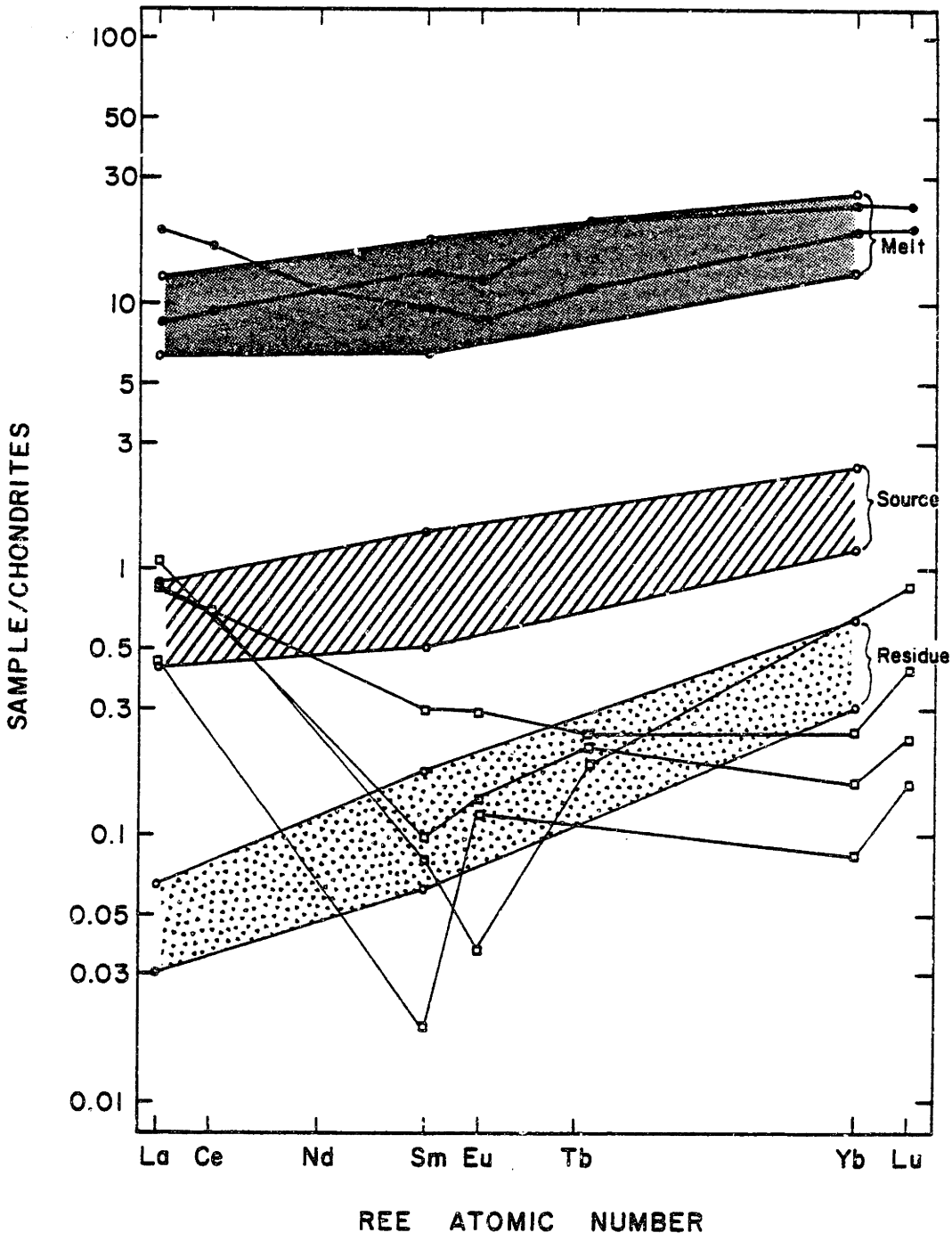
100
50
30
10
5
3
1
0.5
0.3
0.1
0.05
0.03
0.01
SAMPLE/CHONDRITES
Melt
Source
Residue
La
Ce
Nd
Sm
Eu
Tb
Yb
Lu
REE ATOMIC NUMBER

Figure 4-13. Chondrite-normalized REE abundances in eclogites (●) and harzburgites from Garnet Ridge and Green Knobs (□) compared to calculated range of liquids and residues in a partial melting model in which the REE concentrations in the Green Knobs lherzolites define the source REE concentrations. Further details in text.

fluid with peridotite while metasomatized suites in alkalic basalts may reflect the interaction of relatively warm, $CO_2$-rich fluids with peridotite.

(2) The low La/Yb ratios of the lherzolites relative to chondrites indicates that the mantle represented by these lherzolites has oceanic affinities. The data are consistent with the hypothesis of Helmstaedt and coworkers that subducted oceanic lithosphere underlies the Colorado Plateau, but it is more likely that the data are indicative of the widespread occurrence of mantle with oceanic affinities beneath the continents.

(3) The data are consistent with a simple model in which the eclogites and harzburgites represent altered basaltic dikes and residues, respectively, formed by partial melting of source rocks similar to the lherzolites. If the model is an accurate representation of the petrogenesis of these rocks, then the relative LREE depletion of the eclogites and harzburgites may be related to a widespread partial melting event such as the last major plutonism in the area, 1430 million years ago.

## References

Albarede, F., 1976, Some trace element relationships among liquid and solid phases in the course of the fractional crystallization of magmas. Geochim. Cosmochim. Acta, 40, 667-674.

Allen, J. C., A. Boettcher, and G. Marland, 1975, Amphiboles in andesite and basalt: I. Stability as a function of P-T-$f_{O_2}$. Amer. Mineralogist, 63, 1074-1087.

Anderson, A. T., 1975, Some basaltic and andesitic glasses. Rev. Geophys. Space Phys., 13, 37-55.

Arculus, R. J., and J. W. Delano, 1981, Siderophile element abundances in the upper mantle: evidence for a sulfide signature and equilibrium with the core. Geochim. Cosmochim. Acta, 45, 1331-1344.

Arth, J. G., 1976, Behavior of trace elements during magmatic processes - a summary of theoretical models and their applications. Jour. Research U.S. Geological Surv., 4, 41-47.

Basaltic Volcanism Study Project, 1981, Basaltic Volcanism on the Terrestrial Planets. Pergamon Press, Inc., New York, 1286 pp.

Basu, A., and V. R. Murthy, 1977, Kaersutites, suboceanic low-velocity zone, and the origin of mid-ocean ridge basalts. Geology, 5, 365-368.

Best, M. G., 1974, Amphibole-bearing cumulate inclusions, Grand Canyon, Arizona and their bearing on silica-undersaturated hydrous magmas in the upper mantle. Jour. Petrology, 16, 212-236.

Birch, F., 1966, Compressibility; elastic constants. In: S. P. Clark (ed.), Handbook of Physical Constants, Geological Society America Memoir 97, 97-174.

Boettcher, A. L., and J. R. O'Neill, 1980. Stable isotope, chemical, and petrographic studies of high-pressure amphibiles and micas; evidence for metasomatism in the mantle source regions of alkali basalts and kimberlites. Amer. Jour. Sci., 280-A, 594-621.

Bonatti, E., P. Hamlyn, and G. Ottonello, 1981, Upper mantle beneath a young oceanic rift: peridotites from the island of Zabargad (Red Sea). Geology, 9, 474-479.

Brey, G. P., and D. H. Green, 1975, The role of $CO_2$ in the genesis of olivine melilitite. Contr. Mineral. Petrol., 49, 93-103.

Brooks, C., S. R. Hart, A. W. Hofmann, and D. E. James, 1976, Rb-Sr mantle isochrons from oceanic regions. Earth Planet. Sci. Letters, 32, 51-61.

Bryan, W. B., G. Thompson, F. A. Frey, and J. S. Dickey, 1976, Inferred geologic settings and differentiation in basalts from the Deep Sea Drilling Project. Jour. Geophysical Research 81: 4285-4304.

Bultitude, R. J., and D. H. Green, 1968, Experimental study at high pressures on the origin of olivine nephelinite and olivine melilite nephelinite magmas. Earth Planet. Sci. Letters, 3, 325-337.

Cameron, W. E., E. G. Nisbet, and V. J. Dietrich, 1980, Petrographic dissimilarities between ophiolitic and ocean floor basalts. In: Ophiolites, Proceedings Internation Ophiolite Symposium, Geol. Survey Dept., Nicosia, Cyprus, 182-192.

Carlson, R. W., J. D. Macdougall, and G. W. Lugmair, 1978, Differential Sm/Nd evolution in oceanic basalts. Geophysical Research Letters, 5, 229-232.

Carlson, R. W., G. W. Lugmair, and J. D. Macdougall, 1981, Columbia River volcanism: the question of mantle heterogeneity or crystal contamination. Geochim. Cosmochim. Acta, 45, 2483-2500.

Carmichael, I. S. E., F. J. Turner, and J. Verhoogen, 1974, Igneous Petrology, McGraw-Hill Book Co., 739 pp.

Chen, C. Y., F. A. Frey, and S. R. Hart, 1981. The evolution of Haleakala Volcano, East Maui: evidence for heterogeneous mantle sources. EOS, 62, 1068-1069.

Church, W. R., and L. Riccio, 1977, Fractionation trends in the Bay of Islands ophiolite of Newfoundland: polycyclic cumulate sequences in ophiolites and their classification. Can. Jour. Earth Sci., 14, 1156-1165.

Churkin, M., Jr., C. Carter, and J. H. Trexler, Jr., 1980, Collision-deformed Paleozoic continental margin of Alaska - foundation for microplate accretion. Geological Soc. Amer. Bull., 91, 648-654.

Clague, D. A., and F. A. Frey, 1982, Petrology and trace element geochemistry of the Honolulu Volcanic Series, Oahu: implications for the the oceanic mantle beneath Hawaii. Submitted to Jour. Petrology.

Coish, R., M. Roden, F. Frey, and C. J. Suen, 1979, Rare earth element abundances in ultramafic ro2ks from the ocean floor, ophiolites and alpine peridotites (abst.), GSA abstracts with Programs, 11, 403.

Cox, K. G., J. D. Bell, and R. J. Pankhurst, 1979, The Interpretation of Igneous Rocks, George Allen & Unwin, London, 450 pp.

Dale, I. M., and P. M. Henderson, 1972, The partitioning of transition elements in phenocryst-bearing basalts and the implications about melt structure. 24th .nternational Geological Conference, Section 10, 105-111.

Dawson, J. B., and J. V. Smith, 1977, The MARID (mica-amphibole-rutile-ilmenite-diopside) suite of xenoliths in kimberlite. Geochim. Cosmochim. Acta, 41, 309-324.

Deer, W. A., R. A. Mowie, and J. Zussman, 1962, Rock Forming Minerals: Vol. 1, Ortho- and Ring Silicates. Longmans, Green and Co., Ltd., London, 333 pp.

Delaney, J. S., J. V. Smith, D. A. Carswell, and J. B. Dawson, 1980, Chemistry of micas from kiberlites and xenoliths-II. Primary- and secondary-textured micas from peridotite xenoliths. Geochim. Cosmochim. Acta, 44, 857-872.

DePaolo, D. J., and G. J. Wasserburg, 1976a, Nd isotopic variations and petrogenetic models. Geophysical Research Letters, 3, 249-252.

DePaolo, D. J., and G. J. Wasserburg, 1976b, Inferences about magma sources and mantle structure from variations of $^{143}Nd/^{144}Nd$. Geophysical Research Letters, 3, 743-746.

DePaolo, D. J., and R. W. Johnson, 1979, Magma genesis in the New Britain Island-Arc: constraints from Nd and Sr isotopes and trace-element patterns. Contr. Mineral. Petrol., 70, 367-379.

Dickey, J. S. Jr., F. A. Frey, S. R. Hart, E. B. Watson, and G. Thompson, 1977, Geochemistry and petrology of dredged basalts from the Bouvet triple junction, South Atlantic. Geochim. Cosmochim. Acta, 41, 1105-1118.

Dostal, J., and G. K. Muecke, 1978, Trace element geochemistry of the peridotite-gabbro-basalt suite from DSDP Leg 37. Earth Planet Sci. Letters, 40, 415-422.

Drake, M. J., and D. F. Weill, 1975, Partitioning of Sr, Ba, Ca, Y, Eu, Eu, and other REE between plagioclase feldspar and magmatic liquid: an experimental study. Geochim. Cosmochim. Acta, 39, 689-712.

Eggler, D. H., 1978, The effecto of $CO_2$ upon partial melting of peridotite in the system $Na_2O$-CaO-$Al_2O_3$-MgO-$SiO_2$-$CO_2$ to 35 kb, with an analysis in a peridotite-$H_2O$-$CO_2$ system. Amer. Jour. Sci., 278, 305-343.

Ehrenberg, S. N., 1979, Garnetiferous ultramafic inclusions in minette from the Navajo volcanic field. In: F. R. Boyd and H. O. A. Meyer (eds.), The Mantle Sample: Inclusions in Kimberlite and Other Volcanics, Amer. Geophysical Union, Washington, 330-344.

Ehrenberg, S. N., 1982, Rare earth geochemistry of garnet lherzolite and megacrystalline nodules from minette of the Colorado Plateau province. Earth Planet Sci. Letters, 57, 191-210.

Erlank, A. J., and R. S. Rickard, 1977, Potassic richterite bearing peridotites from kimberlite and the evidence they provide for upprr mantle metasomatism. In: Second International Kimberlite Conference Extended Abstracts.

Evensen, N. M., P. J. Hamilton, and R. K. O'Nions, 1978, Rare-earth abundances in chondritic meteorites. Geochim. Cosmochim. Acta, 42, 1199-1213.

Flanagan, F. J., 1976, 1972 Compilation of data on USGS standards. U.S. Geological Survey Professional Paper, 840, 131-183.

Flower, M. F. J., H. V. Schmincke, and R. N. Thompson, 1975, Phlogopite stability and the $^{87}Sr/^{86}Sr$ step in basalts along the Reykjanes Ridge. Nature, 254, 404.

Francis, D. M., 1974, Xenoliths and the nature of the upper mantle and lower crust. Ph.D. thesis, MIT, 236 pp.

Francis, D. M., 1976a, Corona bearing pyroxene granulite xenoliths and the lower crust beneath Nunivak Island, Alaska. Can. Mineralogist, 14, 291-298.

Francis, D. M., 1976b, The origin of amphibole in lherzolite xenoliths from Nunivak Island, Alaska. Jour. Petrology, 17, 357-378.

Francis, D. M., 1976c, Amphibole pyroxenite xenoliths: cumulate or replacement phenomena from the upper mantle, Nunivak Island, Alaska, Contr. Mineral. Petrol., 58, 51-61.

Francis, D. M., 1978, The implications of the compositional dependence of texture in spinel lherzolite xenoliths. Jour. Geology, 86, 473-485.

Frey, F. A., 1969, Rare earth abundances in a high temperature peridotite intrusion: Geochim. Cosmochim. Acta, 33, 1429-1447.

Frey, F. A., 1970, Rare earth and potassium abundances in St. Paul's Rocks. Earth Planet. Sci. Letters, 7, 351-360.

Frey, F. A., 1980, The origin of pyroxenites and garnet pyroxenites from Salt Lake Crater, Oahu, Hawaii: trace element evidence. Amer. Jour. Sci., 280-A, 427-450.

Frey, F. A., and D. H. Green, 1974, The mineraology and origin of lherzolite inclusions from Victorian basanites. Geochim. Cosmochim. Acta, 38, 1023-1059.

Frey, F. A., and M. Prinz, 1978, Ultramafic inclusions from San Carlos, Arizona: petrologic and geochemical data bearing on their petrogenesis. Earth Planet. Sci. Letters, 38, 129-176.

Frey, F. A., and C. J. Suen, ms, The Ronda High-temperature Peridotite: geochemistry and petrogenesis.

Frey, F. A., W. B. Bryan, and G. Thompson, 1974, Atlantic Ocean floor: geochemistry and petrology of basalts from Legs 2 and 3 of the Deep-Sea Drilling Project. Jour. Geophysical Research, 79, 5507-5527.

Frey, F. A., J. S. Dickey, Jr., G. Thompson, W. Bryan, and H. Davies, 1980, Evidence for heterogeneous primary MORB and mantle sources, NW Indian Ocean. Contr. Mineral. Petrol., 74, 387-402.

Frey, F. A., D. H. Green, and S. Roy, 1978, Integrated models of basalt petrogenesis: a study of quartz tholeiites to olivine melilitites from southeastern Australia utilizing geochemical and experimental petrological data. Jour. Petrology, 19, 463-513.

Gast, P. W., 1968, Trace element fractionation and the origin of tholeiitic and alkaline magma types. Geochim. Cosmochim. Acta, 32, 1057-1086.

Green, D. H., and A. E. Ringwood, 1967, The genesis of basaltic magmas. Contr. Mineral. Petrol., 15, 103-190.

Green, D. H., W. O. Hibberson, and A. L. Jaques, 1979, Petrogenesis of mid-ocean ridge basalts. In: M. W. McElhinny (ed.) The Earth: Its Origin, Structure, and Evolution, Academic Press, London, 265-299.

Griffin, W. L., and V. R. Murthy, 1969, Distribution of K, Rb, Sr, and Ba in minerals relevant to basalt genesis. Geochim. Cosmochim. Acta, 33, 1389-1414.

Gurney, J. J., and B. Harte, 1980, Chemical variations in upper mantle nodules from southern African kimberlites. Philosophical Trans. Royal Soc. London, A 297, 273-293.

Harris, P. G., 1957, Zone refining and the origin of potassic basalts, Geochim. Cosmochim. Acta, 12, 195-208.

Hart, S. R., 1971, K, Rb, Cs, Sr, and Ba contents and Sr isotopic ratios of ocean floor basalts. Philosophical Trans. Royal Soc. London, A 268, 573-587.

Hart, S. R., 1976, LIL-element geochemistry, Leg 34 basalts. In: R. S. Yeats, S. R. Hart, et al. (eds.), Initial Reports of the Deep Sea Drilling Project, Volume 34, U.S. Government Printing Office, Washington, 283-288.

Hart, S. R., 1981, Diffusion compensation in natural silicates. Geochim. Cosmochim. Acta, 45, 279-292.

Hart, S. R., and C. Brooks, 1974, Clinopyroxene-matrix partitioning of K, Rb, Cs, Sr, and Ba. Geochim. Cosmochim. Acta, 38, 1799-1806.

Hart, S. R., and C. Brooks, 1977, The geochemistry and evolution of the early Precambrian mantle. Contr. Mineral. Petrol., 61, 109-128.

Hart, S. R., and K. Davis, 1978, Nickel partitioning between olivine and silicate melt. Earth Planet. Sci. Letters, 40, 203-219.

Hart, S. R., and C. J. Allegre, 1980, Trace element constraints on magma genesis. In: R. B. Hargraves (ed.), Physics of Magmatic Processes, Princeton University Press, Princeton, 121-141.

Hart, S. R., W. E. Glassley, and D. E. Karig, 1972, Basalts and sea floor spreading behind the Mariana Island Arc. Earth Planet Sci. Letters, 15, 12-18.

Harte, B., 1977, Rock nomenclature with particular relation to deformation and recrystallization textures in olivine-bearing xenoliths. Jour. Geology, 85, 279-288.

Haskin, L. A., and R. L. Korotev, 1977, Test of a model for trace element partitioning during closed-system solidication of a silicate liquid. Geochim. Cosmochim. Acta, 41, 921-939.

Hawkesworth, C. J., R. K. O'Nions, P. J. Pankhurst, P. J. Hamilton, and N. M. Evensen, 1977, A geochemical study of island-arc and back-arc tholeiites from the Scotia Sea. Earth Planet Sci. Letters, 36, 253-262.

Helmstaedt, H., and R. Doig, 1975, Eclogite nodules from kimberlite pipes of the Colorado Plateau - samples of subducted Franciscan-type oceanic lithosphere. Physics Chemistry Earth, 9, 95-111.

Helmstaedt, H., and D. J. Schulze, 1979, Garnet clinopyroxenite - chlorite eclogite transition in a xenolith from Moses Rock: further evidence for metamorphosed ophiolites under the Colorado Plateau. In: F. R. Boyd and H. O. A. Meyer (eds.), The Mantle Sample: Inclusions in Kimberlites and Other Volcanics, American Geophysical Union, Washington, 357-365.

Hervig, R. L., and J. V. Smith, 1981, Dolomite-apatite inclusion in chrome-diopside crystal, Bellsbank Kimberlite, South Africa. Amer. Mineralogist, 66, 346-349.

Herzberg, C. T., 1978, Pyroxene geothermometry and geobarometry: experimental and thermodynamic evaluation of some subsolidus phase relations involving pyroxenes in the system $CaO$-$MgO$-$Al_2O_3$-$SiO_2$. Geochim. Cosmochim. Acta 42, 945-958.

Hickey, R. L., and F. A. Frey, 1981, Rare-earth element geochemistry of Mariana Fore-arc volcanics: Deep Sea Drilling Project Site 458 and Hole 459B. In: D. M. Hussong, S. Uyeda, et al. (eds.), Initial Reports of the Deep Sea Drilling Project, Volume 60, U.S. Government Printing Office, Washington, 735-742.

Hoare, J. M., W. H. Condon, A. Cox, and G. B. Dalrymple, 1968, Geology, paleomagnetism, and potassium-argon ages of basalts from Nunivak Island, Alaska. Geological Soc. Amer. Memoir 116, 377-412.

Hofmann, A., and S. R. Hart, 1978, An assessment of local and regional isotopic equilibrium in the mantle. Earth Planet. Sci. Letters, 38, 44-62.

Hunter, W. C., and D. Smith, 1981, Garnet peridotite from Colorado Plateau diatremes: hydrates, carbonates, and comparative geothermometry. Contr. Mineral. Petrol., 76, 312-320.

Irving, A. J., 1976, On the validity of paleogeotherms determined from xenoliths suites in basalts and kimberlites. Amer. Mineralogist, 61, 638-642.

Irving, A. J., 1978, A review of experimental studies of crystal/liquid trace element partitioning. Geochim. Cosmochim. Acta, 42, 743-770.

Irving, A. J., 1980, Petrology and geochemistry of composite ultramafic xenoliths in alkalic basalts and implications for magmatic processes within the mantle. Amer. Jour. Sci., 280-A, 389-426.

Irving, A. J., and R. C. Price, 1981, Geochemistry and evolution of lherzolite-bearing phonolitic lavas from Nigeria, Australia, East Germany and New Zealand. Geochim. Cosmochim. Acta, 45, 1309-1320.

Ito, K., and G. C. Kennedy, 1970, The fine structure of the basalt-eclogite transition. Mineralogical Soc. Amer. Special Paper 3, 77-83.

Jacobsen, S. B., and G. J. Wasserburg, 1980, Sm-Nd isotopic evolution of chondrites. Earth Planet. Sci. Letters, 50, 139-155.

Jagoutz, E., H. Palme, H. Baddenhausen, K. Blum, M. Cendales, G. Dreibus, B. Spettel, V. Lorenz, and H. Wanke, 1979, The abundances of major, minor and trace elements in the earth's mantle as derived from primitive ultramafic nodules. Proc. Lunar Planet. Sci. Conf., 10th, 2031-2050.

Jagoutz, E., R. W. Carlson, and G. W. Lugmair, 1980, Equilibrated Nd-unequilibrated Sr isotopes in mantle xenoliths. Nature, 286, 708-710.

Jaques, A. L., and B. W. Chappell, 1980, Petrology and trace element geochemistry of the Papuan Ultramafic Belt. Contr. Mineral. Petrol., 75, 55-70.

Jenkins, D. M., 1981, Experimental phase relations of hydrous peridotites modelled in the system $H_2O$-CaO-MgO-$Al_2O_3$-$SiO_2$. Contr. Petrol., 77, 166-176.

Jensen, B. B., 1973, Patterns of trace element partitioning, Geochim. Cosmochim. Acta, 37, 2227-2242.

Kay, R. W., and P. W. Gast, 1973, The rare earth content and origin of alkali-rich basalts. Jour. Geology, 81, 653-682.

Kay, R. W., and R. G. Senechal, 1976, The rare earth geochemistry of the Troodos ophiolite complex. Jour. Geophysical Research, 81, 964-970.

Kay, R. W., and N. J. Hubbard, 1978, Trace elements in ocean ridge basalts. Earth Planet. Sci. Letters, 38, 95-116.

Kay, R., N. J. Hubbard, and P. W. Gast, 1970. Chemical characteristics and origin of oceanic ridge volcanic rocks. Jour. Geophysical Research, 75, 1585-1613.

Kesson, S. E., 1973, The primary geochemistry of the Monaro alkaline volcanics, southeastern Australia - evidence for upper mantle heterogeneity. Contr. Mineral. Petrol., 42, 93-108.

Korzhinsky, D. S., 1970, Theory of Metasomatic Zoning (translated by J. AAgrell). Clarendon Press, Oxford, 162 pp.

Kurat, G., H. Palmer, B. Spettel, H. Baddenhausen, H. Hofmeister, C. Palme, and H. Wanke, 1980, Geochemistry of ultramafic xenoliths from Kapfenstein, Austria: evidence for a variety of upper mantle processes. Geochim. Cosmochim. Acta, 44, 45-60.

Langmuir, C. H., R. D. Vocke, Jr., G. N. Hanson, and S. R. Hart, 1978, A general mixing equation with applications to Icelandic basalts. Earth Planet. Sci. Letters, 18, 380-392.

Lanphere, M. A., and G. B. Dalrymple, 1980, Age and strontium isotopic composition of the Honolulu Volcanic Series, Oahu, Hawaii. Amer. Jour. Sci., 280-A, 736-751.

Leake, B. E., 1978, Nomenclature of amphiboles. Amer. Mineralogist, 63, 1023-1052.

Leeman, W. P., 1976, Petrogenesis of McKinney (Snake River) olivine tholeiite in light of rare-earth element and Cr/Ni, distributions. Geological Soc. Amer. Bull., 87, 1777-1792.

Lindsley, D. H., and S. A. Dixon, 1976, Diopside-enstatite equilibria at 85-° to 1400°C, 5-35 kb. Amer. Jour. Sci., 276, 1285-1301.

Lindstrom, D. J., 1976, Experimental study of the partitioning of the transition metals between clinopyroxene and coexisting silicate liquid. Ph.D. thesis, University of Oregon.

Lindstrom, D. J., and D. F. Weill, 1978, Partitioning of transition metals between diopside and coexisting silicate liquids - I. Nickel, cobalt, and manganese. Geochim. Cosmochim. Acta, 42, 817-832.

Lloyd, F. E., and D. K. Bailey, 1975, Light element metasomatism of the continental mantle: the evidence and the consequences. Physics Chemistry Earth, 9, 389-416.

Loubet, M., N. Shimizu, and C. J. Allegre, 1975, Rare earth elements in alpine peridotites. Contr. Mineral. Petrol., 53, 1-12.

Mark, R. K., 1971, Strontium isotopic study of basalts from Nunivak Island, Alaska, Ph.D. thesis, Stanford University, 50 pp.

Mathez, E. A., and J. R. Delaney, 1981, The nature and distribution of carbon in submarine basalts and peridotite nodules. Earth Planet. Sci. Letters, 56, 217-232.

McCulloch, M. T., R. T. Gregory, G. J. Wasserburg, and H. P. Taylor, Jr., 1981, Sm-Nd, Rb-Sr, and $^{18}O/^{16}O$ Isotopic systematics in an oceanic crustal section: evidence from the Samail Ophiolite. Jour. Geophysical Research, 86, 2721-2735.

McGetchin, T. R., and L. T. Silver, 1972, A crustal-upper mantle model for the Colorado Plateau based on observation of crystalline rock fragments in the Moses Rock dike. Jour. Geophysical Research, 77, 7022-7037.

McGetchin, T. R., L. T. Silver, and A. A. Chodos, 1970, Titanoclinohumite: a possible mineralogical site for water in the upper mantle. Jour. Geophysical Research, 75, 255-259.

McKay, G. A., and D. F. Weill, 1976, Petrogenesis of KREEP. Proc. Lunar Sci. Conf. 7th, 2427-2447.

Melson, W. G., S. R. Hart, and G. Thompson, 1972, St. Paul's Rocks, equatorial Atlantic: petrogenesis, radiometric ages, and implications on sea floor spreading. Geological Soc. Amer. Memoir 132, 244-272.

Menzies, M. A., 1976, Rare earth geochemistry of fused ophiolitic and alpine lherzolites - I. Othris, Lanzo, and Troodos. Geochim. Cosmochim. Acta, 40, 645-656.

Menzies, M. A., and V. R. Murthy, 1978, Strontium isotope geochemistry of alpine tectonite lherzolites: data compatible with a mantle origin. Earth Planet, Sci. Letters, 38, 346-354.

Menzies, M. A., and V. R. Murthy, 1980a, Nd and Sr isotope geochemistry of hydrous mantle nodules and their host alkali basalts: implications for local heterogeneities in metasomatically veined mantle. Earth Planet. Sci. Letters, 46, 323-334.

Menzies, M. A., and V. R. Murthy, 1980b, Mantle metasomatism as a precursor to the genesis of alkaline magmas - isotopic evidence. Amer. Jour. Sci., 280-A, 622-638.

Menzies, M., and V. R. Murthy, 1980c, Enriched mantle: Nd and Sr isotopes in diopsides from kimberlite nodules. Nature, 283, 634-636.

Murck, B. W., R. C. Buruss, and L. S. Hollister, 1978, Phase equilibria in fluid inclusions in ultramafic xenoliths. Amer. Mineralogist, 63, 40-46.

Mysen, B. O., 1976, Experimental determination of some geochemical parameters relating to conditions of equilibration of peridotite in the upper mantle. Amer. Mineralogist, 61, 677-683.

Mysen, B. O., 1977, Partitioning of cerium, samarium, and thulium between pargasite, garnet peridotite minerals, and hydrous silicate liquid at high temperature and pressure. Carnegie Inst. Wash. Yearbook, 76, 588-594.

Mysen, B. O., 1979, Trace element partitioning between garnet peridotite minerals and water-rich vapor: experimental data from 5 to 30 kb. Amer. Mineralogist, 64, 274-287.

Norman, J. C., and L. A. Haskin, 1968, The geochemistry of Sc: a comparison to the rare earths and Fe. Geochim. Cosmochim. Acta, 32, 93-108.

O'Hara, M. J., and E. L. P. Mercy, 1966, Eclogite peridotite and pyrope from the Navajo country, Arizona and New Mexico, Amer. Mineralogist, 51, 336-352.

O'Nions, R. K., Hamilton, P. J., and N. M. Evensen, 1977, Variations in $^{143}Nd/^{144}Nd$ and $^{87}Sr/^{86}Sr$ ratios in oceanic basalts. Earth Planet. Sci. Letters, 34, 13-22.

Ottonello, G., 1980, Rare earth abundances and distribution in some spinel peridotite xenoliths from Assab (Ethiopia). Geochim. Cosmochim. Acta, 44, 1885-1902.

Pallister, J. S., and R. J. Knight, 1981, Rare-earth element geochemistry of the Samail Ophiolite near Ibra, Oman. Jour. Geophysical Research, 86, 2673-2697.

Papanastassiou, D. A., and G. J. Wasserburg, 1969, Initial strontium isotopic abundances and the resolution of small time differences in the formation of planetary objects. Earth Planet. Sci. Letters, 5, 361-376.

Polve, M., and C. J. Allegre, 1980, Orogenic lherzolite complexes studied by $^{87}Rb$-$^{87}Sr$: a clue to understand the mantle convection processes? Earth Planet. Sci. Letters, 51, 71-93.

Richard, P., and C. J. Allegre, 1980, Neodymium and strontium isotope study of ophiolite and orogenic lherzolite petrogenesis. Earth Planet. Sci. Letters, 47, 65-74.

Richard, P., N. Shimizu, and C. J. Allegre, 1976, $^{143}Nd/^{146}Nd$, a natural tracer: an application to natural basalts. Earth Planet. Sci. Letters, 31, 269-278.

Ringwood, A. E., 1975, Composition and Petrology of the Earth's Mantle. McGraw-Hill Book Co., New York, 618 pp.

Ringwood, A. E., 1979, Origin of the Earth and Moon. Springer-Verlag, New York, 295 pp.

Roden, M. F., 1981, Origin of coexisting minette and ultramafic breccia, Navajo Volcanic Field. Contr. Mineral. Petrol., 77, 195-206.

Roden, M. F., and D. Smith, 1979, Field geology and petrology of the Buell Park minette diatreme, Apache County, Arizona. In: F. R. Boyd and H. O. A. Meyer (eds.), Kimberlites, Diatremes, and Diamonds: Their Geology, Petrology, and Geochemistry, Amer. Geophysical Union, Washington, 364-381.

Roden, M. F., F. A. Frey, and D. M. Francis, 1980, REE, K, Rb, Sr, and Sr isotopic geochemistry of peridotite xenoliths in basalt from Nunivak Island, Alaska (abs.). EOS, 61, 401.

Roden, M. F., F. A. Frey, and S. R. Hart, 1981, The mantle source for the Honolulu Volcanic Series: Nd isotope evidence (abs.). EOS, 62, 423.

Roedder, E., 1965, Liquid $CO_2$ inclusions in olivine-bearing nodules and phenocrysts from basalts. Amer. Mineralogist, 50, 1746-1782.

Roeder, P. L., and R. F. Emslie, 1970, Olivine-liquid equilibrium. Contr. Mineral. Petrol., 29, 275-289.

Sato, M., 1977, Oxygen fugacity of the mantle environment. In: H. J. B. Dick, Jr. (ed.), Magma Genesis, State of Oregon Dept. of Geology and Mineral Industries Bull. 96, 309-310.

Selverstone, J., ms, Fluid inclusions as petrogenetic indicators in granulite xenoliths, Pali-Aike Volcanic Field, Chile.

Serri, G., 1980, Chemistry and petrology of gabbroic complexes from the northern Apennine ophiolites. In: Ophiolites, Proceedings International Ophiolite Conference, Geol. Survey Dept., Nicosia, Cyprus, 296-313.

Shaw, D. M., 1970, Trace element fractionation during anatexis. Geochim. Cosmochim. Acta, 34, 237-243.

Shih, C. Y., 1972, The rare earth geochemistry of oceanic igneous rocks. Ph.D. thesis, Columbia University.

Shimizu, N., 1974, An experimental study of the partitioning of K, Rb, Cs, and Sr and Ba between clinopyroxene and silicate liquid at high pressures. Geochim. Cosmochim. Acta, 38, 1789-1798.

Shimizu, N., and R. J. Arculus, 1975, Rare earth element concentrations in a suite of basanitoids and alkali olivine basalts from Grenada, Lesser Antilles. Contr. Mineral. Petrol., 50, 231-240.

Shimizu, N., M. P. Semet, and C. J. Allegre, 1978. Geochemical applications of quantitative ion-microprobe analysis. Geochim. Cosmochim. Acta, 42, 1321-1334.

Smith, D., 1979, Hydrous minerals and carbonates in peridotite inclusions from the Green Knobs and Buell Park kimberlitic diatremes on the Colorado Plateau. In: F. R. Boyd and H. O. A. Meyer (eds.), The Mantle Sample: Inclusions in Kimberlites and Other Volcanics, Amer. Geophysical Union, Washington, 345-356.

Smith, D., and S. Levy, 1976, Petrology of the Green Knobs diatrem and implications for the upper mantle below the Colorado Plateau. Earth Planet. Sci. Letters, 29, 107-125.

Smith, D., and M. Zientek, 1979, Mineral chemistry and zoning in eclogite inclusions from Colorado Plateau diatremes. Contr. Mineral. Petrol., 69, 119-131.

Sneeringer, M. A., 1981, Strontium and samarium diffusion in diopside. Ph.D. thesis, MIT, 235 pp.

Solomon, S. C., 1976, Geophysical constraints on radial and lateral temperature variations in the upper mantle. Amer. Mineralogist, 61, 788-803.

Spera, F. J., 1981. Carbon Dioxide in igneous petrogenesis: II. fluid dynamics of mantle metasomatism. Contr. Mineral. Petrol., 77, 56-65.

Staudigel, H., 1980, Chemical analyses of interlaboratory standards. In: T. Donnelly, J. Francheteau, et al. (eds.), Initial Reports of the Deep Sea Drilling Project, Volumes 51, 52, 53, Part 2, U.S. Government Printing Office, Washington, 1331-1333.

Stolper, E., 1980, A phase diagram for mid-ocean ridge basalts: preliminary results and implications for petrogenesis. Contr. Mineral. Petrol. 74, 13-27.

Stosch, H. G., 1982, Rare earth element partitioning between minerals from anhydrous spinel peridotite xenoliths. Geochim. Cosmochim. Acta, in press.

Stosch, H. G., and H. A. Seck, 1980, Geochemistry and mineralogy of two spinel peridotite suites from Dreiser Weiher, West Germany. Geochim. Cosmochim. Acta, 44, 457-470.

Stosch, H. G., R. W. Carlson, and G. W. Lugmair, 1980, Episodic mantle differentiation: Nd and Sr isotopic evidence. Earth Planet. Sci. Letters, 47, 263-271.

Suen, C. J., F. A. Frey, and J. Malpas, 1979, Bay of Islands ophiolite suite, Newfoundland: petrologic and geochemical characteristics with emphasis on rare earth element geochemistry. Earth Planet. Sci. Letters, 45, 337-348.

Sun, S.-S., 1980, Lead isotopic study of young volcanic rocks from mid-ocean ridges, ocean islands and island arcs. Philosophical Trans. Royal Soc. London, A 297, 409-445.

Sun, S.-S., and G. N. Hanson, 1975, Origin of Ross Island basanitoids and limitations upon the heterogeneity of mantle sources for alkali basalts and enphelinites. Contr. Mineral. Petrol., 52, 77-106.

Sun, S.-S, R. W. Nesbitt, and A. Y. Sharaskin, 1979, Geochemical characteristics of mid-ocean ridge basalts. Earth Planet. Sci. Letters, 44, 119-138.

Taylor, H. P. Jr., 1980, The effects of assimilation of country rocks by magmas on $^{18}O/^{16}O$ and $^{87}Sr/^{86}Sr$ systematics in igneous rocks. Earth Planet. Sci. Letters, 47, 243-254.

Thompson, G., and D. C. Bankston, 1970, Sample contamination from grinding and sieving determined by emission spectrometry. Applied Spectroscopy, 24, 210-219.

Tiezzi, L. J., and R. B. Scott, 1980, Crystal fractionation in a cumulate gabbro, mid-atlantic ridge, 26°N. Jour. Geophysical Research, 85, 5438-5454.

Varne, R. and A. L. Graham, 1971, Rare earth abundances in hornblende and clinopyroxene lherzolite xenoliths: implications for upper mantle fractionation processes. Earth Planet. Sci. Letters, 13, 11-18.

Wass, S. Y., 1979, Multiple origins of clinopyroxenes in alkali basaltic rocks. Lithos, 12, 115-132.

Wass, S. Y., 1980, Geochemistry and origin of xenolith-bearing and related alkali basaltic rocks from the southern Highlands, New South Wales, Australia. Amer. Jour. Sci., 280-A, 639-666.

Wass, S. Y., and N. W. Rogers, 1980, Mantle metasomatism - precursor to continental alkaline volcanism. Geochim. Cosmochim. Acta, 44, 1811-1824.

Wass, S. Y., P. Henderson, and C. J. Elliot, 1980, Chemical heterogeneity and metasomatism in the upper mantle - evidence from rare earth and other elements in apatite-rich xenoliths in basaltic rocks from eastern Australia. Philosopical Trans. Royal Soc. London, A 297, 333-346.

Wasserburg, G. J., S. B. Jacobsen, D. J. DePaolo, M. T. McCulloch, and T. Wen, 1981, Precise determination of Sm/Nd ratios, Sm and Nd isotopic abundances in standard solutions. Geochim. Cosmochim. Acta, 45, 2311-2325.

Watson, E. B., 1977, Partitioning of manganese between forsterite and silicatr liquid. Geochim. Cosmochim. Acta, 41, 1363-1374.

Watson, E. B., and T. H. Green, 1981, Apatite/liquid partition coefficients for the rare earth elements and strontium. Earth Planet. Sci. Letters, 56, 405-421.

Wendlandt, R. F., and W. J. Harrison, 1979, Rare earth partitioning between immiscible carbonate and silicate liquids and $CO_2$ vapor: results and implications for the formation of light rare earth-enriched rocks. Contr. Mineral. Petrol., 69, 409-419.

White, W. M., and J.-G. Schilling, 1978, The nature and origin of geochemical variation in Mid-Atlantic Ridge basalts from the central North Atlantic. Geochim. Cosmochim. Acta, 42, 1501-1516.

White, W. M., and A. W. Hofmann, 1978, Geochemistry of Galapagos Islands: implications for mantle dynamics and evolution. Carnegie Inst. Wash. Yearbook, 77, 596-606.

Wilshire, H. G., and J. W. Shervais, 1975, Al-augite and Cr-diopside ultramafic xenoliths in basaltic rocks from western United States. Physics Chemistry Earth, 9, 257-272.

Wilshire, H. G., J. E. Nielson Pike, C. E. Meyer, and E. C. Schwarzman, 1980, Amphibole-rich veins in lherzolite xenoliths, Dish Hill and Deadman Lake, California. Amer. Jour. Sci., 280-A, 576-593.

Wood, D. A., 1979, A variably veined suboceanic upper mantle - genetic significance for mid-ocean ridge basalts from geochemical evidence. Geology, 7, 499-503.

Wyllie, P. J., 1978, Mantle fluid compositions buffered in peridotite-$CO_2$-$H_2O$ by carbonates, amphibole, and phlogopite. Jour. Geology, 86, 687-713.

Wyllie, P. J., 1979, Magmas and volatile components. Amer. Mineralogist, 64, 469-500.

Wyllie, P. J., 1980, The origin of kimberlite. Jour. Geophysical Research, 85, 6902-6910.

Yoder, H. S., 1976, Generation of Basaltic Magma. National Academy Sciences, Washington, 263 pp.

Zartman, R. E., and F. Tera, 1973, Lead concentration and isotopic composition in five peridotite inclusions of probable mantle origin. Earth Planet. Sci. Letters, 20, 54-66.

Zindler, A., 1980, Geochemical processes in the earth's mantle and the nature of crust-mantle interactions: evidence from studies of Nd and Sr isotope ratios in mantle-derived igneous rocks and lherzolite nodules. Ph.D. thesis, MIT.

Zindler, A., and E. Jagoutz, 1980, Isotope and trace element systematics in mantle-derived peridotite nodules from San Carlos (abs.). EOS, 61, 374.

Zindler, A., S. R. Hart, F. A. Frey, and S. P. Jakobsson, 1979, Nd and Sr isotope ratios and rare earth element abundances in Reykjanes Peninsula basalts: evidence for mantle heterogeneity beneath Iceland, Earth Planet. Sci. Letters, 45, 249-262.

Zindler, A., S. R. Hart, and C. Brooks, 1981. The Shabogamo intrusive suite, Labrador: Sr and Nd isotopic evidence for contaminated mafic magmas in the Proterozoic. Earth Planet. Sci. Letters, 54, 217-235.

APPENDIX A: LIST OF TABLES AND FIGURES

Tables

Figures